The Retinal Explant as a Model to Investigate Neuronal Pathology and Neuroprotective Strategies

Kate Evelyn Binley

Acknowledgements

Abstract

Despite the association of neuronal cell loss with a wide range of neurodegenerative disorders, the mechanisms leading to this cell death remain poorly understood. In this thesis I have investigated these mechanisms and tested whether they represent viable targets for therapeutic intervention. The adult mouse retinal explant is a popular model of axotomy-induced neuronal degeneration but has been limited by the lack of morphometric data. Since dendritic pruning is well-evidenced to precede cell loss in neurodegenerative diseases, including glaucoma and Alzheimer's disease, I investigated whether the quantification of dendritic morphology of retinal ganglion cells in the retinal explant could be used as a more sensitive measure of neuronal health after axotomy. I report here that retinal ganglion cell dendrite loss precedes cell loss by at least 7 days and that this retraction is substantially retarded following treatment with brain-derived neurotrophic factor applied at the time of explantation. Perhaps most importantly, I demonstrate for the first time in this model that delayed application of brain-derived neurotrophic factor significantly protects against dendritic retraction of retinal ganglion cells. The work outlined in this thesis thus supports the targeting of dendritic outgrowth and/or synaptic connectivity for the treatment of neurodegenerative disorders.

Abbreviations

AMD	Age-related macular degeneration
AUC	Area under the curve
BCA	Bicinchoninic acid
BDNF	Brain-derived neurotrophic factor
BSA	Bovine serum albumin
CaRE	Calcium response element
ChABC	Chondroitinase ABC
CNS	Central nervous system
CNTF	Ciliary neurotrophic factor
CREB	cAMP response element binding protein
CS	Chondroitin sulphate
CS-GAG	Chondroitin sulphate-glycosaminoglycan
CSPG	Chondroitin sulphate proteoglycan
DF	Dendritic field
DiI	1-1'-dioctade-cyl-3,3,3',3'-tetramethylindocarbocyanine perchlorate
DiO	3,3 dioctadecyloxacarbocyanine perchlorate
ECM	Extracellular matrix
ELISA	Enzyme-linked immunoabsorbent assay
ESC	Embryonic stem cell
GAG	Glycosaminoglycan
GCL	Ganglion cell layer
GFP	Green fluorescent protein
HRP	Horseradish peroxidase
INL	Inner nuclear layer

IOP	Intraocular pressure
IPL	Inner plexiform layer
iPSC	Induced pluripotent stem cell
JNK	c-JUN N-terminal kinase
LB	Luria-Bertani
LTP	Long-term potentiation
MAPK	Mitogen-activated kinase
MMP	Matrix metalloprotease
MNP	Magnetic nanoparticle
NCAM	Neural cell adhesion molecule
NGF	Nerve growth factor
NMDA	N-methyl-D-aspartate
NPC	Neural progenitor cell
NS	Not significant
NSC	Neural stem cell
NT-3	Neurotrophin-3
NT-4	Neurotrophin-4
OLM	Outer limiting membrane
ONL	Outer nuclear layer
OPL	Outer plexiform layer
$P75^{NTR}$	p75 neurotrophin receptor
PBS	Phosphate-buffered saline
PFA	Paraformaldehyde
PI3K	Phosphoinositide 3-kinase
PLC	Phospholipase C
PNN	Perineuronal net

PSD-95   Post-synaptic density 95

RF   Receptive field

RGC   Retinal ganglion cell

ROS   Reactive oxygen species

RPC   Retinal progenitor cell

RPE   Retinal pigment epithelium

RT   Room temperature

Shh   Sonic hedgehog

tPA   Tissue plasminogen activator

Trk   Tropomyosin receptor kinase

TUNEL   Terminal deoxynucleotidyl transferase dUTP nick end labelling

UTR   Untranslated region

Contents

List of Figures

List of Tables

List of Equations

Chapter 1: Introduction

1.1 The retina

Retinal ganglion cells (RGCs) are neurons in the inner retina that collect information from photoreceptors. This information is transmitted via RGC axons, which leave the back of the eye through the optic nerve head and terminate in the lateral geniculate nucleus or the superior colliculus in humans. There are two parallel pathways in retinal processing, the ON and the OFF pathways. In the ON pathway bipolar cells and RGCs are depolarised by light, but in the OFF pathway bipolar cells and RGCs are hyperpolarised by light. Following light transduction, photoreceptors synapse to horizontal cells and bipolar cells. Cone-driven bipolar cells synapse directly to RGCs of the same ON/OFF pathway (i.e. ON bipolar → ON RGC; OFF bipolar → OFF RGC), whereas rod-driven bipolar cells transmit signals to ON and OFF RGCs via AII amacrine cells (Figure 1.1) (Famiglietti and Kolb 1976; Nelson et al. 1978). Whilst the majority of RGCs carry out a visual processing role, a small percentage, termed intrinsically photosensitive RGCs, contain melanopsin and are important for the circadian rhythm and controlling the pupillary light reflex (Schmidt et al. 2011; Pickard and Sollars 2012).
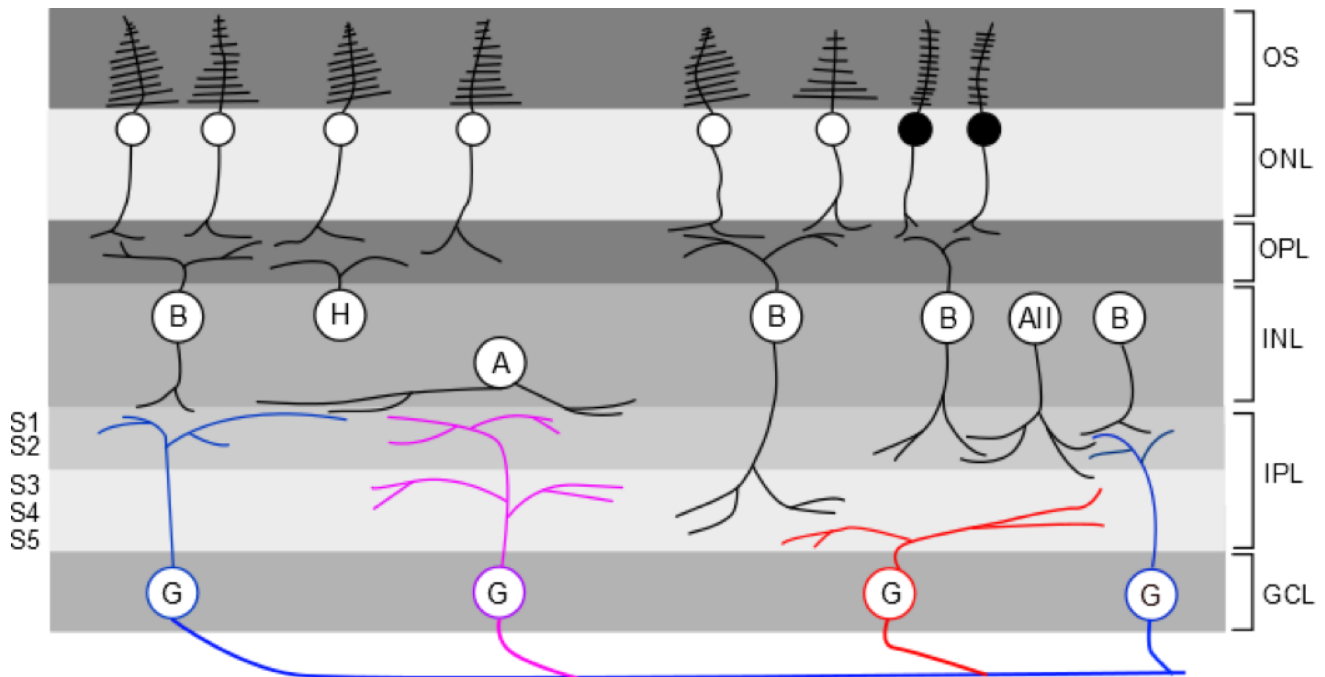
Figure 1.1. Neural processing in the mammalian retina. Under *scotopic* conditions photoreceptors are depolarised and release glutamate, which hyperpolarised cone-driven ON bipolar cells and rod-driven bipolar cells via metabotropic glutamate receptors (Shiells and Falk 1990). Glutamate depolarises OFF bipolar cells via ionotropic glutamate receptors. Under *photopic* conditions glutamate release from photoreceptors is suppressed, resulting in depolarisation of ON bipolar cells and rod-driven bipolar cells, and hyperpolarisation of OFF bipolar cells (Stryer 1986). Cone-driven ON bipolar cells synapse to ON RGCs, and cone-driven OFF bipolar cells synapse to OFF RGCs. Bistratified RGCs receive signals from ON and OFF bipolar cells (Kolb 1970; Famiglietti and Kolb 1976; Nelson et al. 1978). Rod-driven bipolar cells synapse to AII amacrine cells, which in turn depolarise cone-driven ON bipolar cells via gap junctions, and hyperpolarise cone-driven OFF bipolar cells and OFF RGCs via glycine (Tagawa et al. 1999; Bloomfield and Dacheux 2001; Xu and Tian 2008). G (ganglion cell); A (amacrine cell); AII (AII amacrine cell); H (horizontal cell); B (bipolar cell); white cells in ONL (cones); black cells in ONL (rods); GCL (ganglion cell layer); IPL (inner plexiform layer); INL (inner nuclear layer); OPL (outer plexiform layer); ONL (outer nuclear layer); OS (outer segments). The IPL is divided into 5 strata (S1-S5); OFF cells (blue) stratify in S1-S2 (sublamina a); ON cells (red) stratify in S3-S5 (sublamina b); bistratified cells (purple) stratify in sublaminas a and b.

1.2 Classes of retinal ganglion cells

RGCs are a very heterogeneous population of neurons in terms of morphology, as demonstrated in Figure 1.2. Not only does the dendritic field size of RGCs increases with distance from the optic nerve head (Doi et al. 1995), but other morphological parameters, such as soma area, branching complexity and dendritic field asymmetry, vary greatly between neighbouring cells. The variance in the mouse is particularly well demonstrated by the number of different morphological classes of RGCs identified: 14 types by Sun et al. (2002) and Coombs et al. (2006). In addition to classification by cell shape, RGCs have recently begun to be classified by function, of which there has been found to be at least 30 types (Baden et al. 2016), and this number is likely to increase as neuronal recording methods are optimised. Transgenic mouse lines offer a method of labelling specific classes of RGCs, such as Isl2+ RGCs (Triplett et al. 2014) or ON-OFF direction-selective RGCs (Kay et al. 2011). For a summary of available transgenic mouse lines that label specific classes of RGCs, the reader should refer to Sanes & Masland (2015).
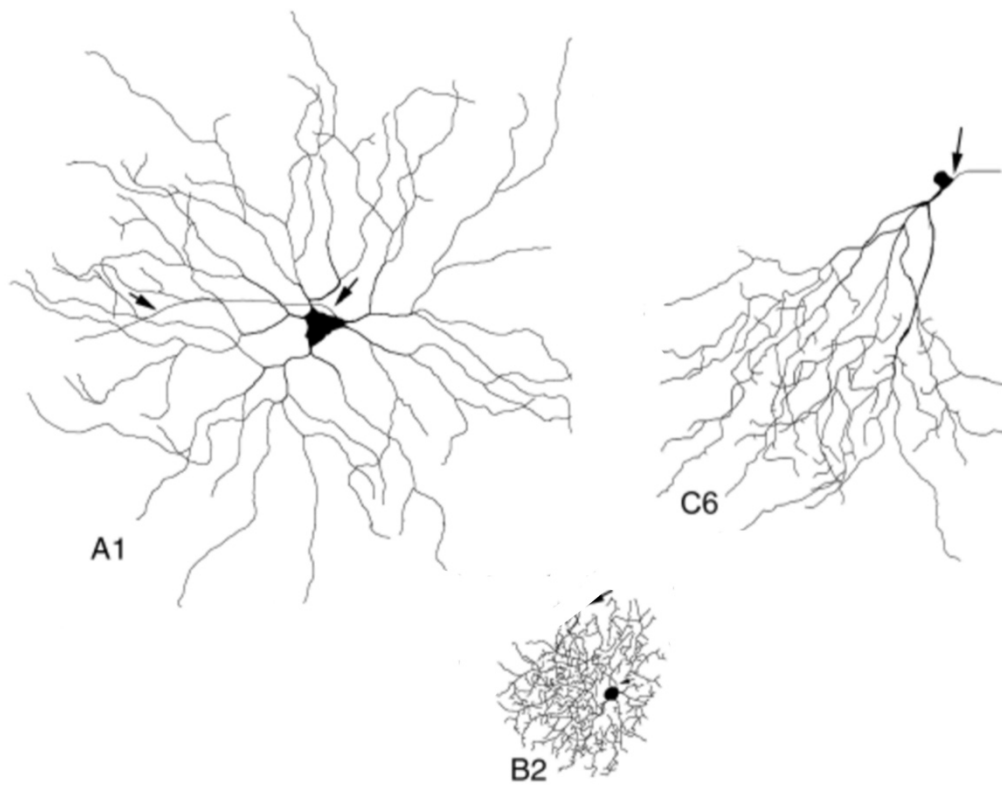
Figure 1.2. Example types of mouse RGCs classified by soma diameter, dendritic field diameter and stratification depth, demonstrating the morphological variety of these neurons. Figure adapted from Sun et al. (2002).

1.3 Normal retinal neurogenesis and dendritogenesis

1.3.1 Retinal neurogenesis

The developing retina contains a population of stem cells capable of differentiating into all cell types in the retina. In the retinae of fish and amphibians a retinal stem cell population also exists in the adult in the ciliary margin zone (Fischer et al. 2013). While many groups have attempted to find this stem cell niche in higher vertebrates for the application of stem cell replacement therapies, several reports suggest that the ciliary margin zone is reduced in more highly evolved vertebrates and is completely absent in the mouse (Li et al. 2013). Nevertheless, there is evidence that a population of retinal stem/progenitor cells does exist in the retinae of mice (Kubota et al. 2002) and humans (Mayer et al. 2005; Johnsen et al. 2012), which may act to repair the tissue following ocular injury.

The 10 layers of the vertebrate retina consist of 7 types of neuronal and glial cells, which all originate from retinal progenitor cells (RPCs). Differentiation of the different cell types occurs in waves and it is imperative, therefore, that there is tight regulation of both extrinsic and intrinsic cues to ensure the correct sequence of differentiation (Zhang and Yang 2001). Ca^{2+} waves are important for controlling the expression of specific genes by binding to calcium response elements and for proliferation of NPCs (Tao et al. 1998; West et al. 2001; Stroh et al. 2011).

In general, neurons in the retina are formed from RPCs in descending size order, with the differentiation of RGCs as the first cell type (Jeffery 1997). In addition, the position relative to the optic nerve seems to be important; RGCs with axons deepest in the optic tract are formed first (alpha cells in rat, beta cells in cat) (Reese and Colello 1992). Low sonic hedgehog (Shh) concentrations induce expression of several genes, including *atonal*, and mitogen-activated kinase (MAPK) waves, which stimulate naïve RPCs to become competent for differentiation. RGCs themselves secrete Shh. Increased concentration of Shh inhibits further RGC differentiation and stimulates the next wave of neuronal differentiation (amacrines) (Zhang and Yang 2001).

1.3.2 Dendrite and axon guidance

The processes of dendrite and axon development are mediated through a collection of extracellular guidance molecules or receptors and intracellular signal molecules. A list of the most important of these molecules can be found in Table 1.1.

Table 1.1. Summary of molecules and proteins involved in the signalling cascades upstream of dendritic and axonal changes during development.

Extracellular guidance molecules	Transmembrane proteins	Intracellular signal molecules
Semaphorins (secreted)	Integrins	Cyclic AMP/GMP
Extracellular matrix components	NMDA receptor	Calcium
	Cadherins	Rho GTPases
	Neuropilins	LIM domain kinase 1
	Plexins	Focal adhesion kinase
		CAMKII

Once cells have fully differentiated into RGCs, the process of dendrite outgrowth and branching occurs. After dendrite growth initiation, one dendrite is selected to become the axon and the process of axon guidance to the midbrain and the thalamus via the optic nerve begins. Simultaneously, the remaining primary dendrites continue to grow and branch in response to a number of positive and negative guidance cues (Erskine and Herrera 2007). Neurite outgrowth is mediated by intrinsic factors, such as intracellular cyclic nucleotide concentration (Marrs et al. 2006), and extrinsic factors, including ephrins (Xu and Henkemeyer 2012) and neurotrophins (Bosco and Linden 1999; Lom and Cohen-Cory 1999).

Regulation of cytoskeleton dynamics is controlled by cyclic nucleotides and proteins affecting the equilibrium between actin polymerisation and actin depolymerisation. Rho GTPases and Ca^{2+} currents play a role in regulation of actin dynamics, therefore regulation of these affects dendrite and axon growth (Shi and Ethell 2006). One protein downstream of Rho GTPases is LIM domain kinase 1, which phosphorylates cofilin, causing actin polymerisation. LIM domain kinase 1 activity is important for RGC axon outgrowth and is expressed in Xenopus RGCs at the time of axon extension (Hocking et al. 2009). Actin remodelling is important to enable synaptic plasticity, which is essential in the cortex for information processing (Meng et al. 2004).

Integrin-extracellular matrix (ECM) interactions are also important in synaptogenesis and modulation of dendrites and axons. This is thought to be achieved through integrin interaction with N-methyl-D-aspartate (NMDA) receptors in hippocampal neurons. In these neurons dendrite length and branching is modulated by activation of CaMKII by increases in Ca^{2+} concentration within dendritic spines (Shi and Ethell 2006). Cadherin-integrin interaction may play an integral role in dendrite development. Experiments in Drosophila and Xenopus suggest that type I cadherins and β1 integrins are required for dendrite extension, and N-cadherin inhibits dendritic branching (Marrs et al. 2006).

Semaphorins are a class of guidance cues that bind to their receptors neuropilins and plexins (Nakamura et al. 2000). The class 3 semaphorin Sema3A stimulates dendrite growth and branching (Fenstermaker et al. 2004) by increasing focal adhesion kinase phosphorylation at sites Y397 and Y576/577, however this is dependent on simultaneous β1 integrin activation. Sema3A signalling also increases cGMP production in neurons (axons and dendrites) (Polleux et al. 2000; Schlomann et al. 2009). Sema3A causes integrin inhibition in axons and as a result has a repulsive effect on axon growth and causes growth cone collapse (Luo et al. 1993; Nakamura et al. 2000; He et al. 2002; Judas et al. 2003). These opposing effects of Sema3A in dendrites and axons is indicative of bidirectional signalling between semaphorins and integrins (Schlomann et al. 2009), and the differences may be due to cGMP signalling downstream of the receptors (Nakamura et al. 2000).

1.3.3 Synaptic formation and remodelling

Throughout development of the central nervous system (CNS) dendritic spines and axons undergo stages of growth and retraction. Dendritic spine stability is essential for synaptogenesis since both pre- and post-synaptic partners need to be present for long enough for a synapse to form (Bourne and Harris 2008). Changes to dendrites and synapses occur in parallel during CNS development and in the adult to facilitate plasticity in the brain (Calverley and Jones 1990; Titus et al. 2007). Dendritic and synaptic remodelling has been observed in neurons in the hippocampus (Fischer et al. 1998; Dunaevsky et al. 1999), frontal and prefrontal cortex (Huttenlocher 1979; Elston et al. 2009; Petanjek et al. 2011), cat visual cortex (Cragg 1975), and rabbit auditory cortex (Rihn and Claiborne 1990). In the developing retina glutamate signalling is important for the regulation of the final dendritic structure and synaptic contacts of RGCs (Bodnarenko & Chalupa 1993). Glutamate released by bipolar cells in a spontaneous fashion before eye opening (Wong 1999) and as a result of light stimulation after eye opening causes increased calcium signalling following activation of the RGC glutamate receptors (Xu & Tian 2007). The resultant increased stability of dendrites and synapses may be due to increased brain-derived neurotrophic factor (BDNF) signalling (Landi et al. 2007), which regulates dendritic and synaptic structure and function in an activity-dependent manner (see 1.6 Neurotrophin signalling).

In addition to development it has been postulated that dendritic and synaptic changes are important in memory and learning (De Roo et al. 2008; Woronowicz et al. 2010). In particular, the size of dendritic spines is an important factor in calcium signalling in Purkinje cells during memory formation (Matsuzaki 2007). Dendritic remodelling in the hippocampus and amygdala is also involved in stress response (Watanabe et al. 1992; Magarinos and McEwen 1995; Vyas et al. 2002).

Importantly, although the retina is often considered an extension of the CNS (London et al. 2013) there is limited plasticity in adult RGCs. At the end of the critical period, an inhibitory mesh-like structure, termed the perineuronal net (PNN) (see 1.7.1), is laid down in the visual cortex to stabilise the

synapses formed during development (Guimaraes et al. 1990; Pizzorusso et al. 2002). The PNN can be considered a specialised form of extracellular matrix and is predominantly comprised of chondroitin sulphate proteoglycans (CSPGs), which are highly negatively charged. PNN components are secreted by neurons and glial cells and the net-like structure is laid down around the soma and proximal dendrites of neurons. It is interesting to note that the secretion of PNN components is regulated by neuronal activity; inhibition of sodium channels inhibits the formation of the PNN (Reimers et al. 2007). The PNN has been evidenced to play important roles in neuronal protection, by acting as an ion buffering system, as well as the modulation of synaptic activity, by restricting the lateral diffusion of AMPA receptors (Frischknecht et al. 2009). Stabilisation of synapses in this way restricts neuronal plasticity, which has been demonstrated in several areas of the CNS, including the mouse barrel cortex (Nowicka et al. 2009) and amygdala (Gogolla et al. 2009). In addition, ON RGC-bipolar synapses may be stabilised by light-induced inhibition of AMPA receptor cycling (Xia et al. 2007). The timing of the critical period in the visual cortex may be modulated by brain-derived neurotrophic factor (BDNF) (Huang et al. 1999).

1.3.4 Dendritic arbor tiling of the retina

During the process of dendrite outgrowth, contact inhibition occurs between dendrites of the same cell/cell type, creating a mosaic of dendritic arbors across the retina. The dendritic fields (DFs) of RGCs partially overlap with the DFs of amacrine and bipolar cells. This allows both excitatory and inhibitory input to control the receptive fields (RFs), and therefore the basics of spatial detection (Barlow and Levick 1965; Torre and Poggio 1978). RGC RFs and DFs are approximately equal in size, although directionally selective RGCs show a slight shift in RF (<30%) relative to the DF, towards the null direction, allowing spatial information to be provided (Yang and Masland 1994). Further information is provided by virtue of the fact that within RGC RFs areas of high activity exist. Both of these features of RFs may be controlled by the specific morphology of each dendritic tree (Amthor et al. 1984; Brown

et al. 2000). In addition to spatial information, dendritic tiling of the retina permits maximum sensitivity to light, and means that there is little redundancy in the system (Han et al. 2012).

1.3.5 Cell surface antigens

Cells membranes contain a wide array of proteins. Cell sub-types can be defined by the specific collection of cell surface antigens they display. This is often useful to define as it allows, for example, the monitoring of the health of a sub-type of neuron that may be of interest under a given disease state, which may allow predictions in terms of disease mechanisms or therapeutic targets. Examples of some retinal cell-specific antigens are outlined in this section.

Thy-1 is a membrane glycoprotein that binds ECM components, such as laminin (Liesi et al. 1990). Thy-1 is present on the cell membrane of many cell types, including lymphocytes (Aoki et al. 1969; Owen and Raff 1970) and RGCs (Barnstable and Drager 1984). Whilst Thy-1 is one of the most widely used RGC markers, it is by no means ideal; 30% of Thy-1 expression in the retina is on the membranes of cells which are not RGCs (Perry et al. 1984), and Thy-1 does not allow targeting of sub-types of RGCs. Further, it has been found that following optic nerve damage, Thy-1 may be downregulated (Nash and Osborne 1999; Schlamp et al. 2001; Huang et al. 2006) or upregulated (Lee et al. 1998; Astafurov et al. 2014). Thy-1 is upregulated in other cells in the retina, including Müller cells (Dabin and Barnstable 1995). This may mark an important ECM remodelling step in the damaged retina. Since amacrine cells express Thy-1 receptors (Dreyer et al. 1995), changes in Thy-1 expression may permit amacrine-Müller cell interactions.

Brn3 is a transcription factor that has roles in axon guidance and cell survival (Gan et al. 1999; Wang et al. 2000; Badea et al. 2009). In the mouse approximately 70% of RGCs express Brn3b (Erkman et al. 1996; Gan et al. 1996), and in the rat 70% of RGCs express at least 2 of Brn3a, Brn3b and Brn3c (Nadal-Nicolas et al. 2012). Brn3b is commonly used as an RGC-specific marker, for example in the study using yellow fluorescent protein-tagged channel rhodopsin molecules expressed downstream of Thy-1 (Zhang et al. 2012). However, as with Thy-1, Brn3 does not allow sub-type targeting.

There are several bipolar cell markers, including *Bhlhb4* (Bramblett et al. 2004), *Irx5* (Cheng et al. 2005) and *Gli5* (Blackshaw et al. 2004). Recently *Grm6*, the promoter for the gene encoding mGluR6 (required for ON-bipolar cell response to glutamate released from photoreceptor cells (Nawy and Jahr 1990; Shiells and Falk 1990, 1992; Nomura et al. 1994; Nawy 1999)), has been found to stimulate the expression of genes that result in the translation of proteins found in ON-bipolar cells (Dhingra et al. 2008). This presents exciting prospects of sophisticated visual circuitry control.

1.4 Aberrant dendritic morphology in ageing and disease

Retinal degeneration is one of the leading causes of blindness in the world today (Quigley 1996; Congdon et al. 2004; Quigley and Broman 2006). Age-related macular degeneration (AMD) commonly involves the deposition of drusen and degeneration of retinal pigment epithelium (RPE), leading to photoreceptor damage (Green et al. 1985; Coleman et al. 2008). AMD is often associated with increased oxidative damage and the presence of splice variants of Complement factor H. These splice variants, for example the Y402H mutation, increase the activity of the complement pathway and are linked to increased likelihood of AMD development (Rutar et al. 2012).

Glaucoma is an umbrella term for a group of diseases associated with optic nerve damage and RGC degeneration (Quigley et al. 1995). Glaucoma is often associated with, although is not defined by, increased intraocular pressure (IOP) (Quigley et al. 1987; Quigley et al. 1988). Eyes with an IOP of >21 mmHg are classified as glaucomatous (Weber et al. 2008). Current treatments focus on reducing IOP (Peeters et al. 2010), however future therapies should aim to preserve cell function in the GCL and prevent further degeneration since it is the RGC loss which ultimately leads to vision loss (Howell et al. 2007).

Retinitis pigmentosa is associated with degeneration of the photoreceptor layer (Dryja et al. 1990; Hartong et al. 2006). RGCs are still present following photoreceptor death. However, it has been shown that transneuronal degeneration occurs through the neuronal pathway, ultimately resulting in loss of RGCs (although this has been disputed in one mouse model), with evidence of abnormal electrical activity (Stone et al. 1992; Strettoi et al. 2002; Mazzoni et al. 2008; Stasheff 2008). It is postulated, therefore, that although introduction of photosensitive cells or stimulation of resident cells, for example by introduction of photosensitive bacterial proteins via gene therapy (Tomita et al. 2009; Busskamp and Roska 2011; Deisseroth 2011), can still result in RGC action potential firing (Margolis et al. 2008; Jensen and Rizzo 2009), neuroprotective agents must be given in combination to prevent secondary degeneration.

1.4.1 Dendritic changes

During normal development of the nervous system, neuronal degradation and dendrite retraction occurs. Dendritic pruning is an important process in ensuring correct neuronal networks are created. Mice lacking caspase-3 have an abnormally large number of dendritic spines, implicating caspase-3 in the modulation of dendritic remodelling (Erturk et al. 2014). Indeed, numerous studies have provided evidence for the role of caspases in dendritic pruning in class IV dendritic arborisation sensory neurons in Drosophila melanogaster undergoing morphogenesis (Kuo et al. 2006; Williams et al. 2006). Interestingly, the location of caspases determines the downstream effects; local caspase activation in dendrites causes dendritic pruning, whereas inhibition of the ubiquitin-proteasome machinery permits global caspase activation and results in cell death (Rumpf et al. 2011; Erturk et al. 2014). Other regulatory factors, such as reactive oxygen species or duration of caspase activation, may modulate the downstream effects, i.e. cell death or dendritic remodelling (Snigdha et al. 2012). In addition, it has been demonstrated in mice and Drosophila that a parallel NAD+-dependent pathway may regulate axonal pruning of neurons during development (Schoenmann et al. 2010). Although specific details are yet to be determined, it is likely that the process of dendritic retraction involves destabilisation of the cytoskeleton, fragmentation and finally removal of debris by glial cells/macrophages (Hyman & Yuan 2012).

Downstream signalling of the excitatory neurotransmitter glutamate has been shown to increase the rate of dendritic pruning (Andres et al. 2008). Since retinal degeneration is associated with reactive gliosis, which involves excessive glutamate signalling and activation of inflammatory pathways, it would be logical to predict that retinal degeneration could be associated with dendritic pruning. Further, it has been postulated that the degree of pruning could be indicative of the level of degeneration within the retina since it seems likely that the reduction of dendritic branching occurs before the onset of RGC death (Morquette and Di Polo 2008).

Morphological remodelling has been demonstrated in a range of disease/injury models affecting the CNS. Firstly, Alzheimer's disease models show dendritic pruning of pyramidal neurons and reduced complexity of glial cells in the hippocampus and entorhinal cortex (Beauquis et al. 2013; Williams et al. 2013b), as well as atrophy of astrocyte processes in amyloid cores (Nagele et al. 2004). Secondly, neuroblastoma dendritic atrophy is one of the morphological changes demonstrated in models of prion diseases, including Creutzfeldt-Jakob disease (Ishikura et al. 2005). Thirdly, structural changes in dendrites and synapses of motor neurons have been noted in models of spinal cord injury (Bannerman et al. 2005; Macias 2008). Finally, there is evidence for neuronal remodelling in retinal degeneration (Jones and Marc 2005). In particular, dendritic pruning in RGCs has been suggested to occur prior to cell death in glaucoma (Weber et al. 1998). Rett syndrome is associated with alterations in the MECP2 gene in patients (Amir et al. 1999) and knockout or mutation of *mecp2* produces a mouse model of the disorder (Chen et al. 2001; Guy et al. 2001). MECP2 is a protein involved in the maintenance of the structural integrity of neuronal circuits (Dani and Nelson 2009; Na et al. 2013), as well as the protection of neurons from oxidative stress (De Felice et al. 2014).

Reduction in DF size and dendritic pruning has been shown to occur in cat, rat, and primate models of glaucoma before the cell is committed to the fate of apoptosis (Morgan 2002; Shou et al. 2003; Kisiswa et al. 2010a; Morgan 2012). Dendritic pruning could therefore provide an invaluable early read-out of cell health and illuminate the therapeutic window in which to prevent the onset of apoptosis in order to maintain some vision in patients.

1.4.2 Oxidative damage

In ageing cells, mitochondrial electron transport becomes less efficient, resulting in an accumulation of reactive oxygen species (ROS) (Harman 1981; Liang and Godley 2003). ROS increase apoptosis, stimulate vascular endothelial growth factor-mediated angiogenesis through upregulation of hypoxia inducible factor, and causes degeneration of membrane lipids, especially those in outer segments of photoreceptors (Cano et al. 1986). Oxidative damage is also stimulated by white light and results in

activation of the complement pathway, including upregulation of complement 3 (Maller et al. 2007; Yates et al. 2007). Increased activity of the complement pathway aids in breaking down apoptotic cells, however dysregulated activity may contribute to tissue degeneration.

High ROS levels activate secretion of matrix metalloproteases (MMPs), which break down ECM proteins, causing remodelling. Remodelling affects cell survival, for example gliosis-mediated upregulation of MMP-9 reduces RGC survival and migration (Santos et al. 2012). Similarly, in retinal degeneration the structure of the outer limiting membrane (OLM) is changed to localise damage by restricting cell migration. Cell replacement therapies rely on the ability of inserted cells to migrate to their target. For these therapies it has been found that integration efficiency can be increased by manipulating ECM remodelling, for example by the addition of MMP-2, and compromising the integrity of the OLM (Zhang et al. 2007; Barber et al. 2012).

1.4.3 Neuroprotection

RGC death is the final step in most cases of retinal degeneration, and since they are the cells that transmit the retinal output to the brain, if this step can be prevented some visual function may be preserved. One mechanism contributing to RGC apoptosis in glaucoma is postulated to be blockage of axonal retrograde transport of growth factors to the soma (Quigley 1995), which may lead to cell stress. Since autophagy is upregulated by oxidative stress and excitotoxicity, and under high stress conditions may stimulate cell death, this may be implicated in glaucoma. On the other hand, downregulation of autophagy in the Atg4B$^{-/-}$ mouse model is combined with reduced RGC survival (Caprioli et al. 1996; Zhu et al. 2005; White et al. 2009; Rodriguez-Muela et al. 2012), therefore further study of the mechanisms linking cell stress and neuronal death are required.

It has been proposed that a more achievable method to manage retinal degenerative diseases may be to provide neuroprotection to the existing healthy cells (Morquette and Di Polo 2008; Bull et al. 2011; Johnson et al. 2011). This protection could come from the addition of growth factors, such as ciliary neurotrophic factor (CNTF) or BDNF, inhibition of glutamate receptor activation, or addition of factors

to inhibit apoptosis (Morquette and Di Polo 2008). The evidence for this approach in the literature is mixed. CNTF reduces photoreceptor death in patients with retinal degeneration (Tibbetts et al. 2012), but in a clinical trial with sustained release of CNTF there was no effect on visual acuity or visual field sensitivity (Talcott et al. 2011). Neuroprotection, in theory, should retard disease progression by maintaining the connections between healthy cells and reducing gliosis, thereby preserving visual acuity. It should be noted that this method can only prevent further deterioration of vision, whereas successful transplantation of neurons has the potential to improve vision, therefore ideally the two approaches would be combined. On the other hand, application of an agent capable of stimulating regrowth of neurons could re-wire the damaged neuronal network and restore visual function (Morgan 2012).

1.5 Neurotrophin signalling

Growth factors are small proteins that act to regulate cell processes in every tissue in the body via intracellular signalling pathways or by binding to plasma membrane receptors. Neurotrophic factors are generally, although not exclusively, expressed in the nervous system (Levi-Montalcini et al. 1996). Neurotrophic factors consist of 3 main groups of growth factors: glial cell-line derived neurotrophic factor family ligands, e.g. glial cell-line derived neurotrophic factor; neuropoietic cytokines, e.g. CNTF; and neurotrophins. The term 'neurotrophin' specifically refers to the 4 proteins nerve growth factor (NGF), BDNF, neurotrophin-3 (NT-3) and NT-4, which share 55% sequence identity for amino acids (Suter et al. 1992) and most have low affinity for the p75 neurotrophin receptor (NTR). Neurotrophins exert their primary downstream effects via binding to tropomyosin receptor kinase (Trk) receptors (Table 1.2). Neurotrophins have essential roles during development and adult homeostasis of the nervous system, particularly with respect to cell survival, differentiation, synaptogenesis and long-term potentiation.

Table 1.2. Summary of neurotrophins and their respective affinities for neurotrophin receptors (Dechant et al. 1997; Chao 2003). The relative affinities are important when considering interplay between Trk and p75^{NTR} signalling (see text for explanation).

Neurotrophin	High affinity receptor	Low affinity receptor(s)
NGF	TrkA	P75^{NTR}
BDNF	TrkB	P75^{NTR}
NT-3	TrkC; p75^{NTR}	TrkA; TrkB
NT-4	TrkB	P75^{NTR}

1.5.1 BDNF gene expression and regulation

BDNF was first isolated from porcine brain in 1982 (Barde et al. 1982). The *bdnf* gene is encoded on chromosome 11p13. In the murine retina expression of mRNA and protein of both BDNF and its candidate receptor, TrkB, is predominantly seen in RGCs (Gao et al. 1997; Bennett et al. 1999), as well as displaced amacrine cells (Cellerino & Kohler 1997; Vecino et al. 2002). Although mRNA expression of the low affinity receptor, p75^{NTR}, is seen in RGCs (Suzuki et al. 1998), at the protein level it has only been observed in Muller cells, with no detectable levels in RGCs in the adult murine retina (Hu et al. 1999).

In the rodent, *bdnf* contains one 3' protein-coding exon (exon IX) and nine 5' non-coding exons (Aid et al. 2007), each containing separate promoter sites, which, in combination with multiple splice sites and polyadenylation sites, can result in the formation of 18 different mRNA transcripts, all of which are ultimately translated into the same protein (Greenberg 2010). It has been postulated that BDNF gene expression has so many points of regulation because BDNF signalling is so important in neuronal structure, function and survival, therefore it is imperative that BDNF levels are able to be modulated downstream of multiple cell signalling cascades. For example, transcripts that include exon IV are associated with dendritic localisation, whereas exon III transcripts are associated with localisation within the soma (Pattabiraman et al. 2005). Post-transcriptional modifications offer another level of control. *Bdnf* transcripts are polyadenlyated at 2 sites, resulting in a 3' untranslated region (UTR). The length of the UTR appears to be important for localisation of the transcript; in the hippocampus short UTRs restrict the transcript to the soma, whereas long UTRs promote transport to dendrites (An et al. 2008).

Expression of *bdnf* is sensitive to cell signalling and neuronal activity due to the presence of 3 calcium response elements (CaRE1-3) upstream of the promoter (Tao et al. 1998; Zheng et al. 2012). Increased intracellular calcium levels results in increased recruitment of nuclear binding proteins binding to CaREs via calcium-dependent kinases and phosphatases (Schuh et al. 2004), resulting in an increase in

the rate of transcription of exon IV (Figure 1.3). Intracellular calcium concentration can be increased through membrane recruitment of phospholipase Cγ (PLCγ), which results in efflux of calcium from calcium stores via binding of inositol 1,4,5-trisphosphate to inositol 1,4,5-trisphosphate receptors. Calcium influx into the cytosol is also increased through voltage-gated calcium channels following membrane depolarisation.
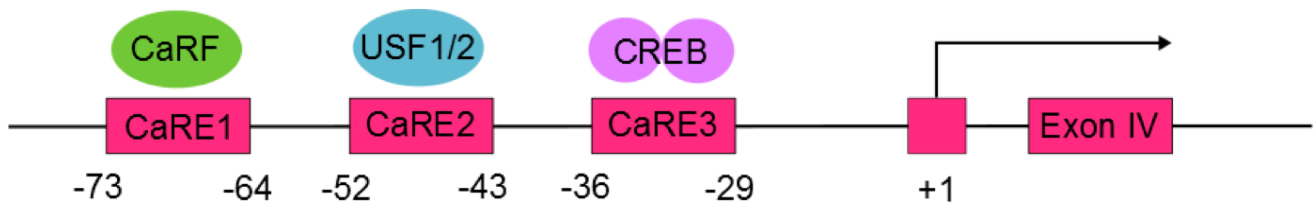
Figure 1.3 Calcium response elements regulate transcription of *bdnf* exon IV in response to calcium. CaRE1 is bound by calcium responsive factor (CaRF) in response to calcium levels via signalling cascades including protein kinase A and PI3K. CaRE2 is bound by upstream stimulatory factor 1/2 (USF1/2), a basic helix-loop-helix member. CaRE3 is bound by cAMP response element binding protein (CREB) in response to calcium levels via voltage-gated calcium channels and NMDA receptors. The positions of each CaRE is shown relative to the initiation site. Figure modified from Zheng et al. 2012.

Epigenetic regulation of *bdnf* is another level of control that is linked to altered expression of *bdnf* in relation to neuronal activity and disease. Exon IV contains a CpG island – these are reported to be important sites for the epigenetic regulation of genes. This CpG island is demethylated by activation-induced cytidine deaminase (Ratnu et al. 2014) following upregulation of the CaMK pathway through either TrkB activation or membrane depolarisation. Neuronal activity is also associated with decreased binding of MeCP2 (binds methylated DNA) and increased binding of CREB, both of which have specific binding sites on exon IV. These binding profiles are associated with increased transcription levels of *bdnf* (Martinowich et al. 2003; Boulle et al. 2012; Karpova 2014). Downregulation of BDNF in Schizophrenia and bipolar disorder is correlated with overexpression of DNA methyltransferase1 (DNMT1), which binds to the *bdnf* promoter on exon IX in glutamatergic neurons of the prefrontal cortex, and seems to be independent of a methylation mechanism (Dong et al. 2014).

1.5.2 P75^{NTR} receptor signalling

P75^{NTR} is a member of the tumour necrosis factor receptor family and as such is capable of activating downstream signalling pathways, predominantly c-JUN N-terminal kinase (JNK), NF-kappaB and RhoA (Carter et al. 1996; Yamashita et al. 1999; Friedman 2000; Harrington et al. 2002). These pathways are associated with apoptosis induction, long-term depression, neurite retraction and synapse loss (Bamji et al. 1998; Frade and Barde 1999; Woo et al. 2005; Zagrebelsky et al. 2005; Yang et al. 2009). P75^{NTR} forms a dimer, linked through a disulphide bond at cys257, which is essential for neurotrophin-mediated p75^{NTR} signalling (Vilar et al. 2009). It has been proposed that neurotrophin binding to the extracellular domain causes separation of the death domains inside the cell, thus permitting binding of adapter proteins to the death domains (Vilar et al. 2009). These adapter proteins are associated with cell death and modulation of neurite retraction (Friedman 2000).

Downstream signalling of p75^{NTR} is not activated in the absence of neurotrophin binding. Apoptosis may be mediated through NGF binding to p75^{NTR}, which facilitates binding of the adapter protein p75^{NTR}-associated death executor to the death domain of p75^{NTR} (Mukai et al. 2000). Knock-out of

either p75^{NTR} or NGF results in an approximately 50% reduction in cell death in retinae and spinal cord

of E15.5 mice (Frade and Barde 1999). During development, NGF-p75^{NTR} signalling promotes cell death

in cells that do not express TrkA (Dechant and Barde 1997). These studies provide strong evidence for

the role of p75^{NTR} signalling in apoptosis.

It should be noted that p75^{NTR} signalling also has positive roles. During development p75^{NTR} is strongly

expressed by neurons, particularly in neurons with long-spanning axons, such as spinal motor neurons,

and neurons with dense dendritic arbors, such as RGCs. In the absence of neurotrophin, RhoA, a small

GTPase, binds to amino acids 331-416 in the death domain of p75^{NTR} (Roux and Barker 2002) and

inhibits neurite outgrowth. However, following neurotrophin binding to p75^{NTR} RhoA is not activated

(Yamashita et al. 1999), which may explain the expression pattern of p75^{NTR} in developing neurons. In

the adult p75^{NTR} is reduced in these neurons (Yan and Johnson 1988). Following axonal injury p75^{NTR}

expression is upregulated in a range of neuronal populations (Ibanez and Simi 2012) and is

subsequently restored to normal levels following axonal re-growth (Ernfors et al. 1989).

1.5.3 Trk receptor signalling

Neurotrophins elicit their primary effect by binding to one of the 3 structurally related receptors TrkA,

TrkB and TrkC. BDNF and NT-4 bind to TrkB with picomolar affinity, while NT-3 binds with nanomolar

affinity. BDNF and NT-4 form a salt bridge with TrkB, but NGF does not form a salt bridge with TrkA,

which may explain the relative binding affinities (Banfield et al. 2001; Naylor et al. 2002). Upon ligand

binding, the Trk receptors dimerise and are autophosphorylated at up to 3 Tyr residues; Tyr670, Tyr

674 and Tyr675 in TrkA (Middlemas et al. 1994). Tyr phosphorylation recruits scaffold proteins, such

as PLC and phosphatidylinositol 3-kinase (PI3K) and MAPK to the membrane (Minichiello et al. 2002;

Schratt et al. 2004). Resultant downstream signalling leads to cell survival, neurite outgrowth, synapse

formation and strengthening, and long-term potentiation (Korte et al. 1995; Xu et al. 2000; Yacoubian

and Lo 2000). Following receptor dimerisation, TrkB is internalised by clathrin-mediated endocytosis,

which is a key step in continuation of the signal. TrkB and p75[NTR] signalling pathways are summarised in Figure 1.4.

Neurotrophin signalling can have opposing downstream effects. While this may seem nonsensical, one key factor that ultimately determines the final outcome (cell death or survival) is the relative affinities for each receptor. As outlined in Table 1.1, with the exception of NT-3, mature neurotrophins have higher affinity for the 'positive' Trk receptors than for the 'negative' p75[NTR]. For the unprocessed, pro-neurotrophins the reverse affinity pattern exists (Rodriguez-Tebar et al. 1990; Lee et al. 2001). This means that processes like apoptosis can be subtly modulated on a temporal scale by the ratio of pro-neurotrophins and mature neurotrophins, which may be modulated through neurotrophin processing or secretion, as well as the relative expression/membrane recruitment of each neurotrophin receptor.
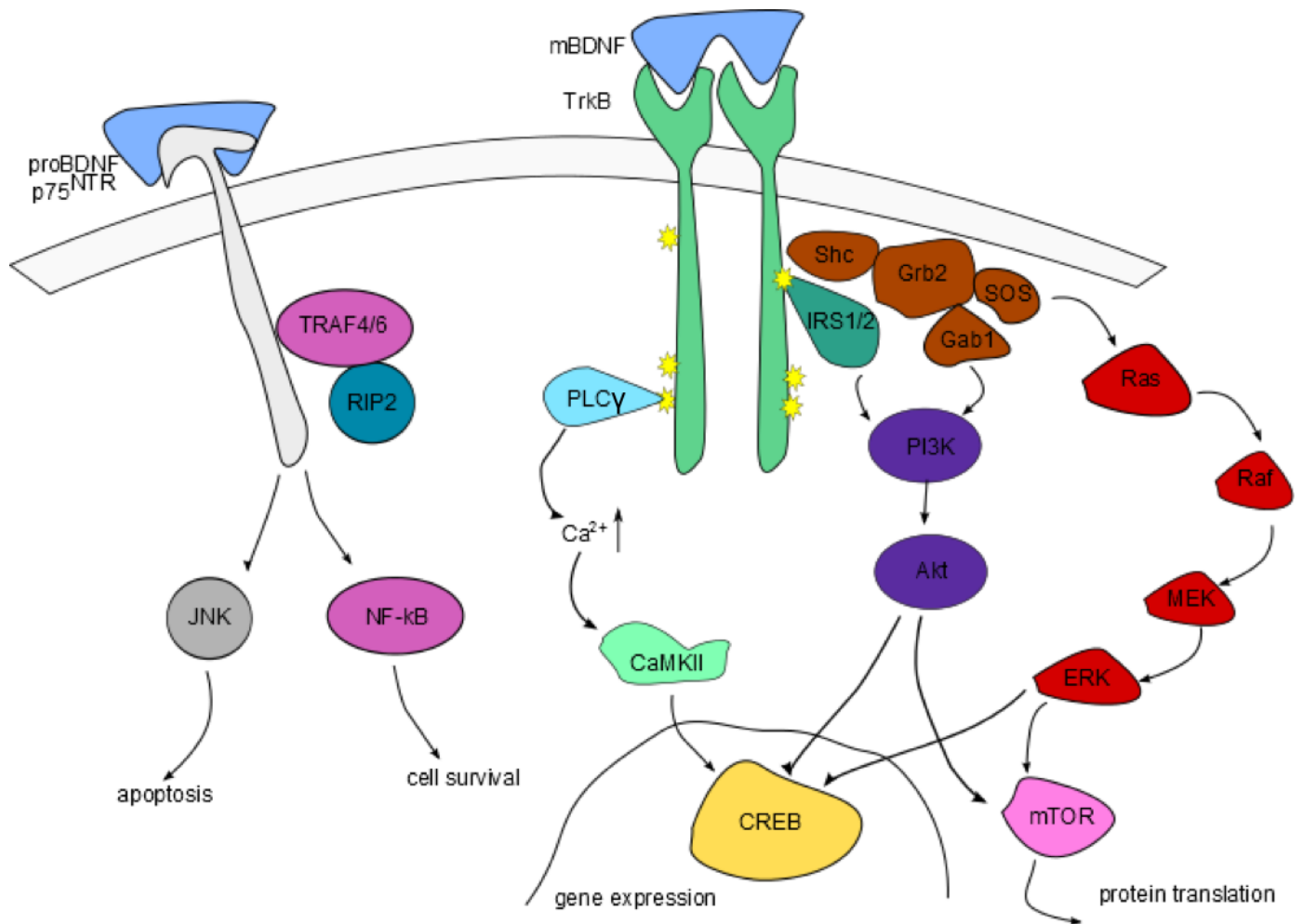
Figure 1.4 Summary of signalling cascades downstream of p75[NTR] and TrkB receptors via ligand binding. Pro-BDNF binds p75[NTR] and mature BDNF (mBDNF) binds TrkB. Pro-BDNF binding to p75[NTR] recruits sortilin and results in downstream JNK signalling, leading to cell death. Mature BDNF can bind to p75[NTR] and may inhibit downstream TrkB signalling through JNK and RhoA (not shown), or may strengthen BDNF binding to TrkB, increase MAPK and Akt signalling, and promote cell survival through NF-kB. Mature BDNF binds TrkB and stimulates downstream signalling of PLCγ, Akt and MAPK, leading to cell survival, neurite outgrowth, as well as increased BDNF transcription through upregulation of CREB (Longo and Massa 2013).

The Trk receptor family is another group of proteins that p75^{NTR} can interact with. Interaction of Trk receptors with p75 may increase the affinity of the Trk receptor for the ligand, and therefore strengthen downstream signalling (Benedetti et al. 1993; Bibel et al. 1999). Indeed, sensory deficits are observed in animals with a mutated NGF, which is able to bind TrkA but not p75 (Horton et al. 1997; Ryden et al. 1997), or with a mutated p75 (Lee et al. 1992; Lee et al. 1994). TrkA and TrkC are localised in lipid rafts, along with the enzyme γ-secretase. In the absence of ligand (NGF/NT-3) TrkA/C associates with p75 ^{NTR} within the lipid raft, allowing γ-secretase to cleave the intracellular death domain of p75 ^{NTR} and activate apoptosis signalling via stimulation of cytochrome c release from mitochondria. In the presence of ligand TrkA/C dimerise, permitting recruitment of scaffold proteins: Shc recruitment to Tyr490 stimulates the Ras pathway; PLCγ recruitment to Tyr785 stimulates the PKC pathway; and PI3K recruitment to Tyr751 stimulates the Akt pathway. Ras and PKC pathways are associated with neurite outgrowth and differentiation, while the Akt pathway suppresses apoptosis and promotes cell survival. In this way, TrkA and TrkC are 'dependence' receptors, that is they depend on the presence of their ligand in order for them not to induce programmed cell death (Dekkers et al. 2013).

TrkB, which contains a structurally different transmembrane domain to TrkA/C, is localised in the lipid bilayer. In the absence of BDNF/NT-4, TrkB associates with p75^{NTR}, however, since γ-secretase is absent in the lipid bilayer, the death domain of p75^{NTR} is not cleaved and therefore apoptosis is not induced. Studies have demonstrated that knocking out BDNF/NT-4 and not TrkB does not result in wide-spread cell death, as seen in similar studies with TrkA/C (Nikoletopoulou et al. 2010). In this way, TrkB is **not** a dependence receptor. Dekkers et al. created a mosaic TrkB receptor that contained the transmembrane domain of TrkA, thereby confining it to lipid rafts, and demonstrated that in the absence of BDNF this mosaic receptor causes cell death (Dekkers et al. 2013). This elegant experiment supports the theory that membrane localisation is key to the downstream effects of these receptors.

1.5.4 BDNF post-translational processing and sorting

In common with other secreted peptides, all neurotrophins are translated as a precursor, or pro-neurotrophin. As outlined above, pro-neurotrophins and mature neurotrophin signalling cascades have largely opposing effects, therefore the relative amounts of precursor versus processed neurotrophin is likely to be a determining factor of whether the end result is pro-apoptotic or pro-survival. Since the ratio can be rapidly modulated by pro-neurotrophin processing, this enables neurotrophin secretion to be rapidly switched on and off – an essential property of molecules that must respond to changes in neuronal activity. In general, precursor proteins are inactive, but pro-neurotrophins are able to stimulate intracellular signalling pathways. Pro-neurotrophins have a higher affinity for $p75^{NTR}$ than Trk receptors, therefore pro-neurotrophin signalling stimulates apoptosis and neurite retraction (Lee et al. 2001).

Mature neurotrophins are generated by proteolytic cleavage of the signal peptide on pro-neurotrophins, followed by dimerization (Heymach and Shooter 1995; Lee et al. 2001). Pro-NGF is processed intracellularly, processed through the constitutive pathway, and secreted as the mature NGF. Pro-BDNF may be cleaved intracellularly or extracellularly. Intracellularly, pro-BDNF is cleaved by furin in the endoplasmic reticulum, or by proconvertases in secretory vesicles (Matsumoto et al. 2008). In non-neuronal cells, such as astrocytes, BDNF is sorted through the constitutive pathway. Neuronal cells use both the constitutive pathway and the regulated pathway in the golgi, which is mediated through the binding of sortilin to the signal peptide of pro-BDNF, or by the binding of CPE to a motif on the mature BDNF section of the protein. The constitutive pathway corresponds to constitutive BDNF release and the regulated pathway corresponds to activity-dependent secretion. The precursor and mature forms of BDNF are released via secretory vesicles into the extracellular milieu, where pro-BDNF can be processed by plasmin (a serine protease; Figure 1.5) or by MMP-3 and MMP-7 (Lee et al. 2001; Pang et al. 2004; Dwivedi 2012). Plasmin is inhibited by the blood-derived protein α-2-macroglobulin, which may reduce BDNF processing as well as directly blocking TrkB

phosphorylation in dopaminergic neurons (Hu and Koo 1998). Processing may be particularly important in the hippocampus, where BDNF is secreted as the precursor protein in response to neuronal activity (Pang et al. 2004).
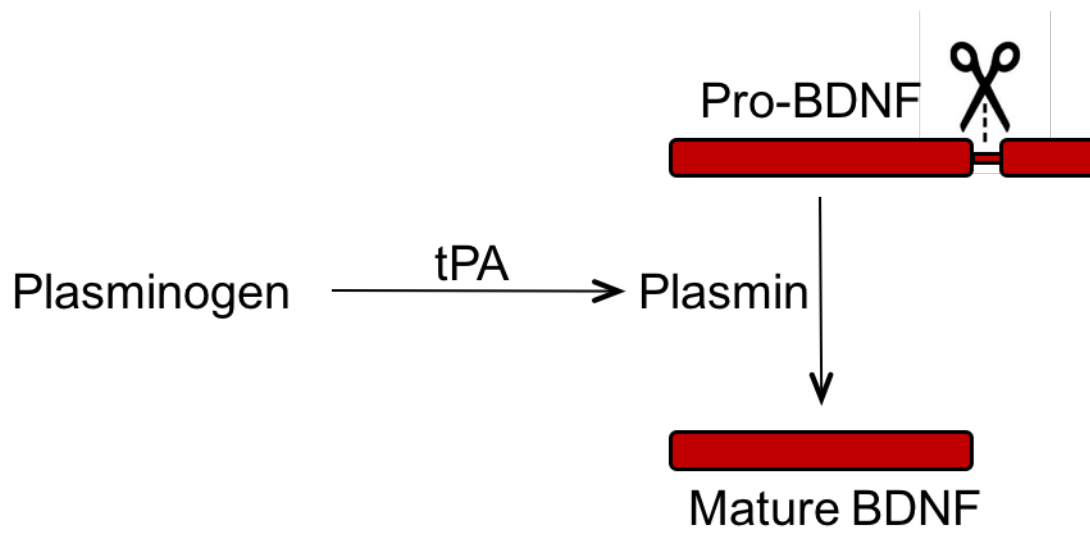
Figure 1.5 Extracellular BDNF processing. Extracellular pro-BDNF is cleaved at Arg-125-Val by plasmin, the activity of which is dependent on tPA (Lee et al. 2001; Gray and Ellis 2008).

1.5.5 BDNF-TrkB signalling and neuronal activity

BDNF-TrkB signalling and neuronal activity are closely linked. BDNF is released pre-synaptically and binds as a dimer to TrkB receptors located on the post-synaptic membrane. BDNF signalling results in formation and stabilisation of synapses through transcriptional changes associated with long-term potentiation (LTP) and dendritic spine growth, in part through regulation of the translation of Homer2, a scaffold protein implicated in dendritic spine function (Schratt et al. 2004), and upregulation of the cytoskeletal protein Arc (Yin et al. 2002). BDNF also increases neurotransmitter release from presynaptic terminals, which, along with stabilisation of synapses, results in an increase in neuronal activity. In turn, neuronal firing causes upregulation of *bdnf* expression via increased calcium influx. Neuronal activity results in an increase in intracellular cAMP. In the hippocampus cAMP regulates BDNF downstream effects by modulating BDNF phosphorylation of TrkB as well as modulating membrane recruitment of TrkB, possibly through strengthening the connection between TrkB and Post-synaptic density 95 (PSD-95) (Ji et al. 2005). PSD-95 is recruited to dendrites through BDNF signalling via the PI3K-Akt pathway (Yoshii and Constantine-Paton 2007), which, in turn, stimulates the production of more TrkB-PSD-95 complexes through activation of PI3K and PLCγ (Yoshii and Constantine-Paton 2010). Neuronal activity causes increased release of tissue plasminogen activator (tPA), resulting in increased cleavage of pro-BDNF. In this way, BDNF processing and signalling acts as a positive feedback loop. This is important to consider when targeting BDNF signalling, as a change in any part of the loop will feed forward to the rest of the loop.

1.5.6 Retinal levels of neurotrophins and their receptors

In the retina, protein expression of TrkA, TrkB and TrkC is low but widespread, with TrkB expression strongest in RGCs, amacrine cells and Muller cells (Cui et al. 2002; Harada et al. 2011). In the rat, axonal injury results in a 5-fold increase in TrkB protein expression in RGCs (Cui et al. 2002). However, changes to Trk receptor levels likely varies with the type of injury. In the rat TrkB is upregulated following optic nerve injury (Cui et al. 2002), whereas in glaucomatous retinas the mRNA level of TrkB remains

constant (Figure 1.6) (Rudzinski et al. 2004). Although it is interesting to map the transcription profiles of neurotrophins and their receptors post-injury, levels of mRNA do not necessarily equate to levels of protein. Consequently, conclusions cannot be drawn regarding the relative levels of pro-neurotrophins and mature peptides, nor the localisation of the receptors within the retina. When investigating profiles of Trk receptors it is also important to consider their phosphorylation state since protein expression alone is not sufficient to promote Trk signalling. Under glaucomatous stress TrkB may be deactivated (dephosphorylated) through increased interaction with the phophatase Shp-2 via hyperphosphorylation of caveolin (Gupta et al. 2012).
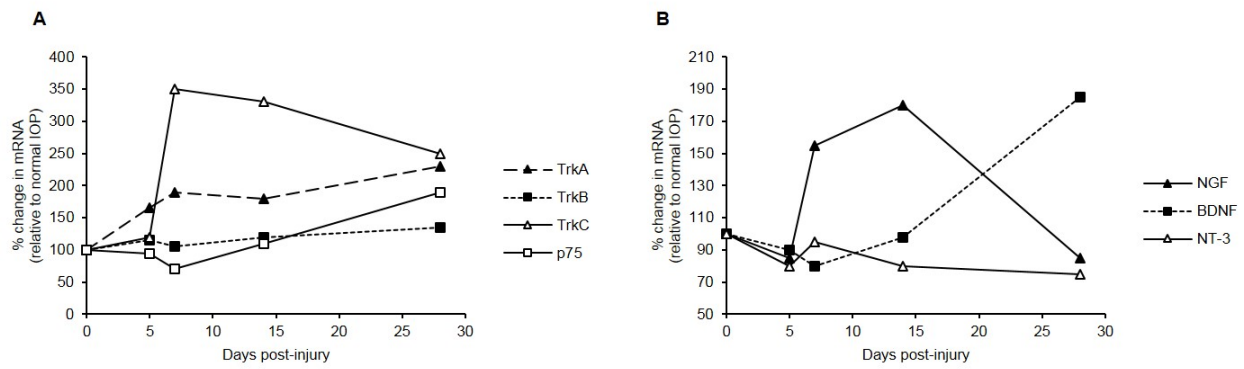
Figure 1.6. Levels of neurotrophins and their receptors in the rat retina. mRNA levels of **(A)** neurotrophin receptors and **(B)** their ligands from whole retinas following injury to induce high IOP. Modified from (Rudzinski et al. 2004).

1.6 Neurotrophin signalling in disease

Given their role in neuronal development and maintenance, it is perhaps not surprising that there have been numerous reports of links between levels of neurotrophins and/or their receptors in injury or disease in the CNS. A PubMed search of "BDNF"+"disease" generates a result of 474 publications in 2015 alone. This section will explore some of these associations.

1.6.1 Alterations in neurotrophin signalling implicated in disease

$P75^{NTR}$ is upregulated following injury (Ernfors et al. 1989; Beattie et al. 2002) and in disease, particularly where neuroinflammation is a component of the disorder, such as Alzheimer's disease (Mufson and Kordower 1992) and multiple sclerosis (Dowling et al. 1999). Levels of proneurotrophins have also been found to be increased in diseases affecting the CNS. Pro-NGF is upregulated in Alzheimer's disease (Fahnestock et al. 2001), and CNS injury (Beattie et al. 2002; Harrington et al. 2004). There is evidence that in depression pro-BDNF and $p75^{NTR}$ are upregulated, whilst mature BDNF and TrkB are downregulated (Zhou et al. 2013).

Reduced expression and protein levels of TrkB and its ligands have been reported in a range of neurological disorders. Rett syndrome patients and the *Mecp2*-null mouse model, have reduced expression of BDNF (Wang et al. 2006; Abuhatzira et al. 2007). Schizophrenia and bipolar disorder are associated with decreased mRNA expression levels of *bdnf* and *trkb* (Weickert et al. 2003; Ray et al. 2014). In Huntington's disease BDNF signalling may be impaired (Baydyuk and Xu 2014). There is evidence that mutations in the gene encoding NT-4 may be a risk factor for primary open-angle glaucoma (Pasutto et al. 2009). In the hippocampus and temporal cortex of Alzheimer's disease patients, the levels of BDNF mRNA and protein are reduced (Phillips et al. 1991; Connor et al. 1997; Fahnestock et al. 2002). The Val66Met polymorphism on codon 66 of the *bdnf* gene is associated with an increased risk of Alzheimer's disease and depression. It has also been reported that the levels of the catalytic form of TrkB are decreased in the temporal and frontal cortex in Alzheimer's disease

(Allen et al. 1999), which is likely to have important implications for TrkB-targeted treatment strategies.

1.6.2 BDNF processing in disease

In many CNS disorders BDNF levels are not notably decreased relative to healthy controls. In the rat prefrontal cortex and hippocampus the normal ratio of pro-BDNF:BDNF is 1:1 (Tang et al. 2014). Because the signalling pathways of the 2 forms of BDNF have opposing effects, it may be that the ratio of these 2 proteins, rather than absolute concentrations, ultimately determines the downstream effect, for example whether the cell will be signalled to survive or to undergo apoptosis. Since this ratio is controlled by how much pro-BDNF is cleaved to form BDNF, there is mounting evidence to suggest that the level of BDNF processing may be a major contributing factor to the pathological state of numerous neurological disorders. Indeed, levels of the tissue inhibitor of MMPs have been reported to be increased in Huntington's disease and Parkinson's disease (Lorenzl et al. 2003). Finally, knockout of tPA accelerates the onset and increases the severity of disease in a mouse model of multiple sclerosis (East et al. 2005).

As previously stated, the Val66Met mutation in the *bdnf* gene is associated with neurological disease. The reduced activity-dependent secretion of BDNF associated with this mutation is presumably the result of steric hindrance caused by the bulky sidechain of methionine at the site that interacts with the binding pocket of sortilin (Egan et al. 2003; Chen et al. 2004). Truncation or siRNA inhibition of sortilin similarly cause missorting of BDNF to the constitutive pathway, resulting in reduced activity-dependent release, but no change to constitutive release (Chen et al. 2005). This demonstrates the importance of sortilin in BDNF processing. Paradoxically, although a decline in activity-dependent BDNF processing is hypothesised to cause reduced plasticity, the presence of the Val66Met polymorphism may enable cognitive processing to override the decelerated plastic motor response. This may explain how the mutation may be beneficial in initial visual adaptation (Barton et al. 2014) as well as in memory-based task switching in elderly subjects (Gajewski et al. 2011).

As discussed, there are multiple proteolytic enzymes involved in BDNF processing, but one of the most attractive enzymes to target is the serine protease, tPA. TPA cleaves the precursor peptide plasminogen to form plasmin, which is then available to process pro-BDNF into BDNF. Reduced plasma levels of tPA and BDNF are associated with depression (Shi et al. 2010), although this study did not distinguish between pro-BDNF and mature BDNF. A recent study found that the anti-depressant effects (increased BDNF, CREB phosphorylation and TrkB phosphorylation) of a VGF-derived peptide were essentially eliminated following block of tPA or TrkB phosphorylation (Lin et al. 2014). Knock-down or overexpression of tPA using lentiviral vectors resulted in significantly reduced or increased levels, respectively, of BDNF in the mouse hippocampus (Bahi and Dreyer 2012). A study by Pang et al. demonstrated that tPA and plasminogen knockout mice have reduced late-LTP in the hippocampus, which can be rescued with mature BDNF, but not uncleavable pro-BDNF. In a report by Scaini et al. administration of branched chain amino acids led to increased pro-BDNF:BDNF, as well as decreased tPA protein level. Since there were no changes in tPA gene expression level, the effects were likely at a protein-level – the authors postulated that the branched chain amino acids generated oxidative stress, which increased expression of plasminogen activator inhibitor-1, an inhibitor of tPA (Scaini et al. 2015). This work provides evidence that oxidative stress, which is commonly generated in a number of neurodegenerative disorders, could reduce levels of tPA, and therefore decrease BDNF.

The studies outlined above provide strong evidence that tPA is one of the most important enzymes involved in BDNF processing when considering pharmaceutical targets. Further, since tPA already has FDA-approval for the treatment of numerous conditions, including ischemic stroke and myocardial infarction (Zivin 2009), this enzyme may have potential as a treatment for a range of neurodegenerative disorders if delivery can be optimised. Alternatively, drugs that increase levels of tPA could be used. Statins may be useful in treatment of depression due to their ability to induce tPA and inhibit plasminogen activator inhibitor-1 (a tPA inhibitor) (Tsai 2007). This research may explain the association between cases of major depressive disorder and cardiovascular disease; lowered levels of tPA could increase the likelihood of both of these disorders (Hou et al. 2009).

Although tPA is able to increase BDNF levels via plasmin activation, the therapeutic effect of increasing

tPA levels may instead be mediated through NMDA receptor activation (Rodier et al. 2014). It has been

proposed that tPA can proteolytically cleave the N-terminus of the NR1 subunit of the NMDA receptor,

which, in turn, increases Ca^{2+} influx through the NMDA receptor (Nicole et al. 2001; Benchenane et al.

2007). The increased intracellular Ca^{2+} levels upregulate BDNF transcription via binding to *bdnf* CREs.

This potential mechanism of action of tPA should be carefully considered when planning the use of

tPA as a therapeutic drug, since overactivation of NMDA receptors could lead to NDMA-induced

excitotoxicity (Traynelis and Lipton 2001). Adverse effects of this include widespread cell death and

seizures.

A number of recent publications have investigated the observed association between physical exercise

and increased BDNF levels (Neeper et al. 1995; van Praag et al. 1999; Adlard et al. 2004). One study

used chronic unpredictable mild stress as a depression model to provide evidence that *bdnf* expression

is decreased with stress. In this model physical exercise (swimming) resulted in a significant increase

in transcription level of *bdnf* in both the stressed and normal groups. The increase in *bdnf* mRNA

correlated with increased transcription levels of the anti-apoptotic protein Bcl-xl with exercise (Jiang

et al. 2014). Further research suggested that the increase in BDNF with exercise may be mediated

through upregulation of *tpa* (Sartori et al. 2011).

Dietary intake of polyunsaturated fatty acids has been shown to increase levels of tPA and BDNF in

the plasma of diabetic rats (Nobukata et al. 2000), and in the hippocampus and prefrontal cortex of a

rat model of depression (Tang et al. 2014). The effect in the hippocampus was enhanced when the

treatment was combined with physical exercise (Wu et al. 2008a). This work may begin to explain the

known beneficial effect of dietary polyunsaturated fatty acids on mental health.

1.6.3 Manipulating neurotrophin signalling as a neuroprotective therapy

BDNF promotes neuronal survival in vitro (Alderson et al. 1990; Cheng and Mattson 1994; Wilkins et

al. 2009). BDNF treatment can preserve the structure of cat RGC dendritic arbors in vivo (Weber and

Harman 2008). Neurite outgrowth is stimulated by BDNF application in cultured neurons (McAllister et al. 1995; McAllister et al. 1996; Bosco and Linden 1999; Baquet et al. 2004; Bonnet et al. 2004) as well as in the guinea pig auditory nerve (Miller et al. 2007). However, BDNF is unsuitable for chronic treatment due to its physical properties: it has a very short half-life ($T_{1/2}$<1 minute); it crosses the blood-brain barrier poorly (Poduslo and Curran 1996); it is pharmacologically 'sticky' (its highly positively charged residues restrict its dispersion) (Lu 2003); and it has some affinity for p75[NTR].

Vector-based delivery of BDNF is a method to provide sustained supply of BDNF to the target tissue (Zhang et al. 2011; Rodger et al. 2012). One caveat with this approach, however, is that the BDNF processing enzymes could become saturated, potentially resulting in a large supply of pro-BDNF. As outlined above, pro-BDNF signalling is not desirable in the context of ameliorating neurodegeneration, and may in fact worsen the condition.

BDNF mimetics are small molecules designed to bind to the active site of TrkB that BDNF binds to in order to stimulate downstream signalling events (Bai et al. 2010). Mimetics are typically modelled on the binding domain of BDNF but with subtle alterations to improve binding efficiency (T_{ON}), decrease unbinding efficiency (T_{OFF}), improve blood brain barrier crossing (by making the molecule more lipophilic or creating a caging structure), or decrease degradation time ($T_{1/2}$). Mimetics may also be able to better target desired signalling pathways by being designed to have poorer efficiency for p75[NTR], whilst maintaining high efficiency for TrkB (Qian et al. 2006; Bai et al. 2010; Massa et al. 2010; Brahimi et al. 2014; Liu et al. 2016). Mimetics have already been shown to have at least the same neuroprotection efficacy, with respect to neuronal survival, as BDNF in the hippocampus and striatum (Massa et al. 2010). The TrkB agonist, LM22A-4, has been shown to restore wildtype levels of TrkB phosphorylation in the medulla and pons in a mouse model of Rett syndrome (Schmid et al. 2012). Finally, TrkB agonists have been evidenced to increase RGC survival in models of glaucoma (Bai et al. 2010).

1.7 Extracellular matrix manipulation

1.7.1 Perineuronal net structure

The PNN, first described by Camillo Golgi in 1873, is a specialised form of ECM that contacts the surface of neurons around the soma and proximal dendrites (Golgi 1873). The PNN is primarily composed of chondroitin sulphate proteoglycans (CSPGs), keratin sulphate proteoglycans, tenascin, and the scaffolding molecule hyluronan. Importantly, the PNN is not a homogeneous structure; the types and ratios of components are specific to each region of the CNS (Virgintino et al. 2009), indicative of region-specific roles of the PNN (Mouw et al. 2014).

The PNN is laid down during development at the end of the critical period following secretion of cartilage link protein Crtl1 (Carulli et al. 2010) and acts to stabilise neuronal networks and synaptic connections (Guimaraes et al. 1990; Pizzorusso et al. 2002). This is achieved partly through CSPGs (e.g. neurocan) and keratin sulphate proteoglycans, which act as physical barriers to synaptic contacts or inhibit axonal outgrowth via negatively charged elements (Wang and Fawcett 2012). Before the PNN is present, neuronal networks are incredibly plastic and experiments, such as monocular deprivation, can have dramatic effects on the re-wiring of the visual processing pathway (Gordon and Stryker 1996). Such changes occurring after the PNN has been laid down, however, do not result in the same rewiring (Sur et al. 1988; Pizzorusso et al. 2002). The PNN has also been reported to contain astrocyte cell (a type of glial cell) processes, intertwined with the ECM components of the net. These astrocytes provide a buffering role by mopping up excess glutamate from the extracellular space, mainly through their Na^+-dependent glutamate transporters (Bruckner et al. 1993; Anderson and Swanson 2000). In addition, the fact that CSPGs are highly charged may allow them to buffer cations. In this way, the PNN may protect neurons, particularly those with high activity levels, from oxidative stress and glutamate-induced excitotoxicity (Morawski et al. 2004). Finally, CSPGs have been found to have binding sites for growth factors, including TGF-beta (Wang et al. 1991) and bFGF (Rapraeger et al.

1991), suggesting that the PNN may play a role in the modulation and localisation of growth factor signalling (Flaumenhaft and Rifkin 1991).

1.7.2 ECM remodelling in injury and disease

Following injury to the CNS or in models of neurodegeneration, including Parkinson's disease and Alzheimer's disease, microglia are activated by lipopolysaccharides and other factors via JNK and p38 MAPK pathways (Dheen et al. 2007). Initially, activated microglia, characterised by their amoeboid shape (Kettenmann et al. 2011), are beneficial as they phagocytose damaged cells and debris. Chronic activation of microglia results in accumulation of pro-apoptotic cytokines and reactive oxygen species, therefore may be detrimental to neurons. Indeed, microglial activation is evidenced to be a major cause of RGC death in retinal degeneration (Yuan and Neufeld 2001). Microglial activation is one of the hallmarks of many neuropathologies (Dheen et al. 2007).

Both types of macroglia in the retina, astrocytes and Muller cells, are also activated following injury or in disease. Astrocytes play important roles in Amyotrophic lateral sclerosis and Alzheimer's disease (Wiese et al. 2012). Activation of macroglia involves the upregulation of glial fibrillary acidic protein, nestin and glutamine synthetase, a key protein in the prevention of glutamate-induced excitotoxicity (Chang et al. 2007). Activated astrocytes secrete matricellular proteins, including glycoproteins, which play roles in synaptic plasticity, remodelling, angiogenesis, as well as recruitment of immune cells. Activated astrocytes are implicated in the maintenance and repair of the blood brain barrier, and ablation of astrocytes can lead to damaging oedema in the brain (Sofroniew 2005). Hevin is secreted by activated astrocytes and is involved in the regulation of pre- and post-synaptic connections (Singh et al. 2016), therefore may help with neuronal re-wiring post-injury. Interestingly, there are multiple combinations of secreted factors from activated astrocytes depending on the specific injury or disease profile, giving each disease its own activated astrocyte 'fingerprint' (Jones and Bouvier 2014). If ECM remodelling is to be a target for neuronal injury and disease it will likely be important to identify the matricellular protein makeup in each case so that treatment can be tailored as appropriate.

Chronically activated astrocytes make up the majority of glial scars, which function as physical barriers around the site of injury to protect nearby cells from inflammation and invading macrophages. Unfortunately, the highly negatively charged CSPG components of the glial scar inhibit axonal outgrowth, which limits the regeneration of native neurons (Ekstrom et al. 1988; Fawcett and Asher 1999; Chua et al. 2013). If the site of damage is small enough, adjacent neurons may be able to re-form connections through a process termed neural remodelling, as demonstrated in the outer retina in retinal degeneration and in the visual cortex (Marc et al. 2003). Although compensation is possible, if scarring is too widespread or number of neurons lost is too large, neural remodelling may not be capable of re-wiring the neuronal network, resulting in loss of function (Hausmann 2003).

In addition to restricting migration, gliosis may increase RGC death by causing scarring around the lamina cribrosa, leading to RGC axonal damage (Howell et al. 2007). Activation of microglia and astrocytes is evidenced to be a major cause of RGC death in glaucoma and other models of retinal degeneration (Tezel et al. 2012; Vecino et al. 2015). The PNN may play a role in the pathology other neurodegenerative disorders, for example in Alzheimer's disease, where PNN components (Karetko and Skangiel-Kramska 2009), such as tenascin-C, are biomarkers for Alzheimer's disease (Hall 2012). CSPGs are upregulated following CNS injury (Morgenstern et al. 2002), including in the degenerating retina (Barber et al. 2012). PNN disregulation may be an underlying cause of epilepsy (McRae and Porter 2012). Digestion of PNN components, specifically brevican, by MMPs ADAMTS1 and 4 may be induced by kainite-induced seizures (Yuan et al. 2002). Indeed it should be noted that the PNN is not a fixed structure; endogenous MMPs continuously remodel ECM components according to neuronal activity and local environmental changes. TPA is upregulated following monocular deprivation (Wiesel and Hubel 1963) and spinal cord injury (Bukhari et al. 2011). It has been postulated that the substrate for tPA is components of the PNN (Mataga et al. 2002). It should also be considered that BDNF may contribute to this plasticity, since tPA is an important enzyme in BDNF processing (see section 1.5.4).

1.7.3 Is the PNN an inhibitor of neuronal plasticity?

Although some areas of the brain do respond to injury by stimulating stem cell differentiation (Magavi et al. 2000) or upregulating neurotrophin receptors (Cui et al. 2002), complete repair following moderate to severe injury is rare. In these cases, therapeutic approaches are required to replace lost neurons, or to stimulate endogenous repair mechanisms. One method is to stimulate the neurite outgrowth of resident neurons. This can be attempted by application of growth factors (Thanos et al. 1989), growth cone stimulation via Sema3a (Fenstermaker et al. 2004), or mechanical elongation (Magdesian et al. 2016). Alternatively, cells could be replaced by stem cell-derived neurons (see stem cell section 1.8). These approaches have shown some success, but the presence of inhibitory CSPGs in the PNN has been theorised to limit the regenerative capacity of neurons, particularly in the case of spinal cord injury (Bukhari et al. 2011). It has therefore been postulated that CSPG remodelling may be required in combination with other therapeutic strategies for complete recovery to occur.

1.7.4 Could PNN digestion permit neuronal regeneration or is it an essential component to protect neurons?

The highly negatively charged elements of glycoproteins present in the PNN and glial scars inhibit the positively charged growth cone of axons, and present an obstacle for synaptic and dendritic remodelling. CSPGs in the PNN and glial scars can be partially digested by the bacterial enzyme chondroitinase (ChABC) (Bradbury et al. 2002). ChABC cleaves chondroitin sulphate glycosaminoglycan (GAG) chains (the main inhibitory components of the molecules) to leave stubs (Figure 1.7) that can be detected by immunohistochemistry (Bradbury et al. 2002; Lin et al. 2008; Orlando et al. 2012).
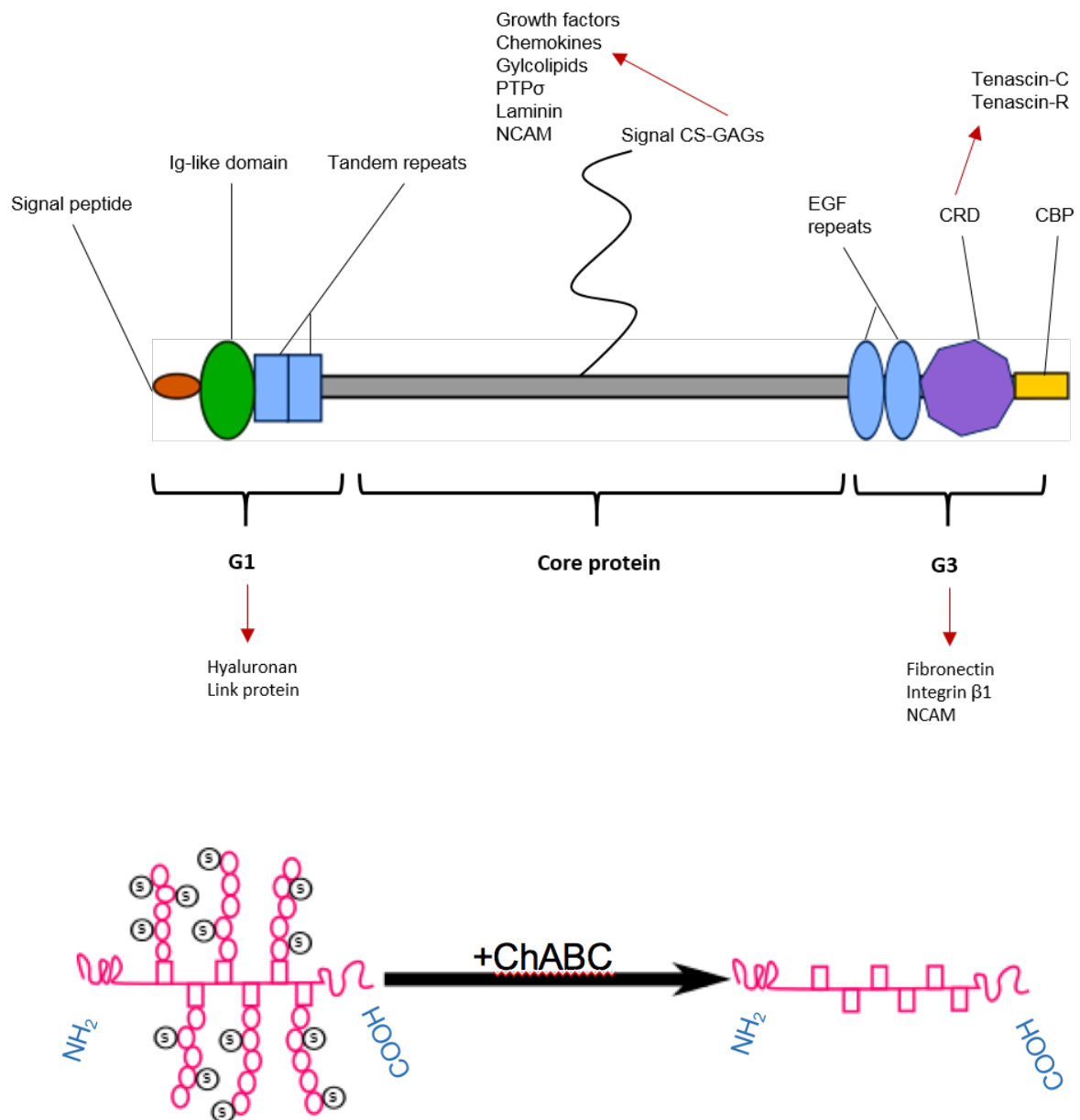
Figure 1.7. Basic structure of CSPG (*top*) with interaction points. Multiple CS-GAGs may be present but only one is shown for clarity. GAGs can be digested using the bacterial enzyme ChABC, leaving epitope stubs on the core protein (*below*). Note that ChABC digestion removes the inhibitory sulphate chains. G1, globular N-terminal domain; G3, globular C-terminal domain; PTPσ, protein tyrosine phosphatase σ; NCAM, neural cell adhesion molecule; Ig, immunoglobulin; EGF, epidermal growth factor; CRD, carbohydrate recognition domain; CBP, complement binding protein. Modified from (Bartus et al. 2012).

Degradation of GAG chains with ChABC increases the integration efficiency of transplanted cells in spinal cord and brain injury models. ChABC treatment has been shown to increase axonal regeneration following spinal cord injury in rats (Bradbury et al. 2002; Massey et al. 2006; Garcia-Alias et al. 2009). On the other hand, improvement in visual cortex plasticity was limited following ChABC treatment with monocular deprivation in cats (Vorobyov et al. 2013), suggesting that the success of CSPG digestion may be injury-specific, or may require combination therapy. It has been postulated that ChABC treatment may be effective in increasing integration of stem cells in retinal degeneration (Singhal et al. 2008; Barber et al. 2012). Ma *et al* demonstrated that ChABC treatment increases synaptogenesis between transplanted RPCs and recipient neurons in models of retinal degeneration (Ma et al. 2011). The Pearson group used the *Rho*$^{-/-}$ mouse model to investigate the effect of ChABC treatment on integration of photoreceptor precursor cells into the ONL of the retina. The *Rho*$^{-/-}$ retina has an intact OLM and reactive gliosis present, resulting in large CSPG production. In this model, ChABC treatment alone resulted in an 8-fold increase in transplanted cell integration relative to controls. When combined with a siRNA targeting ZO-1 to disrupt the OLM, ChABC treatment also significantly increased the percentage integration relative to control. However, one should interpret the data cautiously as it is not clear that the combined treatment offers a worthwhile increase in percentage integration, relative to ChABC treatment alone. Optokinetic head-tracking behaviour experiments were used to assess how percentage integration relates to improved visual function. These behavioural experiments suggested improved visual function in mice with combined treatment compared to control mice, however only 7 mice were used; greater n numbers are required to verify the result (Barber et al. 2012). Further, it would be interesting to know how the behavioural results differ in mice with ChABC treatment alone.

Although PNN digestion is a promising strategies for some models, it is worth adding a note of caution. The PNN protects neurons from excitotoxicity and oxidative stress. Further, activated microglia may not target neurons that are in contact with the PNN (Karetko and Skangiel-Kramska 2009), therefore removal of PNN components may not be advisable in cases where microglial activation is prevalent.

Disruption of glial scars may expose neighbouring tissue to the highly toxic immune response, and inhibit functional recovery – this was demonstrated with mild to moderate spinal cord injury where the usual return of function was impeded (Sofroniew 2005).

1.8 Stem cells

1.8.1 Stem cell therapy

Stem cell therapy to introduce new cells into the retina has been trialled in disease models. To date this method has had limited success. Several groups claim improved visual acuity (MacLaren et al. 2006; Pearson et al. 2012), however this is frequently proposed upon the incorrect assumption that the improved light sensitivity of photoreceptors results in increased neuronal processing. Neuronal processing is extremely complex, so much so that if one connection is not correct, the result of photoreceptor cell stimulation may be no signal is passed on to the next cell, or a feedback loop may be created, whereby the stimulated cell re-stimulates itself (Rao et al. 2000). For both of these results, increasing the light intensity would increase photoreceptor cell activation, as measured by increased cell membrane depolarisation, however the signal would not be passed to the visual centre in the brain, thus there would be no improvement in visual acuity. Reactivating plasticity is likely to be key in the treatment of neuronal degeneration when attempting to re-wire neuronal circuits (Marc et al. 2003; Grimaldi et al. 2005; Hong and Chen 2011; Morimoto 2012).

There are several different stem/progenitor cell niches have been investigated for use with cell replacement therapy in retinal degeneration. All of these protocols are associated with their own advantages and disadvantages, which will be explored in this section.

Embryonic stem cells

Embryonic stem cells (ESCs) are an attractive option for cell replacement therapies because they are pluripotent, meaning that they have the potential to differentiate into any of the 3 germ layers. The drawbacks of ESCs include the risk of tumour formation if their proliferation becomes uncontrolled, and controversial ethical issues. There is also the risk of immune-rejection (Schraermeyer et al. 2001; Baker and Brown 2009). Studies to date have provided mixed results; a recent study in humans with macular degeneration involving ESC-derived RPE suggested that visual function could be stabilised

(Song W et al. 2015), although since the duration of this study was only one year, one must remain cautious when making inferences about the potential of ESC-derived cells from this study. The recent initiation of another clinical trial, in which stem cell-derived RPE cells were transplanted into retinas of AMD patients (https://www.mrc.ac.uk/news/browse/first-patient-treated-with-stem-cell-therapy-for-wet-age-related-macular-degeneration/, last accessed 16.02.16), suggests that there may be hope for the treatment of AMD. It should be noted, however, that transplantation and integration of neuronal cells, as opposed to epithelial cells described here, is likely to be a substantially greater challenge for the future. ESCs also offer a virtually limitless supply of cells that can be differentiated into neurons in vitro with the application of retinoic acid (Bibel et al. 2004). This has allowed researchers to investigate genes/proteins involved in neuronal degeneration, and may highlight target pathways for neuroprotection and repair.

Induced pluripotent stem cells

Induced pluripotent stem cells (iPSCs) are cells that have been reprogrammed by expression of the transcription factors *Oct4*, *Sox2*, *Klf*, and *Myc*, to create an embryonic stem cell-like cell (Takahashi and Yamanaka 2006). These cells are favoured by many groups because they offer the same level of pluripotency as ESCs but come without the ethical issues and rejection problems since the cells can in theory be derived from the patient's own cells, creating an explosion in the field of personalised medicine. Despite this, iPSCs are in no way ideal because the teratoma risk remains, and their production is a very lengthy process: approximately 2 weeks from mouse fibroblasts, and 3-4 weeks from human fibroblasts (Sommer and Mostoslavsky 2013). In addition, it should be noted that if the disease genotype is inherited, the iPSCs made from the patient's cells will contain the same mutation, therefore the affected gene must be corrected prior to generation of iPSCs (Tibbetts et al. 2012). Despite these drawbacks, iPSCs have proved an invaluable research tool for modelling neurodegenerative disorders, including ALS (Dimos et al. 2008), Rett Syndrome (Marchetto et al. 2010)

and Huntington's disease (Zhang et al. 2010), elucidating contributory mechanisms to disease and repair.

Neural stem cells

Neural stem cells (NSCs) are multipotent stem cells that are capable of generating all cells in the neural lineage (neurons and glia). The advantage of using NSCs in place of ESCs or iPSCs for the purpose of cell replacement therapy is their lineage is restricted so they are more likely to differentiate into the correct cell type, whilst maintaining high self-renewal capability. However, the price of self-renewal is the risk of tumour formation, so, as always, the potential benefits must outweigh the risks. Nevertheless, NSC transplantation has been shown to improve neuronal survival and/or functional outcome in a range of neurodegenerative disease models, including Alzheimer's disease (Wu et al. 2008b; Blurton-Jones et al. 2009) and amyotrophic lateral sclerosis (Mitrecic et al. 2010).

 NSCs have proved useful for researching genes and signalling pathways implicated in neurodegenerative disorders. It has been recently reported that the forced expression of three transcription factors, Brn2, Ascl1 and Myt1l, can convert fibroblasts to induced neuronal cells (Pang et al. 2011). This is a faster method of producing neuronal cells from somatic cells, therefore this may improve the availability of patient-derived neurons or cells for the investigation of neuronal degeneration.

Retinal progenitor cells

Retinal progenitor cells are unipotent cells, usually taken from embryonic tissue. Because they are not true stem cells there is a reduced risk of tumour formation, however trials to date have demonstrated poor integration efficiency, particularly in diseased retinas (Klassen et al. 2004; Mansergh et al. 2010). It may be that CSPG remodelling is required to improve integration efficiency (Ma et al. 2011). There may be some promise using ESC-derived retinal progenitor cells, which have been reported to increase visual function in rats (Qu et al. 2015).

Retinal sheets

An alternative approach for patients who have complete photoreceptor loss is transplantation of retinal sheets. Embryonic *retinal sheets* have been transplanted into retinal degeneration models but may stimulate formation of a glial scar (Peng et al. 2007). Foetal retinal sheets, with attached RPE, are able to integrate into the host IPL (Woch et al. 2001) and in some cases have been evidenced to increase light sensitivity (Sagdullaev et al. 2003; Seiler and Aramant 2012), while in others little effect on visual function was measured (Seiler et al. 2009). Greater success has been achieved with retinal sheets that contain both photoreceptors and RPE because the RPE is required to support photoreceptors. More recently, retinal sheets constructed from ESCs and iPSCs have been shown to be capable of integration into the host retina in mice (Assawachananont et al. 2014) and primates (Shirai et al. 2016).

Retinal prostheses

Artificial electrical stimulation of neurons is one approach to treat retinitis pigmentosa that may address the problem of trying to connect new neurons into an existing neuronal network. Implantation of an electronic prosthesis does not result in good visual function by any means, however for blind patients it may offer some level of contrast sensitivity for identifying obstructions, and motion detection (Dobelle et al. 1974; Veraart et al. 1998). It should be noted that this approach is only suitable for patients who have complete vision loss as the prosthesis is likely to interfere with native retinal outputs. In addition, the risk of side effects is high; 30% of patients experienced severe adverse effects in one clinical trial with electronic implants (Humayun et al. 2012).

1.8.2 Photoreceptor replacement

A large proportion of the literature to date regarding stem cell therapy to treat retinal degeneration focuses on photoreceptor transplantation. One approach involves the transplantation of *Nrl*-GFP labelled post-mitotic photoreceptor precursor cells into the OLM of wildtype mice. This is a promising

method, but will likely be more successful if the efficiency can be improved. The current transplantation efficiency is 0.01% and the percentage integration is even lower (Ma et al. 2011). If sufficient cell numbers could be introduced into the retina, the result could be therapeutically beneficial, however it has been estimated that 150,000 cells are required to produce an ERG response across the whole retina (Pearson et al. 2012). Despite this, the question remains as to whether integrated stem cells are capable of connecting to the visual circuitry and improving visual acuity. Numerous groups claim improved light sensitivity with transplanted photoreceptor precursor cells, however, as outlined previously, increased photoreceptor cell activation in response to light does not necessarily equate to increased neuronal firing to the visual centre in the brain. If transplanted cells are not able to reliably connect to the neuronal circuitry, no increase in number of integrated cells will increase the therapeutic benefit of any stem cell therapy. Therefore, future work in this field must endeavour to improve methods to measure connectivity of transplanted cells, and also develop techniques to facilitate formation of functional synapses between host neurons and transplanted cells.

It should be noted that a lot of the proclaimed success to date in photoreceptor transplantation has been in wildtype retinas. The environment in the degenerating retina is very different to that of the wildtype retina (glial scarring is just one example), therefore transplantation efforts are likely to have very different outcomes in disease models (Barber et al. 2012). The normal retina has an intact OLM, which may mean that the transplantation efficiency is better in disease models with disrupted OLM compared to wildtype models.

1.8.3 Cell-based delivery of agents

Cell-based delivery of drugs is an attractive method to target largely inaccessible areas, such as the brain. Cells can be made to endocytose drug-filled endosomes or they can be transfected with genes encoding a particular protein. In both cases, the cells pump out the agent and in this way can provide a more sustained delivery than alternative methods to cross the blood brain barrier, such as

nanocarriers or ultrasound beams (Hynynen et al. 2001; Koo et al. 2006). NSCs and ESCs have been used to deliver neurotrophic agents, such as NGF, with neuroprotective results in animal models of Alzheimer's disease (Wu et al. 2008b) and Huntington's disease (Kordower et al. 1997). Further advances in genetic engineering will enable greater control of delivery of agents, for example with the use of the light-sensitive transcription (Stuber and Mason 2013).

1.8.4 Future prospects

Different models of retinal degeneration have different characteristics regarding speed of degeneration, extent of OLM disruption, and gliosis (Barber et al. 2012). Since all of these factors affect the migration, integration, differentiation, and stability of donor cells, the disease aetiology will determine the most appropriate line of treatment. Some animal models with varied diseases timelines are currently available, such as the $Gnat1^{-/-}$ model, which loses 10% of photoreceptors over a period of 12 months, and the $PDE6\beta^{rd1}$ model, which loses virtually all the photoreceptors in a period of 3 weeks (Barber et al. 2012). More models with a greater variety of neuropathologies are required to aid the development of tailored therapies.

One problem limiting stem cell replacement therapy is the need for transplanted cells to be stable for several years to reduce the need for repeated surgery. The MacLaren group reported that 33.3% of twelve eyes from $rd1$ mice had surviving transplanted photoreceptor cells by week 12 (Singh et al. 2013), which would not be an acceptable percentage nor survival period in human patients. Cell survival, and indeed neuronal connectivity, remain key issues to be addressed if injected cells are to become and remain part of a functional neural network. On the other hand, numerous studies have shown promise of functional recovery in models of a number of disorders, however in some cases the therapeutic effect measured may be due to a downstream effect, such as secretion of BDNF (Blurton-Jones et al. 2009), rather than neuronal activity of transplanted cells.

1.9 Manipulation of stem cell migration

Stem cells have widespread potential for the treatment of neurodegenerative disorders. However, since many target areas of the CNS are largely inaccessible and stem cells may not be viable when injected directly next the injury site (Kelly et al. 2004), there is a need for stem cell migration to be controlled in a way that is safe and that allows deep tissue penetration.

1.9.1 Electrical fields

All cells have membrane potentials generated by the distribution of ions and charged molecules. It was proposed as early as the 19th century that electric fields could be used to stimulate cell migration (McCaig et al. 2005). In fact, endogenous electric fields have shown to be important for guiding mesenchymal stem cells to wound sites, including the rat cornea (Reid et al. 2005; Zhao et al. 2006), therefore there has been interest in the utilisation of external electrical fields to direct stem cell migration. Electrical activation (0.2 V) has been shown to stimulate neurite extension of rodent NSCs (Kobelt et al. 2014) and axonal outgrowth of cultured rat RGCs (Goldberg et al. 2002). There is evidence that direct current electrical fields can direct the migration of rodent NSCs and human ESCs towards the cathode in vitro (Li et al. 2008; Meng et al. 2011; Feng et al. 2012), as well as promoting neuronal differentiation from neural precursor cells (Thrivikraman et al. 2014; Zhao et al. 2015).

Electrical field-directed cell migration is promising. However, it is important to consider the potentially serious drawbacks with this method, the main one of which is that application of an electric current over long time periods result in an increase in temperature, which may cause protein denaturation or cytotoxicity.

1.9.2 Magnetic fields

Magnetic fields have been widely researched for their potential use in the direction of cell migration. Given that magnetic fields can penetrate non-transparent tissue very well, can be controlled remotely, and are relatively safe (Long et al. 2015), they may offer a better method of targeting largely inaccessible areas of the brain compared to optogenetics. It is known that iron is required by cells (as

much as 4 g may be present in the body (Bulte 2009)) and can be bound to proteins. Further, since iron is ferromagnetic, it seems plausible that there would be a way to control protein function using magnetic fields.

Magnetic particles

The basic principle of magnetism is that electrons possess the property of spin and orbital angular momentum, which together contribute to the electron's magnetic moment. If the magnetic moments are aligned (intrinsically or due to an external magnetic field) the atoms are said to have the property of magnetism. All materials are magnetic to a certain degree. Most materials are only magnetic when in the presence of an applied magnetic field, i.e. diamagnetic or paramagnetic. This type of magnetism is usually very weak. Ferromagnetism, however, is a much stronger type of magnetism; the magnetisation value, M, may be 10^4 times greater than that of a paramagnetic material (Whitesides et al. 1983). The value of M is dependent on the strength of the external magnetic field, H, and on the temperature (Sattler 2010). Superparamagnetic nanoparticles (iron oxide particles) are often favoured in the context of medicine, since they lose their magnetism in the absence of an external magnetic field, meaning they do not aggregate following removal of the magnetic field (Bonnemain 1998).

Magnetic particles used in biological research usually fall into two categories: nanoparticles (diameter 1-100 nm) and microparticles (diameter 1-1000 μm). The size of magnetic particle is a very important factor. For instance, to enable targeting to specific tissue intercellular space, particles should ideally be <10 nm diameter, or <1 nm for the brain and kidney tubules (Berry and Curtis 2003). Nanoparticles are optimally endocytosed if their diameter is <60 nm (Zhang et al. 2009), but this process can be promoted with larger particles using a polymer coating (Zhang et al. 2002). The maximum number of particles that may be taken up by a cell is predicted to be 500-5000 (Zhang et al. 2009).

The basic structure of magnetic nanoparticles (mnps) is shown in Figure 1.8. Due to their ferrite core, magnetic nanoparticles have the property of superparamagnetism: in the absence of an external

magnetic field mnps have a magnetisation value of essentially zero; and in the presence of an external magnetic field, the particles are magnetised (Obaidat et al. 2015). In the latter state they can be described as obeying Coulomb's law and can be influenced by the magnetic gradient. The silicon-based coating of mnps allows the iron oxide to be stable in aqueous solution and has the added benefit of permitting conjugation of drug molecules (Yang et al. 2012).

Due to their size, it should be possible to use mnps to target cells, proteins, and even specific DNA sequences. In the era of genome sequencing and rapid advances in genetic engineering mnps have great prospects in many areas of biomedicine and regenerative medicine. Mnps can be used to introduce DNA or RNA into cells, and as such present a novel transfection method, magnetofection, to introduce new DNA or to knock down genes using siRNA (Schillinger et al. 2005). In magnetofection, DNA of interest is mixed with mnps coated with a charged polymer, which allows binding of the DNA to the particle surface via electrostatic interactions. The DNA-coated particles are then introduced into cells with the use of an external magnetic field. Advances in this technology have shown that an oscillating magnetic field increases the efficiency of transfection, as outlined by the Nanotherics website (http://www.nanotherics.com/whatismat.htm, last accessed 15.02.2016).
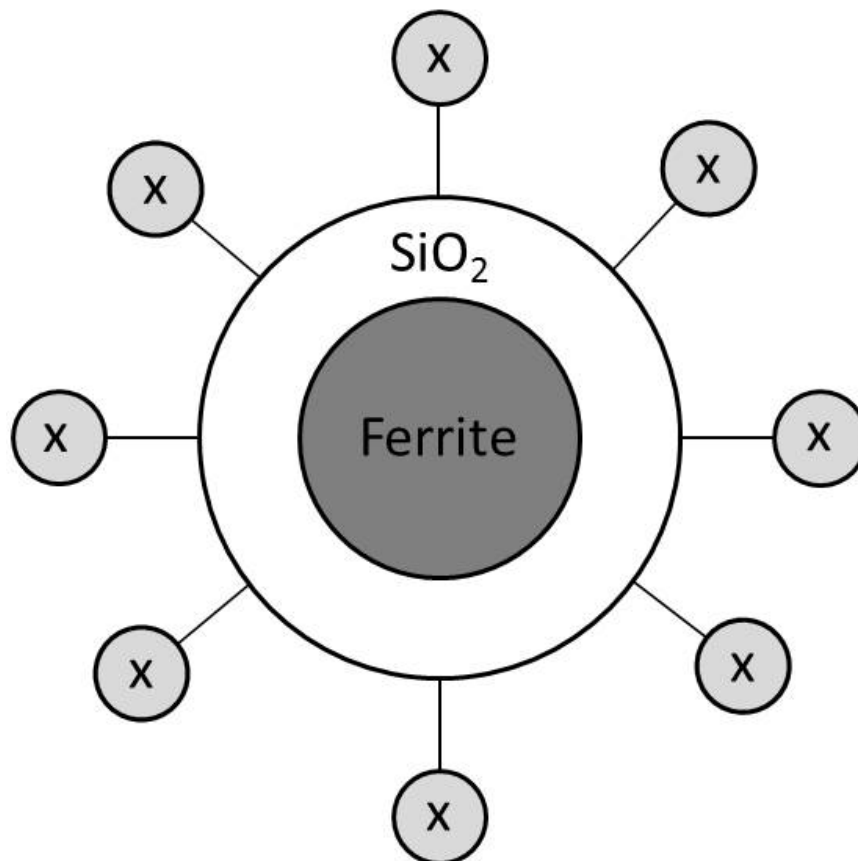
Figure 1.8 Structure of a magnetic nanoparticle. The ferrite core (comprised of iron oxides plus a mixture of oxides of nickel, manganese and zinc) is surrounded by a silica coat, to which functional groups (x) may be attached. Adapted from (McBain et al. 2008).

Uses in drug targeting and diagnostics

The use of magnetic particles as a drug delivery system is by no means a new idea (Senyei et al. 1978; Widder et al. 1980). There has been a great deal of interest in the use of mnps in cancer treatment. It has been theorised that mnps could be conjugated to an anti-cancer drug or to radionucleotide atoms, injected into the bloodstream and directed towards the tumour using an external magnet. NSCs have been used to deliver magnetic discs (2 μm diameter) with an external magnetic field to cause mechanical destruction of malignant glioma cells (Muroski et al. 2016). These treatments are attractive since the procedure is non-invasive and the particles can be easily tracked using MRI (Mejias et al. 2011). Further, by combining knowledge about specific cancer cell markers, mnps could be targeted to cancer cells using cell type-specific antibodies (Babincova et al. 2002). This would mean that theoretically the dose of the anti-cancer drug could be increased while minimising the risk of adverse effects.

Other uses of magnetic particles in targeted drug delivery include treatment of disorders affecting the brain. The blood-brain barrier is an important structure that impedes the passing of molecules that are larger than 400 Da or are poorly lipohillic (Pardridge 2012) to protect the brain, however, this can make it difficult to deliver drugs to the target site. Mnps may circumvent this problem. Drug molecules can be encapsulated within magnetic particles, injected into the bloodstream, and directed to the target site with an externally positioned magnet (McBain et al. 2008).

Other therapeutic uses

When an alternating magnetic field is applied following the magnetic hysteresis loop, mnps generate heat. Since mnp solutions tend to pool around tumour cells, rather than surrounding normal cells, this technology can be used to target heat to cancer cells (Babincová et al. 2001; Babincova et al. 2004). In one study, median temperatures of approximately 50°C in the centre of tumours were achieved, causing death of the cancer cells (Kumar and Mohammad 2011). It should be noted that whilst the

effect to surrounding cells was minimal, a 2°C increase is not negligible and therefore caution should be exercised, particularly in vulnerable tissue such as the brain, where cytotoxicity could be devastating. In order to minimise damage to non-target cells these mnps are usually injected into the centre of the tumour. This method, using temperatures of 43-55°C, is termed magnetic thermoblation. A similar method, magnetic hyperthermia, involves temperatures of 45-47°C and although this also causes tumour regression, the regression is often not permanent (Hilger et al. 2001). Magnetic field-induced warming technology also has potential for the treatment of hypothermia (Pankhurst et al. 2003).

Uses in cell signalling research

As eluded to previously, specific proteins can be conjugated to magnetic particles, which facilitates the investigation of signalling pathways. In addition, the protein concentration, using knowledge about the number of mnps per protein, and the spatiotemporal effects, using controlled magnetic fields, may be explored. Further, conjugation of mnps to ligands/agonists may enable magnet-controlled manipulation of signalling cascades, which may be useful as a research tool and as a potential therapeutic approach. It should be noted that although some signalling pathways, such as those downstream of integrins, are mechanosensitive, the magnetic force applied to each mnp is similar to that required to stimulate downstream signalling (Sniadecki 2010).

Uses in whole cell migration

Since cells can be made to take up mnps via endocytosis, it would be logical to hypothesise that it may be possible to control the migration of cells containing mnps using a magnet. Indeed, this has been demonstrated using mnp-containing stem cells in vitro (Raffa et al. 2009; Song et al. 2010) and in vivo (Song *et al.*, 2010). By applying the same principle as is used in cell sorting, resident cells may be controlled using a magnet by using antibody-conjugated mnps. Permanent magnet-directed migration of mnp-labelled stem/progenitor cells in vivo has been demonstrated in the repair of vasculature

injury and wound healing (Kyrtatos et al. 2009; Riegler et al. 2013). Permanent magnets have also been reported to control the migration of cells from the blood to a lesion site using mnps bound via cell surface antigens in vivo in the rabbit. In this study mnps were coated with anti-CD34 antibodies via polyethylene glycol, which were injected intravenously and bound to stem cells via their cell surface antigen CD34. A permanent magnet was then held next to a femoral artery and it was found that mnp-bound stem cells accumulated at a lesion site in the femoral artery following application of a magnetic field (Chen et al. 2013). This is an interesting approach as it would permit higher specificity. Although promising, the reach of this approach is limited by the fact that the strength of magnetic fields decreases exponentially as a function of distance from the magnet surface (Figure 1.9). Consequently, it may be difficult to control the migration of cells deep in the brain without the implantation of magnets, which has been demonstrated in the spinal cord (Tukmachev et al. 2015), retina (Yanai et al. 2012) and brain (Carenza et al. 2014). Alternatively, electromagnets can be used to generate large magnetic fields with controlled gradients, and since MRI machines are commonplace in hospitals, the equipment for magnetic field-directed migration may already be available (Riegler et al. 2010).
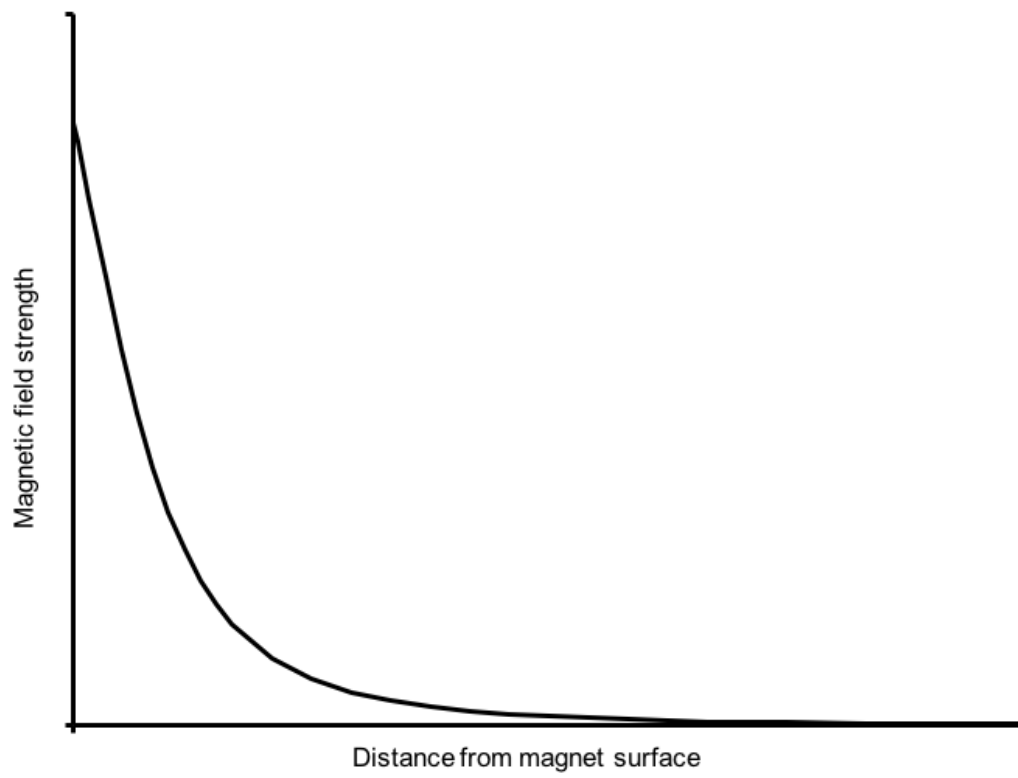
Figure 1.9 Magnetic field strength, Br, follows the inverse square law with distance from the magnet surface.

Mnp toxicity

The potential toxicity of mnps is a concern in the field, and breakdown of iron within cells via the Fenton reaction produces free radicals that can damage DNA (Imlay et al. 1988). Despite this, there has been no reported adverse effects on the viability or migration of stem cells when nanoparticles are used at 10 pg iron/cell (Bulte 2009; Loebinger et al. 2009; Richards et al. 2012). One recent study demonstrated that neuronal activity is not affected by the movement of magnetic nanoparticles in brain slices (Ramaswamy et al. 2015). Mnps have been widely used in medicine for cell tracking and imaging (using MRI scanning), and are rapidly removed from circulation within 3 hours (Sun et al. 2008). The size of mnp is an important consideration since particles with a diameter of <5.5 nm are filtered out of the body via the renal system (Choi et al. 2007) and particles with a diameter of >500 nm are removed from circulation by phagocytes in the spleen (Chen and Weiss 1973).

1.9.3 Magnetic field-sensitive receptors

Magnetoreception describes a phenomenon where organisms are able to sense the Earth's magnetic field. To date, evidence for the existence of a magnetic field-sensitive receptor, or magnetoreceptor, has ben limited to the cases of migratory organisms. Magnetic field-sensitive migratory behaviour has been detected in bacteria (Baumgartner et al. 2013), Drosophila (Qin et al. 2016), Zebrafish (Takebe et al. 2012), sea turtles (Lohmann et al. 1999), lobsters (Boles & Lohmann 2002), and several species of bird, including homing pigeons (Leask 1977; Mora et al. 2004). There have been three possible mechanisms for magnetoreception proposed: electromagnetic induction, magnetite magnetoreception, and chemical magnetoreception. Electromagnetic induction is proposed to involve detection of magnetic fields using an electrical conductor. When the conductor passes through a magnetic field, a force Is applied, termed Lorentz force, the magnitude of which is relative to the parameters (strength, direction, etc.) of the magnetic field (Johnsen & Lohmann 2005). There is evidence for electromagnetic induction in studies with elasmobranch fish (e.g. sharks and rays), for example rays conditioned to respond to changes in a magnetic field had their responses blocked

following introduction of magnets in their nasal cavities (Molteno & Kennedy 2009). Magnetite (Fe_3O_4) magnetoreception is proposed to involve a molecule containing iron, which aligns itself to the geomagnetic field and rotation of the magnetic field may result in opening of a connected ion channel (Kirschvink et al. 2001). This could result in downstream neuronal firing that may cause a change in migratory behaviour. The chemical magnetoreception hypothesis relies on free radical reactions that are influenced by the Earth's magnetic field. Since light-absorbing reactions, such as in photoreceptors, typically involve free radical reactions, it has been proposed that chemical magnetoreception may be associated with light-responsive organs (Ritz et al. 2000). In line with this, there is evidence for crytochromes in migratory, but not non-migratory, songbirds (Mouritsen et al. 2004).

There is little evidence for a magnetoreceptor in non-migratory animals, however if it does exist, perhaps the alignment of a molecule with the geomagnetic field may have a use for the detection of orientation during embryogenesis, but there have been no studies supporting this theory. Although debated to be present in humans, a recently presented two models for a magnetically-sensitive receptor, the magnetoreceptor. In this report, one model suggested that magnetite may help protein complexes align with external magnetic fields and stimulate movement of stretch receptors, while a second model suggested the involvement of photoreceptors where phototransduction leads to the exchange of radicals, leading to different chemical products in the presence or absence of an external magnetic field (Lohmann 2016). Rat mesenchymal stem cells have been shown to migrate in response to a permanent magnet array without mnps, which provides evidence of a mammalian magnetoreceptor. In this study, mesenchymal stem cells from rats were grown on a microarray of magnets for up to 3 days and at the end of the culture period it was found that the cells grew on the surface of the magnets, unlike in the non-magnetic array control, where cells grew in a more random fashion (Zablotskii et al. 2013).

1.9.4 Magnetogenetics

The recent construction of iron containing proteins has brought the advent of magnetogenetics –
control of transcription by the application of an external magnetic field. Using these proteins, neuronal
action potential firing (Long et al. 2015) and calcium-regulated insulin release (Leibiger and Berggren
2015) can be remotely controlled. It may be possible to combine this technology with cell-based
delivery of neurotrophins, particularly as *bdnf* has calcium response elements.

1.10 The retinal explant: a model for neurodegeneration

The retinal explant is an ideal model to investigate the mechanisms involved in neuronal degeneration. The axotomy, performed at the time of explantation, is a consistent injury, unlike the optic nerve crush (Weber and Harman 2008). The resultant rapid cell death is a major advantage of this model over similar in vivo models, as well as the minimal contribution of an immune response. Experiments with cell culture and brain slices are rapid, but do not permit investigation of an intact neuronal network. In addition, the fact that the concentration and location of agents can be controlled relatively easily has resulted in the widespread use of this model for the study of neuroprotective strategies (Ogilvie et al. 1999; Wang et al. 2002; Koizumi et al. 2007; Moritoh et al. 2010; Niyadurupola et al. 2011) and cell replacement therapies (Johnson and Martin 2008; Bull et al. 2011; Denk et al. 2015).

Results from explant experiments are primarily assessed using cell counts or viability markers, such as propidium iodide and calcein-AM (Grieshaber et al. 2010), or terminal deoxynucleotidyl transferase dUTP nick end labelling (TUNEL) (Gavrieli et al. 1992), which can underestimate tissue health. Recent reports indicated that retinal explants are viable for at least 7 days (Lye et al. 2007; Johnson and Martin 2008; Kobuch et al. 2008). However, it should be noted that a retina containing 'viable' cells is not necessarily capable of transmitting signals along the entire visual pathway. RGCs that contain active esterases, and therefore stain positive for calcein-AM, may not be capable of receiving input from bipolar cells and amacrine cells if dendritic pruning has occurred. Lack of morphometric analysis of RGCs, from which functional potential may be inferred, is a major limitation of work to date.

In order for morphometric analysis of RGCs to be carried out, cells must be labelled in a sparse and random manner. Golgi staining remains a gold standard staining method but does not combine well with other histological techniques (Golgi 1873). Microinjection of dyes is technically challenging and is biased towards larger cells. Retrograde labelling with fluoro-gold (Chiu et al. 2008) relies on intact axons and commonly results in over-labelling. The use of transgenic animals, for example Thy1-dependent expression of green fluorescent protein (GFP) for labelling of RGCs, can produce sparse

labelling but underreports dendritic pruning (Williams et al. 2013a). Ballistic labelling (diolistics and biolistics) (Lo et al. 1994; Christianson and Lo 2011) labels cells in a sparse manner. Diolistics uses tungsten particles as microcarriers of lipophilic dyes, which are delivered to cells under high pressure helium blasts. The lipophilic dyes diffuse through cell membranes in a temperature-dependent nature, therefore the resultant labelling is considered random since it is independent of cell health or ATP machinery. Biolistics uses gold particles to deliver plasmids to cells using helium blasts. In addition to labelling cell morphology by transfection with, for example GFP, biolistiocs also permits visualisation of synaptic or mitochondrial markers, which may be useful to monitor in parallel with changes to the whole cell morphology.

1.10.1 TrkB signalling in the retinal explant

Since the retinal explant is an axotomy model, it is important to consider the potential signalling pathways initiated by axotomy that may contribute to dendritic retraction and neuronal cell death in this model. Wallerian degeneration describes the degenerative events contributing to axotomy-induced axonal retraction (Gerdts et al. 2016). The study of Wallerian degeneration has provided target proteins and signalling cascades that would be interesting to study in the context of dendritic atrophy and/or neuroprotection. Following axotomy, Sarm1 (a protein with multiple protein interaction sites) activation leads to upregulation of MKK4 and MKK7 (Gerdts et al. 2013; Yang et al. 2015). A resultant energy deficit, possibly due to the disruption of a stem in glycolysis by Sarm1-MAPK, results in intracellular build-up of Ca^{2+}. Calpain (a cysteine protease) can be activated by caspases, or independently activated by high intracellular levels of calcium (George et al. 1995). In axotomy models, calpain is postulated to be activated in a caspase-independent manner. Activated calpain digests actin, resulting in axonal retraction (Yang et al. 2015). MKK4 is antagonised by Akt, which is upregulated by BDNF-TrkB signalling. From this we can postulate that BDNF treatment of axotomised RGCs may retard axonal retraction. Further, BDNF signalling is capable of inducing neurite extension via Ras-activated actin polymerisation, therefore BDNF treatment has the potential to not only retard

axonal degeneration but to stimulate outgrowth, as observed in adult rodent retinal explants (Thanos

et al. 1993; Goldberg et al. 2002).

1.11 Aims and hypothesis

Based on the evidence that dendritic retraction precedes cell loss in neurodegenerative disorders, I hypothesise that morphometric analysis of RGCs in adult mouse retinal explants will provide a more sensitive readout of neuronal cell health, compared to cell counts. Further, I postulate that the quantification of dendritic morphology in these neurons will aid identification of mechanisms implicated in neuronal degeneration and therefore targets for neuroprotection and repair.

Specific aims of this thesis will be:

- To assess the timeline of onset of dendritic retraction versus cell loss of RGCs in the mouse retinal explant.

- To test whether dendritic retraction may be retarded following treatment with neurotrophic agents (pan-caspase inhibitor and BDNF).

- To investigate the potential inhibitory role of the PNN on neuronal plasticity; specifically, whether PNN digestion will facilitate dendritic remodelling of RGCs following axotomy.

- To test whether external magnetic fields can increase migration depth of NSCs into the GCL of mouse retinal explants, and thereby test this a potential method to deliver neurotrophic agents to specific cell layers in the central nervous system.

The methods to be used in this thesis will now be outlined.

Chapter 2. Materials and Methods

2.1 Animal use

2.1.1 Housing of animals

Mice were housed in a 12 h light/dark cycle with access to food and water ad libitum.

2.1.2 Animals used

C57/Bl6 mice of either sex aged 6 weeks – 8.5 months were used for all experiments (Table 2.1).

Table 2.1. Animal numbers for all experiments.

Experiment	Number of explants	Number of animals
Explant area measurements	4	4
Nuclear staining	18	15
Immunohistochemistry	21	17
TUNEL	14	13
Calcein-AM	13	13
Diolistics	123	88
ELISA	29	15
Neural stem cell migration	6	3

2.2 Retinal explant preparation and culture

Mice were killed by cervical dislocation in accordance with the Home Office (UK) and eyes were marked for nasal orientation using a sterile 18 gauge needle. Eyes were enucleated, washed with 1x phosphate-buffered saline (PBS, pH 7.4) to remove blood and hair, and placed into ice-cold Hanks-balanced Salt Solution (Life Technologies Ltd., Paisley, UK) supplemented with 1% penicillin-streptomycin. Under a light dissecting microscope (Leica DFC 420C) the retina was rapidly dissected as outlined in Figure 2.1. The prepared explant was cultured on a 0.4 μm PTFE culture insert (Millipore, Watford, UK) in a 35 mm culture dish (Millipore) containing 1.2 mL supplemented Neurobasasl-A culture media (Table 2.2). Explants were cultured at 37°C, 5% CO_2. For culture periods of >1 day the media was changed with fresh pre-warmed (37°C) media to prevent accumulation of toxins.

Table 2.2. Components of culture media. All components were purchased from Life Technologies Ltd. The medium was made up in a sterile 100 mL DURAN® bottle at stored at 4°C for no longer than 2 weeks.

Component	Concentration	Role
Neurobasal-A	-	Maintenance of adult neurons.
Penicillin-Streptomycin	1% (100 U/mL penicillin; 100 µg/mL streptomycin)	Antibiotics to minimise contamination caused by both gram-positive and gram-negative bacteria.
L-glutamine	0.8 mM	Amino acid to improve viability of cells.
N-2 supplement	1%	Supports growth of post-mitotic neurons in primary culture.
B-27 supplement	2%	Supports growth and viability of CNS neurons.
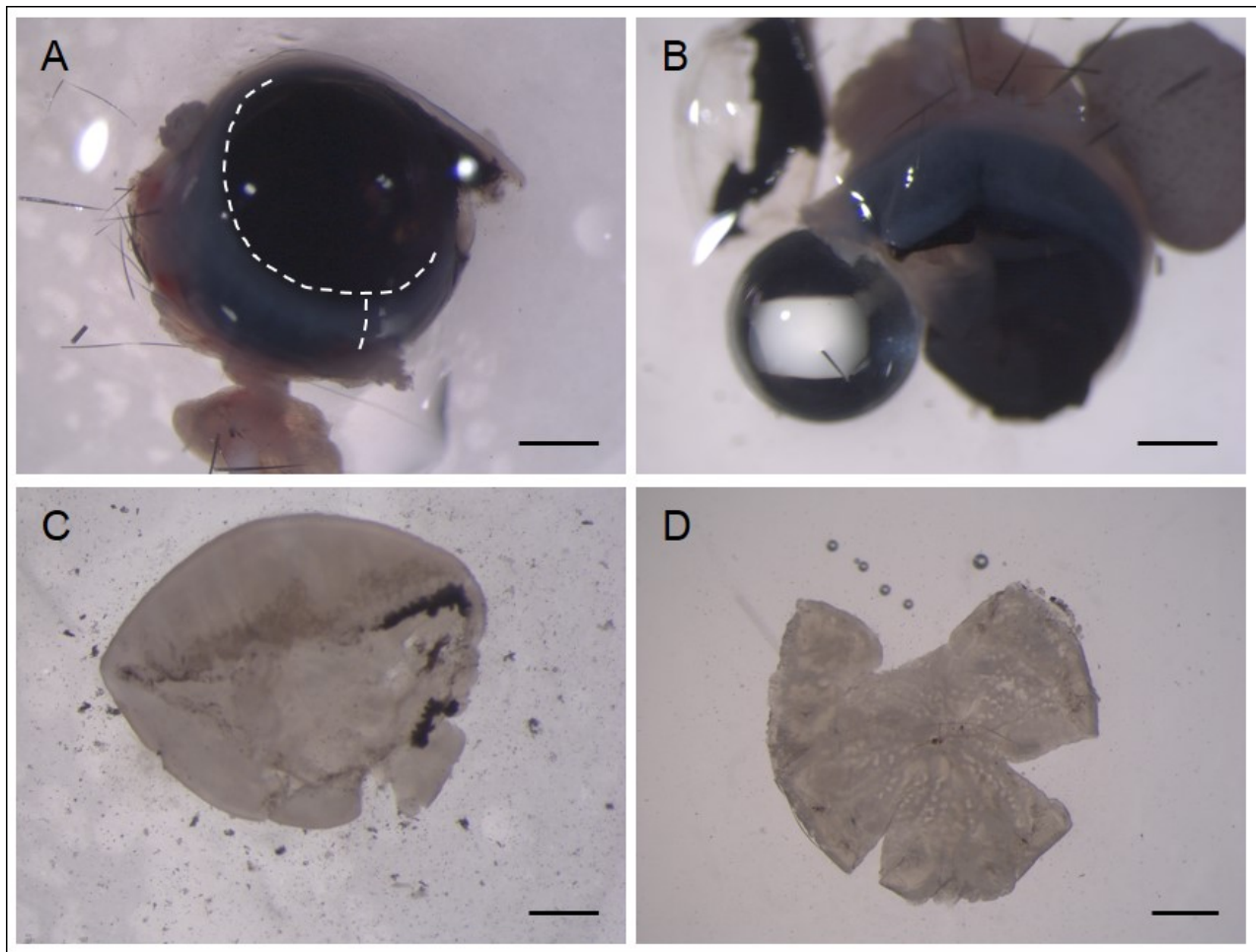
Figure 2.1. Preparation of retinal explant. (**A**) A cut was made from the nasal mark towards the optic nerve head and the anterior chamber was removed by cutting around the ciliary margin zone. (**B**) The lens was removed. (**C**) The retina was gently separated from the retinal pigment epithelium. (**D**) The retina was transferred to a culture insert, GCL facing up. Two additional cuts were made to create a three leaf clover shape and permit the retina to lie flat. Dashed lines indicate cut sites. Scale bars: 1 mm.

2.2.1 Pan-caspase inhibition

Explants were cultured in the culture medium as described previously. The pan-caspase inhibitor Q-VD (R&D Systems, Abingdon, UK) was added as a topical aliquot (100 µL) directly onto each explant at a concentration of 100 µM (total concentration 7.7 µM in culture medium) in dimethyl sulphoxide. Controls had a 100 µL topical aliquot of dimethyl sulphoxide. After 1 day the culture medium was replaced and fresh aliquots were applied. After 2 days in culture, explants were labelled diolistically (section 2.8).

2.2.2 BDNF treatment

Explants were treated with 100 ng/mL BDNF (Regeneron/Amgen) for 3 d initiated at day 0 (3 d total) or at day 3 (6 d total). Prior to BDNF treatment, delayed BDNF-treated explants were cultured in normal culture medium for 3 d. BDNF was diluted in 1xPBS + 0.1% bovine serum albumin (BSA) and added to the culture medium to make a final concentration of 100 ng/mL or 1000 ng/mL. Controls had the same volume of vehicle added to the culture medium (2 µL/mL for 100 ng/mL BDNF, 20 µL/mL for 1000 ng/mL BDNF). All medium was replaced daily and cells were labelled diolistically (section 2.8).

2.2.3 ChABC treatment

To digest the PNN, explants were treated with ChABC (a kind gift from Prof. Bruce Caterson, Cardiff University) for 1 d. ChABC was stored at a stock concentration of 10 U/mL in 1xPBS + 0.1% BSA and applied as a topical aliquot (50 µL) diluted in 1xPBS. Controls had a topical aliquot (50 µL) of vehicle.

To visualise chondroitin sulphate (CS) digestion explants were treated with ChABC, and after 1 d explants were fixed and processed for immunohistochemistry as described in section 2.5. To investigate the effect on RGC dendritic morphology explants were treated with ChABC for 1 d and cultured for a further 2 d (3 d total) or 5 d (6 d total), and at the end of the culture period explants were diolistically labelled. To investigate a potential synergistic role of CS digestion and BDNF treatment, explants were treated with BDNF for 3 d from day 0 or from day 3, as outlined in section

2.2.2, in conjunction with 1 d ChABC treatment initiated at day 0. Explants were labelled with diolistics at the end of the culture period (section 2.8).

2.2.4 BDNF blocking with mAb#9

In order to investigate the role of endogenous BDNF, explants were treated with a mouse IgG2b monoclonal antibody raised against BDNF (as described by Kolbeck at al.(Kolbeck et al. 1999)), mAb#9 (a generous gift from Prof. Yves Barde, Cardiff University). MAb#9 (3.8 μg/μL) was added to the culture medium to generate a final concentration of 10 μg/mL. Controls had mAb#9 omitted. Explants were treated with mAb#9 ±BDNF (100 ng/mL) for 3 d, and then diolistically labelled (section 2.8).

2.3 Cryosectioning

At the end of the culture period the medium was replaced with 1 mL 4% paraformaldehyde (PFA, pH 7.4). A topical aliquot (500 μL) of PFA was applied onto the explant to ensure complete submersion of the tissue. Explants were fixed for 4 hours at 4°C, followed by replacement of PFA with 30% sucrose, including a topical aliquot (500 μL) of sucrose onto the explant. Explants were cryoprotected overnight at 4°C. Explants were then carefully placed into moulds containing optimal cutting temperature compound and labelled for orientation. Explants were rapidly frozen using liquid nitrogen-cooled isopentane and stored at -20°C.

Explants were cut using a cryostat (Leica CM 3050S). Sagittal sections were cut (10-14 μm) in the nasal-temporal direction and placed onto coated Superfrost® slides (Scientific Laboratory Supplies Ltd., Yorkshire, UK). Slides were left covered at room temperature overnight to allow any water to evaporate, and then stored at -20°C.

To use as positive controls for apoptotic markers, spleen from mice used for explants were dissected, washed with saline and fixed overnight in 4% PFA. The spleen was cryoprotected in 30% sucrose overnight, frozen in optimal cutting temperature, and stored at -20°C. Spleen was cut into 14 μm sections using a cryostat, placed onto coated Superfrost® plus slides, and stored at -20°C. To use as

positive controls for neuronal/CS markers, brains were fixed, frozen and section as described for spleen. The brains were cut anterior to posterior in the coronal plane.

2.4 Nuclear staining

For all staining protocols using frozen sections the following method was used prior to labelling: sections were left at room temperature (RT) for 30 min to allow all water to evaporate, then washed 3x with 1xPBS. The slides were carefully dried and a pap pen (Sigma-Aldrich, 5 mm tip) was used to draw a hydrophobic barrier around each section.

2.4.1 Staining method

Sections were incubated with TO-PRO-3 (Table 2.3; Life Technologies Ltd.) for 10 min (RT) in the dark. Sections were washed 3x with 1xPBS, the slides were carefully dried and sections were coverslipped with Prolong Gold anti-fade reagent® (Life Technologies Ltd.) and sealed with nail varnish. Sections were stored in the dark to prevent photobleaching.

2.4.2 Confocal microscopy

Sections were imaged by confocal microscopy (Zeiss, LSM 510, release version 4.2 SP1) using the 633 nm laser with 651-704 nm detector. Z-stacked images (1024x1024 pixels) were taken in 1 μm intervals through the entire section.

2.4.3 Image analysis

Images were imported into the image processing software FIJI (Schindelin et al. 2012) as RGB (8-bit) images. To prevent inaccurate measurements caused by overlapping cells the central 1 μm z-slice was analysed in each case. In order to minimise inaccuracies introduced by changes in volume in the z-plane of the tissue, nuclear counts were taken linearly in two-dimensions. The number of cells in a 250 μm line were counted using the multi-point tool, and the number was then calculated as number of cells/mm. Cell layer thicknesses were measured using the line tool, with three measurements taken for each section.

2.5 Immunohistochemistry

2.5.1 Staining method

All incubations were at room temperature, unless stated otherwise. Sections were incubated with 5% chicken serum in 1xPBS (Invitrogen, heat inactivated at 56°C) for 30 min. Sections were washed 3x with 1xPBS and then incubated with primary antibody for 4 h or overnight at 4°C. Sections were washed 3x with 1xPBS, followed by incubation with secondary antibody for 1.5 h. For all antibody concentrations see Table 2.3. Sections were washed 3x with 1xPBS and counter-stained with TO-PRO-3 as previously described or Hoechst (Table 2.3). Finally, sections were coverslipped with Prolong Gold anti-fade reagent and stored in the dark before imaging.

2.5.2 Fluorescence microscopy

Sections were imaged by confocal microscopy (488 nm argon laser with 500-530 nm bandpass filter for secondary antibodies and 633 nm laser with 651-704 nm detector for TO-PRO-3) or fluorescence microscopy (488 nm with FITC filter for secondary antibodies and 361 nm excitation with 497 nm detection for Hoechst). Confocal images were taken as z-stacks in 1 μm intervals. Fluorescence images were taken as single plane images in the centre of the section.

2.5.3 Image analysis

Images were imported as RGB (8-bit) images into FIJI and the central 1 μm z-slice was analysed in each case. Fluorescence was quantified either by counting the number of cells double stained for TO-PRO-3 and the antibody or by measuring the mean channel intensity of the cell layer. The mean channel intensity was normalised for background fluorescence by subtracting the channel intensity for the same cell layer in the negative control.

Table 2.3. Nuclear stains and antibodies used.

Primary antibodies and nuclear stain

Specificity	Target	Source	Clone	Working concentration	Diluent	Company
Thy1.2	RGCs	Rat IgG2b	Monoclonal	2.5 µg/mL	PBS + 0.1% triton	Abcam
Active caspase-3	Apoptotic cells	Rabbit	Polyclonal	10 µg/mL	PBS	Chemicon
1B5	Unsulphated CS disaccharide	Mouse IgG	Monoclonal	1:5	PBS	Bruce Caterson lab
2B6	4-sulphated CS disaccharide	Mouse IgG	Monoclonal	1:5	PBS	Bruce Caterson lab
3B3	6-sulphated CS disaccharide	Mouse IgM	Monoclonal	1:5	PBS	Bruce Caterson lab
TO-PRO-3 iodide 642	Nucleic acids	-	-	1 µM	ddH$_2$O	Life Technologies Ltd.
Hoechst	Nucleic acids	-	-	20 µM	PBS	Life Technologies Ltd.

Secondary antibodies

Specificity	Conjugate	Source	Working concentration	Diluent	Company
Rat IgG	AlexaFluor 488	Goat	4 µg/mL	PBS	Abcam
Rabbit IgG	AlexaFluor 488	Goat	4 µg/mL	PBS	Life Technologies Ltd.
Mouse IgG	AlexaFluor 488	Goat	4 µg/mL	PBS	Life Technologies Ltd.

Mouse IgM	AlexaFluor 488	Goat	4 µg/mL	PBS	Life Technologies Ltd.

2.6 TUNEL assay

2.6.1 Staining method

Sections were labelled for apoptosis using the TUNEL assay (Millipore) according to the manufacturer's instructions. All incubations were at room temperature, unless stated otherwise, and took place in a humidified incubation chamber. Briefly, sections were digested with proteinase K for 20 min at 37°C and incubated with end-labelling cocktail for 60 min at 37°C. Sections were blocked with blocking buffer for 20 min and broken DNA was labelled by incubation with Avidin-FITC for 30 min at 37°C. Sections were nuclear stained with TO-PRO-3 and coverslipped with Prolong Gold anti-fade reagent. Positive controls were sections pre-incubated with proteinase K for 60 min at 37°C. Negative controls had the Avidin-FITC incubation step omitted. Labelled sections were stored in the dark prior to imaging to prevent photobleaching.

2.6.2 Confocal microscopy

1024x1024 pixel 8-bit images of labelled sections were obtained by confocal microscopy (Zeiss). Z-stacked images were taken in 1 µm steps through the entire section. Separate channels were used for FITC (488 nm laser with 500-530 nm bandpass filter) and TO-PRO-3.

2.6.3 Image analysis

Images were imported into FIJI and the central z-slice was analysed in each case to prevent inaccuracies caused by overlapping cells. TUNEL staining was quantified as mean green channel intensity for each cell layer, normalised for negative control fluorescence in the respective cell layer.

2.7 Calcein-AM assay

2.7.1 Staining method

At the end of the culture period explants were labelled with Calcein-AM (Biotium, Inc., CA, USA), applied as a 200 µL topical aliquot (10 µM in 1xPBS) for 30 min at 37°C. Controls were incubated with

the same volume aliquot of vehicle only. Explants were washed 3x with 1xPBS, counterstained with

TO-PRO-3, and coverslipped with Prolong Gold anti-fade reagent.

2.7.2 Confocal microscopy

Explants were imaged immediately after labelling to prevent fading of fluorescence. TO-PRO-3 staining

was used to identify the GCL. Z-stacked images (1024x1024 pixels) in 1 µm intervals through the entire

GCL were taken using separate channels for calcein (488 nm laser with 500-530 nm bandpass filter)

and TO-PRO-3. Images were taken at four locations (Figure 2.2).
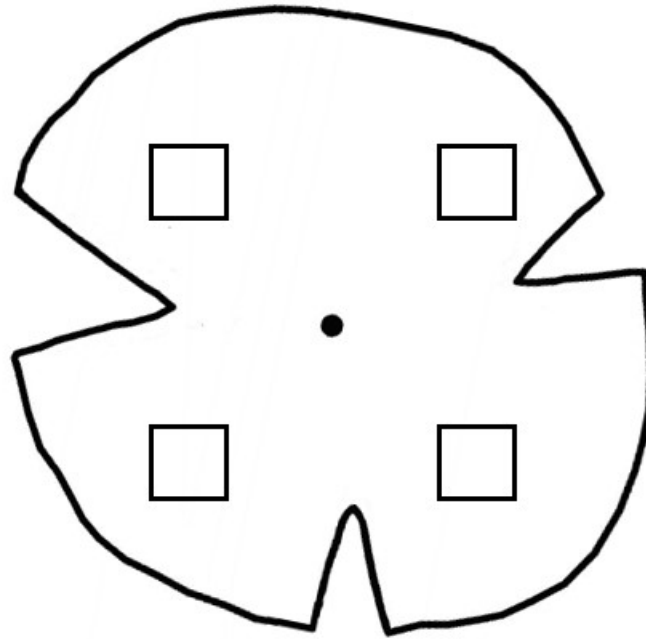
Figure 2.2. Locations imaged for calcein staining. X=0, Y=0 μm was set at the optic nerve and images were collected at the four locations indicated (x=±1000 μm, y=±850 μm).

2.7.3 Image analysis

Calcein positive cells were cells double stained for TO-PRO-3 and calcein. The number of positive cells in a 300x300 μm^2 square were counted in each quadrant of each explant and the mean count was calculated as number of cells/mm^2.

2.8 Diolistics

2.8.1 Bullet preparation

Diolistics bullets were prepared with modifications to the protocol described previously (Gan et al. 2000). 200 mg tungsten particles (1.7 µm diameter) were split between two glass slides. Separately, 3 mg 1-1'-dioctade-cyl-3,3,3',3'-tetramethylindocarbocyanine perchlorate (DiI) and 6 mg 3,3 dioctadecyloxacarbocyanine perchlorate (DiO) were dissolved in 800 µL methylene chloride and mixed with half of the tungsten particles to coat. DiI/DiO-coated tungsten particles were distributed inside Tefzel tubing (Bio-rad, Hertfordshire, UK), which was then sealed at both ends and mounted on a Tubing Prep station (Bio-rad) overnight to ensure even coating. The tubing was wrapped in aluminium foil to protect from light and stored in the dark to prevent photobleaching.

2.8.2 Diolistic labelling method

DiI/DiO-coated tubing was cut into 1.2 cm 'bullets', which were placed inside the cartridge holder of a hand-held Helios gene gun (Bio-rad, Figure 2.3). The gen gun was mounted on a stand (built in-house) to ensure that the barrel was perpendicular to the retinal surface. DiI/DiO-coated tungsten particles were propelled at 120 psi (helium) through a 3 µm polyethylene terephthalate membrane filter (Scientific Laboratory Supplies Ltd.) to prevent clumping. Explants were incubated at 37°C for 30 min to allow the dye to distribute through the cell membranes. Explants were cut out of the culture inserts, mounted on glass slides (Scientific Laboratory Supplies Ltd.), washed with 1xPBS, and fixed in 4% PFA for 10 min in a moist incubation chamber. Explants were washed with 1xPBS and nuclear stained with

TO-PRO-3 for 10 min. Explants were washed with 1xPBS, coverslipped with Prolong gold anti-fade

reagent, sealed with nail varnish, and stored in the dark prior to imaging.

Figure 2.3. Hand-held gene gun for ballistic delivery of lipophilic dye-coated tungsten particles (diolistics). The 'bullets' are loaded in the cartridge holder (white arrowhead). The particles are fired through a 3 μm filter (black arrowhead) into the retina (black arrow), with the barrel (white arrow) at a distance of 5 cm from the explant.

2.8.3 Confocal microscopy

Diolistically-labelled explants were imaged by confocal microscopy (Zeiss) within 24 hours of labelling to prevent fading of fluorescence. RGCs were identified as having a soma in the GCL and an axon projecting towards the optic nerve. 512x512 or 1024x1024 pixel 8-bit z-stacked images were taken in 1 μm intervals through the entire cell, using separate channels for each dye (DiI, 523 nm laser and 565-615 nm bandpass filter; DiO, 488 nm argon laser and 500-530 nm bandpass filter). The eccentricity relative to the optic nerve head was recorded for each cell.

2.8.4 Neuron tracing and Sholl analysis validation

Images were imported into FIJI, split into a single channel image (8-bit), and the dendritic arbor was traced in three-dimensions using the plug-in Simple Neurite Tracer (Longair et al. 2011). The longest primary dendrite was extended back to the soma centre and Sholl analysis (Sholl 1953) was carried out in 10 μm steps up to a maximum radius of 300 μm. For sub-type analysis, RGCs were divided into ON and OFF cells based on their stratification depth. Cells with dendrites terminating in the first 55% of the IPL were classified as ON, those with dendrites terminating in the last 45% of the IPL were OFF, and cells with dendrites in both layers were bistratified.

In order to validate the Simple Neurite Tracer Sholl analysis method, 62 cells were also analysed using the manual method. Concentric rings were digitally traced onto the 8-bit tracing image (Figure 2.4) and the number of dendrites on each ring were counted and plotted as a function of eccentricity. The Sholl profiles for both methods were almost identical and Bland-Altman plots did not indicate the presence of any systematic errors (Binley et al. 2014).
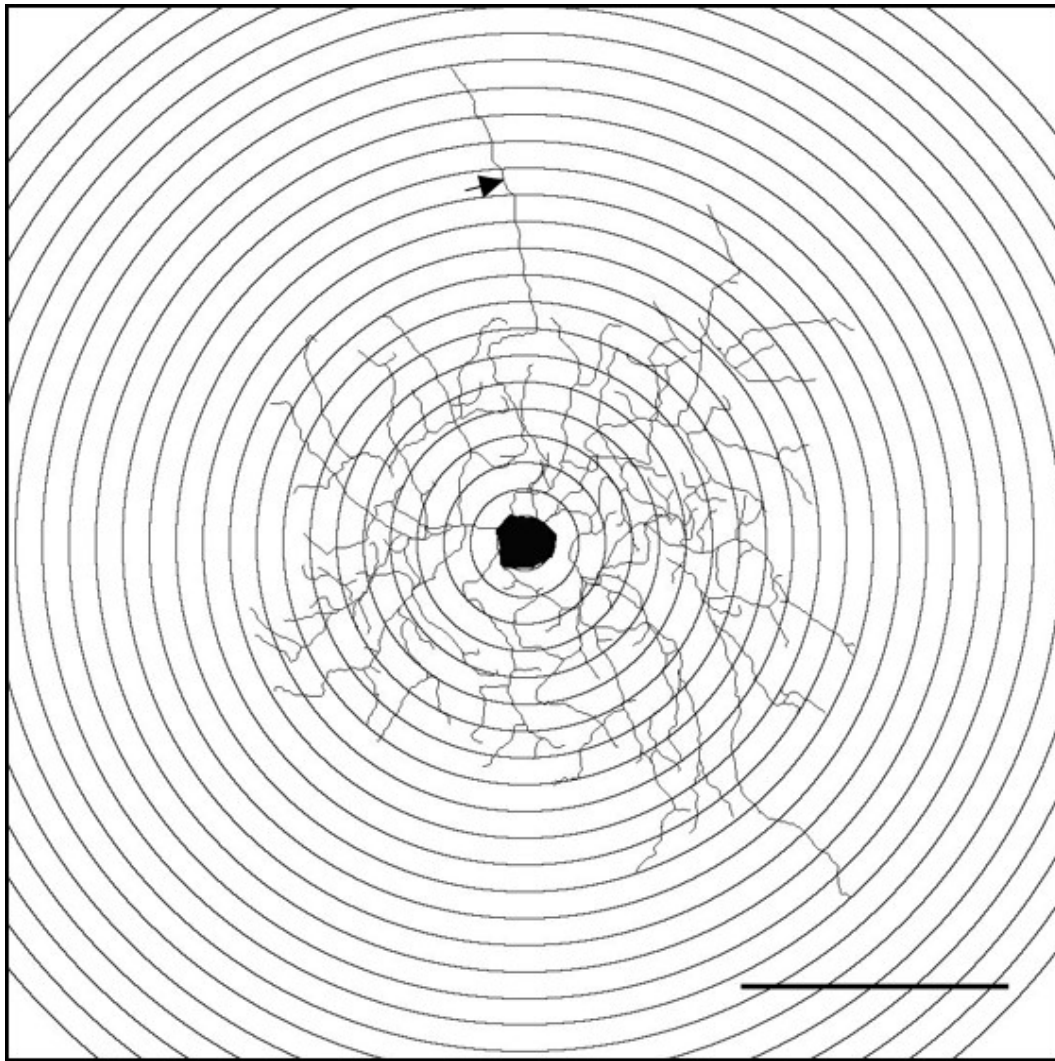
Figure 2.4. 8-bit tracing of RGC with digitally overlain concentric (10 μm apart) circles centred on the soma centre for manual Sholl analysis. The number of dendrites on each ring were counted. Arrow indicates axon (not counted in analysis). Scale bar: 100 μm.

2.8.5 Branching index and dendritic field area calculations

The branching index was calculated using the Sholl analysis output and equation 2.1 (Garcia-Segura and Perez-Marquez 2014),

$$Branching\ index = \sum_{x_{min}}^{x_{max}} [I_x - (I_{x-n})] \cdot x$$

Where $x_{min} = 10\ \mu m$

$\quad x_{max} = 300\ \mu m$

$\quad n = 10\ \mu m$

$\quad [I_x - (I_{x-n})] > 0$

Equation 2.1. Branching index calculation.

The dendritic field area was measured as the area within a polygon connecting the terminal dendrites of a dendritic arbor (Figure 2.5).
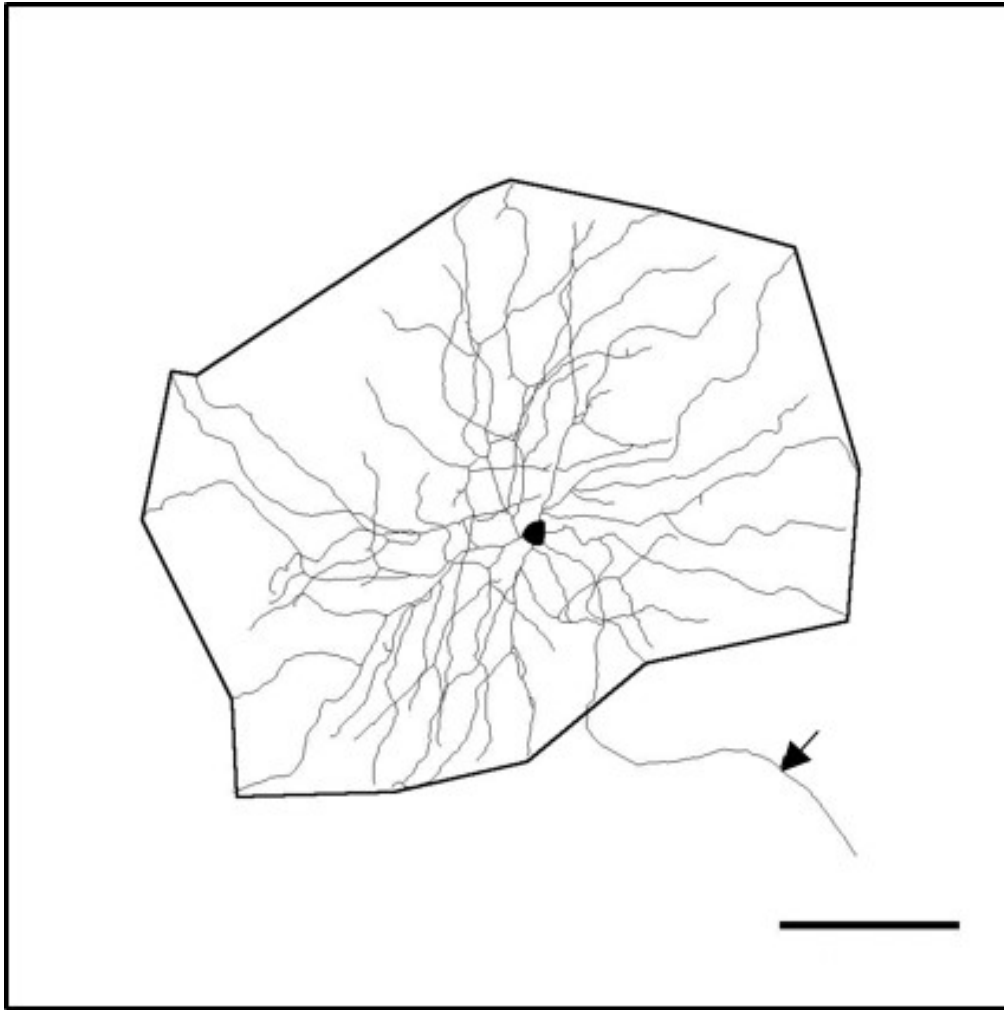
Figure 2.5. Dendritic field area was measured in FIJI by drawing a polygon connecting the terminal dendrites of an 8-bit tracing image. Arrow indicates axon (not included in measurement). Scale bar: 100 μm.

2.9 Bacterial culture and plasmid preparation

For the transformation reaction Luria-Bertani (LB) agar (Sigma-Aldrich) was made at a concentration of 32 g/L in a sterile 250 mL DURAN® bottle. To dissolve, the mixture was microwaved in 30 second periods until boiling and translucent, and autoclaved on a 25 min liquid cycle (135°C) to sterilise. The agar was allowed to cool to approximately 55°C, at which point ampicillin (40 mg/mL stock; 0.2 μm filtered (Scientific Laboratory Supplies Ltd.); Sigma-Aldrich) was added 1:1000 to create a final concentration of 40 μg/mL. The plates were poured (5 mm depth) and allowed to set (20 minutes) with the lids slightly off to allow water to evaporate. The lids were replaced and plates stored inverted to prevent condensation at 4°C.

DH5α cells were used as competent cells. The competent cells and plasmids (PSD-95-GFP, BDNF-myc, CAG-GFP) were put on ice for 2 minutes to defrost. 25 μL competent cells and 1 μL plasmid were added to the same tube, followed by incubation on ice for 30 minutes. The cells were then heatshocked at 42°C for 30 seconds, put on ice for 3 minutes, and 50 μL SOC was added to each tube. The tubes were incubated at 37°C, 200 rpm for 60 minutes. Finally, the cells were plated on LB agar (as described) using glass spreaders (Sigma-Aldrich) and incubated inverted overnight (17-24 hours) at 37°C. Sterile 10 μL pipette tips were used to select individual colonies that were uniform in shape and smaller than 4 mm in diameter. The tips were placed in separate T75 flasks containing 10 mL LB broth (+80 μg/mL ampicillin; Sigma-Aldrich), which were incubated on a rotatory incubator at 37°C, 170 rpm overnight until cloudy.

For the mini-prep reaction, 2 mL culture broth was removed and the plasmid purified as per the manufacturer's protocol. The plasmid concentration was measured using a nanodrop.

2.10 Enzyme-linked immunosorbent assay (ELISA)

2.10.1 Tissue preparation

Explants were cultured as described. At the end of the culture period retinas (left and right retinas pooled) were gently placed into tubes containing 50 µL RIPA buffer + 10 µL protease inhibitor (Roche, Welwyn Garden City, UK) and snap frozen in liquid nitrogen. Samples were stored at -80°C.

Retinas were re-suspended in a total of 300 µL lysis buffer (3.5 mL RIPA buffer + 35 µL protease inhibitor + 35 µL phosphatase inhibitor + 17.5 µL 6-amihexanoic acid + 3.5 µL aprotinin + 3.5 µL phenotroline) and sonicated on ice with a probe sonicator until homogeneity was achieved. Homogenates were kept on ice for 30 min, sonicated on ice, and centrifuged at 1500 rpm, 4°C for 10 min. The supernatants were transferred to clean Eppendorf tubes and the pellets discarded.

2.10.2 Bicinchoninic acid (BCA) assay

The protein concentrations of homogenates were measured using a BCA kit (Life Technologies Ltd.). Nine BSA protein standards (0.20 mg/mL, 0.15 mg/mL, 0.10 mg/mL, 0.075 mg/mL, 0.050 mg/mL, 0.025 mg/mL, 0.0125 mg/mL, 0.00625 mg/mL, 0 mg/mL) were prepared and 100 µL of each standard was added to 100 µL working solution (50 parts reagent A, 1 part reagent B), in triplicate, in a 96-well plate. Tissue samples were run in duplicate; to each well 5 µL sample was added to 95 µL dH$_2$O + 100 µL working solution. The plate was covered and incubated at 37°C for 1 hour and the absorbance at 562 nm was measured using a luminometer (Wallac Victor2 1420 Multilabel Counter; Perkin Elmer, Akron, Ohio, USA).

2.10.3 Sandwich ELISA method

The Sandwich ELISA method is outlined in figure 2.6. The wells of a 96-well plate were coated with 200 µL/well of 3 µg/mL mAb#1 in coating buffer (50 mM NaHCO$_3$, 50 mM Na$_2$CO$_3$, pH 9.7). The plate was covered and incubated overnight at RT. The coating solution was removed and the plate washed 3x with washing buffer (1xPBS, 0.1% Tween-20). 200 µL/well blocking buffer (1xPBS, 4% BSA (Sigma-

Aldrich)) was incubated for 2 hours at 30°C. The plate was washed 3x with washing buffer. 150 µL/well

incubation buffer (0.1 M KH_2PO_4, 0.1 M Na_2HPO_4, pH 7.6) was added, along with 50 µL/well sample or

standard (25 ng/mL, 12.5 ng/mL, 6.25 ng/mL, 3.13 ng/mL, 1.56 ng/mL, 0.781 ng/mL, 0.391 ng/mL,

0.195 ng/mL, 97.7 pg/mL, 48.8 pg/mL, 24.4 pg/mL, 12.2 pg/mL, 0 pg/mL) in triplicate, and incubated

for 3 hours on a rotating platform (300 rpm) at RT. The plate was washed 5x with washing buffer and

200 µL/well 1:4000 (diluted in incubation buffer + 4% BSA) mAb#9 (3.8 µg/µL stock) conjugated to

horseradish peroxidase (HRP; Roche) was added and the plate incubated for 3 hours on a rotating

platform (300 rpm) at RT. The plate was washed 5x with washing buffer. 100 µL/well

chemiluminescent substrate (Roche) was added and luminescence measured using a luminometer.
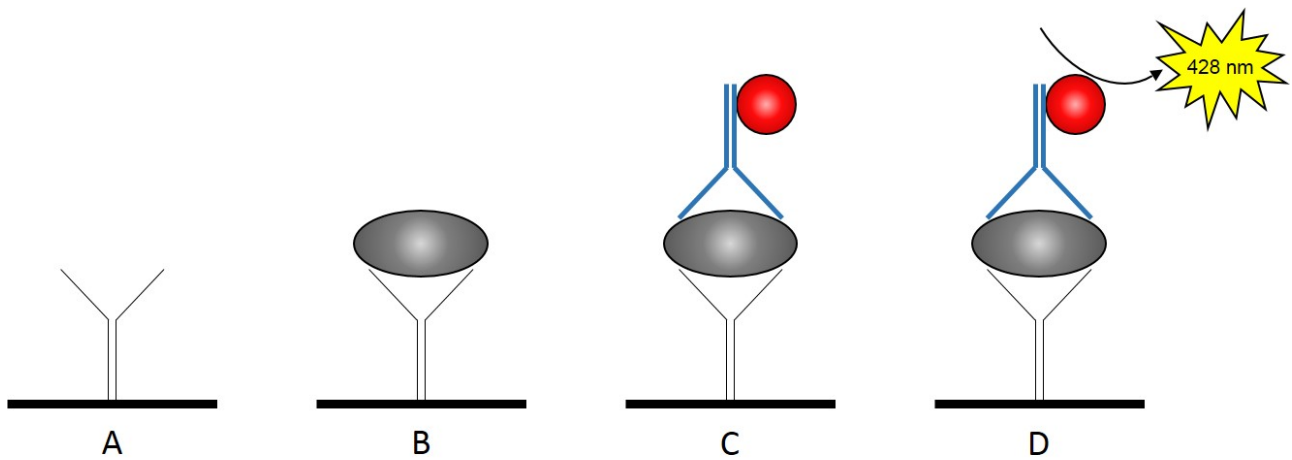
Figure 2.6. Sandwich ELISA method. (**A**) The plate is coated with mAb#9. (**B**) After blocking, the homogenised sample tissue is added to the plate and the target protein (BDNF) binds to the antibody. (**C**) The detecting Ab (mAb#9 conjugated to HRP) is added and binds to BDNF. (**D**) The substrate (luminol) is added and HRP catalyses the oxidation of luminol into 3-aminophthalate. This reaction is accompanied by a 428 nm emission, which is detected by the luminometer and can be converted into protein concentration.

2.11 NSC culture

All work with NSCs was carried out in a laminar flow hood using sterile equipment to minimise risk of contamination. NSCs were originally isolated from lysed whole brains of transgenic C57/Bl6 mice with GFP downstream of the actin promoter. NSCs were cultured in 12 mL DMEM/F-12 medium (+)L-glutamine (+)HEPES, supplemented as outlined in Table 2.4, at 37°C, 5% CO_2. The culture medium was made up in a sterile 100 mL DURAN® bottle and used immediately. Cells were cultured in upright T25 flasks to prevent adherence to the side of the flask, which stimulates auto-differentiation. Cells were grown as neurospheres and split weekly to twice-weekly to prevent cell death in the centre of the neurospheres. To split NSCs, T25 flask contents were decanted into 25 mL universal tubes and spun at 1000 rpm for 5 min. The medium was aspirated, cells were re-suspended in 2 mL Accutase® (Life Technologies Ltd.) and incubated in a 37°C water bath for 10-30 min, or until the neurospheres were no longer visible. Cells were then spun at 1000 rpm for 5 min, the Accutase® was aspirated and cells were re-suspended in the previously aspirated 12 mL medium. Finally, cells were split into 2 sterile T25 flasks (6 mL each) and flasks were topped up to 12 mL using freshly prepared DMEM/F-12, supplemented as described previously, and flasks were replaced at 37°C, 5% CO_2.

Table 2.4. Culture medium and supplements for NSC culture.

Component	Concentration	Role	Company
DMEM/F-12 (+)L-glutamine (+)HEPES	As supplied	Maintenance of mammalian cells in culture.	Life Technologies Ltd.
Penicillin-Streptomycin	1% (100 U/mL penicillin; 100 µg/mL streptomycin)	Antibiotics to minimise contamination caused by both gram-positive and gram-negative bacteria.	Life Technologies Ltd.
Non-Essential Amino Acids Solution	1%	Growth and viability of cells.	Life Technologies Ltd.
B-27 supplement	2%	Supports growth and viability of CNS neurons.	Life Technologies Ltd.
Fibroblast growth factor	10 ng/mL	Maintenance of stem cells in an undifferentiated state.	Peprotech, London, UK
Epidermal growth factor	10 ng/mL	Mitogenic factor.	Peprotech
Accutase®	As supplied	Protease/collagenase to dissociate NSCs. Gentler action than trypsin.	Life Technologies Ltd.

2.12 Magnetic field manipulation of NSC migration

Ten µg/mL laminin was prepared by diluting 1 mg/mL stock laminin in PBS (pH 7.4), followed by filtration through a 0.2 µm filter to sterilise. 1.5 mL 10 µg/mL laminin was added to each 35 mm culture dish and allowed to coat the bottom of the dish for 2 h in a class II hood. Dishes were washed with sterile PBS and allowed to dry for 15 min. Laminin-coated dishes were stored for up to 1 month, sealed, at 4°C prior to use.

To seed NSCs, the laminin-coated dishes were first pre-conditioned with 1.5 mL DMEM/F-12 per dish for 5 min at RT. Meanwhile, NSCs were dissociated with Accutase® to obtain single cells in suspension. The medium in the pre-conditioned dishes was replaced with 3 mL NSC suspension, plated at a density of 1.2-1.9 X 10^5 cells/cm^2. The cells were incubated overnight at 37°C, 5% CO_2 to allow adherence to laminin.

Iron nanoparticles (100 nm diameter; nTMag, Nanotherics Ltd., Newcastle under Lyme, UK) were introduced into the NSCs using a magnefect nano II (Nanotherics). 1.5 µL or 3 µL mnps were inserted into the culture medium of the seeded NSCs and the 35 mm dish was placed on one of the 35 mm magnets of the 6-well plate magnefect plate. The magnefect was placed at 37°C, 5% CO_2 and the introduction of nanoparticles into the cells was stimulated for 30 min using 0.2 mm displacement at 2 Hz. The medium was replaced with Accutase® and cells were incubated at 37°C, 5% CO_2 for 5-10 minutes until >90% of cells had dissociated from the laminin. Cells were spun down at 1000 rpm for 5 minutes and resuspended in culture medium in a clean 35 mm dish. NSCs were immediately imaged by brightfield microscopy using an inverted lens (X10). Images of NSCs in suspension were collected every 2.5 seconds for a total of 125 seconds, and images of NSCs on the bottom surface of the dish were collected every minute for a total of 9 minutes. To investigate the effect of magnetic fields on NSC migration, a 6.7 kg, 23 kg or 38 kg-pull permanent NdFeB magnet (Supermagnete, Germany) or a 25 kg-pull electromagnet (EmagnetsUK, Hertfordshire, UK; operated at 0.2 A, 24 VDC) was positioned against the edge of the culture dish (6.7 kg-pull magnet) or 10 mm away from the edge of the culture

dish (all other magnets). The magnet properties are outlined in Table 2.5 and the theoretical magnetic field strengths are shown in Figure 2.7. The imaging protocol described previously in the absence of magnet were then repeated. Imaging was always carried out immediately after the introduction of mnps as nanoparticles are degraded by cells as part of their normal iron metabolism pathway (Bulte and Kraitchman 2004) and to prevent NSCs adhering to the dish surface.

The magnetic field strengths for all the magnets at the distances used were measured using a Gaussmeter (built in-house, Dr. Turgut Meydan group, Wolfson Centre for Magnetics, Cardiff University). The theoretical field strengths, calculated using Equation 2.2, are shown in Figure 2.7.

Table 2.5. Magnet properties for migration of NSCs. All magnets are cylindrical. Flux density values from http://www.ndfeb-info.com/neodymium_grades.aspx, last accessed 27.02.16.

Magnet (grade)	Diameter (mm)	Height (mm)	Residual flux density, Br (mT)	Pull-force (kg)
NdFeB (N42)	15	8	1280	6.7
NdFeB (N42)	30	15	1280	23
NdFeB (N45)	35	20	1320	38
Electromagnet	18	20	-	25

$$B(X) = \frac{Br}{2}\left[\left(\frac{H+X}{\sqrt{R^2+(H+X)^2}}\right) - \left(\frac{X}{\sqrt{R^2+X^2}}\right)\right]$$

Where   B = Magnetic flux density

X = distance from magnet surface

Br = Residual flux density

H = Height of magnet

R = Radius of magnet

Equation 2.2. Magnetic field strength, B, for permanent cylindrical magnets at a given distance from the magnet surface (https://product.tdk.com/en/products/magnet/pdf/e371_circuit.pdf, last accessed 28.02.16).
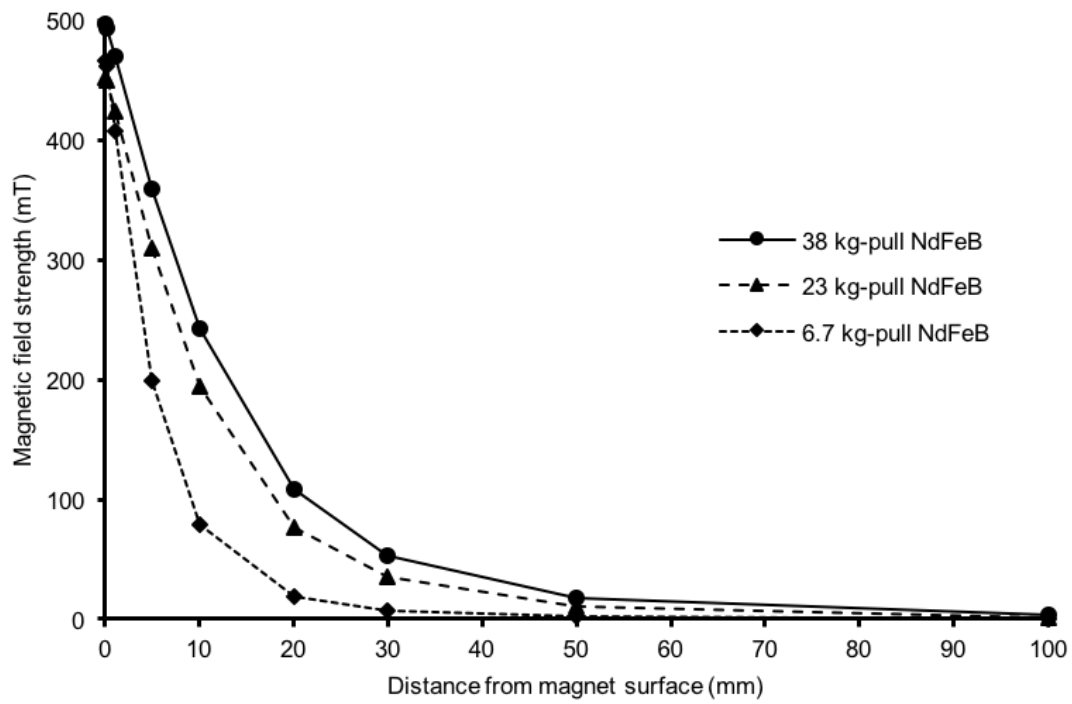
Figure 2.7. Hypothetical magnetic field strengths of all NdFeB magnets used as a function of distance from the magnet surface calculated using the properties in Table 2.5 and Equation 2.2.

Images were exported as TIFF files and imported into FIJI for cell tracking analysis. To measure the

migration paths of the cells, the manual tracking plugin (http://fiji.sc/Manual_Tracking; last accessed

14.01.16) was used to track all cells present in the first 1200 μm from the edge of the dish next to the

magnet surface (6.7 kg-pull magnet) or in the first 900 μm from the edge of the dish (all other

magnets). The track data were then imported into Chemotaxis plugin

(http://ibidi.com/xtproducts/en/Software-and-Image-Analysis/Manual-Image-Analysis/Chemotaxis-

and-Migration-Tool; last accessed 14.01.16), which was used to analyse the mean accumulated

distance, mean euclidean distance (figure 2.8), mean velocity, x forward migration index, y forward

migration index, x centre of mass, and y centre of mass for all experiments. Equations S1-S4 for all

calculated indices can be found in the Appendix.
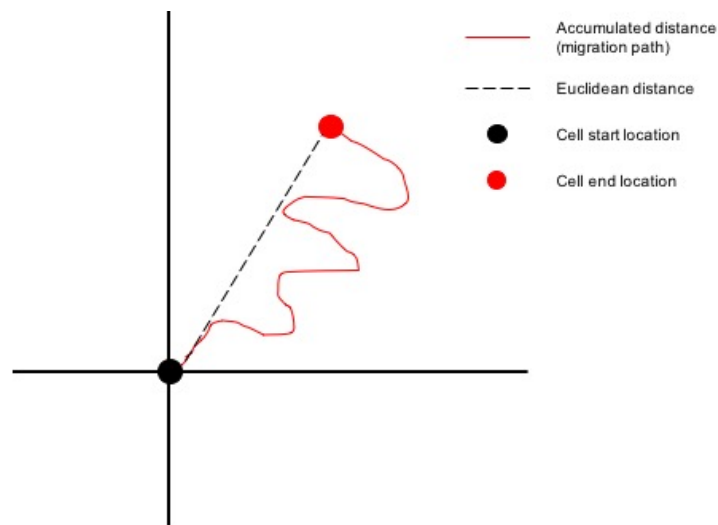
Figure 2.8. The accumulated distance is calculated as the distance covered by a cell throughout its migration track. The euclidean distance is the straight-line distance connecting the start and end positions of the cell, as shown. Both distances are calculated automatically using the Chemotaxis plugin.

2.13 Cell transplantation into explants

To test the depth and speed of migration of NSCs within tissue, retinal explants were prepared as described in 2.2 and a topical 2 mL aliquot of NSCs immediately post-splitting (re-suspended in NSC culture medium) at a density of 1×10^5 cells/cm^2 was placed directly on the explant. The explant was incubated at 37°C, 5% CO_2 for 3 h with the 35 mm dish positioned on top of a 38 kg-pull magnet, or on the incubator shelf only as control. At the end of the culture period the explant was fixed in 4% PFA for 15 minutes, nuclear stained using TO-PRO-3 (10 min), and coverslipped with Slo-fade diamond mountant (Invitrogen). Explants were immediately imaged by confocal microscopy using the 633 nm laser for TO-PRO-3 visualisation, and the 488 nm argon laser (500-530 nm bandpass filter) for GFP. The stage was centred on the optic nerve (X=0, Y=0) and four z-stacked images in each quadrant of the retina were collected. Z-stacked 1024x1024 pixel 8-bit images were taken in 1 μm slices from the start of the GCL to the INL. The green channel settings were kept constant for all images. Images were imported into FIJI and in each case the depth of the IPL was measured. All GFP+ve cells were drawn around using the polygon tool and the green channel intensity was measured in every slice. The green channel intensity was expressed as % IPL depth.

Chapter 3: Characterisation of the Mouse Retinal Explant

3.1 Introduction

The murine retinal explant remains a popular model for the investigation of CNS disorders (Johnson and Martin 2008; Guerin et al. 2011; Wood et al. 2011). Since the neuronal cell loss resulting from axotomy performed at the time of dissection is a common end point in all neurodegenerative diseases, this model has widespread applications. Further, short experimental time and the acquisition of translatable data are major advantages of the explant over in vivo and in vitro models, respectively. The primary readout for this model is typically cell loss, which fails to provide information regarding synaptic and structural changes to the cells prior to cell death, nor does it allow investigation of mechanisms under a pathological state. The lack of morphometric data is a major limitation of this work to date.

Predicated on widespread evidence that dendritic pruning precedes cell loss in neurodegenerative diseases including Parkinson's disease (Patt et al. 1991), Alzheimer's disease (Selkoe 2002) and glaucoma (Weber et al. 1998), I investigated whether morphometric analysis of RGC dendritic arbors could provide information about neuronal cell health. Sholl analysis (Sholl 1953) quantifies dendrites as a function of eccentricity, with loss of distal dendrites manifesting as a leftward shift in the Sholl profile, and a reduced peak amplitude indicates a loss of proximal dendrites. The data from Sholl analysis can be used to derive the branching index, described by Garcia-Segura and Perez-Marquez (Garcia-Segura and Perez-Marquez 2014), which quantifies the shape of the dendritic arbor (Figure 3.1).

Branching index: 2   8   13   36
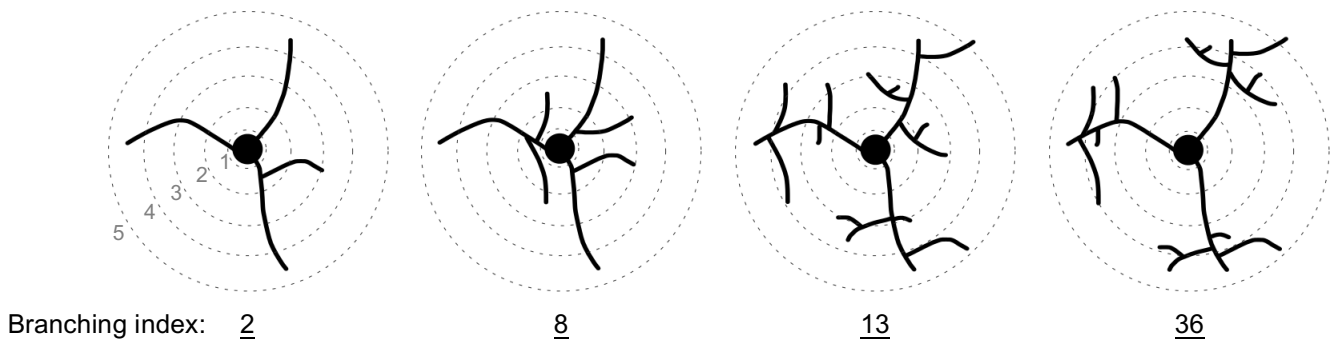
Figure 3.1. The branching index is an indicator of cell shape. A small branching index indicates a low number of branching events or that branching is predominantly proximal. A large branching index indicates a high number of branching events or that branching mainly occurs distally. Note that the two cells on the far right have the same number of dendrites, but due to different branching eccentricities they have very different branching indices. The branching index is calculated using Equation 2.1 (see Materials and Methods).

In order to quantify dendritic arbors, cells must be discretely labelled. Morphologically, RGCs are an extremely heterogeneous population of neurons; their shape varies with sub-type as well as eccentricity (Sun et al. 2002; Coombs et al. 2006). In order to reduce bias, it is essential that labelling is random. Techniques such as the use of transgenic animals that rely on reporter gene expression are inherently biased since they select for the healthiest cells that can afford the energy demands of translating reporter proteins. Consequently, the unhealthiest cells, which may have undergone the greatest morphological changes, are less likely to express the reporter protein, thus resulting in underreporting of dendritic pruning, as demonstrated by Williams et al. (2013a). Further, the expression of Thy1, a commonly used driver for RGC-specific expression, has been found to be both downregulated (Huang et al. 2006) and upregulated (Lee et al. 1998; Astafurov et al. 2014) following optic nerve injury or stress. Single cell filling is technically challenging and may be biased towards larger cells. Retrograde labelling commonly results in dense staining patterns and requires an intact axon, which may result in bias towards cells resistant to axonal degeneration or cells with more efficient axonal transport machinery. Ballistic delivery of dye particles (diolistics) or plasmids (biolistics) labels cells in a random manner. Since biolistics requires a 2 d incubation period to permit sufficient expression levels of XFP and the only requirement for successful diolistics labelling is an intact plasma membrane, I used diolistics to label RGCs for their morphometric analysis over a 3 day period. This was compared to cell counts data in order to delineate degenerative events in this model.

3.2 Gross tissue morphology

En-face photographs were taken of 4 explants immediately after dissection, after 6 h, 1 d and daily thereafter up to 14 d. Images were used to measure the surface area of explants in order to account for potential oedema, which has been reported to occur in organotypic culture (Wurm et al. 2009). Measurements indicated no significant change in area (P>0.05 by ANOVA with TUKEY post-hoc) throughout the 14 d culture period (Figure 3.2).
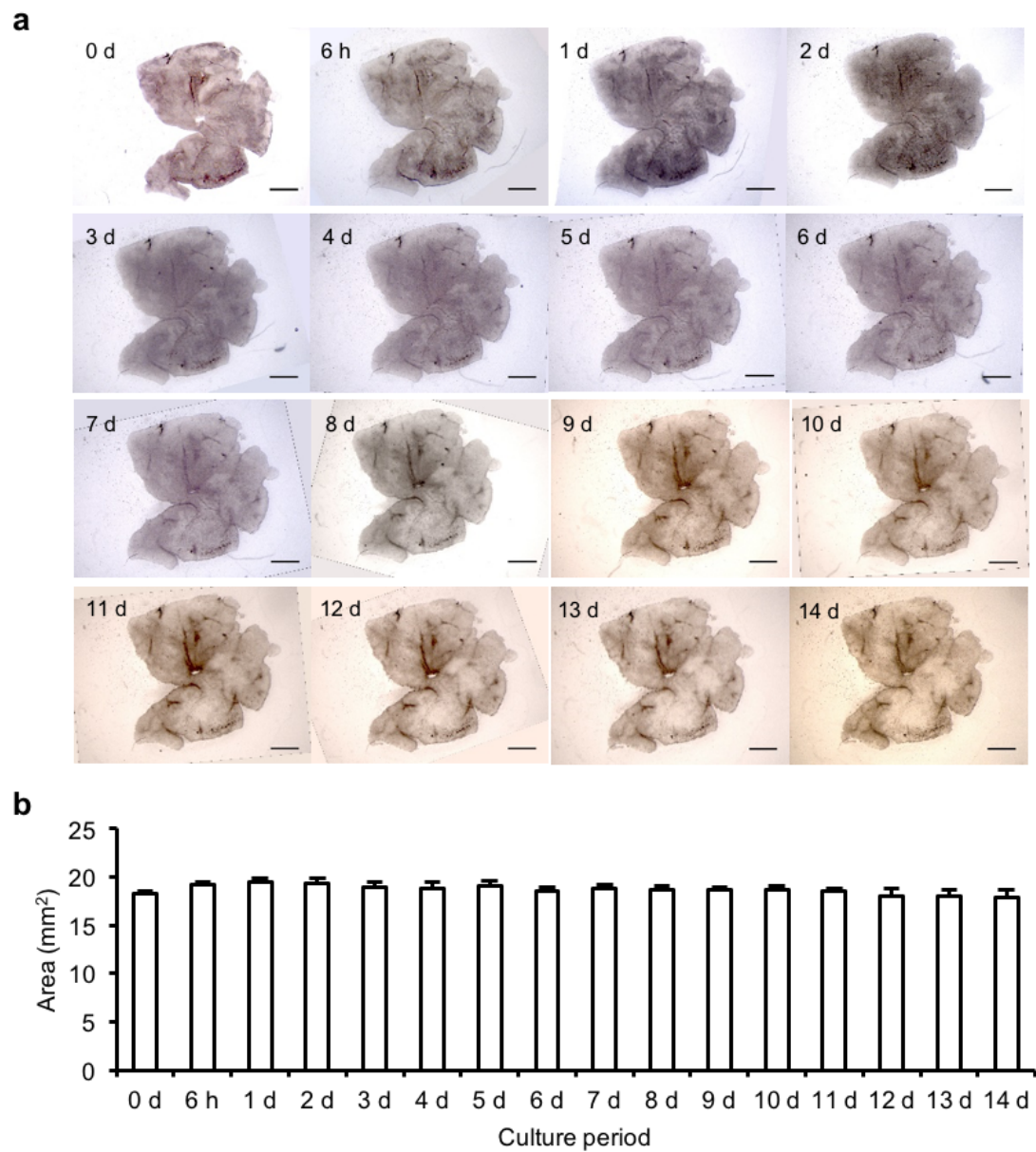
Figure 3.2 Gross tissue area measurements of explants cultured for up to 14 d. (**a**) En face photographs of explants at each time point. (**b**) Mean areas of explants. P>0.05, ANOVA with TUKEY post-hoc. Scale bar: 1 mm. Error bars: SEM. N=4 retinas, 4 animals for all time points.

3.3 Retinal layer architecture

Cryosections of 18 explants cultured for up to 14 d were nuclear stained, with half of sections in each group defined as peripheral and the remainder as central. To minimise the effects of oedema, linear cell counts of the GCL were made. Cell layer thickness was measured for the INL and ONL to complete histological analysis of cell layers.

GCL nuclear counts remained relatively constant until 14 d, when there was a decrease of 37.5% (P=0.001 by ANOVA with Tukey post-hoc). The INL and ONL both showed thinning after 3 d, which subsequently plateaued. The INL thickness reduced by 24.5% (P<0.001 by ANOVA with TUKEY post-hoc) after 3 d, and 25.2% (P<0.001) by 14 d. The ONL thickness reduced by 16.4% (P<0.001 by Mann-Whitney with Bonferroni correction) after 3 d, and by 25.3% (P<0.001) by 14 d (Figure 3.3).
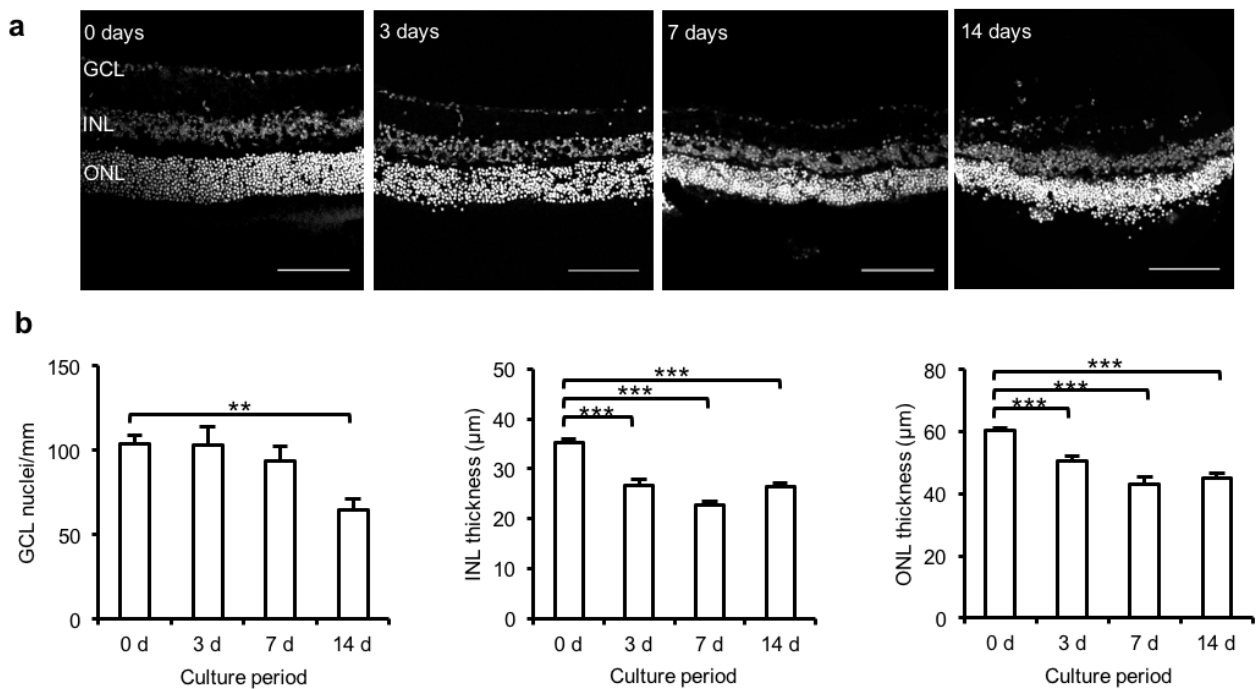
Figure 3.3. Retinal cell layer measurements for explants cultured for up to 14 days, as shown. (**a**) Confocal images of TO-PRO-3 stained sagittal cryosections. (**b**) Nuclei counts for GCL (*left*) and measured thicknesses of INL (*middle*) and ONL (*right*). **$P<0.005$, ***$P<0.001$, ANOVA with TUKEY post-hoc (GCL and INL), Mann-Whitney with Bonferroni correction (ONL). Scale bar: 100 µm. Error bars: SEM. N=5 retinas (0 days), n=6 retinas (3 days), n=3 retinas (7 days), n=4 retinas (14 days). GCL=ganglion cell layer, INL=inner nuclear layer, ONL=outer nuclear layer. At least 3 sections from each retina were used at each time point.

3.4 Thy1.2 and active caspase-3 levels

Frozen sections of explants cultured for 0 d, 3 d, 7 d and 14 d were analysed immunohistochemically for the expression of neuronal marker Thy1.2 and apoptotic marker active caspase-3. Thy1.2 levels were significantly higher in the GCL and IPL relative to the other layers, and could therefore be used to successfully identify the GCL at all time points. In the GCL and IPL Thy1.2 staining significantly increased after day 0 (3.5-fold increase at day 3, $P<0.005$, ANOVA with TUKEY post-hoc), and remained elevated for the remainder of the experiment (Figure 3.4a-b). The number of active caspase-3 positive cells in the GCL and INL showed a trend of increasing with the number of days cultured but this did not reach statistical significance ($P>0.05$, Mann-Whitney tests with Bonferroni correction; Figure 3.4c-e). After 14 d active caspase-3 staining increased 4.4-fold ($P<0.05$, Mann-Whitney tests with Bonferroni correction) in the ONL (Figure 3.4f).
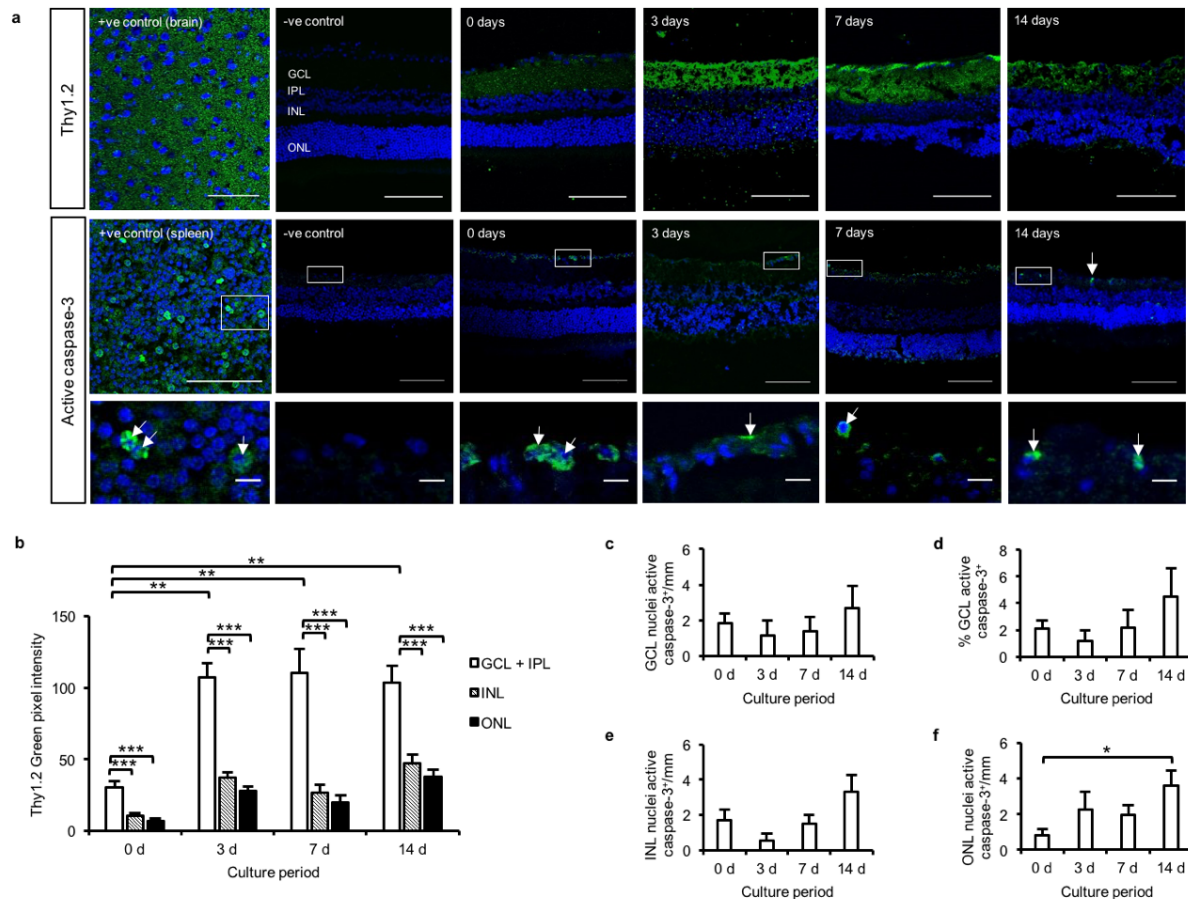
Figure 3.4. Immunohistochemistry staining for the neuronal marker Thy1.2 and the apoptotic marker active caspase-3. (**a**) Frozen sections of retinas cultured for up to 14 d, as indicated. White arrows indicate active caspase-3 positive cells in magnified sections of the above images, as indicated. Scale bars: 100 μm (*top* and *middle*); 10 μm (*bottom*). (**b**) Quantification of Thy1.2 staining in each layer measured by mean green channel intensity. **P<0.005, ***P<0.001, ANOVA with TUKEY post-hoc. (**c**) The number of active caspase-3 positive cells in the GCL. (**d**) The number of active caspase-3 positive cells in the GCL expressed as a percentage of total number of cells in the GCL. (**e**) The number of active caspase-3 positive cells in the INL. (**f**) The number of active caspase-3 positive cells in the ONL. *P<0.05, Mann-Whitney with Bonferroni correction. Error bars: SEM. Thy1.2: n=3 retinas, 2 animals (0 d); n=3 retinas, 3 animals (3 d); n=3 retinas, 3 animals (7 d); n=5 retinas, 5 animals (14 d). Active caspase-3: n=5 retinas, 3 animals (0 d); n=3 retinas, 3 animals (3 d); n=3 retinas, 3 animals (7 d); n=5 retinas, 5 animals (14 d).

3.5 Cell viability in the degenerating explant

Frozen sections of explants cultured for 0 d, 3 d, 7 d and 14 d were analysed for DNA breakdown, a marker of apoptosis, by TUNEL assay. In all layers there was minimal staining at day 0. In the GCL staining peaked at day 3 (4.0-fold increase, $P<0.001$). In the other two layers staining peaked at day 7 (INL 3.5-fold increase, $P<0.05$; ONL 24-fold increase, $P<0.001$, Mann-Whitney tests with Bonferroni correction for all; Figure 3.5).
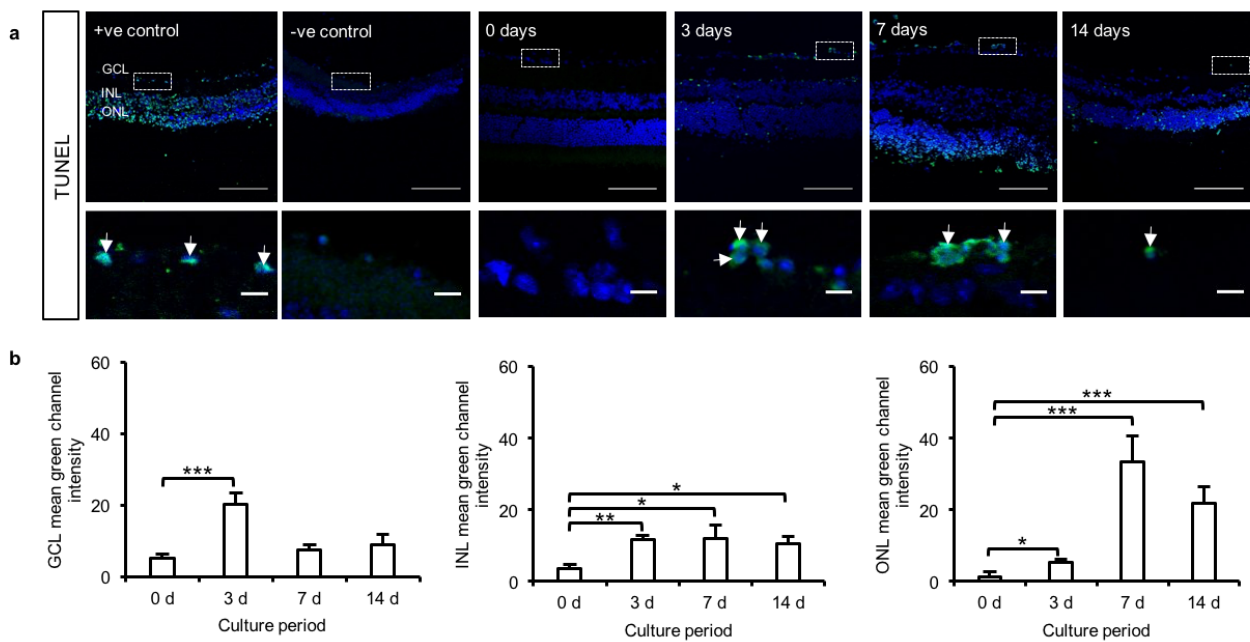
Figure 3.5. TUNEL staining. (**a**) Frozen sections of retinal explants cultured for up to 14 d labelled for DNA breakdown using TUNEL assay. TUNEL positive cells are stained for both FITC (green) and TO-PRO-3 nuclear stain (blue). Positive controls were sections pre-incubated in proteinase K for 1 hour. Negative controls had no incubation with Avidin-FITC. White arrows indicate TUNEL positive cells in magnified sections of the above images, as indicated. Scale bars: 100 μm (*top*), 10 μm (*bottom*). (**b**) Quantification of TUNEL staining in each layer measured by green channel fluorescence. *P<0.05, **P<0.005, ***P<0.001 (Mann-Whitney with Bonferroni correction). Error bars: SEM. N=4 retinas, 3 animals (0 d); n=4 retinas, 4 animals (3 d); n=3 retinas, 3 animals (7 d); n=3 retinas, 3 animals (14 d).

The number of viable cells was quantified in 13 whole, unfixed explants cultured for 0 d, 1 d, 7 d and 14 d using the calcein-AM assay. Calcein-AM passes across cell membranes and if the cell contains active esterases, the AM is cleaved, allowing the fluorescent protein, calcein, to be quantified as a measure of cell viability (Decherchi et al. 1997). Although there was a trend towards a decrease in calcein positive cells after 1 d, this did not reach statistical significance at any point (P>0.05, ANOVA with TUKEY post-hoc). Indeed, it was noted that there was a large amount of variation between explants at the same culture period, as indicated by the large error bars in Figure 3.6.
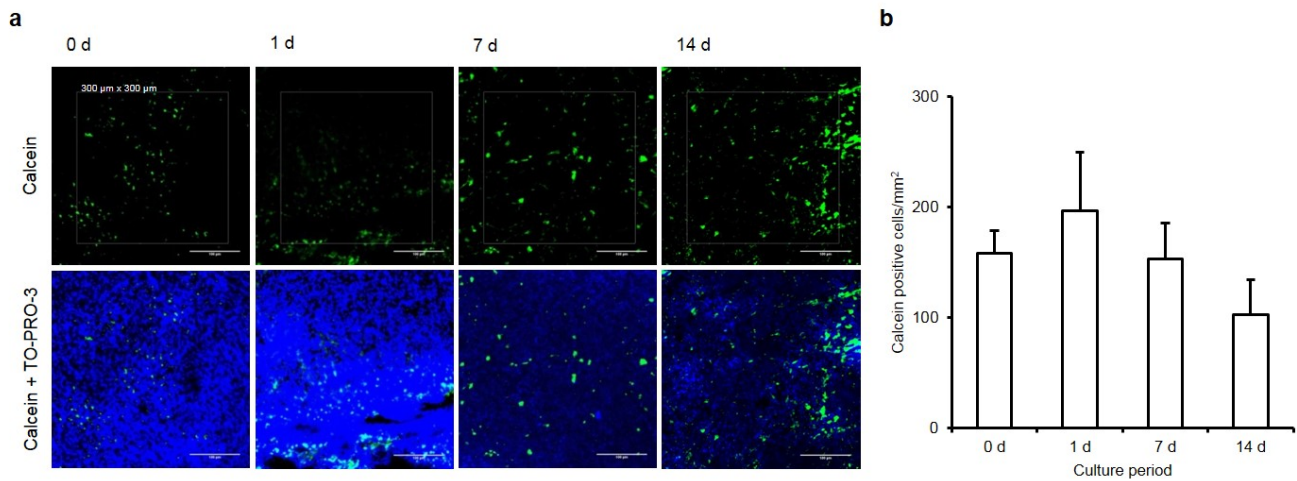
Figure 3.6. Calcein staining. (**a**) En face images of retinal wholemounts stained with calcein (green) and TO-PRO-3 (blue) immediately after dissection (0 d) and after 1, 7 and 14 days in culture, as indicated. Cells stained for both calcein and TO-PRO-3 were counted in the central 300x300 µm, as shown. Scale bars: 100 µm. (**b**) Quantification of calcein staining measured as number of calcein positive cells per mm^2 at the same locations in each explant (x=1000 µm, y=850 µm; x=1000 µm, y=-850 µm; x=-1000 µm, y=-850 µm; x=-1000 µm, y=850 µm where the origin is the optic nerve as described in Figure 2.2). Error bars: SEM. N=4 retinas, 4 animals (0 d), n=3 retinas, 3 animals (1 d), n=3 retinas, 3 animals (7 d), n=3 retinas, 3 animals (14 d). P>0.05, ANOVA with TUKEY post-hoc.

3.6 Morphometric analysis of RGCs over 3 days

One hundred and ninety-five RGCs from fifty explants (n=38 animals of both sex, aged 1.5 – 5 months) cultured for 0 d, 6 h, 1 d, 2 d and 3 d were labelled diolistically and their dendritic arbors quantified by Sholl analysis. There was an obvious loss of dendrites over the 3 d culture period (Figure 3.7a-c), which was quantified as a leftward shift in the Sholl profile over the first 24 h, proceeded by a reduction in peak amplitude between day 1 and day 2 (Figure 3.7d). The Sholl area under the curve (AUC) decreased by 14.5% (P<0.05) after 6 h, and continued to decrease by a maximum of 56.7% (P<0.001, Mann-Whitney tests with Bonferroni correction for both) at day 3 (Figure 3.7e). The branching index decreased by 41.9% (P<0.005, ANOVA with TUKEY post-hoc) after 1 d and remained relative constant thereafter (Figure 3.7f).

In order to account for sub-type bias, all RGCs were grouped based on stratification depth and categorised as ON, OFF or bistratified (see section 2.8.4). There was no significant difference in Sholl AUC between sub-groups within the same culture period (P>0.05). Sholl AUC showed a general trend of reducing with increased culture period, irrespective of sub-group. ON cells showed a reduction in Sholl AUC of 49.0% (P<0.001) after 2 d and 61.0% (P<0.001) after 3 days (Figure 3.7g). OFF cells had a decreased Sholl AUC of 37.9% (P<0.005) after 1 day and 30.1% (P<0.05) after 2 days (Figure 3.7h). The Sholl AUC of ON-OFF cells was reduced by 49.9% (P<0.05, Mann-Whitney tests with Bonferroni correction for all) after 2 days (Figure 3.7i).
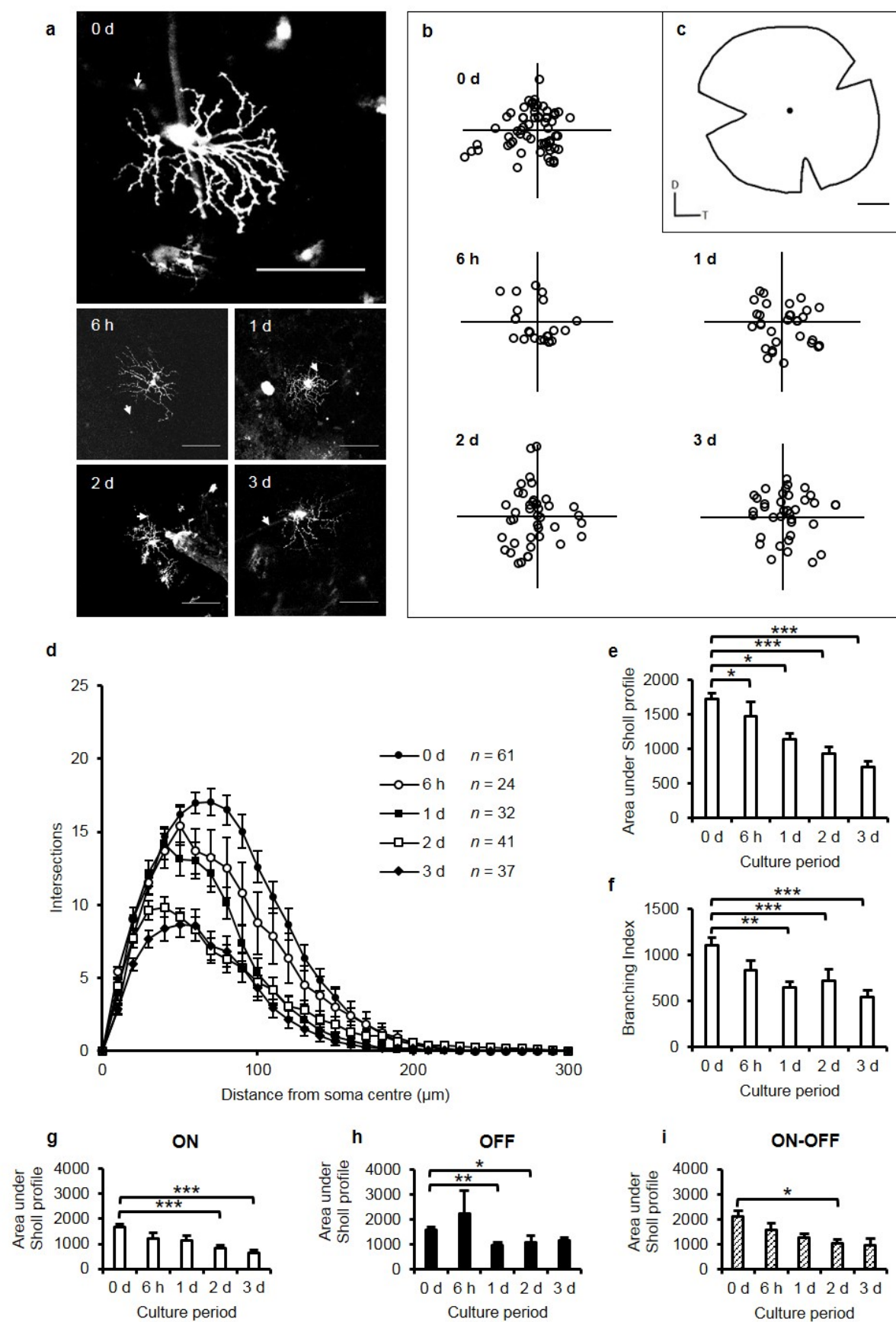
Figure 3.7

Figure 3.7 (previous page). Morphometric analysis of RGCs. (**a**) Representative fluorescent images of RGCs labelled by diolistics after 0 days, 6 hours, 1 day, 2 days, and 3 days explant culture, as shown. Images are 512x512 pixels (0 d) or 1024x1024 pixels (rest). Scale bars: 100 μm. Arrows indicate axons. (**b**) Locations of all analysed RGCs at each time point where the origin in the optic nerve. All plots show no evidence of bias in terms of eccentricity. (**c**) Diagram of prepared explant for orientation of location plots. D = dorsal, T = temporal. Scale bar: 1 mm. (**d**) Sholl profiles for RGCs at each time point, with the number of cells indicated. (**e**) Sholl AUC at each time point calculated using the trapezoidal model. (**f**) Branching index for RGCs at each time point, calculated using the Sholl analysis output as described in chapter 2.8.5. (**g**) Sholl AUC plots for ON stratifying cells only. N=28 cells (0 d), n=14 cells (6 h), n=13 cells (1 d), n=26 cells (2 d), n=28 cells (3 d). (**h**) Sholl AUC plots for OFF stratifying cells only. N=12 cells (0 d), n=4 cells (6 h), n=8 cells (1 d), n=8 cells (2 d), n=5 cells (3 d). (**i**) Sholl AUC plots for ON-OFF stratifying cells only. N=11 cells (0 d), n=6 cells (6 h), n=11 cells (1 d), n=7 cells (2 d), n=4 cells (3 d). *P<0.05, **P<0.005, ***P<0.001 (Mann-Whitney tests with Bonferroni correction for all Sholl AUC; ANOVA with TUKEY post-hoc for branching index). Error bars: SEM.

To check that labelling was random, all 61 cells labelled at 0 d were classified according to the RGC classification system outlined by Sun et al. using soma diameter, DF diameter and stratification depth (Sun et al. 2002). The proportion of cells in each classification group were found to be similar to those reported by Sun et al. and more importantly, there was a good spread of different sub-types of RGC labelled (Table 3.1).

Table 3.1. Proportion of RGC sub-types from 0 d explants classified according to Sun et al., 2002.

Group	Number	% of population	% in Sun et al.
A1	2	3.3	4.5
A2	8	13.1	5.5
Total A	**10**	**16.4**	**10.0**
B1	4	6.6	4.5
B2	2	3.3	9.0
B3	11	18.0	10.6
B4	3	4.9	5.7
Total B	**20**	**32.8**	**29.8**
C1	1	1.6	3.1
C2	8	13.1	10.2
C3	0	0.0	2.4
C4	2	3.3	5.9
C5	3	4.9	11.2
C6	4	6.6	4.5
Total C	**18**	**29.5**	**37.3**
D1	3	4.9	7.3
D2	10	16.4	15.5
Total D	**13**	**21.3**	**22.8**

In order to check that there were no confounding variables that may have affected Sholl analysis data, a multiple regression analysis was carried out on all Sholl AUC results from all explants cultured for 0 – 3 days. The dependent variable was AUC, and the independent variables were culture period, age, and sex. This regression model was described to be a good fit of the data (P<0.001, ANOVA). Culture period was the only explanatory variable of Sholl AUC (B = -228, P<0.001, Table 3.2), indicating that the length of culture period was the only factor that caused a change in the RGC dendritic morphology.

Table 3.2. Multiple regression model exploring predictive factors of Sholl AUC (dependent variable). In this model culture period (0=0 d, 1=6 h, 2=1 d, 3=2 d, 4=3 d), age (number of months), and sex (1=male, 2=female) were predictors.

Variable	Coefficient (B)	P
Culture period	-228	7.08×10^{-10}
Age	93.6	0.126
Sex	-82.4	0.410

3.7 Pan-caspase inhibition

To explore the involvement of pan-caspase activation in dendritic atrophy of RGCs and to test the sensitivity of the morphometric readout in the explant model 9 explants (n=6 animals, aged 3-4 months, female) were cultured with the pan-caspase inhibitor Q-VD for 2 d. A 2 d treatment window was selected based on the evidence that there is substantial dendritic atrophy within this time frame. RGCs were diolistically labelled (Figure 3.8a-b) and their dendritic arbors quantified by Sholl analysis, as outlined previously. Q-VD-treated cells were partially protected from dendritic retraction; 3 points on the Sholl profile 10-30 µm from the soma (Figure 3.8c) were increased relative to control ($P<0.05$, Kruskal-Wallis), indicating an effect on proximal dendrites only. Although none reached statistical significance ($P>0.05$), all three morphometric parameters measured (Sholl AUC, branching index and dendritic field area) showed the trend of an increase with Q-VD treatment, relative to controls, although all measurements for control and Q-VD-treated cells were significantly reduced ($P<0.001$, ANOVA with TUKEY post-hoc) compared to 0 d cells (Figure 3.8d-f). The experimental timeline is illustrated in Figure 3.8g.

To account for cell sub-type bias and to investigate any group-specific effects of pan-caspase inhibition the cells were split into ON, OFF and ON-OFF, according to their stratification depth in the IPL. There was no significant difference ($P>0.05$) between Sholl AUC for control cells and Q-VD-treated cells that were ON or OFF stratified, however for both treatment groups both ON and OFF subtypes had Sholl AUCs that were significantly reduced ($P<0.05$, ANOVA with TUKEY post-hoc) relative to 0 d cells of the same subtype (Figure 3.8h-i). There were no control cells that were bistratified so comparisons between controls and Q-VD-treated cells could not be made for this subtype, however Q-VD-treated ON-OFF cells had a significantly reduced ($P<0.05$, ANOVA) Sholl AUC relative to 0 d cells (Figure 3.8j).
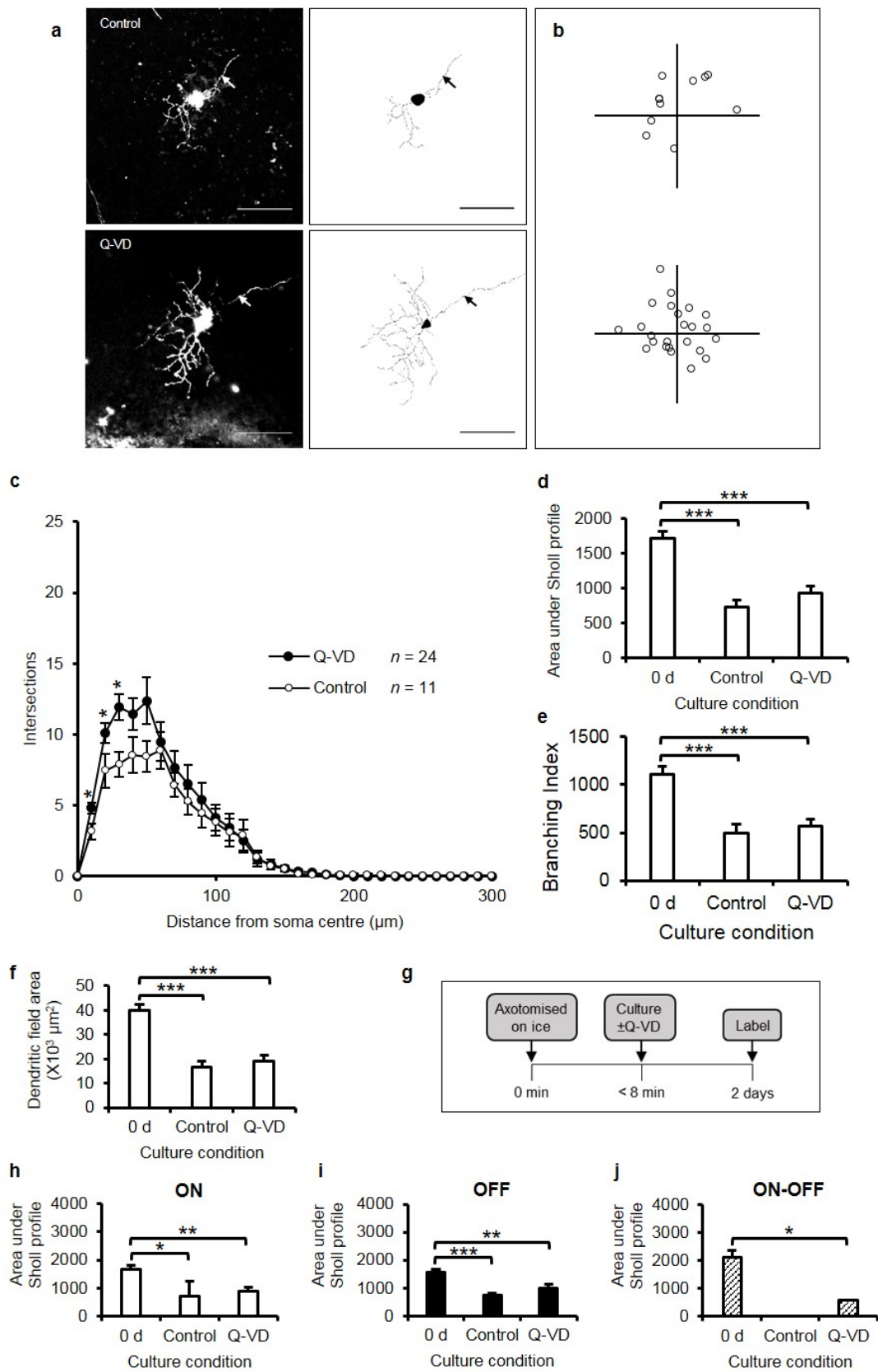
Figure 3.8

Figure 3.8 (previous page). Morphometric analysis of RGCs treated with the pan-caspase inhibitor Q-VD over 2 d. (**a**) Representative fluorescent images (*left*) of diolistically labelled RGCs and their respective 8-bit tracing images (*right*) from explants treated with Q-VD or vehicle only as control. Arrows indicate axons. Scale bars: 100 µm. (**b**) Locations of all analysed cells in each treatment group plotted relative to the optic nerve (origin). Neither group displayed any sign of bias in terms of eccentricity. (**c**) Sholl plots for both treatment groups with the number of cells analysed for each group shown *$P<0.05$, Kruskal-Wallis. (**d**) Sholl AUC for both treatment groups shown with the value for 0 d cells for comparison. ***$P<0.001$, ANOVA with TUKEY post-hoc. (**e**) Branching index for both treatment groups shown with the value for 0 d cells for comparison. ***$P<0.001$, ANOVA with TUKEY post-hoc. (**f**) Dendritic field area for both treatment groups shown with the value for 0 d cells for comparison. ***$P<0.001$, ANOVA with TUKEY post-hoc. (**g**) Experimental time scale. (**h**) Sholl AUC plots for ON stratifying cells only. N=28 cells (0 d), n=2 cells (control), n=10 cells (Q-VD). *$P<0.05$, **$P<0.005$, ANOVA with TUKEY post-hoc. (**i**) Sholl AUC plots for OFF stratifying cells only. N=12 cells (0 d), n=9 cells (control), n=13 cells (Q-VD). **$P<0.005$, ***$P<0.001$, ANOVA with TUKEY post-hoc. (**j**) Sholl AUC plots for ON-OFF stratifying cells only. N=11 cells (0 d), n=0 cells (control), n=1 cell (Q-VD). *$P<0.05$, ANOVA. Error bars: SEM.

In order to check that age was not a confounding factor, a multiple regression analysis was run on Sholl AUC values for Q-VD-treated cells. The model was a good fit of the data ($p<0.005$, ANOVA). Culture condition (i.e. Q-VD treatment) and age were explanatory variables ($p<0.05$) of Sholl AUC (Table 3.3).

Table 3.3. Multiple regression model exploring predictive factors of Sholl AUC (dependent variable). In this model culture condition (1=control, 2=Q-VD), age (number of months), were explanatory variables.

Variable	Coefficient (B)	P
Culture condition	464	0.005
Age	538	0.001

3.8 Conclusions

In this chapter the aim was to characterise the mouse retinal explant in terms of cellular changes over time and to investigate the potential of morphometric analysis of RGCs to quantify neuronal cell health.

Prior work (Johnson and Martin 2008) has shown that the retinal architecture can be maintained for at least 14 d. Although the number of cells in the INL and ONL were not counted, the respective layer thicknesses can be used as a reasonable estimate of cell loss since there was no evidence of lateral expansion of the tissue over time. It was interesting to note that the INL and ONL begun to show signs of degeneration 11 days before the GCL, in line with the literature (Mazzoni et al. 2008; Garcia-Ayuso et al. 2010). This is likely because photoreceptors are more susceptible to oxidative stress and degeneration has been shown to pass along neuronal pathways by a process termed 'transneuronal degeneration' (Lei et al. 2008).

The pattern of viability markers did not correlate with cell loss in the GCL. Further, the timelines of viability assays were inconsistent with one another; in the GCL active caspase-3 and calcein staining did not change over 14 d but TUNEL staining peaked at 3 d. Although the patterns of TUNEL and active caspase-3 labelling resembled those in the literature (Johnson and Martin 2008; Ferrer-Martin et al. 2014), measurement of DNA damage may not be a good indicator of apoptosis. It has been proposed that it is the ability of cells to repair DNA damage, and not the DNA damage itself, that determines the likelihood of cell death (Brown and Wilson 2003). Further, the TUNEL assay also labels DNA breaks associated with normal DNA turnover and necrosis (Elmore 2007), the latter of which has been reported to be a major cause of cell death in axotomy models (Kashimoto et al. 2008). Additionally, active caspase-3 may not be a reliable marker of apoptosis, particularly as it remained constant in every cell layer, other than the ONL. This suggests that active caspase-3 was not implicated in cell loss in the explant. This idea is supported by the evidence that cultured RGCs can die by caspase-independent apoptosis (Tezel and Yang 2004; McKernan et al. 2007). The lack of significant apoptotic

staining reported here could indicate that cell death occurred rapidly, i.e. the period in which cells were undergoing apoptosis and would be labelled as such was so short that cells either appeared healthy or were completely degraded, however this seems unlikely since cell loss in the GCL was not significant until 14 days. A more plausible explanation is that caspase-independent cell death pathways had been triggered, resulting in DNA damage, but cell death did not begin to occur until after 7 days. These data support the use of cell loss to quantify cell death. The lack of supporting calcein staining is likely due to poor tissue penetration and therefore would require future validation – calcein staining may be more appropriate to test viability in cell-based assays rather than tissue preparations. Although it has been reported in the rat retinal explant (Grieshaber et al. 2010), calcein staining is more commonly used to label cells (Goldberg et al. 2002; Kador et al. 2013). Tissue penetration is a confounding factor for assays that require access to cells deeper than 40 μm, such as antibody labelling (Melvin and Sutherland 2010), therefore the reliability of calcein staining in tissues cannot be assured. This may explain some of the inconsistencies observed between viability assays presented here.

Dendritic retraction of RGCs preceded cell loss by at least 7 d. It should be kept in mind that RGCs are a heterogeneous population of neurons, as evidenced by the large number of sub-types identified in the mouse (Coombs et al. 2006). It is therefore important that labelling is random so as to ensure that any difference in morphology is not due to sub-type bias. Labelling bias can be discounted here because the distribution of sub-types identified at 0 d closely matched that reported by Sun et al. (Sun et al. 2002). Other factors, such as age and sex of the animal, can be discounted as confounding factors, since culture time or treatment group were found to be the only predictive factors of dendritic arbor morphology (for 0-3 d cells).

It is important to point out that absence of evidence for bias does not necessarily exclude this possibility. The small number of cells analysed for some conditions, such as the Q-VD controls, was perhaps too small for the presence of bias to be tested. Indeed, this may be the reason that age was

an explanatory variable of cell morphology, despite age not being a factor with any other set of cells analysed (some of which had a much larger age range). However, since the Sholl profile for these cells was very similar to that of the untreated 2 d cells (Figure 3.7), it is likely that these results are reliable. Finally, it is important to consider the limitations of the experiment investigating pan-caspase inhibition, given that a single concentration of Q-VD was used. In the future a dose-response assay should be carried out to obtain the most optimal concentration of Q-VD in order to validate the results presented here.

Given the well-evidenced role of caspases in dendritic pruning during development (Williams et al. 2006; D'Amelio et al. 2010; Erturk et al. 2014) it was surprising to find that pan-caspase inhibition had only a modest protective effect on dendritic pruning of RGCs in the explant. There are several possible explanations for this. Firstly, the number of cells may have been insufficient for a difference to be measured. Secondly, 2 days may not have been a long enough time course for the protective effect to have been identified. Thirdly, dilution of the Q-VD aliquot in the remaining culture medium may resulted in a sub-optimal concentration (7.7 µM). Finally, the age distribution may have masked the effect of Q-VD. Age was found to positively correlate with an increase in Sholl AUC, but all control cells were from mice aged 4 months and Q-VD-treated cells were split equally from mice aged 3 and 4 months.

3.9 Summary

Retinas from adult mice were cultured as wholemounts for up to 14 d. In the GCL significant cell loss was not observed until day 14, whilst significant dendritic pruning of RGCs occurred after 6 hours. This suggests a treatment window between 6 hours and 14 days where neuronal structure may be restored. In addition, the sensitivity of this assay was demonstrated by pan-caspase inhibition, which successfully retarded dendritic retraction of RGCs within the time frame investigated.

Chapter 4: BDNF-TrkB Signalling in the Mouse Retinal Explant

4.1 Introduction

In chapter 3 I provided evidence that morphometric analysis of axotomised RGCs in the adult mouse retinal explant provides a rapid readout of neuronal cell health. I next sought to use this model to investigate the mechanisms involved in neuronal degeneration and to test the utility of the assay to evaluate neuroprotective agents. In this context, the most promising agent to prevent dendritic atrophy is BDNF, which has well-evidenced roles in the outgrowth and maintenance of dendrites in the brain and retina (Thanos et al. 1989; McAllister et al. 1995; Bosco and Linden 1999).

There is considerable evidence that BDNF mRNA and protein levels are reduced in models of neuronal degeneration (Fahnestock et al. 2002; Weickert et al. 2003; Baydyuk and Xu 2014), therefore one therapeutic avenue to explore is the restoration of normal levels of BDNF to repair neuronal function. Although the levels of BDNF in the rodent retinal explant have been reported (Seki et al. 2003; Domenici et al. 2014), these have not been published in parallel with morphometric changes. I therefore investigated the temporal relationship between endogenous BDNF protein levels and RGC dendritic retraction, and then to explore whether dendrite loss could be accelerated by blocking endogenous BDNF.

BDNF treatment has been shown to be neuroprotective in a range of neurodegeneration models (Weber and Harman 2008; Nagahara et al. 2009; Rodger et al. 2012), however the physical properties of BDNF (pharmacologically 'sticky' and short half-life (Poduslo and Curran 1996; Lu 2003)) make it difficult to precisely control its concentration and location in vivo. Given that the mouse retina is only approximately 200 μm thick (Ferguson et al. 2013), the explant is an ideal model in which to examine the effects of BDNF treatment on axotomy-induced neuronal degeneration. Finally, given that a major limitation in this field is the lack of clinically-relevant data, I sought to investigate whether the neuroprotective effects of BDNF could be achieved when treatment was initiated after injury.

4.2 Levels of endogenous BDNF in the retinal explant

Twenty-nine adult mouse retinal explants (n=15 animals of both sex, aged 4-7 months) were cultured ex vivo for 0 d, 1 d, 3 d, 7 d, and 14 d, after which time right and left explants were pooled and snap frozen in RIPA buffer containing 20% protease inhibitor. Pooled explants were lysed and total protein content was quantified by BCA assay and BDNF protein was quantified by ELISA using mouse anti-BDNF antibody mAb#9 (see 2.10).

Total retinal protein decreased by 22.0% ($p<0.05$) after 1 d, and was lowest after 14 d (50.0% decrease, $p<0.001$, ANOVA, Figure 4.1a). This correlates with cell loss in the INL and ONL (the majority protein components of the retina) as shown in Figure 3.3 (see Chapter 3). BDNF protein levels in the explant followed a similar trend, but did not reach significance at any time point ($p>0.05$, ANOVA, Figure 4.1b). The level of BDNF protein, when expressed per mg total protein, also did not change ($p>0.05$, ANOVA) over 14 d (Figure 4.1c-d).
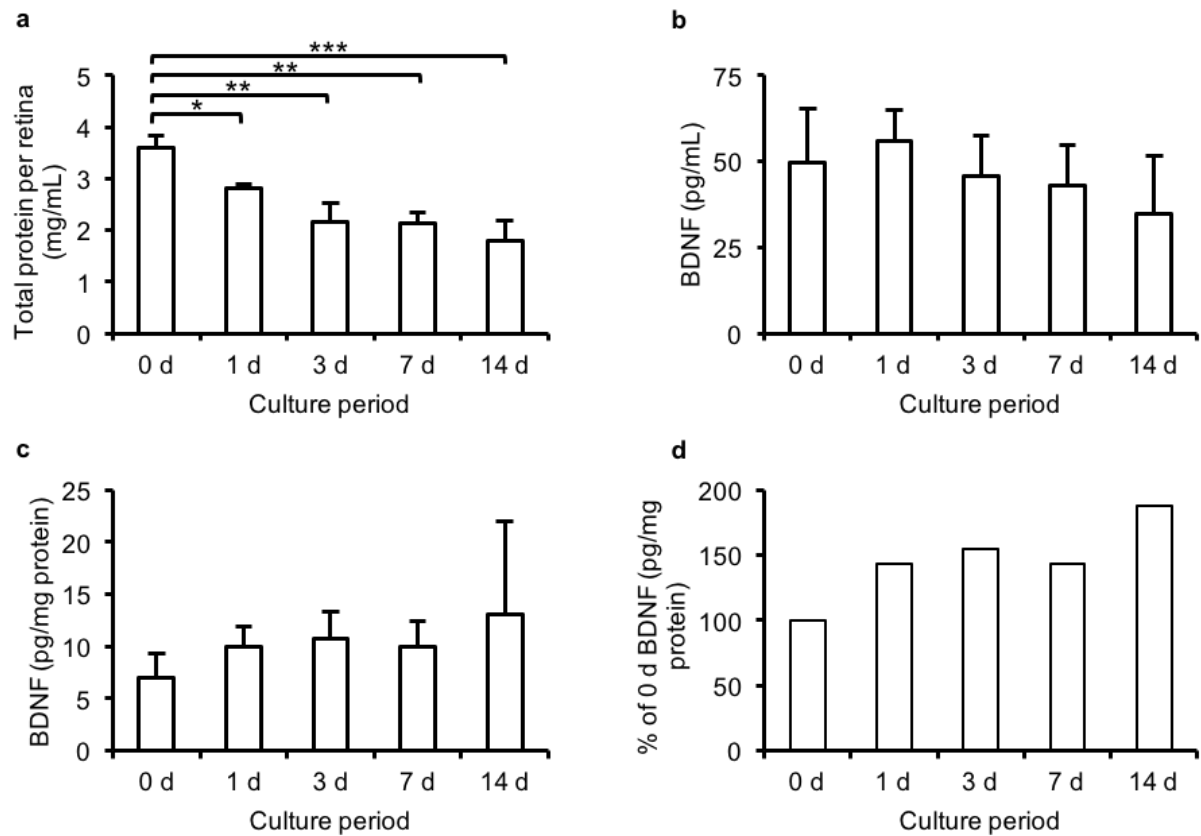
Figure 4.1 Quantification of total protein (BCA assay) and BDNF protein (ELISA) in retinal explants after culture periods of up to 14 d. (**a**) Total protein. *p<0.05, **p<0.005, ***p<0.001, ANOVA. (**b**) Total BDNF protein levels. p>0.05, ANOVA. (**c**) BDNF protein relative to total protein. p<0.05, ANOVA. (**d**) BDNF protein relative to total protein, expressed as a percentage of the value at 0 d. n=6 explants, 3 animals (0 d); n=6 explants, 3 animals (1 d); n=6 explants, 3 animals (3 d); n=6 explants, 3 animals (7 d); n=5 explants, 3 animals (14 d). All values were calculated per retina. Means ±SD.

4.3 BDNF treatment retards RGC dendritic atrophy

Seven explants (n=7 mice of either sex, aged 2-5.5 months) were treated with 100 ng/mL BDNF for 3 d, at which point RGCs were diolistically labelled and their dendritic arbors quantified. The culture timeline is shown in Figure 4.2a. BDNF-treated cells had visibly more complex dendritic arbors (Figure 4.2b-c). Following BDNF treatment, Sholl curve peaks were greatly increased 20-80 µm (p<0.05, Kruskal-Wallis) from the soma centre (Figure 4.2d). BDNF treatment resulted in a 75.8% increase (p<0.005, ANOVA with Tukey post-hoc) in Sholl AUC and an 81.0% increase (p<0.001, ANOVA with Tukey post-hoc) in branching index, relative to controls, but neither measures were significantly different from 0 d cells (Figure 4.2e-f). The dendritic field area of BDNF-treated cells was 61.2% larger (p<0.05) than control cells but 28.8% smaller (p<0.005, test) than 0 d cells (Figure 4.2g). RGCs were divided into ON, OFF and ON-OFF based on INL stratification (see section 2.8.4) to check for sub-type-specific effects of BDNF. Following BDNF treatment, the Sholl AUC of ON cells increased by 109% (p<0.005) relative to controls but was not significantly different (p>0.05, ANOVA with Tukey post-hoc) from 0 d cells (Figure 4.2h). The Sholl AUC for BDNF-treated OFF cells was 73.6% increased (p<0.05) relative to controls, but was not significantly different (p>0.05, ANOVA with Tukey post-hoc) from 0 d cells (Figure 4.2i). There was no significant difference (p>0.05, ANOVA with Tukey post-hoc) between groups for Sholl AUC of bistratified cells (Figure 4.2j).

Figure 4.2

Figure 4.2 (previous page) Morphometric analysis of RGCs from explants treated with 100 ng/mL BDNF for 3 d. (**a**) Culture timeline of experiment. (**b**) Fluorescent images (*left*) and 8-bit tracing images (*right*) of diolistically labelled RGCs. Scale bar: 100 µm. Arrows indicate axon. (**c**) Locations of all analysed RGCs relative to the optic nerve (origin). (**d**) Sholl profiles for control cells and BDNF-treated cells demonstrating increased dendritic complexity with BDNF treatment. The number of cells in each group is shown. *p<0.05, **p<0.005, ***p<0.001, Kruskal-Wallis. (**e**) Area under the Sholl profile for each group, shown with the value for 0 d cells for comparison. **p<0.005, ***p<0.001, ns not significant, test. (**f**) Branching index for each group, shown with the value for 0 d cells for comparison. ***p<0.001, ns not significant, test. (**g**) Dendritic field area for each group, shown with the value for 0 d cells. *p<0.05, **p<0.005, ***p<0.001, test. (**h**) Area under the Sholl profile for ON-stratifying cells in each group. **p<0.005, ***p<0.001, test. (**i**) Area under the Sholl profile for OFF-stratifying cells in each group. *p<0.05, test. (**j**) Area under the Sholl profile for bistratified cells in each group. p>0.05, test. Means ±SEM.

In order to check that age and sex were not confounding factors, a multiple regression analysis was run on Sholl AUC values for BDNF-treated cells. The model provided a good fit of the data ($p < 0.05$, ANOVA). Culture condition (i.e. BDNF treatment) was the only explanatory variable ($p < 0.05$) of Sholl AUC (Table 4.1).

Table 4.1. Multiple regression model to test the possible confounding effects of variance in age and sex on Sholl AUC (dependent variable). Culture condition (1=control, 2=BDNF), age (number of months), and sex (1=male, 2=female) were the predictors.

Variable	Coefficient (B)	P
Culture condition	665	0.008
Age	-29.4	0.797
Sex	51.5	0.831

4.4 Delayed BDNF treatment retards RGC dendritic atrophy

To investigate the mechanism of BDNF action and to test BDNF treatment in a more clinically relevant paradigm that could be translated to clinical treatment 6 explants (n=6 mice, male, aged 8.5 months) were cultured in normal culture medium for 3 d, at which point 100 ng/mL BDNF was added for a further 3 d (6 d total). The culture timeline is outlined in Figure 4.3a. Delayed BDNF treatment resulted in RGCs with more complex dendritic arbors (Figure 4.3b-c), in which the Sholl profile was increased 20-100 µm from the soma centre (p<0.05, Kruskal-Wallis) (Figure 4.3d). The Sholl AUC of delayed BDNF-treated cells was increased by 136% (p<0.001) compared to controls, decreased by 32.9% (p<0.05) relative to 0 d cells, and increased by 56.6% (p<0.005, ANOVA with Tukey post-hoc) compared to 3 d cells (Figure 4.3e). Delayed BDNF treatment resulted in a 107% increase in branching index (p<0.05), relative to controls, but a 45.1% decrease in branching index (p<0.005, ANOVA with Tukey post-hoc) compared to 0 d cells (Figure 4.3f). The dendritic field area of delayed BDNF-treated cells was 134% increased (p<0.001) relative to controls but was 43.1% decreased (p<0.001, ANOVA with Tukey post-hoc) compared to 0 d cells (Figure 4.3g). Cells were split into ON, OFF, and ON-OFF to check for sub-type-specific effects of delayed BDNF treatment. Following delayed BDNF treatment the Sholl AUC of ON cells was 95.8% increased (p<0.05) relative to controls, 55.3% increased (p<0.05) relative to 3 d cells, and 39.5% decreased (p<0.05, ANOVA with Tukey post-hoc) compared to 0 d cells (Figure 4.3h). The Sholl AUC of delayed BDNF-treated OFF cells was 253% increased (p<0.005) compared to controls but was not significantly different (p>0.05, ANOVA with Tukey post-hoc) from any other group (Figure 4.3i). No control cells were identified as ON-OFF cells and for all other groups the Sholl AUCs were not significantly different (p>0.05, ANOVA with Tukey post-hoc, Figure 4.3j).

Although age and sex were constant in this group, a multiple regression analysis was used to check the predictive effect of delayed BDNF treatment on Sholl AUC. The model was a good fit of the data (p=0.001, ANOVA) with the culture condition (i.e. delayed BDNF treatment/no BDNF) was a significant explanatory variable for the change in Sholl AUC (B=671, p=0.001).
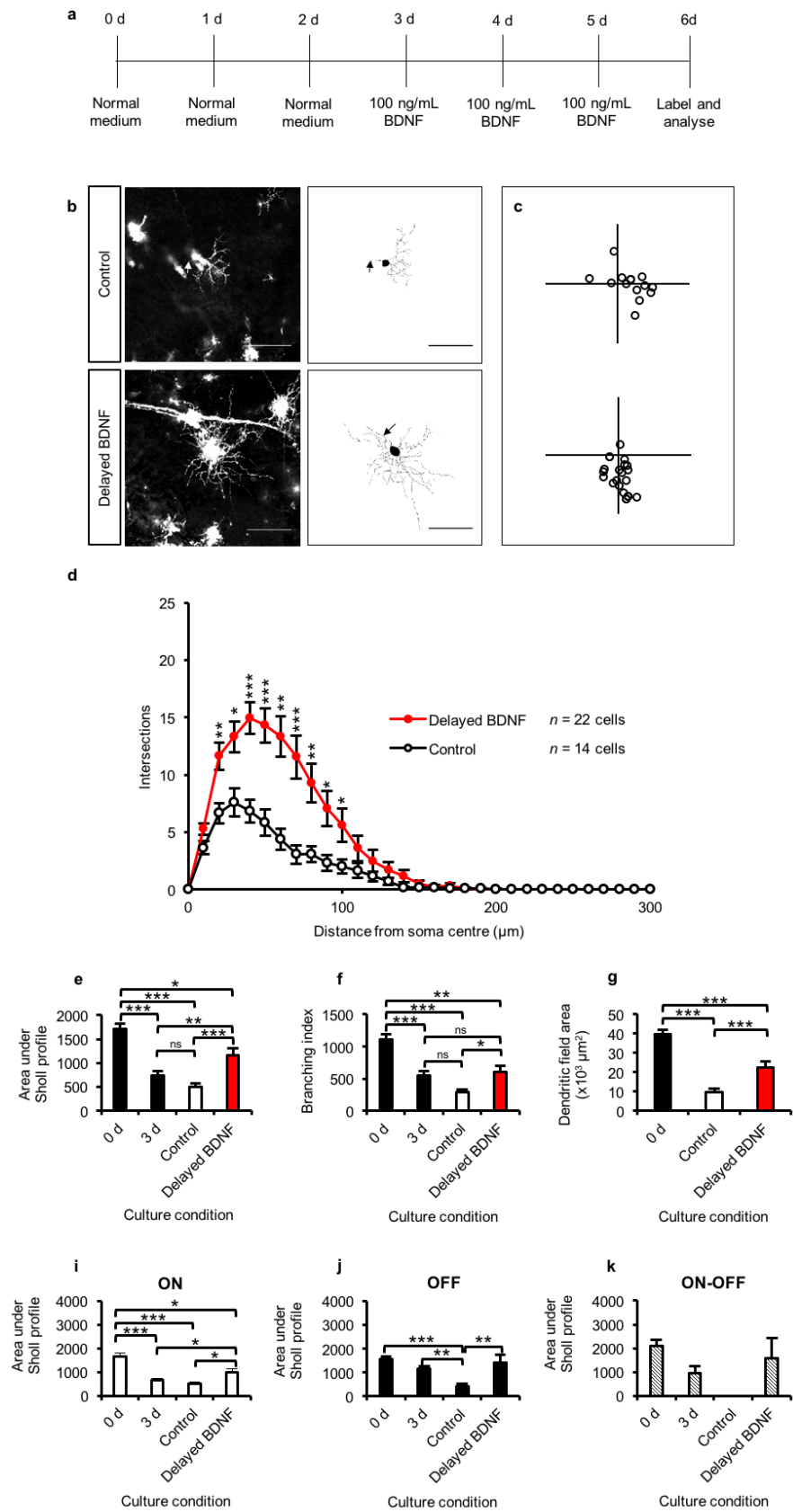
Figure 4.3

Figure 4.3 (previous page) Morphometric analysis of RGCs from explants treated with 100 ng/mL BDNF initiated 3 d-post axotomy. (**a**) Culture timeline. (**b**) Fluorescent images (*left*) and 8-bit tracing images (*right*) of RGCs from each group. Scale bars: 100 µm. Arrows indicate axons. (**c**) Locations of all analysed RGCs relative to the optic nerve (origin) showing no evidence of labelling bias. (**d**) Sholl profiles for each group. The number of cells in each group is shown. *p<0.05, **p<0.005, ***p<0.001, Kruskal-Wallis. (**e**) Area under the Sholl profile, shown with the values for 0 d and 3 d cells for comparison. *p<0.05, **p<0.005, ***p<0.001, ns not significant, ANOVA with Tukey post-hoc. (**f**) Branching index with 0 d and 3 d cell values. *p<0.05, **p<0.005, ***p<0.001, ns not significant, ANOVA with Tukey post-hoc. (**g**) Dendritic field area with 0 d cell value. *p<0.05, **p<0.005, ***p<0.001, ns not significant, ANOVA with Tukey post-hoc. Areas under the Sholl profile split by RGC sub-type (**i-k**) provide no evidence of sub-type-specific effects of delayed BDNF treatment. (**i**) Sholl AUCs for ON cells, with the corresponding value for 0 d and 3 d cells for comparison. *p<0.05, ***p<0.001, ANOVA with Tukey post-hoc. (**j**) Sholl AUCs for OFF cells, with the corresponding value for 0 d and 3 d cells. **p<0.005, ***p<0.001, ANOVA with Tukey post-hoc. (**k**) Sholl AUCs for bistratified cells, with the corresponding value for 0 d and 3 d cells for comparison. p>0.05, ANOVA with Tukey post-hoc. Means ±SEM.

4.5 The effect of BDNF is dose-dependent

To test for the presence of a dose-dependent effect of BDNF, 6 explants (n=3 animals, female, aged 2 months) were treated with 1000 ng/mL BDNF for 3 d initiated at day 3 (6 d total). At the end of the culture period RGCs were labelled and analysed as before. The culture timeline is shown in Figure 4.4a. RGCs treated with 1000 ng/mL BDNF had visibly larger and more complex dendritic arbors (Figure 4.4b-c), quantified as a large increase in Sholl peak amplitude between 30-110 µm and 130-160 µm from the soma centre ($p < 0.05$, Kruskal-Wallis) as well as a rightward shift in the Sholl profile (Figure 4.4d). Delayed 1000 ng/mL BDNF-treated cells had Sholl AUCs that were 119% increased ($p < 0.001$) relative to controls and 136% increased ($p < 0.001$) relative to 3 d cells, but were not significantly different ($p > 0.05$, ANOVA with Tukey post-hoc) from 0 d cells (Figure 4.4e). The branching index of delayed 1000 ng/mL BDNF-treated cells was increased by 83.6% ($p < 0.05$) relative to controls and by 95.1% ($p < 0.005$) relative to 3 d cells. The index did not differ significantly ($p > 0.05$, ANOVA with Tukey post-hoc) compared with 0 d cells (Figure 4.4f). The soma diameters of treated cells were unchanged ($p > 0.05$, ANOVA with Tukey post-hoc) compared to controls (Figure 4.4g). The dendritic field area of delayed 1000 ng/mL BDNF-treated cells was 67.9% increased ($p < 0.05$) relative to controls, but was not significantly different ($p > 0.05$, ANOVA with Tukey post-hoc) compared to 0 d cells (Figure 4.4h).
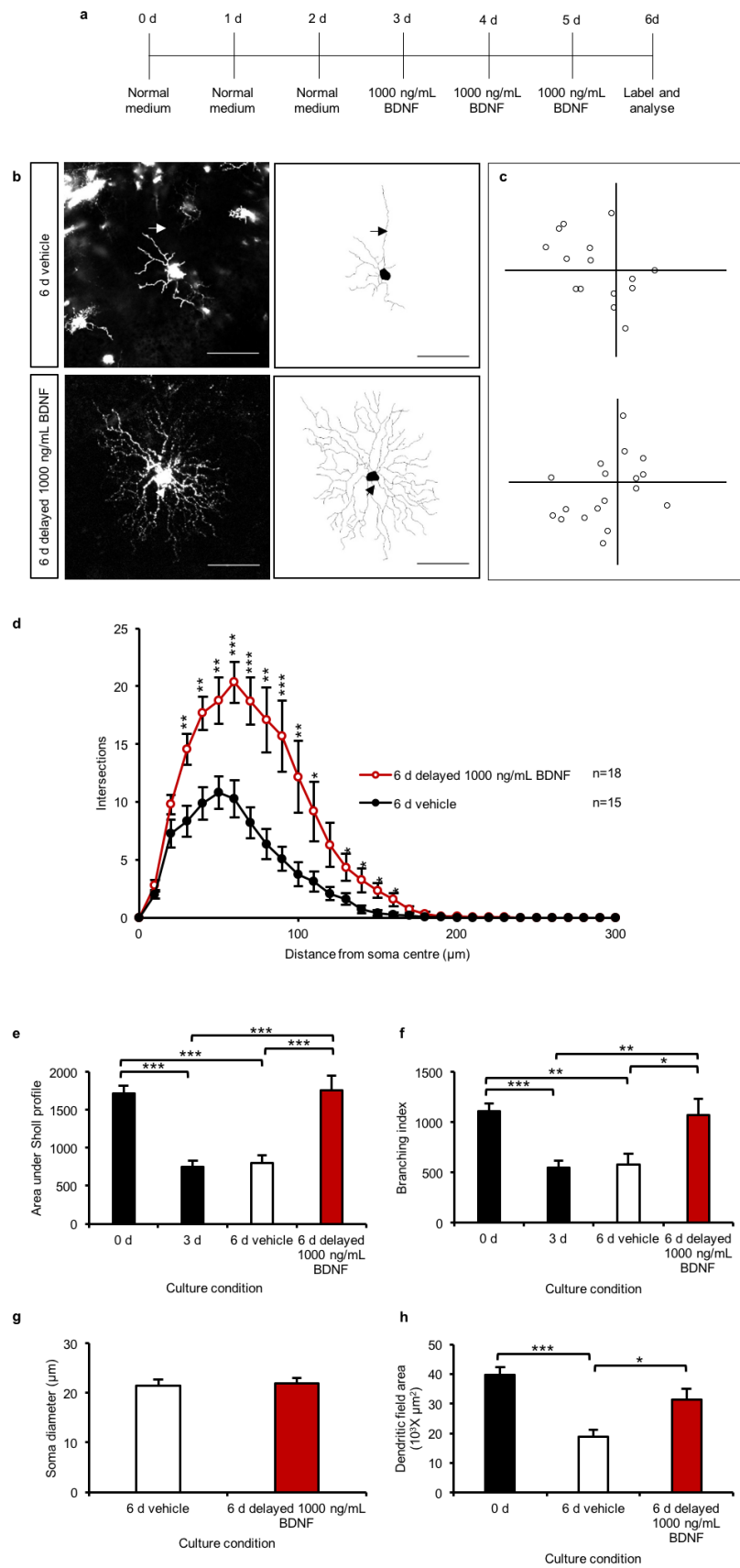
Figure 4.4

Figure 4.4 (previous page) Morphometric analysis of RGCs from explants treated with 1000 ng/mL BDNF initiated at day 3. (**a**) Culture timeline. (**b**) Fluorescent images (*left*) and 8-bit tracings (*right*) of diolistically labelled RGCs in each treatment group. The number of cells in each group is shown. Scale bars: 100 μm. Arrows indicate axons. (**c**) Locations of all analysed cells relative to the optic nerve (origin) showing no evidence of labelling bias. (**d**) Sholl profile for each group. The number of cells in each group is shown. *p<0.05, **p<0.005, ***p<0.001, Kruskal-Wallis. (**e**) Area under the Sholl profile, shown with the values for 0 d and 3 d cells for comparison. ***p<0.001, ANOVA with Tukey post-hoc. (**f**) Branching index with 0 d and 3 d cell values. *p<0.05, **p<0.005, ***p<0.001, ANOVA with Tukey post-hoc. (**g**) Soma diameter. p>0.05, test. (**h**) Dendritic field area with 0 d cell value for reference. *p<0.05, ***p<0.001, ANOVA with Tukey post-hoc. Means ±SEM.

4.6 Blocking endogenous BDNF has no effect on RGC morphology

To investigate the effect of endogenous BDNF on dendritic retraction of RGCs, 9 explants (n=7 animals of both sex, aged 4-6 months) were cultured for 3 d with the mouse anti-BDNF antibody mAb#9 (10 μg/mL) to block endogenous BDNF. To ensure that mAb#9 was binding to its target protein, 11 explants (n=10 animals of both sex, aged 2-5 months) were cultured for 3 d with 100 ng/mL BDNF ±10 μg/mL mAb#9. At the end of the culture period RGCs were labelled and analysed as before. The culture timeline is shown in Figure 4.5a. There was no visible effect of mAb#9 treatment on the dendritic arbors of RGCs, compared to controls, and RGCs treated with both BDNF and mAb#9 appeared unchanged relative to control cells, in contrast to the highly branched arbors of BDNF-treated cells (Figure 4.5b-c). These observations were quantified by Sholl analysis, indicating no difference ($p>0.05$, Kruskal-Wallis) in Sholl profile between controls and mAb#9-treated cells (Figure 4.5d), and combined treatment of mAb#9 with BDNF completely abolished the effect of BDNF on the Sholl profile (Figure 4.5e). The area under the Sholl profile and branching index of BDNF-treated cells were increased ($p<0.05$) relative to the other three treatment groups, which were all unchanged ($p>0.05$, ANOVA with Tukey post-hoc) from each other (Figure 4.5f-g). The soma diameter of RGCs was constant ($p>0.05$, ANOVA with Tukey post-hoc) throughout every treatment group (Figure 4.5h). The dendritic field area of BDNF-treated cells was 55.2% increased ($p<0.005$) relative to control cells, but there were no other differences ($p>0.05$, ANOVA with Tukey post-hoc) between treatment groups (Figure 4.5i).
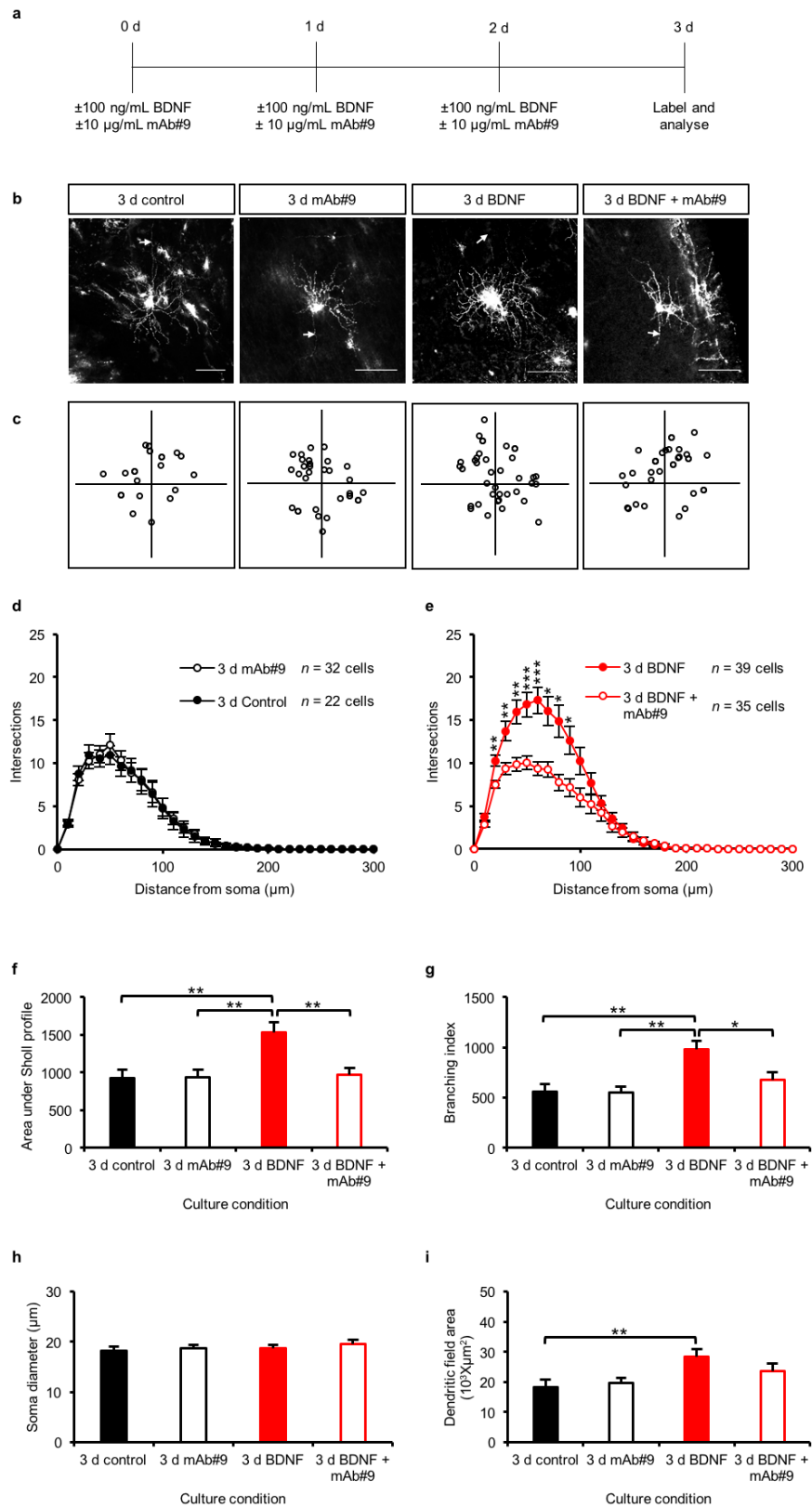
Figure 4.5

Figure 4.5 (previous page) Morphometric analysis of RGCs from explants treated with BDNF blocking antibody mAb#9 or 100 ng/mL BDNF for 3 d. (**a**) Culture timeline. (**b**) Fluorescent images of diolistically labelled RGCs from each treatment group. Scale bars: 100 µm. Arrows indicate axons. (**c**) Locations of all analysed cells relative to the optic nerve (origin). (**d**) Sholl profiles for mAb#9-treated cells and control cells, showing no effect of blocking endogenous BDNF. $p > 0.05$, Kruskal-Wallis. (**e**) Sholl profiles for BDNF-treated cells ±mAb#9, showing that mAb#9 treatment blocks the positive effect of exogenously-applied BDNF. *$p < 0.05$, Kruskal-Wallis. The number of cells in each treatment group (**d-e**) is shown. (**f**) Area under the Sholl profile for all treatment groups shows no difference between groups, except BDNF-treated cells. **$p < 0.005$, ANOVA with Tukey post-hoc. (**g**) Branching index for all groups. *$p < 0.05$, **$p < 0.005$, ANOVA with Tukey post-hoc. (**h**) Soma diameter for each group. $p > 0.05$, ANOVA with Tukey post-hoc. (**i**) Dendritic field area measurements. **$p < 0.005$, ANOVA with Tukey post-hoc. Means ±SEM.

4.7 Conclusions

In this chapter I used the morphometric analysis assay established in Chapter 3 to test the roles of exogenous and endogenous BDNF in the maintenance of dendritic arbor structure. The data indicate that endogenous BDNF does not play a role in the dendritic retraction of RGCs and that BDNF treatment can retard RGC dendrite loss. In addition, I present for the first time evidence that delayed application of BDNF can not only protect against dendritic retraction but may stimulate dendritic outgrowth in RGCs.

The data presented in this chapter demonstrate that BDNF is a potent neuroprotective agent that prevents dendrite loss in RGCs, although this protection was mainly seen for primary and secondary dendrites (20-80 μm from the soma) in the case of 3 d treatment initiated immediately after axotomy (Figure 4.2d). The limited protective effect on terminal dendrites may restrict the number of synaptic connections that can be protected, therefore may be important to consider for the strategy of re-wiring neuronal networks as only partial restoration of neuronal function may be achievable.

The evidence presented here is consistent with a neurite outgrowth mechanism of BDNF. This is particularly exciting because it demonstrates that it may be possible to treat neuronal degeneration even after a significant amount of neuronal damage has occurred. Application of a compound such as BDNF could theoretically promote re-wiring of neuronal networks, thereby restoring neuronal function. It is important to note that this mechanism of BDNF cannot be confirmed with the results shown here; it may simply be a consequence of biased populations of cells. As outlined in section 1.2 (Introduction), RGCs are an extremely heterogeneous population morphologically, therefore it is possible that the evidence for BDNF-mediated dendritic outgrowth demonstrated here is a result of BDNF selecting for the survival of RGC sub-types that are more highly branched with larger dendritic field areas, resulting in this morphology becoming a higher proportion of the remaining population. Nevertheless, the data are convincing, given the lack of evidence of labelling bias and the evidence that age and sex were not confounding factors. However, the absence of sampling bias may simply be

due to the low number of cells in some groups. Although this weakens the statistical power of differences between groups, the Sholl profiles for control cells were very similar to those for cells cultured for the same time period. Nevertheless, time-series imaging is required in order to validate this mechanism.

The evidence shown here supports the theory that endogenous BDNF does not play a role in dendritic retraction of RGCs in the explant, however two points should be considered. Firstly, the ELISA did not measure the location of BDNF within the retina. Secondly, mAb#9 was shown to block exogenous BDNF, but if it could not penetrate the tissue sufficiently, it would have been unable to bind endogenous BDNF. In both cases, the possibility that endogenous BDNF *secretion* was reduced following axotomy cannot be discounted.

4.8 Summary

In the retinal explant total protein rapidly decreased after 1 d, however the level of BDNF protein remained constant for at least 14 d. BDNF treatment initiated immediately after axotomy or 3 d-post axotomy retarded RGC dendritic retraction and these data support the theory that BDNF can promote dendritic outgrowth in RGCs. There was also evidence of a dose-dependent effect of BDNF. Blocking endogenous BDNF had no effect on RGC dendrite loss over 3 d. These data support the use of BDNF a therapeutic agent for the treatment of neuronal degeneration.

Chapter 5: CSPG Digestion to Enhance RGC Remodelling in the Retinal Explant

5.1 Introduction

In Chapter 4 I demonstrated that application of BDNF protects RGCs from dendritic retraction and may promote dendritic outgrowth. However, it was noted that the protective effect of BDNF was largely limited to the primary and secondary dendrites. In order to improve neuronal network rewiring, a method was sought to stimulate outgrowth of terminal dendrites.

CSPGs are a major component of the PNN, which is laid down at the end of the critical period to limit neuronal plasticity (Pizzorusso et al. 2002; Carulli et al. 2010; Wang and Fawcett 2012). Following CNS injury, the secretion of CSPGs is increased and, along with activated astrocytes, these form a glial scar to protect neighbouring healthy tissue from an immune response (Sofroniew 2005). Although CSPGs have a protective role, they can also limit remodelling of dendrites and synapses, which is essential after injury if neuronal function is to be repaired. It has been proposed that CSPG digestion may increase synaptic plasticity via the removal of inhibitory signals (Bradbury et al. 2002), as demonstrated in the kitten visual cortex (Gordon and Stryker 1996). However, it should be noted that there may be a limit to plasticity in the adult (Pizzorusso et al. 2002).

The retinal explant is an excellent model to test the effect of CSPG digestion on dendritic remodelling since it contains an intact neuronal network, unlike the brain slice. In this chapter I tested the effect of ChABC treatment on RGC dendritic remodelling, primarily focussing on terminal dendrites. I also explored whether this treatment could be used in combination with BDNF application to enhance dendritic outgrowth.

5.2 ChABC digests CSPGs in each retinal layer

To confirm that ChABC treatment could be used to digest CSPGs in the retinal explant, particularly in and around the GCL, 5 explants were treated with a topical 50 µL aliquot of 0.25 U/mL or 0.5 U/mL ChABC, or vehicle as control, for 1 d. Explants were then fixed and processed for immunohistochemistry to visualise presence of GAG stubs 1B5, 2B6 and 3B3. Antibodies to 1b5, 2B6 and 3B3 bind to the stubs generated following ChABC digestion. 3B3 antibodies also bind to undigested CSPGs. Following treatment with 0.25 U/mL ChABC only faint staining of CS stubs could be seen, compared to the untreated state. With 0.5 U/mL ChABC treatment there was strong staining for 1B5 and 2B6 in the GCL, INL and ONL, and staining for 3B3 was faint but stronger than in explants treated with vehicle only (Figure 5.1). These results support the use of a topical aliquot of 0.5 U/mL ChABC for 1 d to digest CSPGs in the GCL.
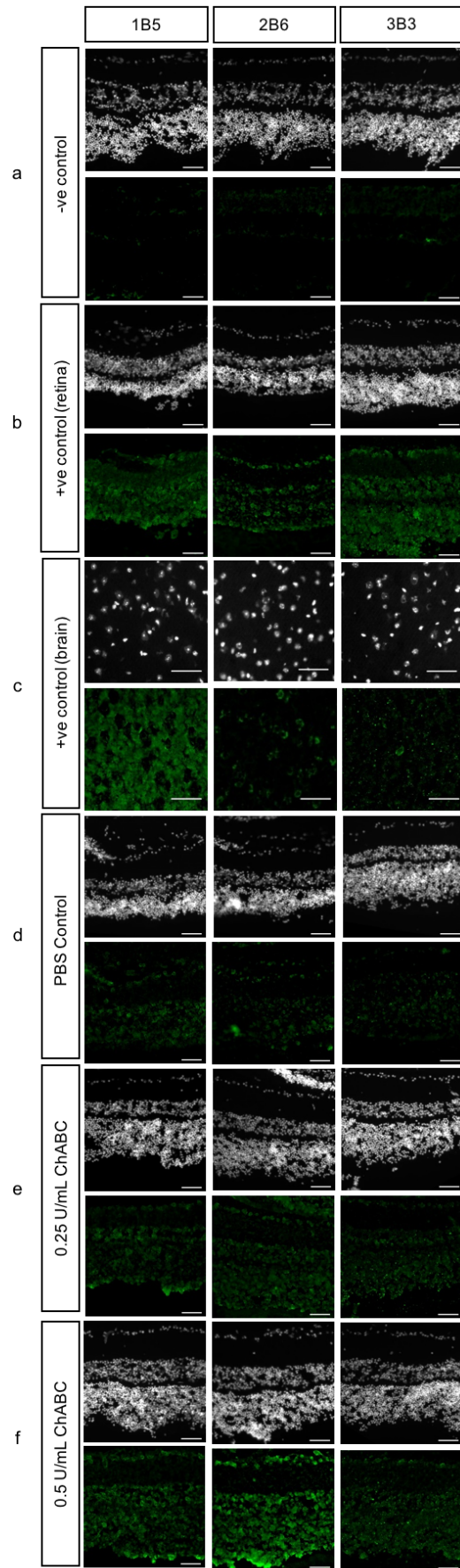
Figure 5.1

Figure 5.1 (previous page). Immunohistochemical staining for products of CSPG digestion in frozen sections of the retinal explant following 1 d treatment with 0.25 U/mL and 0.5 U/mL ChABC. CS stubs (1B5, 2B6 and 3B3) are visualised in green and nuclear staining (Hoechst) is displayed in monochrome above to the corresponding antibody staining panel. (**a**) Negative controls: retinal sections stained for the corresponding antibody with omission of either primary or secondary antibody displaying negligible fluorescence. (**b**) Positive controls (retina): explants were cultured under normal culture conditions for 1 d and their sections were pre-incubated in 0.5 U/mL ChABC for 2 h at 37°C, 5% CO_2 prior to immunohistochemical staining. (**c**) Positive controls (brain): untreated mouse brain sections to visualise normal levels of the CS stubs in the brain. (**d**) PBS control: an explant was cultured with a PBS aliquot for 1 d to visualise normal levels of each CS stub following 1 d ex vivo culture. N=1 explant. (**e**) An explant treated with 0.25 U/mL ChABC displays faint, dispersed staining for all epitopes in all retinal layers. N=1 explant. (f) Explants treated with 0.5 U/mL ChABC shows strong staining for 1B5 (*left*) and 2B6 (*middle*) in each retinal layer. N=3 explants, 3 mice. Scale bars: 50 µm.

5.3 Over 3 d ChABC treatment blocks the protective effect of BDNF

In order to verify that ChABC treatment is not toxic to RGCs, 6 explants (n=4 mice, male, aged 2-7 months) were treated with 0.5 U/mL ChABC as a topical aliquot, or vehicle as control, immediately after wholemount preparation. After 3 d culture RGCs were labelled and analysed as before. The culture timeline is shown in Figure 5.2a. There was no visible difference in morphology of RGCs from ChABC-treated explants compared to controls (Figure 5.2b-c) and this was confirmed by quantification with Sholl analysis ($p > 0.05$, Kruskal-Wallis, Figure 5.2d).

Next, to test whether ChABC treatment could enhance the effect of BDNF on RGC dendritic arbors, 7 explants (n=5 mice of either sex, aged 2-7 months) were treated with 0.5 U/mL ChABC as a topical aliquot, or vehicle as control, and BDNF was added to the medium to make a final concentration of 100 ng/mL. Explants were treated with BDNF for 3 d, at which point RGCs were labelled and analysed as before. The culture timeline is shown in Figure 5.3a. RGCs from explants treated with BDNF were characteristically highly branched, but cells with combined BDNF and ChABC treatment had fewer dendrites (Figure 5.3b-c). This was quantified by Sholl analysis; the Sholl profile was significantly ($p < 0.05$, Kruskal-Wallis) increased 40 µm, 210 and 220 µm from the soma centre in BDNF-treated cells compared to ChABC+BDNF-treated cells (Figure 5.3d).

The outlined patterns in dendritic arbor shape were supported by morphometric analysis. There was no difference ($p > 0.05$, ANOVA with Tukey post-hoc) in soma diameter between groups (Figure 5.4a). There was no significant difference ($p > 0.05$, ANOVA with Tukey post-hoc) between groups for dendritic field area (Figure 5.4b), but the results followed the same trend as the other morphometric measures; area under the Sholl profile was 66.3% increased ($p < 0.05$, ANOVA with Tukey post-hoc) in BDNF-treated cells relative to ChABC-treated cells (Figure 5.4c). The branching index of BDNF-treated cells was 78.5% increased ($p < 0.05$) compared to ChABC-treated cells and 89.6% increased ($p < 0.005$, ANOVA with Tukey post-hoc) compared to ChABC+BDNF-treated cells (Figure 5.4d).
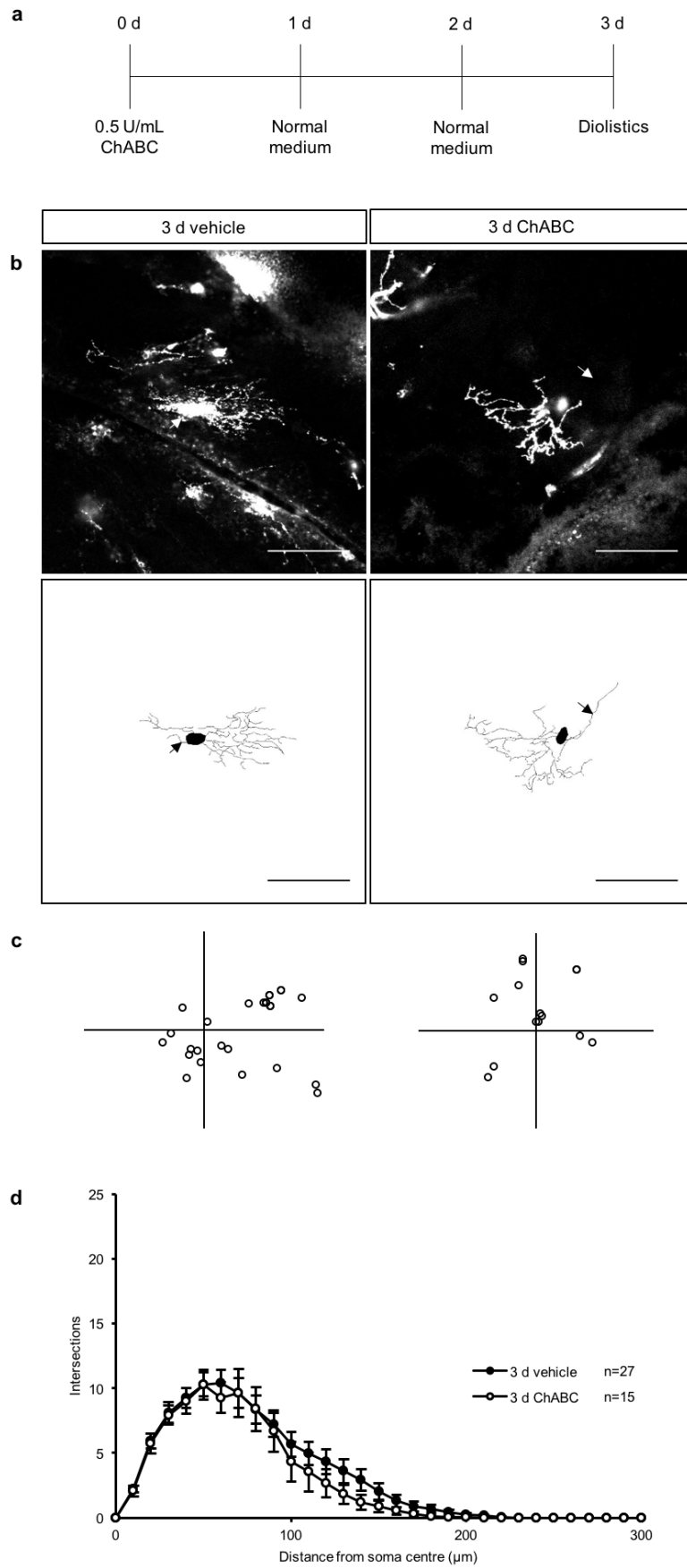
Figure 5.2

Figure 5.2 (previous page) Morphometric analysis of RGCs from explants treated with 0.5 U/mL ChABC as a topical aliquot from day 0 for 1 d and cultured for 3 d. (**a**) Culture timeline. (**b**) 1024x1024 pixel confocal images (*top*) and 8-bit tracings (*bottom*) of diolistically labelled RGCs from each treatment group show no visible difference between treatment conditions. Arrows indicate axons. Scale bars: 100 µm. (**c**) Locations of all cells analysed relative to the optic nerve (origin) demonstrating no evidence of labelling bias. (**d**) Sholl profiles show no difference between treatment groups. p>0.05, Kruskal-Wallis. The number of cells for each group is indicated. Means ±SEM.
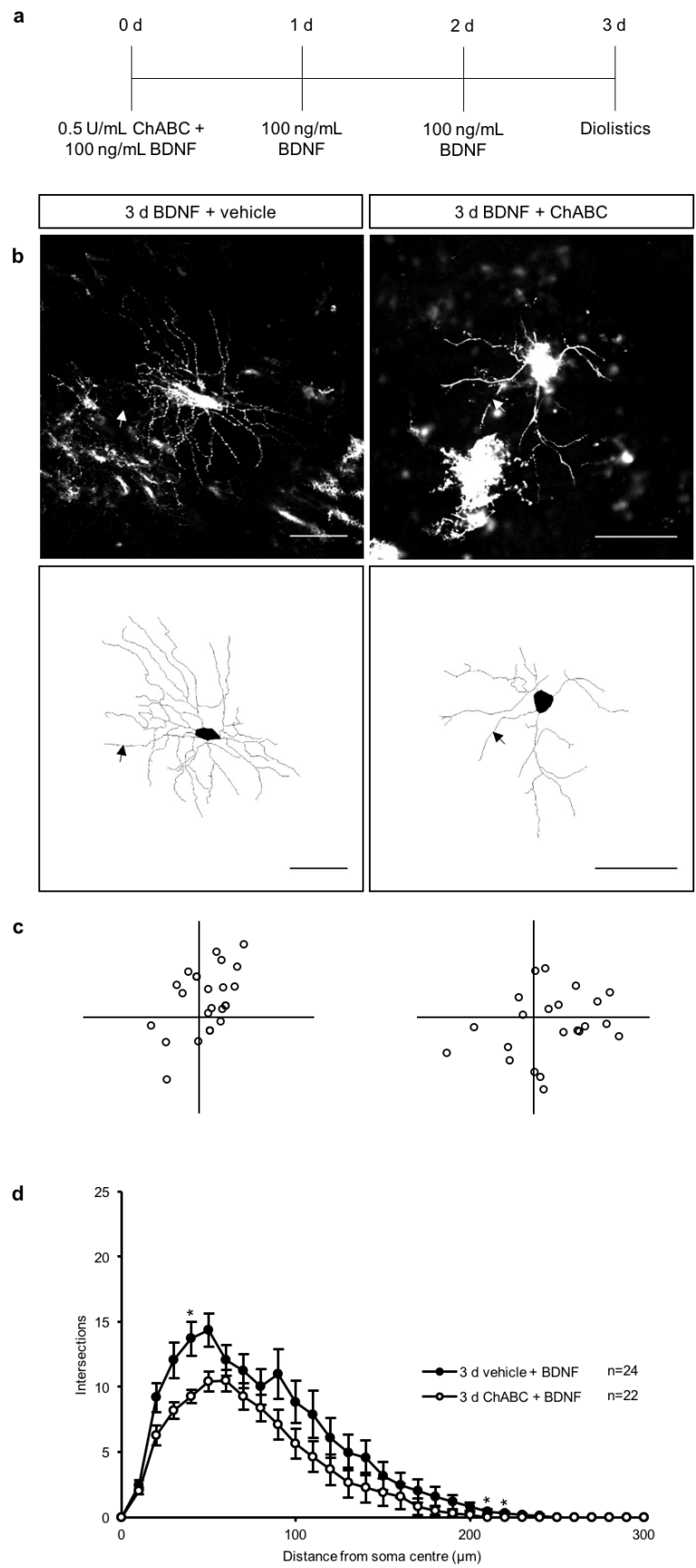
Figure 5.3

Figure 5.3 (previous page) Morphometric analysis of RGCs from explants treated with 100 ng/mL BDNF for 3 d, combined with 0.5 U/mL ChABC applied as a topical aliquot from day 0 for 1 d. (**a**) Culture timeline. (**b**) 1024x1024 pixel confocal images (*top*) and 8-bit tracings (*bottom*) of diolistically labelled RGCs from each treatment group show increased dendritic branching in the absence of ChABC. Arrows indicate axons. Scale bars: 100 µm. (**c**) Locations of all cells analysed relative to the optic nerve (origin) demonstrating no evidence of labelling bias. (**d**) Sholl profiles show increased number of dendrites when ChABC was omitted. *p<0.05, Kruskal-Wallis. The number of cells for each group is indicated. Means ±SEM.
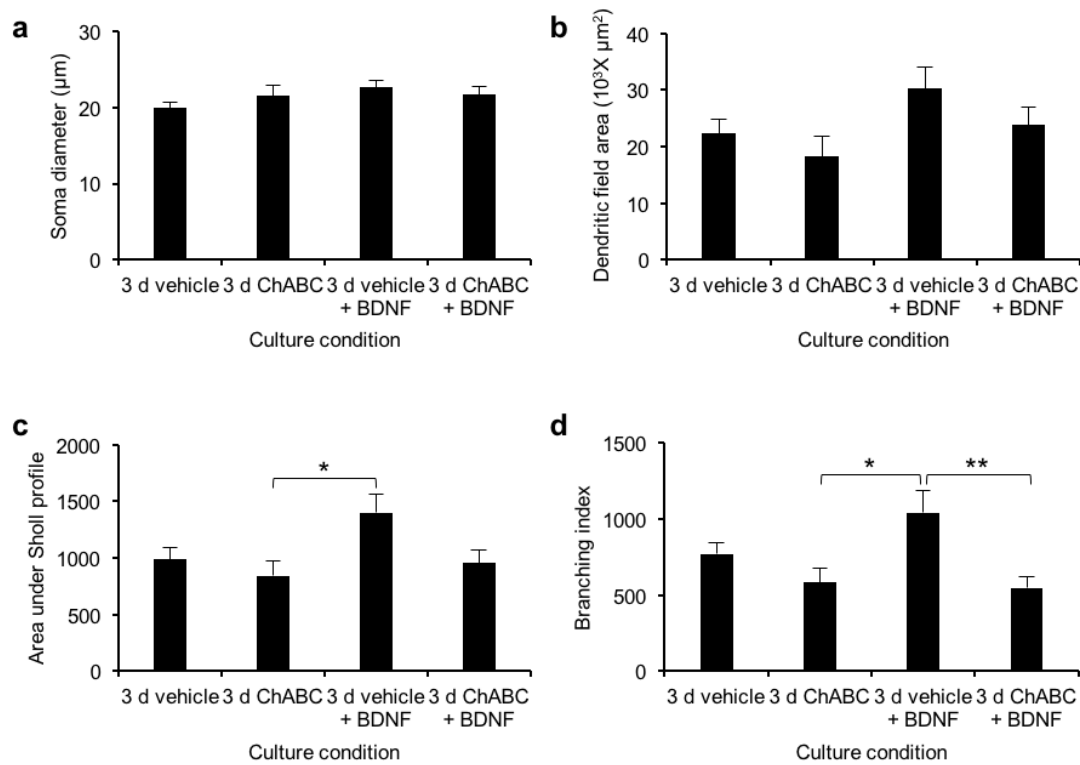
Figure 5.4 Morphometric measures of RGCs from explants treated with 0.5 U/mL ChABC, or vehicle as control, ±100 ng/mL BDNF over 3 d. (**a**) Soma diameters show no difference between groups. p>0.05, ANOVA with Tukey post-hoc. Measures of dendritic arbor morphology (**b-d**) demonstrate a general trend of increased dendritic arbor complexity and size with BDNF –ChABC. (**b**) Dendritic field area for each group. p>0.05, ANOVA with Tukey post-hoc. (**c**) Area under the Sholl profile. *p<0.05, ANOVA with Tukey post-hoc. (**d**) Branching index. *p<0.05, **p<0.005, ANOVA with Tukey post-hoc. Means ±SEM.

5.4 Over 6 d ChABC treatment is neuroprotective but offers no extra protection in combination with BDNF

To investigate whether CSPG digestion is toxic over a longer time period, 6 explants (n=3 animals of either sex, aged 2-4 months) were treated with a topical aliquot of 0.5 U/mL ChABC at day 0, followed by culture for a total of 6 d, at which point RGCs were labelled and analysed as before. The culture timeline is shown in Figure 5.5a. ChABC-treated RGCs had visibly larger, more densely branched dendritic arbors, compared to control cells (Figure 5.5b-c). This observation was quantified by Sholl analysis, which demonstrated a significant increase ($p < 0.05$, Kruskal-Wallis) in Sholl peak amplitude 20-120 μm from the soma centre and a rightwards shift, relative to controls (Figure 5.5d).

To investigate whether ChABC treatment could enhance the neuroprotective effect of BDNF over a longer time period and to test a possible inhibitory interaction between ChABC and BDNF (Figure 5.3), 6 explants (n=3 animals, male, aged 2-6 months) were treated with a topical aliquot of 0.5 U/mL ChABC, or vehicle as control, at day 0, followed by delayed 100 ng/mL BDNF treatment (6 d total). The culture timeline is outlined in Figure 5.6a. RGCs from each treatment group were indistinguishable from each other (Figure 5.6b-c), which was confirmed by Sholl analysis ($p > 0.05$, Kruskal-Wallis, Figure 5.6d).

Morphometric measures further supported the described effects of ChABC and BDNF treatment over 6 d. There was no difference ($p > 0.05$, ANOVA with Tukey post-hoc) in soma diameter between groups (Figure 5.7a). The dendritic field area and Sholl AUC of RGCs in every group treated with ChABC or BDNF were significantly ($p < 0.05$, ANOVA with Tukey-post hoc) larger than RGCs treated with vehicle only (Figure 5.7b-c). The branching index followed the same trend as the results for dendritic field area and Sholl AUC, although no group was significantly different ($p > 0.05$, ANOVA with Tukey post-hoc, Figure 5.7d).

To test whether ChABC treatment affected the stratification depth of RGC dendrites in the IPL when combined with BDNF treatment, the percentage stratification depth of ON-stratifying (0-55%) and OFF-stratifying (55-100%) dendrites was measured. There was no difference ($p > 0.05$, T-test) in stratification depth of ON dendrites between groups, but OFF dendrites stratified 10.4% further into the IPL ($p < 0.05$, T-test) with ChABC+BDNF compared to vehicle+BDNF cells (Figure 5.7e-f).
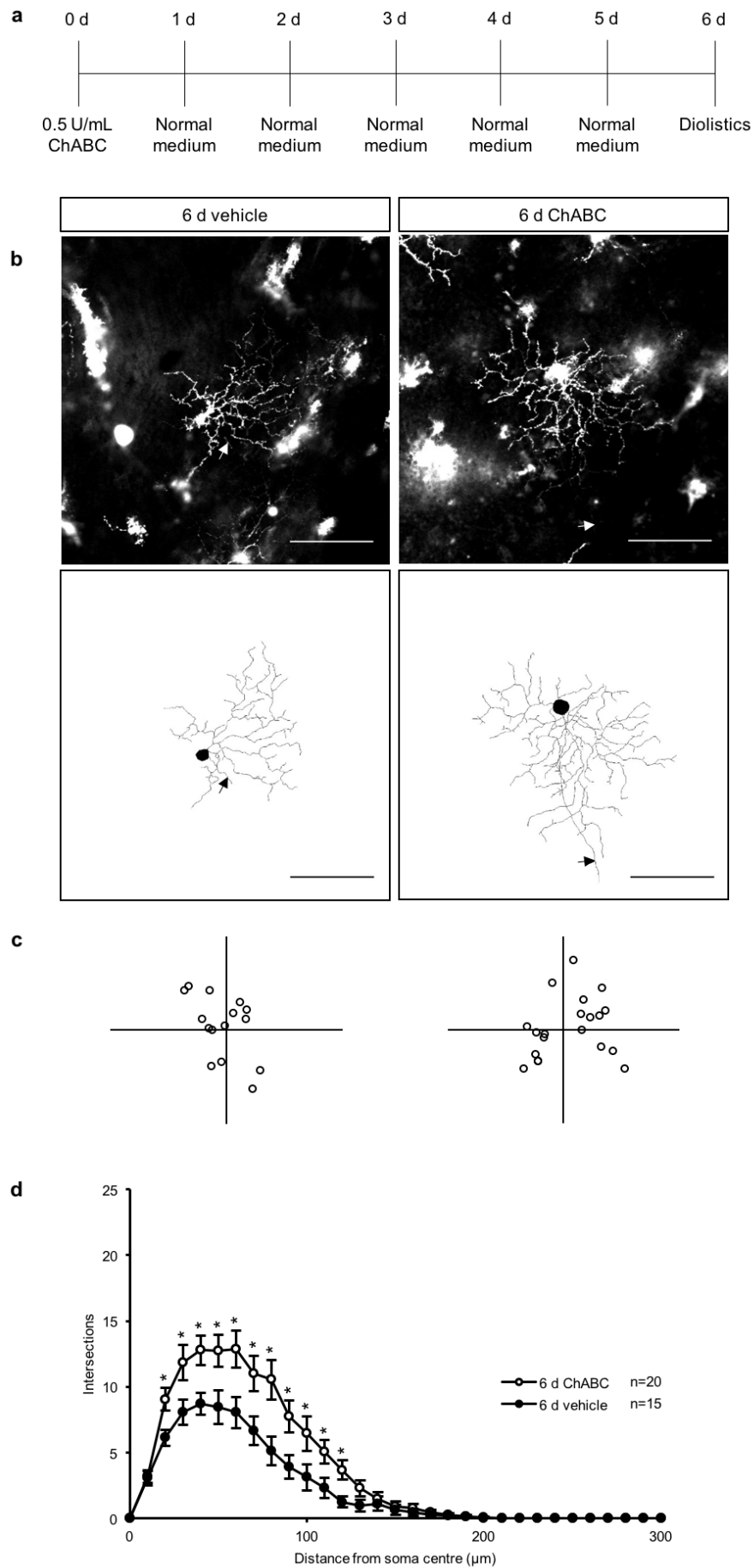
Figure 5.5

Figure 5.5 (previous page) Morphometric analysis of RGCs from explants treated with 0.5 U/mL ChABC as a topical aliquot from day 0 for 1 d and cultured for 6 d. (**a**) Culture timeline. (**b**) 1024x1024 pixel confocal images (*top*) and 8-bit tracings (*bottom*) of diolistically labelled RGCs from each treatment group. Arrows indicate axons. Scale bars: 100 µm. (**c**) Locations of all cells analysed relative to the optic nerve (origin) demonstrating no evidence of labelling bias. (**d**) Sholl profiles. *p<0.05, Kruskal-Wallis. The number of cells for each group is indicated. Means ±SEM.
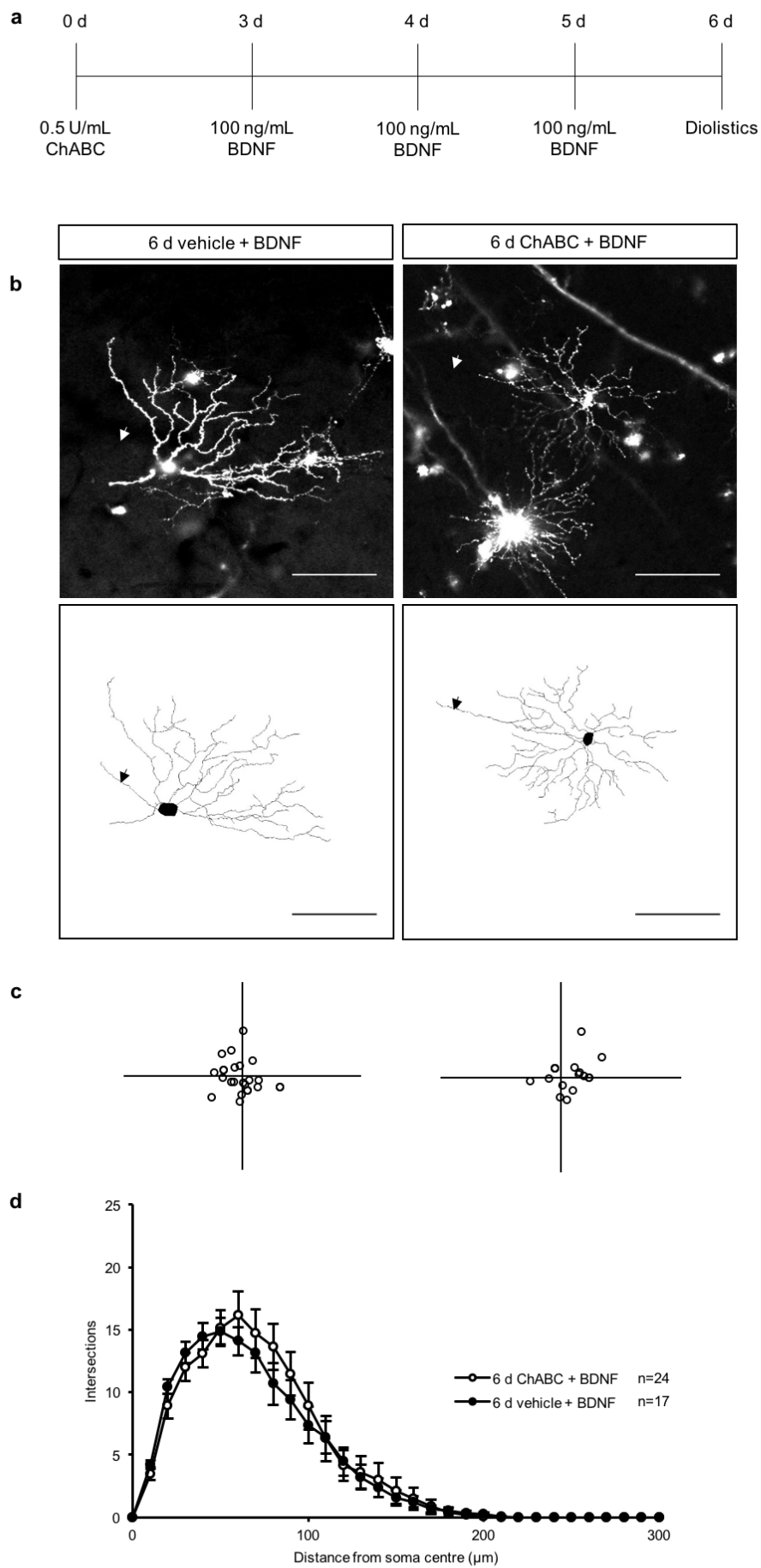
Figure 5.6

Figure 5.6 (previous page) Morphometric analysis of RGCs from explants treated with 0.5 U/mL ChABC applied as a topical aliquot on day 0 for 1 d, followed by 100 ng/mL BDNF treatment for 3 d initiated at day 3 (6 d total). (**a**) Culture timeline. (**b**) 1024x1024 pixel confocal images (*top*) and 8-bit tracings (*bottom*) of diolistically labelled RGCs from each treatment group show no difference in morphology between groups. Arrows indicate axons. Scale bars: 100 µm. (**c**) Locations of all cells analysed relative to the optic nerve (origin) demonstrating no evidence of labelling bias. (**d**) Sholl profiles. p>0.05, Kruskal-Wallis. The number of cells for each group is indicated. Means ±SEM.
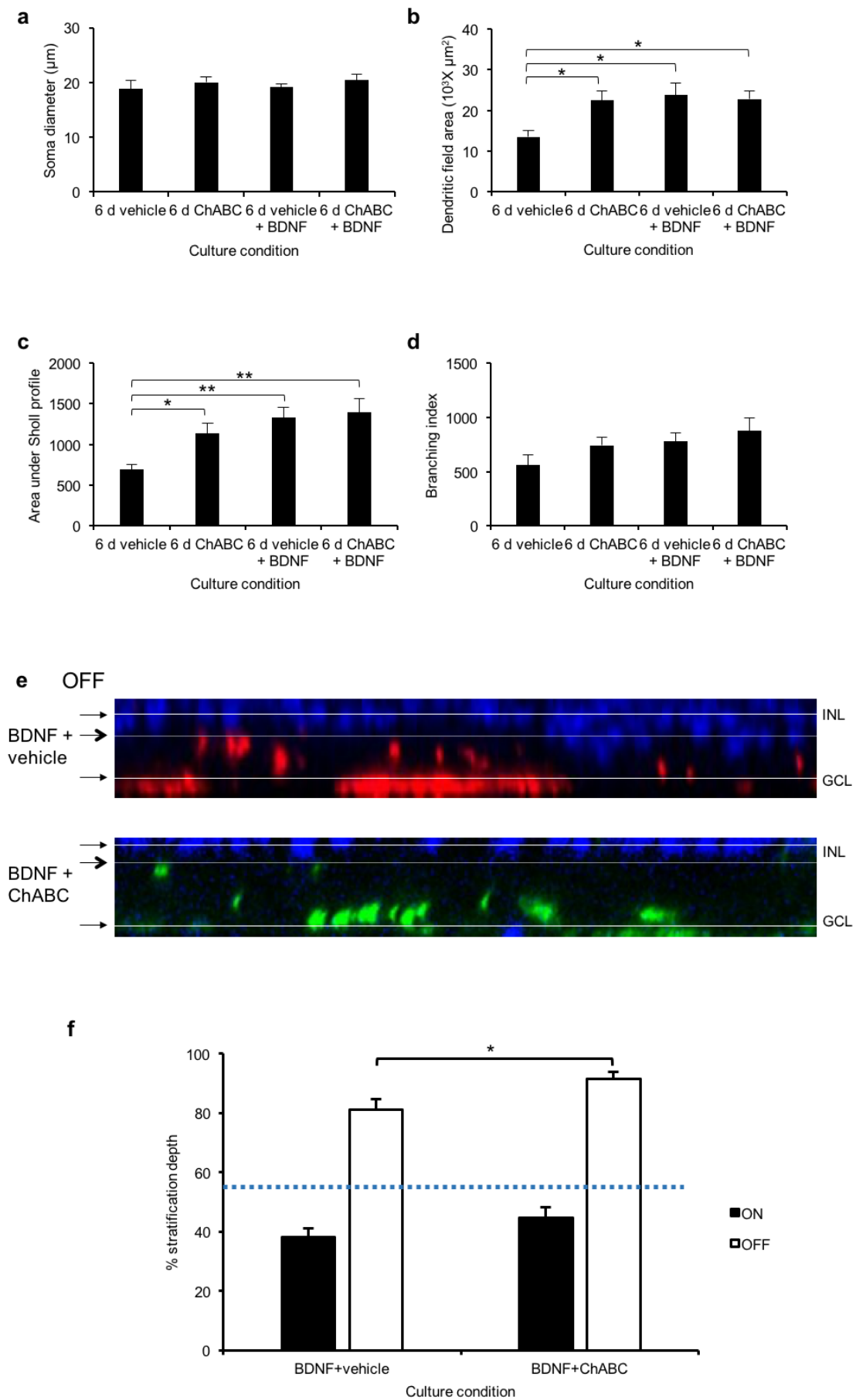
Figure 5.7

Figure 5.7 (previous page) Morphometric measures of RGCs from explants treated with ±0.5 U/mL ChABC ±100 ng/mL BDNF over 6 d. (**a**) Soma diameters show no difference between groups. $p > 0.05$, ANOVA with Tukey post-hoc. Measures of dendritic arbor morphology (**b-d**) demonstrate a general trend of increased dendritic arbor complexity and size with addition of BDNF or ChABC. (**b**) Dendritic field area for each group. *$p < 0.05$, ANOVA with Tukey post-hoc. (**c**) Area under the Sholl profile. *$p < 0.05$, **$p < 0.005$, ANOVA with Tukey post-hoc. (**d**) Branching index. $p > 0.05$, ANOVA with Tukey post-hoc. (**e**) Representative XY orthogonal views of dendritic arbors stratifying in the OFF lamina for cells treated with BDNF (top) or BDNF + ChABC (bottom). In each image lower black arrow indicates GCL, upper black arrow indicates INL, open arrow indicates stratification depth. Nuclei stained with TO-PRO-3 (blue), dendrites stained with DiI (red) or DiO (green). (**f**) Quantification of stratification depth for ON and OFF-stratifying dendrites for cells treated with BDNF or BDNF + ChABC. Blue dotted line represents boundary (55%) IPL depth for classification of ON (below line) or OFF (above line). *$p < 0.05$, T-test. Means ±SEM.

5.5 Following ChABC digestion, BDNF fails to protect against RGC dendrite loss, even when an increased concentration of BDNF is used.

To test the effect of increased concentration of BDNF with ChABC treatment to see if the neuroprotective effect of BDNF could be enhanced. Eleven explants (n=6 animals of either sex, aged 6 weeks-2 months) were treated with a topical aliquot of 0.5 U/mL ChABC, or vehicle as control, at day 0, followed by 1000 ng/mL BDNF treatment initiated at day 3 for 3 d (6 d total). RGCs were analysed as before. The culture timeline is shown in Figure 5.8a. RGCs from explants treated with delayed 1000 ng/mL BDNF had dendritic arbors that were visibly larger and more complex than control cells, but there was no visible difference following ChABC treatment (Figure 5.8b-c). This observation was quantified by Sholl analysis, in which the Sholl profile peak for cells treated with delayed 1000 ng/mL BDNF was approximately doubled between 30-110 μm ($p<0.05$, Kruskal-Wallis) from the soma centre and was translated rightwards relative to the profile for control cells (Figure 5.8d). There was no significant difference ($p>0.05$, Kruskal-Wallis) between curves at any distance from the soma centre for cells from explants treated with ChABC (or vehicle) and 1000 ng/mL BDNF (Figure 5.8e).
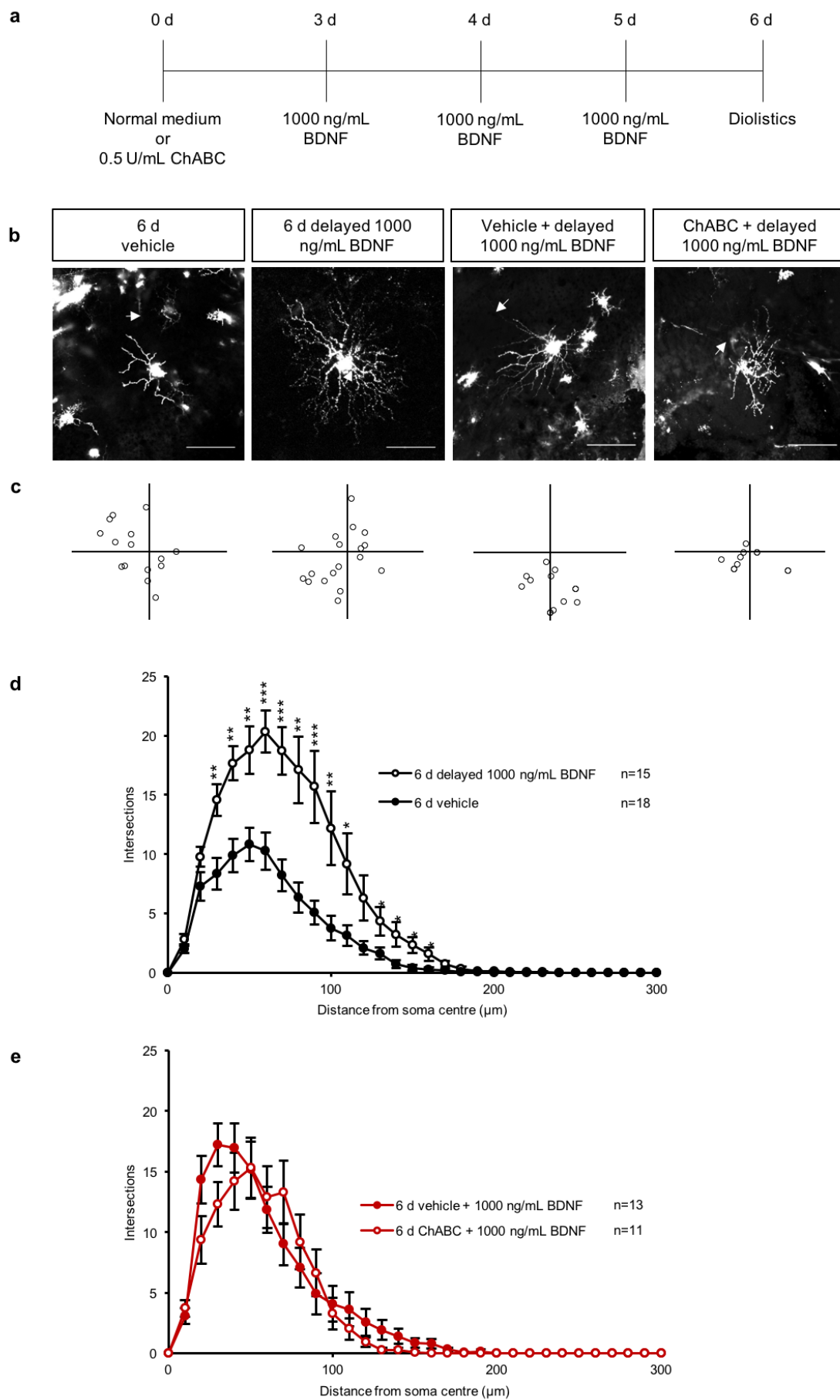
Figure 5.8

Figure 5.8 (previous page) Morphometric analysis of RGCs from explants treated with 0.5 U/mL ChABC, or vehicle as control, applied as a topical aliquot on day 0 for 1 d, followed by 1000 ng/mL BDNF treatment, or vehicle as control, initiated at day 3 for 3 d (6 d total). (**a**) Culture timeline. (**b**) 1024x1024 pixel confocal images of diolistically labelled RGCs from each treatment group show dramatically increased dendritic arbor branching and size following BDNF treatment. Arrows indicate axons. Scale bars: 100 µm. (**c**) Locations of all cells analysed relative to the optic nerve (origin) demonstrating no evidence of labelling bias. (**d**) Sholl profiles. *p<0.05, **p<0.005, ***p<0.001, Kruskal-Wallis. (**e**) Sholl profiles. p>0.05, Kruskal-Wallis. The number of cells for each group is indicated. Means ±SEM.

5.6 Pre-treatment with BDNF may benefit combination therapy with ChABC

In order to test whether reversal of treatment order could enhance the neuroprotective effect of either BDNF or ChABC, 6 explants (n=3 animals, male, aged 4 months) were first treated with 100 ng/mL BDNF, or vehicle as control, at day 0 for 1 d, followed by a topical aliquot of 0.5 U/mL ChABC at day 1, and finally at day 3 RGCs were labelled and analysed as before. The culture timeline is shown in Figure 5.9a. RGC dendritic arbors from explants treated with BDNF and ChABC appeared larger than those treated with ChABC only (Figure 5.9b-c). The Sholl peak amplitudes were unchanged between groups, but the Sholl profile for RGCs treated with BDNF and ChABC was translated rightwards 100-120 μm and 180 μm from the soma centre ($p < 0.05$, Kruskal-Wallis), relative to the curve for ChABC-treated cells (Figure 5.9d). There was no difference in soma diameter between groups ($p > 0.05$, T-test, Figure 5.9e). Although there was no significant difference ($p > 0.05$, T-test) between groups for either dendritic field area or area under the Sholl profile, these results followed the same trend as the branching index, which was 33.8% increased ($p < 0.05$, T-test) in BDNF+ChABC-treated cells, relative to ChABC only-treated cells (Figure 5.9f-h).
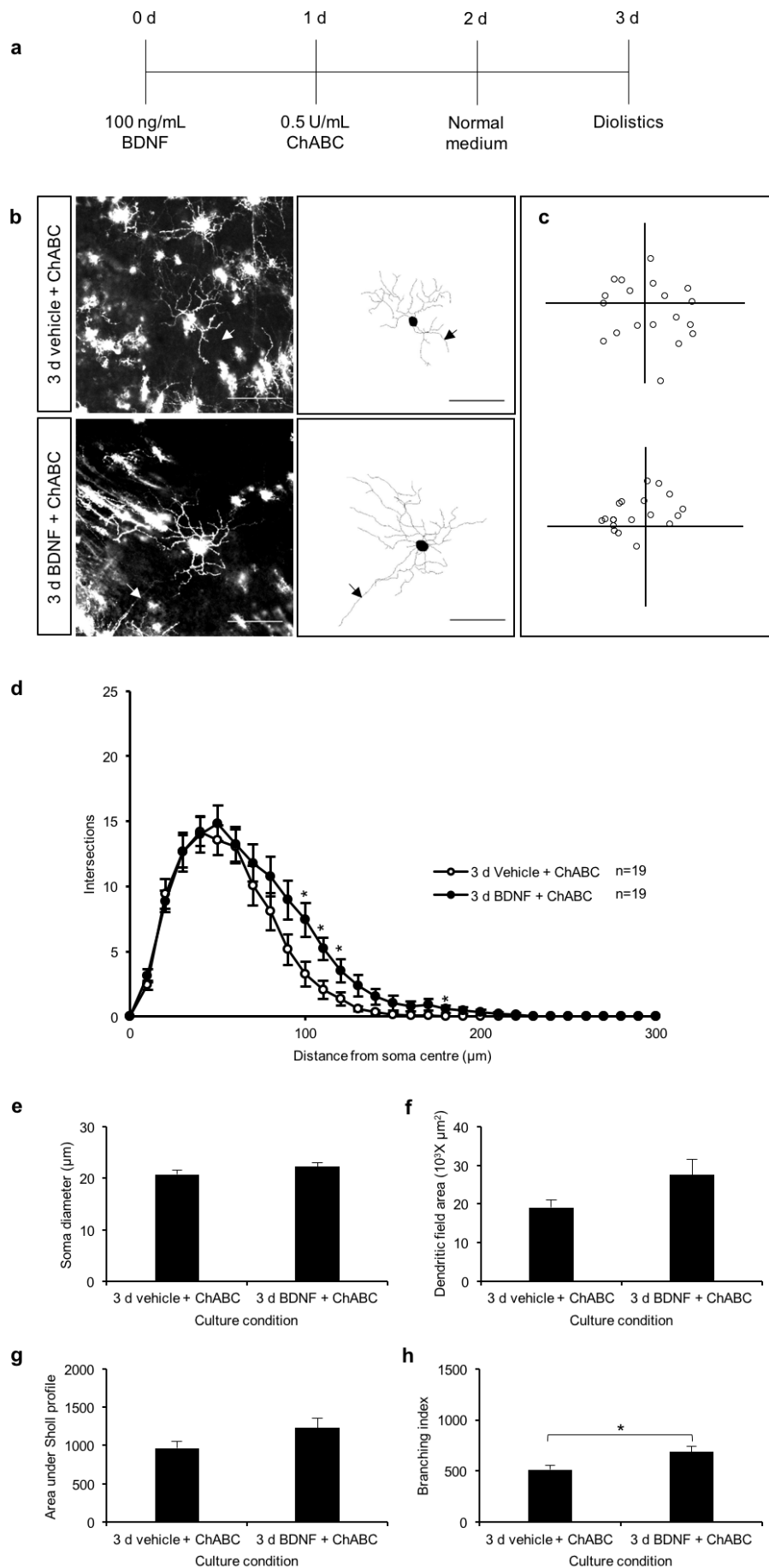
Figure 5.9

Figure 5.9 (previous page) Morphometric analysis of RGCs from explants cultured for 3 d, treated with 100 ng/mL BDNF at day 0 for 1d, followed by 0.5 U/mL ChABC treatment at day 1. (**a**) Culture timeline. (**b**) 1024x1024 pixel confocal images (*left*) and 8-bit tracings (*right*) of diolistically labelled RGCs from each treatment group. Arrows indicate axons. Scale bars: 100 µm. (**c**) Locations of all cells analysed relative to the optic nerve (origin) demonstrating no evidence of labelling bias. (**d**) Sholl profiles. *P<0.05, Kruskal-Wallis. The number of cells for each group is indicated. (**e**) Soma diameter. P>0.05, T-test. (**f**) Dendritic field area. P>0.05, T-test. (**g**) Area under the Sholl profile. P<0.05, T-test. (**h**) Branching index. *p<0.05, T-test. Means ±SEM.

5.7 Conclusions

In this chapter I explored the effect of digesting the CSPG components of the PNN with respect to RGC plasticity and in combination with BDNF treatment. The data shown here suggest that ChABC treatment could facilitate RGC plasticity over longer time periods, but that a combination of ChABC and BDNF does not deliver an additional therapeutic benefit in this model.

There was no effect on RGC dendritic morphology of ChABC treatment after 3 d treatment, but after 6 d there appeared to be an increase in dendritic regrowth. Over both of these time-frames ChABC treatment either blocked or had no positive effect on the neuroprotective effect of BDNF treatment, even when the concentration of BDNF was increased 10-fold. This is perhaps not surprising, given the role of the PNN in stabilising synaptic connections and dendritic morphology. Specifically, CSPGs of the PNN have been shown to bind anchor proteins, such as neural cell adhesion molecule (NCAM), which increase the efficiency of BDNF-TrkB interaction (Vutskits et al. 2001).

It should be noted that as in Chapters 3 and 4, some of the groups in this chapter had small number of cells (especially in Figure 5.9) and that it would be prudent to undertake further work to substantiate these observations. Despite this, the Sholl profiles were similar for all groups of the same culture period, therefore it is likely that there was a similar spread of cell types in each group. All groups seemed to show the same trend, but these patterns should be validated in the future with the use of time-series imaging.

Structural analysis of RGCs provides a sensitive readout of cell stress since cell swelling/dendritic beading can be a marker of stress or necrosis (Pasantes-Morales and Tuz 2006; Liang et al. 2007). There was no evidence of cell stress with ChABC treatment, supporting the notion that ChABC is not toxic.

Reversal of treatment timeline, i.e. BDNF prior to ChABC, may have been protective for distal dendrites. BDNF was only applied for 1 d during this experiment, which may reflect the modest

neuroprotective effect. Nevertheless, it would be interesting to further examine this reversed treatment regime by applying BDNF for a longer period prior to CSPG digestion. In the future it would also be instructive to investigate the duration of the neuroprotective effect of BDNF following removal of BDNF from the culture medium, in order to provide information regarding dosing frequencies for any resultant treatment regimes.

5.8 Summary

ChABC treatment was not toxic to RGCs in the retinal explant, and may even be neuroprotective over longer culture periods, however it appeared to inhibit the neuroprotective effect of BDNF when BDNF was added over 3 d. There was no evidence of inhibition of the positive effect of BDNF with ChABC treatment over 6 d, however there was no additional neuroprotective effect when the two treatments were combined, even when the concentration of BDNF was increased 10-fold. Finally, there was evidence that reversal of the treatment regime, i.e. treatment with BDNF prior to ChABC, may increase neuroprotection of terminal dendrites.

Chapter 6: Neural Stem Cell Migration

6.1 Introduction

I have demonstrated that BDNF application significantly retards RGC dendritic retraction in the degenerating retinal explant, therefore has potential for the treatment of neurodegenerative disorders. Injection of BDNF is not suitable therapeutically because BDNF is pharmacologically 'sticky' and has a short half-life, therefore it is difficult to control concentration and location of injected BDNF (Poduslo and Curran 1996; Lu 2003). Further, BDNF application is undesirable due to the risks associated with repeat injections in the CNS, such as inflammation or infection. An alternative delivery route is via secretion from donor stem cells that can be engineered to translate and secrete peptides of choice. Cell-mediated delivery enables sustained dosing of the agent and, more importantly, permits control of agent release through transcription control techniques including optogenetics (Deisseroth 2011) or magnetogenetics (Long et al. 2015).

Cell-mediated delivery of BDNF is an exciting method and stem cells will migrate into tissue without external influences (Jeon et al. 2008; Li and Jiang 2011), but in order for therapies to be effective with minimal adverse effects, stem cell migration must be controlled. Endogenous magnetic fields have been evidenced to play a role in cell migration during wound healing. Further, magnetic fields are deeply penetrating without compromising safety, and permit dosing to be controlled spatially and temporally (Kyrtatos et al. 2009; Chen et al. 2013). Magnetic fields also have the advantage of allowing stem cells to be sequestered for termination of treatment. For these reasons the use of external magnetic fields is an attractive method to direct stem cell migration in the CNS. The retinal explant is an ideal platform to test whether this technique can improve the efficiency of stem cell migration into the IPL with a view to providing cell-mediated delivery of BDNF to RGCs.

6.2 The effect of permanent magnetic fields on NSCs in suspension

To test the effect of permanent magnetic fields on the movement of NSCs in suspension in vitro, 3 mL GFP-expressing NSCs (passage 39-42) were seeded onto 10 µg/mL laminin-coated 35 mm culture dishes overnight at a density of 1.2-1.8X10^5 cells/cm^2. Volumes of 1.5 uL or 3 uL nTMag were introduced into NSCs using a magnefect at 2 Hz for 30 min at 37°C, 5% CO_2. Control dished contained NSCs with no nTMag. Cells were disassociated from laminin using Accutase® and immediately imaged for tracking analysis. NSCs were imaged by brightfield microscopy at 10X using time-series, with images taken every 2.5 sec for a total of 125 sec (6.7 kg-pull NdFeB magnet) or every 1 min for a total of 9 min (23 kg-pull and 38 kg-pull NdFeB magnets). The imaging set-up is shown in Figure 6.1. Images were taken at the edge of the dish of cells in suspension (6.7 kg-pull magnet) or of cells on the bottom surface of the dish (23 kg-pull and 38 kg-pull magnets). Imaging experiments were conducted in the absence of the magnet prior to imaging in the presence of the magnet, for each dish. Images were exported as TIFFs and tracking was analysed using mTrack and Chemotaxis in FIJI.

6.2.1 NSC movement with 6.7 kg-pull NdFeB magnet

There was no observable change in directionality (a measure of how systematically the cells move in a particular direction, i.e. towards a magnet) of the movement paths of the NSCs in any of the conditions investigated (Figure 6.2). There was no difference (p>0.05, ANOVA with Tukey post-hoc) in migration distance between experimental conditions (Figure 6.3a-b). Although no group was significantly different (p>0.05, ANOVA with Tukey post-hoc), there was a trend of an increase in migration velocity in the presence of the magnet (Figure 6.3c). Forward migration indices and centres of mass were not significant between groups (p>0.05, ANOVA with Tukey post-hoc), but showed a trend of an increase in directionality in the presence of the magnet (Figure 6.3d-e).
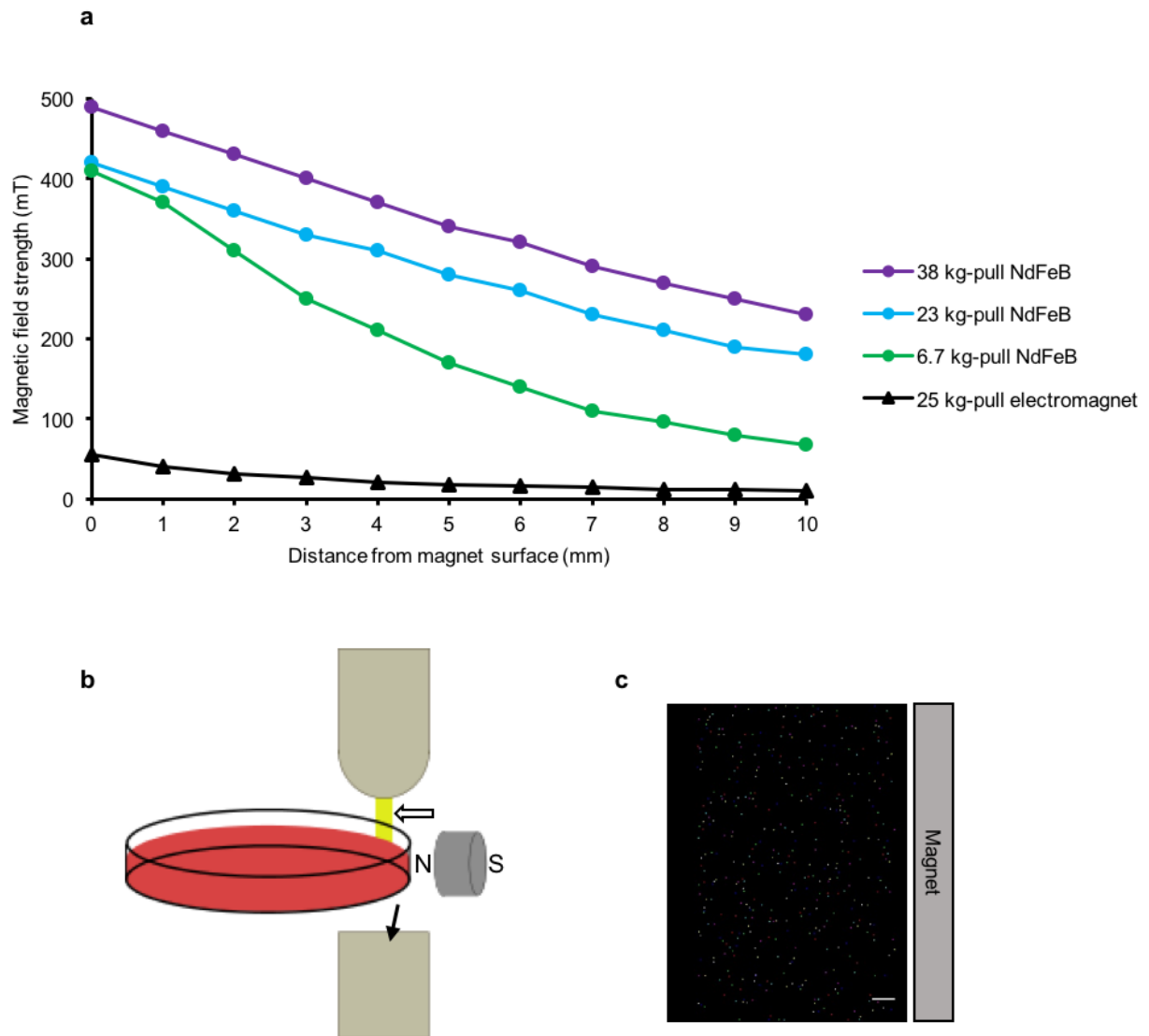
Figure 6.1 Experimental set-up for magnet-directed movement of magnetic nanoparticle-containing NSCs in suspension in vitro. (a) Magnetic field strength of each magnet measured using a gaussmeter at the surface of the magnet and at 1 mm increments up to 10 mm from the magnet surface. (**b**) GFP-NSCs ±nTMag were placed in a 35 mm dish and the magnet was held directly against the edge of the dish (6.7 kg-pull magnet) or 10 mm from the edge of the dish (all other magnets). Cells were imaged by brightfield microscopy at the edge of the dish in the absence of the magnet before introduction of the magnet. Open arrow: light source. Black arrow: detector. The north (N) and south (S) poles are indicated. (**c**) Example image of NSCs after analysis with mTrack to show relative position of magnet. Each dot represents a tracked cell. Scale bar: 50 μm.
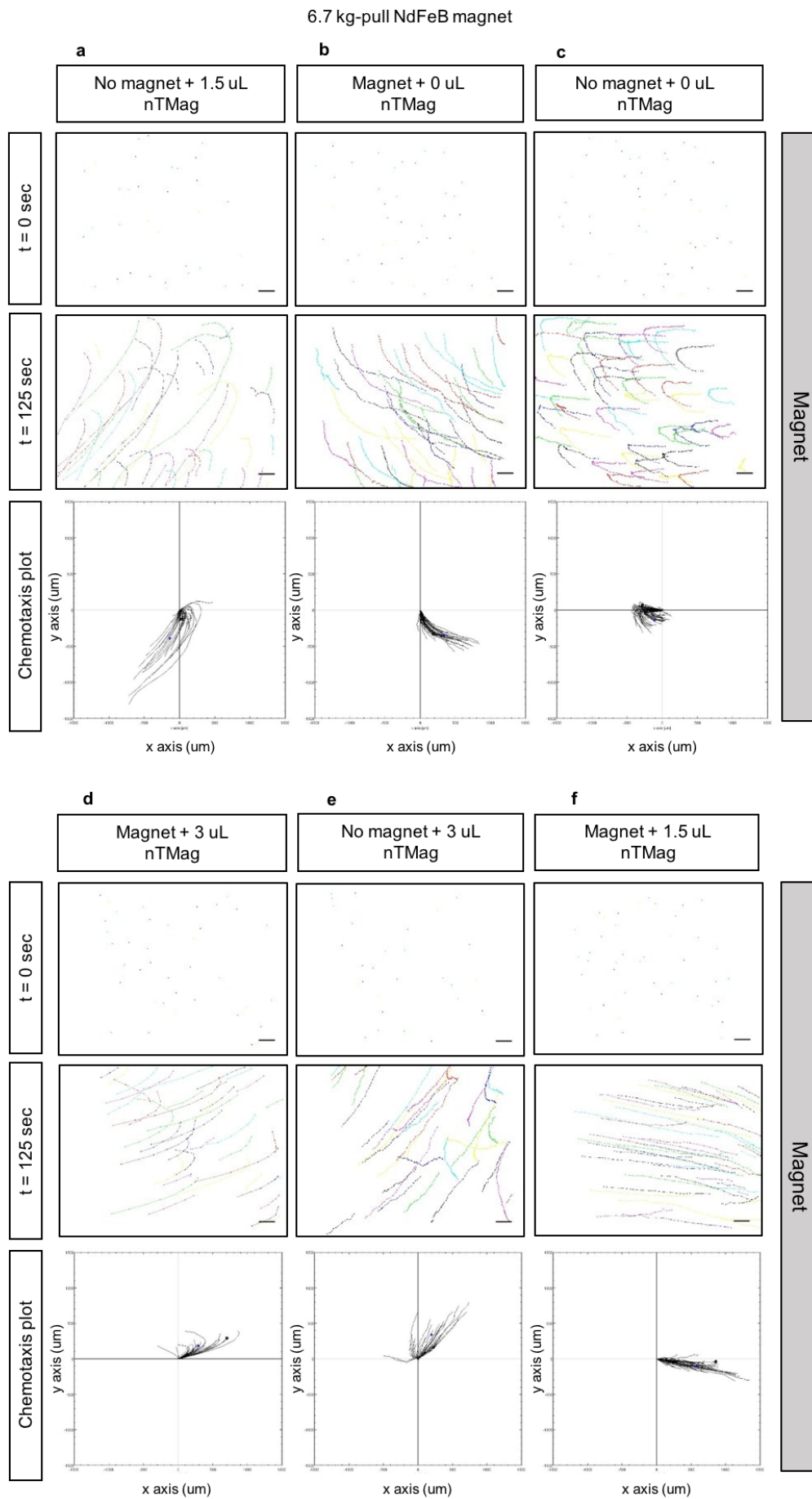
Figure 6.2

Figure 6.2 (previous page) Cell tracking analysis of GFP-NSCs with 6.7 kg-pull NdFeB magnet using the plugin mTrack. The start (*top*) and end (*middle*) frames are shown for each condition. The cell movement plots (*bottom*) show the migration track of each cell relative to its starting position (origin) created using the Chemotaxis plugin in FIJI. Magnet: right of each image, as indicated. (**a**) No magnet, no nTMag. (**b**) Magnet, no nTMag. (**c**) No magnet, 1.5 μL nTMag. (**d**) Magnet, 1.5 μL nTMag. (**e**) No magnet, 3 μL nTMag. (**f**) Magnet, 3 μL nTMag. Scale bars: 50 μm.
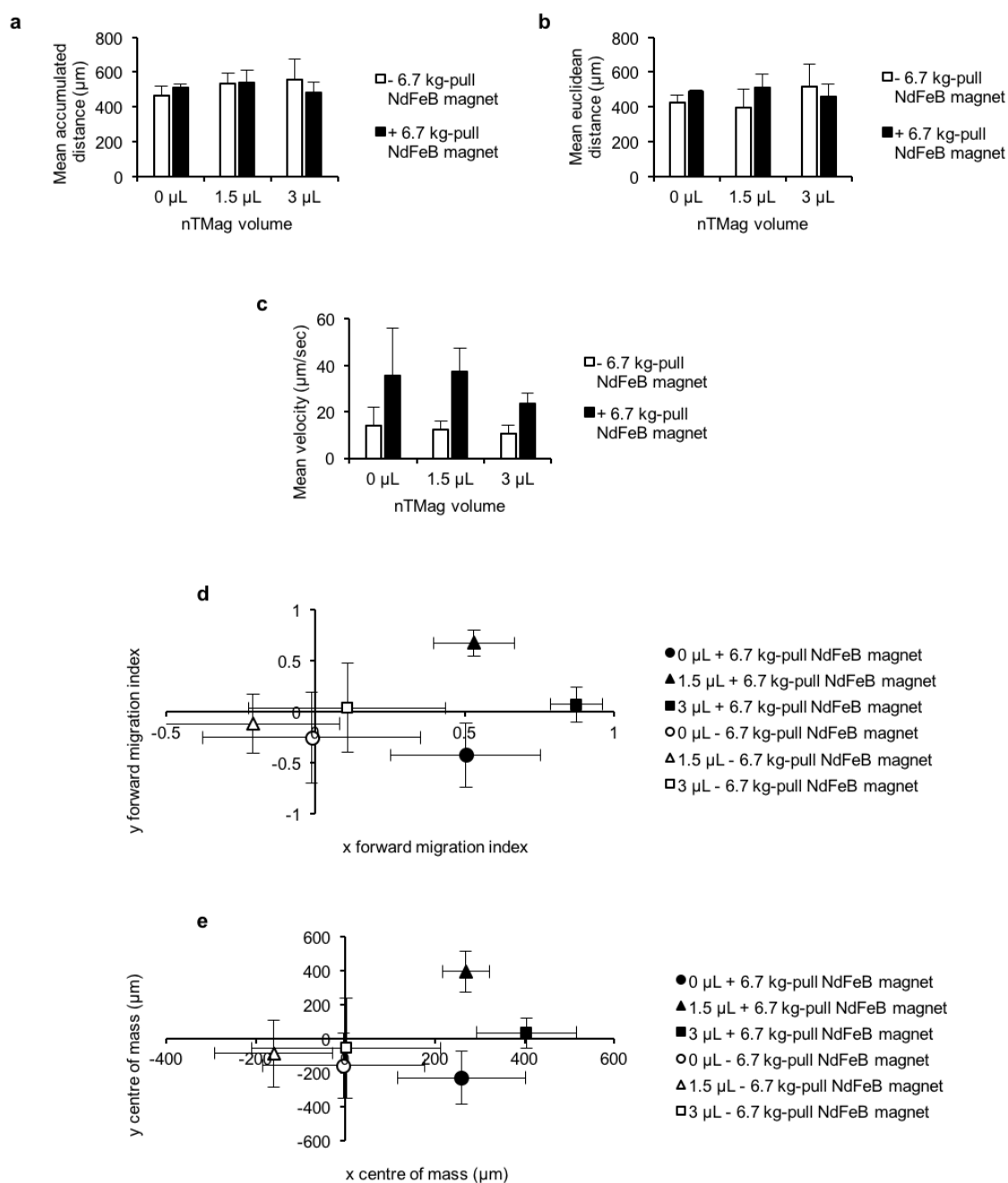
Figure 6.3 Quantification of NSC tracking in the presence of a 6.7 kg-pull NdFeB magnet with 0 µL, 1.5 µL or 3 µL nTMag. (**a**) Mean accumulated distance for each experimental condition. p>0.05, ANOVA with Tukey post-hoc. (**b**) Mean euclidean distance for each experimental condition. p>0.05, ANOVA with Tukey post-hoc. (**c**) Mean velocity for each experimental condition. p>0.05, ANOVA with Tukey post-hoc. (**d**) Mean x and y migration indices for each experimental condition. p>0.05, Mann-Whitney with Bonferroni correction (x forward index); p>0.05, ANOVA with Tukey post-hoc (y forward index). (**e**) Mean x and y centres of mass for each experimental condition. p>0.05, ANOVA with Tukey post-hoc. Error bars ±SEM. n=3 dishes for each experiment.

6.2.2 NSC tracking with 23 kg-pull NdFeB magnet

In the absence of the 23 kg-pull magnet, movement paths were random, but directionality appeared

to improve in the presence of magnet with both volumes of nTMag used (Figure 6.4). There was no

difference in movement distance or velocity between groups ($p > 0.05$, ANOVA with Tukey post-hoc)

(Figure 6.5a-c). Although not significant ($p > 0.05$, Mann-Whitney with Bonferroni correction or ANOVA

with Tukey post-hoc), there was a trend of an increase in directionality in the x axis, measured as

forward migration indices and centres of mass, in the presence of the magnet with no nTMag. The y

forward migration index was significantly greater for NSCs with 0 µL nTMag no magnet compared to

3 µL nTMag with magnet (Figure 6.5d-e).

23 kg-pull NdFeB magnet

a

No magnet + 0 uL nTMag		Magnet + 0 uL nTMag	
t = 0 min	t = 9 min	t = 0 min	t = 9 min

b

c

No magnet + 3 uL nTMag		Magnet + 3 uL nTMag	
t = 0 min	t = 9 min	t = 0 min	t = 9 min

d
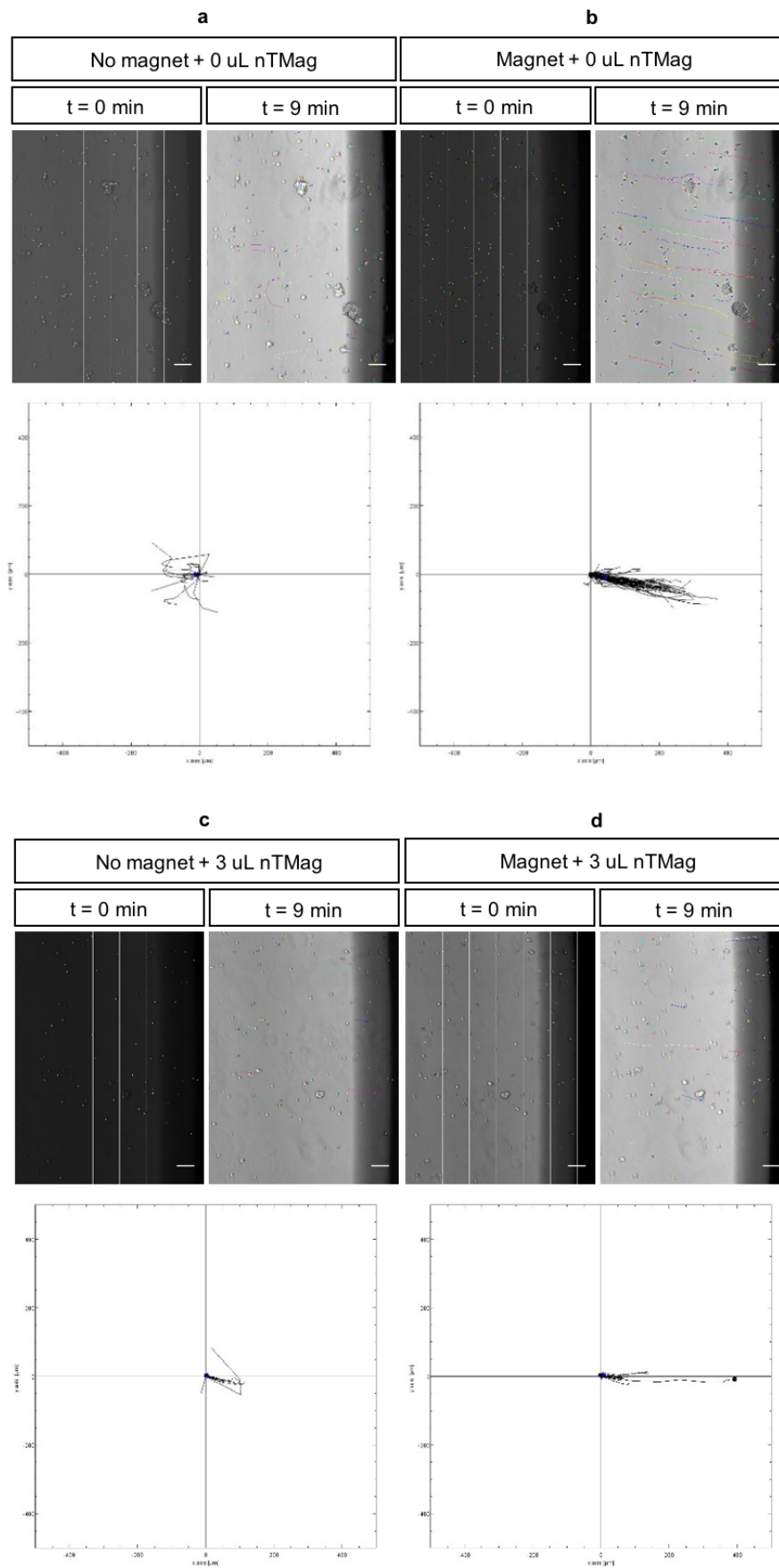
Figure 6.4

Figure 6.4 (previous page) Cell tracking analysis of GFP-NSCs with 23 kg-pull NdFeB magnet using the plugin mTrack. The start (*left*) and end (*right*) frames are shown for each condition. The cell movement plots (*bottom*) show the migration track of each cell relative to its starting position (origin). (**a**) No magnet, no nTMag. (**b**) Magnet, no nTMag. (**c**) No magnet, 3 µL nTMag. (**d**) Magnet, 3 µL nTMag. Scale bars: 50 µm.
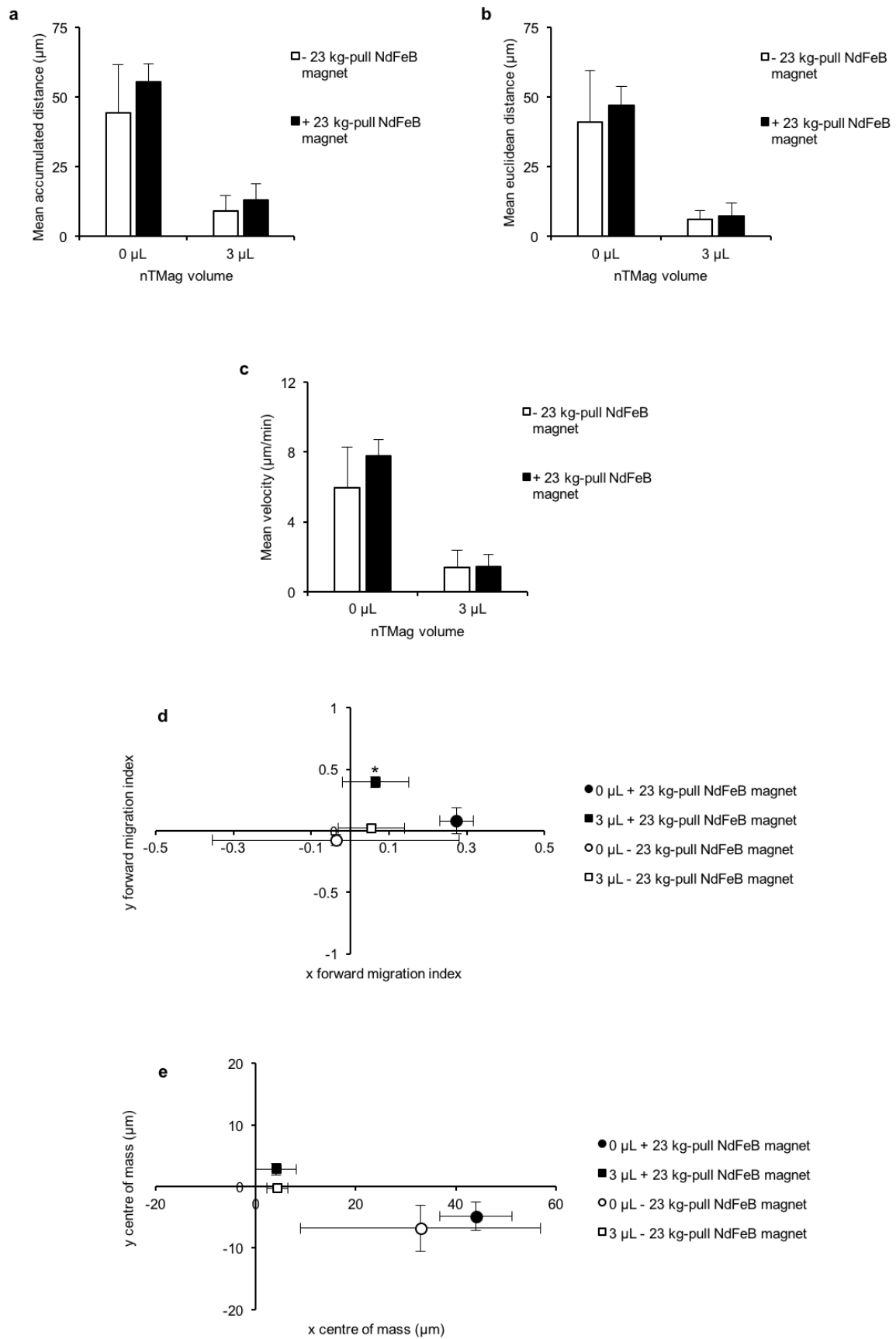
Figure 6.5

Figure 6.5 (previous page) Quantification of NSC movement tracking in the presence of a 23 kg-pull NdFeB magnet with 0 μL or 3 μL nTMag. (**a**) Mean accumulated distance for each experimental condition. p>0.05, ANOVA with Tukey post-hoc. (**b**) Mean euclidean distance for each experimental condition. p>0.05, ANOVA with Tukey post-hoc. (**c**) Mean velocity for each experimental condition. p>0.05, ANOVA with Tukey post-hoc. (**d**) Mean x and y migration indices for each experimental condition. *p<0.05, ANOVA with Tukey post-hoc. *represents 0 μL no magnet vs. 3 μL with magnet y forward migration index. (**e**) Mean x and y centres of mass for each experimental condition. p>0.05, ANOVA with Tukey post-hoc. Error bars ±SEM. n=≥2.

6.2.3 NSC tracking with 38 kg-pull NdFeB magnet

In the absence of the 38 kg-pull magnet, migration paths were random, but there was more coherent directionality in the presence of the magnet with both volumes of nTMag used (Figure 6.6). There was no difference in movement distance or velocity between groups (p>0.05, ANOVA with Tukey post-hoc) (Figure 6.7a-c). Although not significant (p>0.05, ANOVA with Tukey post-hoc), there was a trend of improved migration directionality in the presence of the magnet with both volumes of nTMag (Figure 6.7d-e).

38 kg-pull NdFeB magnet
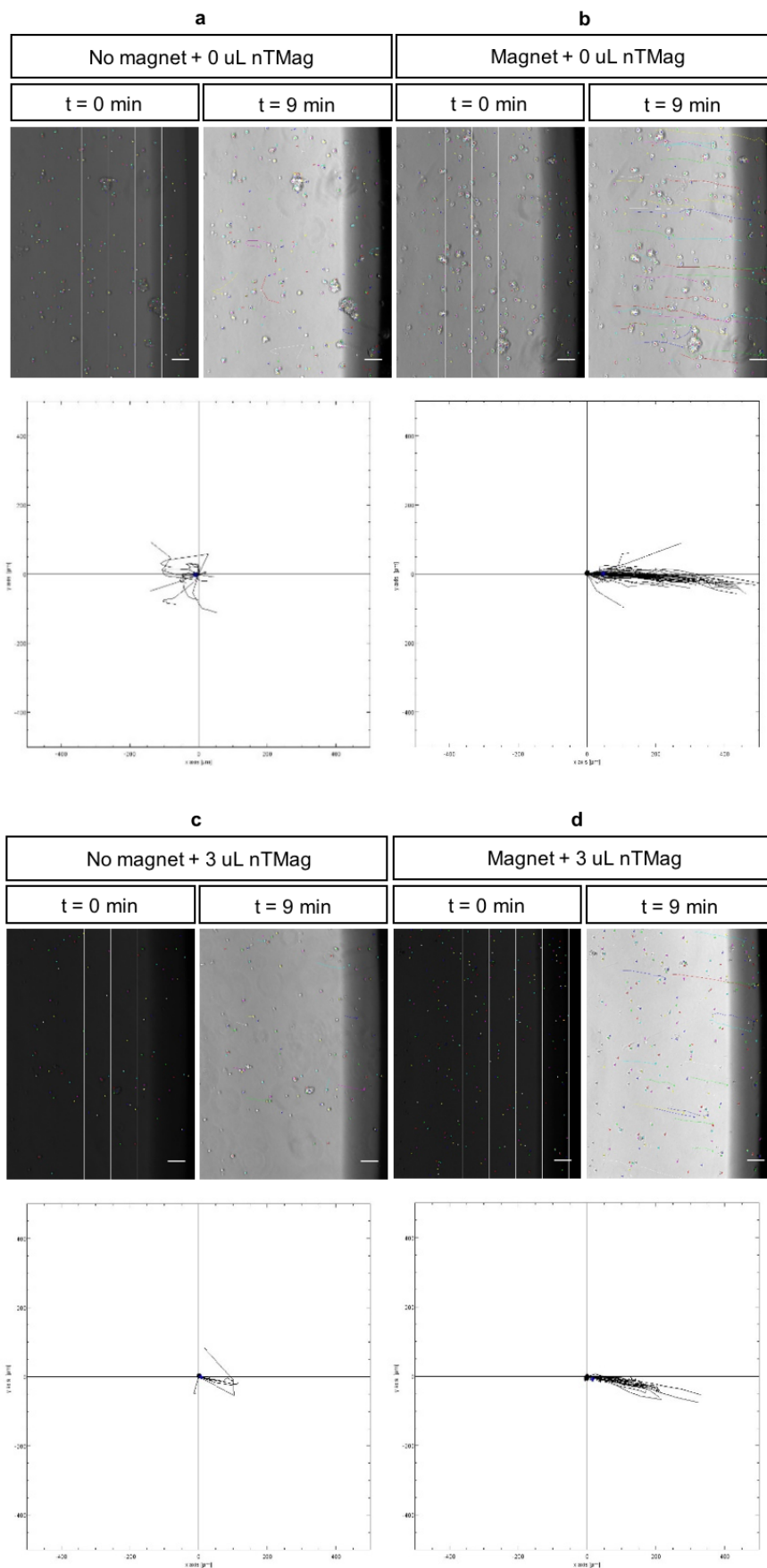
Figure 6.6

Figure 6.6 (previous page). Cell tracking analysis of GFP-NSCs with 38 kg-pull NdFeB magnet using the plugin mTrack. The start (*left*) and end (*right*) frames are shown for each condition. The cell movement plots (*bottom*) show the movement track of each cell relative to its starting position (origin). (**a**) No magnet, no nTMag. (**b**) Magnet, no nTMag. (**c**) No magnet, 3 µL nTMag. (**d**) Magnet, 3 µL nTMag. Scale bars: 50 µm.
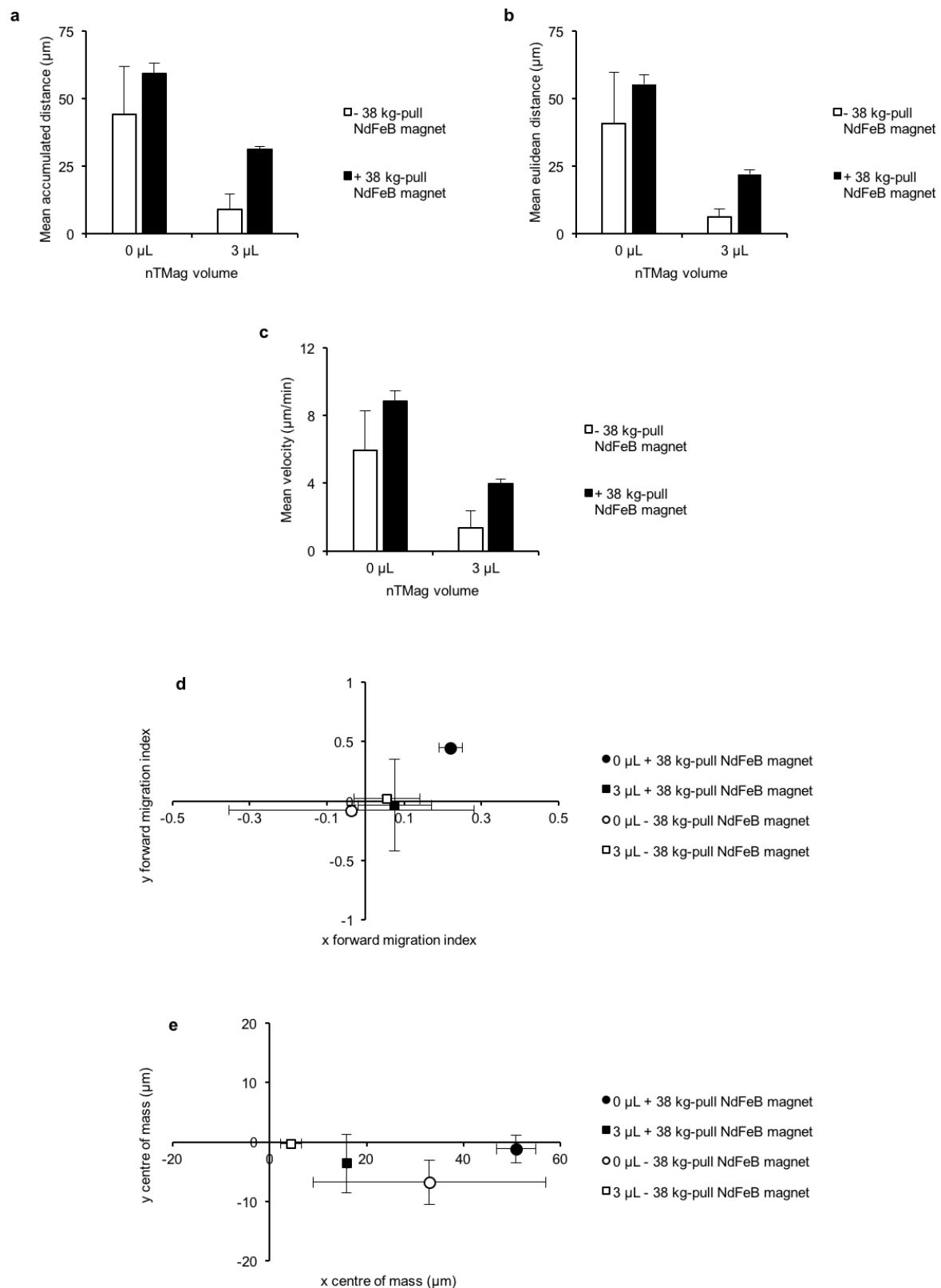
Figure 6.7 Quantification of NSC tracking in the presence of a 38 kg-pull NdFeB magnet with 0 µL or 3

µL nTMag. The data show a trend of increased distance, speed and directionality in the presence of

the magnet. (**a**) Mean accumulated distance for each experimental condition. p>0.05, ANOVA with

Tukey post-hoc. (**b**) Mean euclidean distance for each experimental condition. p>0.05, ANOVA with Tukey post-hoc. (**c**) Mean velocity for each experimental condition. p>0.05, ANOVA with Tukey post-hoc. (**d**) Mean x and y migration indices for each experimental condition. p>0.05, ANOVA with Tukey post-hoc. (**e**) Mean x and y centres of mass for each experimental condition. p>0.05, ANOVA with Tukey post-hoc. Error bars ±SEM. n=≥2.

6.3 The effect of electromagnetic fields on NSC movement

Since electromagnets can be designed to have stronger fields than the same sized permanent magnet, the effect of an electromagnet on the migration patterns of NSCs was investigated. GFP-expressing NSCs (passage 43) were seeded on laminin and disassociated as before and imaging experiments were repeated as described in 6.2 with no nTMag only, with NSCs on the bottom surface of the dish imaged for cell tracking experiments. Images were then taken with a 25 kg pull electromagnet, operated at 0.2 A, 24 V, held 10 mm from the edge of the dish. NSCs were tracked as before.

In the absence of magnet, NSC movement paths were relatively random, but in the presence of the 25 kg-pull electromagnet movement directionality was improved (Figure 6.8a-b). There was no difference (p>0.05, ANOVA with Tukey post-hoc) in migration distance or velocity with the addition of the electromagnet, but NSC migration distance and velocity showed a trend of decrease compared to the data from experiments with the 23 kg-pull and 38 kg-pull NdFeB magnets (Figure 6.8c-e). Although not significant (p>0.05), directionality in the x axis tended to increase in the presence of the electromagnet, as measured by forward migration indices and centres of mass. The y forward migration index was significantly greater (p<0.05, ANOVA with Tukey post-hoc) in NSCs with 0 µL nTMag + 38 kg-pull magnet compared to every other group (Figure 6.8f-g).
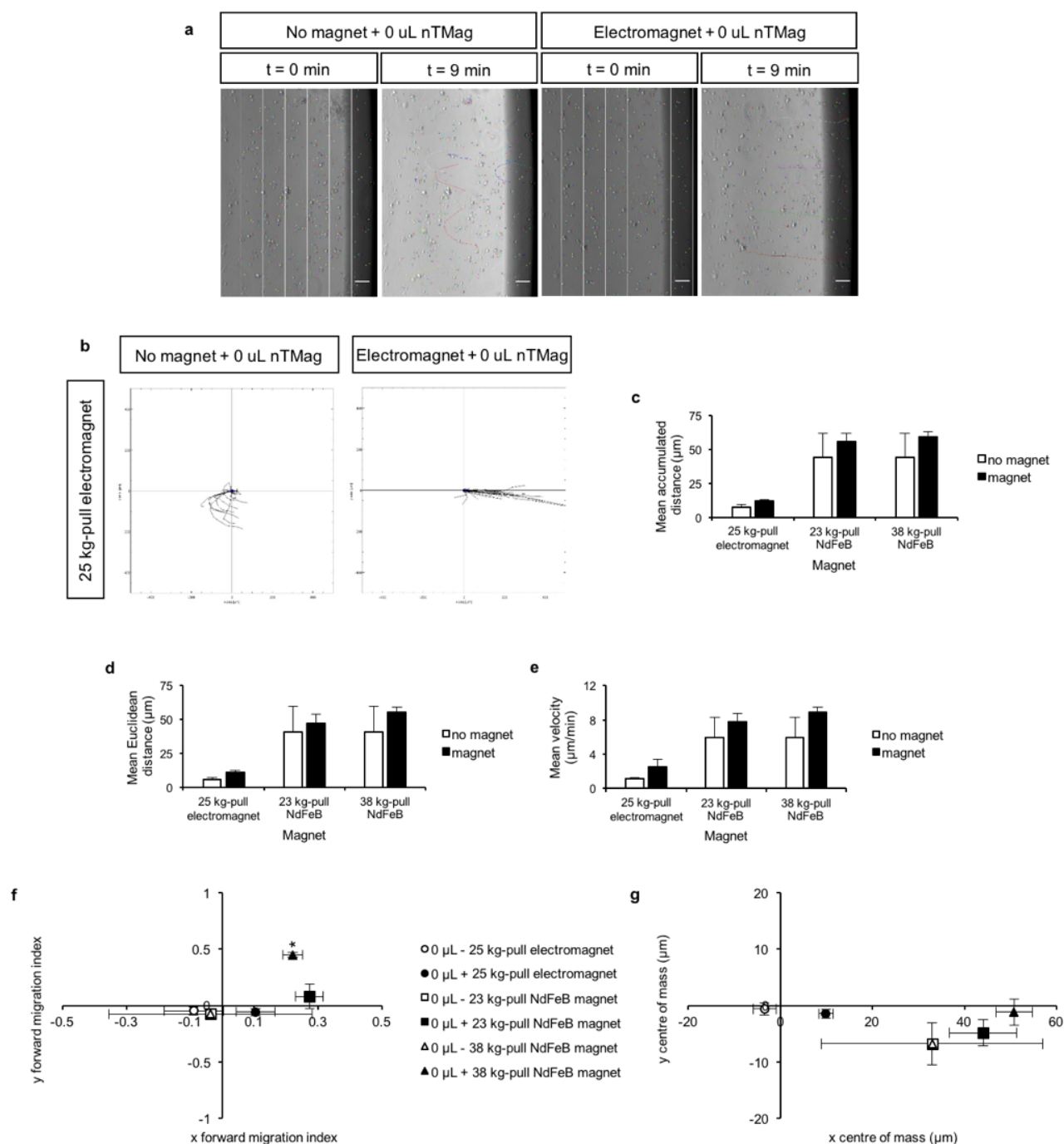
Figure 6.8 Cell tracking analysis of GFP-NSCs with a 25 kg-pull electromagnet using the plugin mTrack. Cell tracking demonstrates increased directionality in the presence of the magnet. (**a**) Images of tracked cells ± the electromagnet, with the starting and final frame shown for each condition. Scale bars: 50 μm. (**b**) Cell movement plots for each condition, showing the movement tracks of every cells relative to its starting position (origin). (**c**) Mean accumulated distance, shown with the values for the tracking experiments with the 23 kg and 38 kg-pull NdFeB magnets with no nTMag for comparison. p>0.05, ANOVA with Tukey post-hoc. (**d**) Mean euclidean distance, shown with the values for the tracking

experiments with the 23 kg and 38 kg-pull NdFeB magnets with no nTMag for comparison. $p > 0.05$,

ANOVA with Tukey post-hoc. (**e**) Mean velocity, shown with the values for the tracking experiments

with the 23 kg and 38 kg-pull NdFeB magnets with no nTMag for comparison. $p > 0.05$, ANOVA with

Tukey post-hoc. (**f**) Mean x and y migration indices, shown with the values for the tracking experiments

with the 23 kg and 38 kg-pull NdFeB magnets with no nTMag for comparison. *$p < 0.05$, ANOVA with

Tukey post-hoc. *represents 0 µL with 38 kg-pull magnet vs. all other groups y forward migration index.

(**g**) Mean x and y centres of mass, shown with the values for the tracking experiments with the 23 kg

and 38 kg-pull NdFeB magnets with no nTMag for comparison. $p > 0.05$, ANOVA with Tukey post-hoc.

Error bars ±SEM. n=3 (electromagnet); n≥2 (23 kg-pull and 38 kg-pull NdFeB magnets).

6.4 Permanent magnetic fields increase integration of NSCs into the retinal explant

To test the effect of a permanent magnetic field on the movement of NSCs in a more clinically relevant model, 6 explants (3 mice, male, 2 months old) were cultured for 3 h with a 2 mL topical aliquot of 1×10^5 NSCs/cm^2 with a 38 kg-pull NdFeB magnet placed directly underneath the culture dish (10 mm from explant) or no magnet as control (Figure 6.9a). At the end of the culture period the explants were fixed and nuclear stained with TO-PRO-3. The entire GCL-IPL of each explant were imaged by confocal microscopy in 1 um steps (1024x1024 pixels images) in each quadrant of each explant (Figure 6.9b). The green channel intensity of every GFP+ NSC was measured in each slice from the GCL to the INL and the IPL depth at each slice was quantified as % IPL depth.

In the presence of the magnet, more GFP+ cells could be seen in the GCL or IPL, whilst GFP+ cells in control retinas seemed to be mostly located above the GCL (Figure 6.9c-d). This was confirmed by quantification, in which explants with the magnet had significantly increased ($p<0.05$, ANOVA with Tukey post-hoc) green channel intensity at depths of >0%-50% IPL (Figure 6.9e).
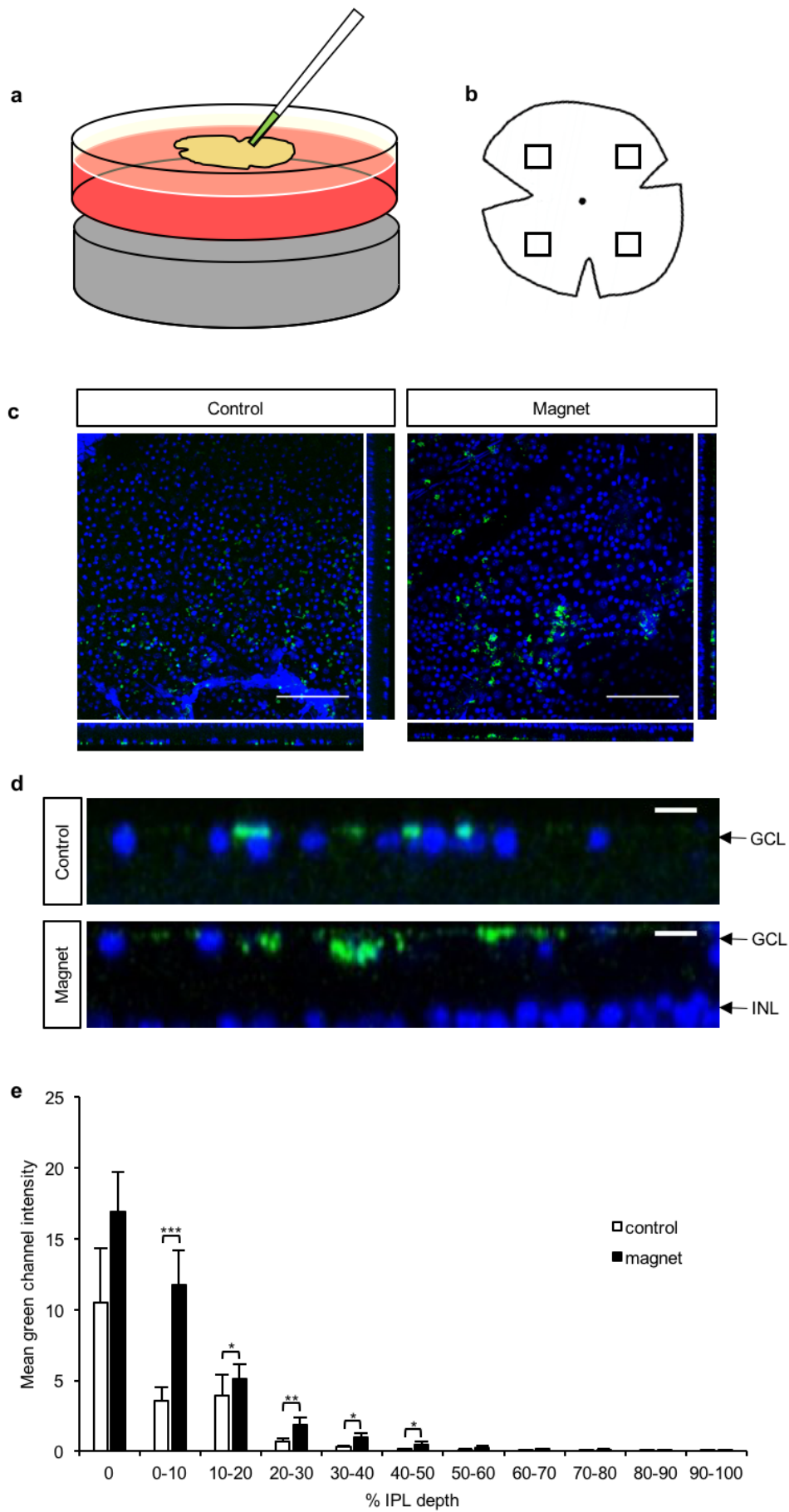
Figure 6.9

Figure 6.9 (previous page) GFP-NSC migration into the mouse retinal explant with a permanent 38 kg-pull magnet. (**a**) Experimental set-up. The magnet was placed directly underneath the culture dish and the NSCs were placed directly on top of the explant, as shown. (**b**) Locations for confocal images of explant following migration experiment. One area in each quadrant of the retina was imaged. (**c**) Representative images of the GCL after 3 hours of NSC migration in the absence (*left*) and presence (*right*) of the magnet. The orthogonal views are presented. Scale bars: 100 µm. (**d**) Orthogonal XZ view of control (*top*) and magnet (*bottom*) explants are shown in higher magnification to demonstrate increased depth of NSC migration in the IPL in the presence of the magnet. Scale bars: 10 µm. (**e**) Quantification of green channel intensity at different depths of the IPL with and without the magnet. *p<0.05, **p<0.005, ***p<0.001, ANOVA with Tukey post-hoc. Error bars: SEM.

6.5 Conclusions

In this chapter I explored the potential of guiding NSCs using external magnetic fields, with a view to using NSCs to deliver a more sustained delivery of BDNF to RGCs within the retinal explant. It should be noted that the in vitro NSC 'migration' measured in this chapter was the directed movement of cells in suspension using magnetic fields, rather than traditional cell migration across a substrate. Without measuring the changes in activation levels of proteins, such as Rac (Ridley et al. 1999), following introduction of a magnetic field the NSC movement in the retinal explant also cannot be confirmed as cell migration. Nevertheless, the results thus far are promising for the use of magnetic fields to direct stem cells for the efficient delivery of neurotrophic agents.

My data demonstrated a trend for movement distance, speed and directionality to increase in the presence of a magnetic field, both with and without addition of mnps, but no significant difference in migration parameters was measured for any group. This may have been because the images were taken at the edge of the dish where cell movement was limited by the dish boundary. In the future it would be interesting to segment migration analysis into smaller bands and examine the effect of distance from magnet surface – especially as magnetic field strength declines exponentially as the inverse square of the distance. The lack of significance also reflects large variability in movement patterns of NSCs in suspension, particularly in vitro. Experiments should therefore be repeated in order to obtain data for a much greater number of cells, and over longer time periods.

Temperature is likely to be a factor that was largely overlooked in the current study. In the experiments described here, the NSCs were taken from a 37°C incubator and imaged in a room that was not temperature controlled. These will likely have resulted in the formation of convection currents, which may have had a confounding effect on the movement of NSCs. Further, since an alteration in temperature of only 1°C affects the apparent magnetic field strength (but not magnetic flux density) (Reiser et al. 2007), there may have been large variations depending on day, and even time of the experiment. For these reasons, it would be instructive to repeat these experiments using

a temperature-controlled chamber. Heat production by the electric current of the electromagnet should also be considered. It was noted that there was considerable heat production during the use of the electromagnet, which may have been cytotoxic and should be checked with a viability assay. Although not significant, it was observed that the movement distances and velocities for NSCs with the electromagnet, including control cells, were generally lower than controls with the other magnets. This may have been a result of low n numbers, which can be easily tested by repeating all the experiments to check for reproducibility. Alternatively, the reduction in motility may have reflected a decrease in viability of the cells, which were of higher passage number for the experiments with the electromagnet, compared to the other magnets. It is well known that stem cell viability decreases with passage number (Martin-Piedra et al. 2014) and this could be tested by Trypan blue staining. Although it has been reported that mnps do not adversely affect cell viability or migration behaviour (Ramaswamy et al. 2015), this should be verified with viability assays.

Although I measured a significant increase in the NSC migration/movement depth with the magnet, migration was limited to the upper 50% of the IPL. In the context of cell-mediated delivery of BDNF, this may result in protection being given to ON-stratified dendrites only. However, since it was reported in the rat magnetic field-mediated retention of cardiosphere-derived cells in the coronary artery took 24 hours (Cheng et al. 2012), it is likely that the experimental timeline used here was not long enough to identify the limit of magnetic field-directed movement of the cells. In line with this, it would be valuable to monitor the movement of NSCs in the explant using time-series imaging, so that migration speed can be assessed.

6.6 Summary

There was no significant effect of external magnetic fields (permanent or electromagnetic) on the movement of NSCs in suspension in vitro, even following inclusion of mnps. In contrast, application of a permanent magnetic field increased the depth of NSC migration into the IPL of explants in the absence of mnps.

Chapter 7: General discussion

7.1 The retinal explant as a model to investigate neuronal degeneration

In this thesis I have shown that the morphometric analysis of RGCs provides a readout of neuronal cell health in a translatable model of neuronal degeneration that is rapid and robust, compared to similar in vivo models, in which neuronal degeneration is markedly slower. I have highlighted a discrepancy between cell loss and dendritic retraction, thus outlining a window in which to delineate degenerative events and to investigate the effects of neuroprotective agents.

There are a number of challenges with working with this model. One problem is that there is no 'perfect' RGC marker. Thy1 is one of the most widely used RGC markers, but only labels 70% of RGCs (Perry et al. 1984) and fluctuates in expression level following optic nerve damage (Schlamp et al. 2001; Astafurov et al. 2014). It would be interesting to compare the levels of Thy1 to the levels of other neuronal markers, such as Brn3, NeuN and TUJ1 to allow a more accurate assessment of the number of RGCs. Given that there is no perfect marker of RGCs and viability markers are not reliable markers of cell death in this model, nuclear staining likely provides the best readout of RGC loss, particularly given that amacrine cells are resistant to cell death (Kunzevitzky et al. 2010) and so their numbers may be considered to be constant (offset). This model is limited as a generic CNS model because, unlike most neurons in the brain, RGCs do not have dendritic spines. Nevertheless, the retinal explant offers a major advantage over the hippocampal brain slice by the presence of intact neuronal networks.

Cell sub-type analysis revealed that OFF-stratifying RGCs may be more susceptible to dendritic pruning than the other sub-types, as reported in the mouse (El-Danaf and Huberman 2015; Johnson et al. 2016). Although intriguing, division of cells into sub-types results in small sample numbers, thereby making it difficult to draw firm conclusions. This is a problem in the mouse, where at least 14 different structural RGC types (Coombs et al. 2006) and 30 different functional types (Baden et al. 2016) have

been identified. Classification is further complicated in disease, where the measurements required for classification (distal dendrites and dendritic field size) are often altered. This problem can be circumvented with the use of parameters that are resistant to change, such as measurements of proximal dendrites (Tribble et al. 2014).

Pan-caspase inhibition was modestly protective against retraction of proximal dendrites (Figure 3.8c in Chapter 3). This was surprising, given the breadth of evidence for caspase-dependent dendritic pruning (Williams et al. 2006; D'Amelio et al. 2010) and the reported role of local caspases activity in dendritic atrophy in glaucoma (Kisiswa et al. 2010b; Erturk et al. 2014). One possibility is that perhaps caspases do not play a major role in axotomy-induced RGC dendropathy. There is good evidence that axotomy activates calpains (serine-threonine proteases) in a calcium-mediated manner via sarm1 (Yang 2015). Calpains degrade cytoskeletal proteins, such as microtubule-associated proteins 1 and 2 (Billger et al. 1988), resulting in proximal axon retraction, a process known as Wallerian degeneration (Waller 1850; Stoll et al. 2002), and glutamate-induced dendritic retraction in hippocampal neurons (Wilson et al. 2000). It would be interesting to apply calpain inhibitors to investigate whether this mechanism exists in axotomy-induced RGC degeneration in the retinal explant.

Absence of light may contribute to neuronal degeneration in the retinal explant. Since light inhibits the plasticity of synapses connecting ON bipolar cells to ON RGCs (Xia et al. 2007), scotopic conditions may remove this inhibition, as demonstrated in the mouse explant (Xia et al. 2006). In the absence of light retinal neurotransmission is increased due to permanent photoreceptor depolarisation (Xu et al. 2007). This increase in neuronal activity may result in increased oxidative stress caused by reactive oxygen species, or glutamate-induced excitotoxicity caused by increased glutamate secretion that have been shown to induce dendritic atrophy in CA1 and CA3 pyramidal neurons (Christian et al. 2011). These mechanisms may have played a role in the dendritic retraction of RGCs measured here.

 Dendrite loss implies synapse loss. Since synapses are formed throughout dendritic arbors (Spruston 2008), it seems logical to infer that dendrite retraction would be associated with synapse loss.

However, this must be verified by future experiments as it has not been explicitly shown in this study. This could be achieved by immunohistochemistry with the post-synaptic marker PSD-95, and the pre-synaptic markers VGlut1 and synaptophysin (Johnson et al. 2007; Ippolito and Eroglu 2010). Alternatively, biolistic labelling could be used (Lo et al. 1994; Morgan et al. 2008). Biolistic labelling would be preferable since it would permit quantification of the rate of synapse loss with time-series imaging. Although widespread dendrite loss is likely to be accompanied by synapse loss, the two events may not occur concurrently, as shown in a mouse model of Alzheimer's disease where dendrite loss precedes synapse loss (Williams et al. 2013b). Biolistics would allow the relationship between dendrite loss and synapse loss to be delineated in the retinal explant, as well as validation of the morphometric changes reported here. Labelling of synaptic locations may also provide information regarding neuronal gain. The combination of inputs onto specific dendritic compartments can greatly alter the functional output of the neuron, i.e. firing rate or spike frequency (Silver 2010; Pouille et al. 2013). It is important to note that biolistics was not suitable in the current study because it requires a 2 d incubation period for the expression of transfected DNA and since DiI and DiO are toxic, temporal 'snapshots' were the best way to quantify dendritic changes.

7.2 The retinal explant as a model to investigate the effect of BDNF

The application of neurotrophic agents is an appealing therapeutic strategy to combat neuronal degeneration. The retinal explant is an ideal model to test potential treatment paradigms and their effect on neuronal morphology. Since BDNF application has been shown to protect against cell loss (Chen and Weber 2001), it is an attractive agent for neuroprotection. However, it is difficult to control the concentration and location of BDNF in vivo because it is a pharmacologically 'sticky' protein that has a short half-life and does not cross the blood-brain barrier well (Poduslo and Curran 1996; Lu 2003). With an ex vivo model BDNF can be applied directly to the target site. Further, since Sarm1 signalling may be implicated in axotomy-induced degeneration, BDNF may target pathways implicated in degeneration. BDNF-TrkB signalling activates Akt, which inhibits MKK4, thus blocking downstream activation of JNK signalling (Longo and Massa 2013). Here I demonstrate that BDNF treatment, initiated immediately after axotomy or 3 d-post axotomy significantly retarded dendritic atrophy of RGCs.

The neuroprotective effect of BDNF shown here is perhaps not surprising, given the well-evidenced role of BDNF in maintenance of dendritic arbor morphology in development (McAllister et al. 1996; Bibel and Barde 2000; Yacoubian and Lo 2000) and in the adult (Xu et al. 2000). Many groups have demonstrated that BDNF application protects against cell death (Ma et al. 1998; Mocchetti and Bachis 2004). In the cat optic nerve crush model BDNF has been shown to reduce RGC loss (Chen and Weber 2001) and retard dendritic retraction of RGCs (Weber and Harman 2008)) . This work is of interest, but since exogenous BDNF is difficult to control in vivo, the ex vivo model is a more reliable platform. Further, the optic nerve crush is not a consistent injury, unlike the total axotomy performed here. In line with the mechanism of BDNF I propose here, it has been reported in the mouse retinal explant that Thy1-YFP labelled RGCs show reduced dendrite loss with a combination of BDNF and CNTF (Johnson et al. 2016). However, the true therapeutic effect is not clear since, as previously outlined, Thy1 labelling underreports dendritic pruning (Williams et al. 2013a). Furthermore, it is uncertain

what role BDNF had in the protective effect shown in this study because only a combination treatment of BDNF+CNTF was used.

One of the major limitations of work investigating neurotrophic support in neuronal degeneration is the pathology vs. treatment timescale. In general, agents are applied at the time of, or even before the time of injury. This is unlikely to be possible in the clinic due to current screening methods and the ability of neuronal networks to compensate for cell loss. Here, I show for the first time that BDNF treatment initiated 3 d-post axotomy offers significant protection against dendritic retraction, and may promote dendritic outgrowth. It will be important to determine how sustained the neuroprotective effects of BDNF are in this model prior to in vivo trials.

The morphometric data from retinal explants treated with delayed BDNF (Figure 4.3 in Chapter 4) presented here are suggestive of a neurite outgrowth mechanism of BDNF, similar to that reported in the adult guinea pig auditory nerve (Miller et al. 2007). However, it should be noted that this hypothesis needs to be confirmed by time-series imaging. Nevertheless, the prospect of an agent that can be applied post-injury and restore neurons to a native-like morphology is exciting because it suggests that it may be possible to re-wire neuronal networks and restore function. In the future it would be interesting to investigate synapse formation in the IPL in parallel with dendrite outgrowth, since the presence of synapses is essential for dendrite extension to have a positive functional effect. This could be achieved by biolistic labelling, for example using PSD-95, which could be used in combination with biolistic labelling of cytoskeletal markers in order to validate the dendritic outgrowth mechanism of BDNF.

BDNF is an attractive candidate for treatment of retinal degeneration because it has been reported that its main receptor, TrkB, is upregulated following optic nerve injury (Cui et al. 2002). The neuroprotective effect of cell-mediated delivery of BDNF is potentially limited by the availability of extracellular BDNF-processing enzymes. High level BDNF secretion in the unprocessed pro-BDNF form could saturate active sites of enzymes such as plasmin, resulting in increased pro-BDNF signalling. The

resultant pro-apoptotic and pro-dendritic retraction signalling could counterbalance the protective effects of BDNF. Fortunately, p75^{NTR} is not expressed by RGCs in the mouse retinal explant (Hu et al. 1999). Confirmation that p75^{NTR} is not expressed by RGCs in the explant would support cell-based delivery of BDNF because presumably any secreted pro-BDNF would not have a negative effect on RGCs. It would be interesting to map the expression levels of TrkB and p75^{NTR} over time in the retinal explant to verify that TrkB is a good target. The phosphorylation state of TrkB should also be measured, since there is evidence that TrkB is inactivated (dephosphorylated) following glaucomatous damage (Gupta et al. 2012).

7.3 Chondroitin sulphate proteoglycan remodelling does not augment neuroprotection in combination with BDNF

The PNN is postulated to be a barrier to neuronal plasticity and stem cell integration (Pizzorusso et al. 2002; Fawcett 2015). I used morphometric analysis to investigate the effect of CSPG digestion on RGC plasticity in the degenerating explants, as well as a potential synergistic effect of combined ChABC and BDNF treatment. Over longer culture periods (6 d) ChABC treatment promoted RGC dendritic remodelling. I was, however, surprised to find that ChABC treatment completely blocked the neuroprotective effect of BDNF, even when the concentration of BDNF was increased.

Successful CSPG digestion by ChABC was evidenced by immunohistochemistry. However, it is worth noting that there was only evidence of CSPG digestion around RGC somas and proximal dendrites, presumably because the PNN tends to be restricted to these areas (Lee et al. 2012). Since the proximal dendrites are most resistant to retraction, this may begin to explain the limited effect on plasticity of ChABC treatment. Alternatively, given the limited immune response in ex vivo preparations, the PNN may not be upregulated to the same extent as in vivo models of CNS damage (Raposo and Schwartz 2014).

NCAM has been reported to improve the efficiency of BDNF-TrkB binding. NCAM interacts with CS GAG chains on CSPGs and also binds directly to TrkB. NCAM binds directly to TrkB and the polysialic acid tail of NCAM interacts with BDNF (Vutskits et al. 2001), thereby increasing the likelihood of BDNF binding to TrkB (Cassens 2010). NCAM interacts with CS GAGs on CSPGs (Figure 1.7), thereby positioning NCAM close to neurites where BDNF-TrkB signalling occurs. Since CSPGs are upregulated in response to CNS injury, it is possible that this may facilitate neurotrophin signalling in an attempt improve neuronal survival in the wake of an immune response. Interaction between BDNF and the PNN may also be explained by the large number of positively charged residues on the BDNF protein, which enable the formation of electrostatic bonds with the highly negatively charged components of CSPGs. Digestion of CSPGs may therefore reduce the binding affinity of BDNF for TrkB, which may

explain the inhibitory effect of ChABC treatment on BDNF-induced neuroprotection, even when ChABC and BDNF were not present at the same time.

The possible effect of NCAM on BDNF-TrkB binding strengthens the case for using TrkB activating agents in place of BDNF. TrkB agonists improved RGC survival in models of optic nerve injury (Hu et al. 2010) and glaucoma (Bai et al. 2010). In addition, TrkB agonists can be designed to have more favourable properties than BDNF, including higher binding affinity, higher specificity to TrkB, longer half-life, and better ability to cross the blood-brain barrier (Qian et al. 2006; Bai et al. 2010; Massa et al. 2010; Brahimi et al. 2014; Liu et al. 2016). Since these agents would presumably not require the presence of CSPGs to strengthen binding to TrkB, they could be used in combination with ChABC treatment. Finally, these agents could be generated as peptides, meaning that DNA encoding their sequence could be used in conjunction with cell-mediated delivery to secrete the agent to the target cells.

7.4 Cell-mediated delivery of neurotrophic agents may be improved by manipulation of NSC migration using external magnetic fields

Here I present data that support of the use of external magnetic fields to guide NSCs in vitro and into ex vivo tissue, with a view to using NSCs to deliver BDNF in a sustained manner. Permanent magnets have been used to direct mnp-containing stem cells or endothelial cells in vitro (Moysidis et al. 2015), as well as to lesion sites in the spinal cord (Vishwakarma et al. 2015) and to the retina (Yanai et al. 2012), with moderate success. To date, work with magnetic field-driven migration in vivo has generally only been applied to target sites bordering the bloodstream. In this study I present the first evidence that this technology may be used to drive migration of stem cells *into* neuronal tissue, offering promise that it may finally be possible to target previously inaccessible parts of the brain.

The data presented here demonstrating increased migration depth of NSCs in the absence of mnps into a retinal explant towards the direction of a permanent magnet (Figure 6.9 in Chapter 6) supports the postulated presence of a magnetoreceptor in mammals. Once a ridiculed idea, the concept of a magnetic field-sensitive receptor has more recently become generally accepted (Lohmann 2016). There is evidence that a magnetoreceptor may explain the migratory behaviour of several organisms, including bacteria, drosophila and homing pigeons (Mora et al. 2004; Baumgartner et al. 2013; Qin et al. 2016) but researchers have debated the existence of such a receptor in mammals, including humans. The data I present here supports the existence of a mammalian magnetoreceptor and poses the exciting possibility of using external magnetic fields to control both the migration and the selective gene expression of stem cells to deliver neurotrophic support to degenerating neurons. Since activation of the magnetoreceptor stimulates calcium influx (Knoepfel and Akemann 2010; Long et al. 2015), it is easy to envisage how magnetic fields could be used to control BDNF expression in transfected NSCs. These cells could then be directed to the target site, where the secretion of BDNF could be remotely controlled.

It has been reported that CSPG digestion improves integration efficiency of photoreceptor precursor cells in the adult mouse retina (Barber et al. 2012). It would be interesting to examine the effects of ChABC treatment on NSC migration depth in the retinal explant. On the other hand, this is unlikely to be clinically useful if the NSCs are used to deliver neurotrophic agents, given the inhibitory effect of ChABC treatment on the action of BDNF. ChABC-digested PNN components are replaced within 5 weeks in vivo (Fawcett 2015). The CSPG replacement time should be investigated in the explant, since it may be that ChABC could be used to aid migration of BDNF-expressing NSCs into the IPL, and after the PNN has been rebuilt, BDNF could elicit its neuroprotective effects.

The specifications of the magnet need to be optimised to enable clinical translation. Small instruments can be placed behind the retina during surgery, therefore the retina is an ideal tissue to test the potential of magnetic field-directed migration of stem cells. However, it should be noted that the 38 kg-pull magnet used here is too large to fit behind the retina in vivo. I have demonstrated a proof-of-principle that magnetic fields can be used to direct migration of NSCs into the retinal explant. This experiment should be repeated with a smaller magnet that could be placed behind the retina. Indeed, the magnets used here may not have appropriate magnetic field strengths for application in vivo. If the field strength is too low, there will be no beneficial effect, but field strengths that are too high could cause neurotoxicity due to an increase in noradrenaline levels (Rajendra et al. 2004). Further, it would be interesting to test the migratory effect of more than one magnet, either to shape magnetic fields outside the eye, or to generate magnetic field gradients.

The use of electromagnets may allow better control of cell migration with the aid of magnetic field gradients. As previously outlined, the electromagnet used in this study generated a large amount of heat, which may have been a confounding factor in migration experiments. In the clinic this problem could be alleviated by the use of electromagnets in MRI scanners, which contain cooling systems. Large electromagnets such as these circumvent the need to implant magnets, and have been demonstrated to be capable of directing mnp-tagged macrophages in vivo (Muthana et al. 2015).

Furthermore, MRI scanners can be used to track mnp-containing MSCs in a rat model of Huntington's

disease (Moraes et al. 2012), thereby providing a visual aid for the direction of cells.

7.5 Conclusions

The adult mouse retinal explant is an excellent model for the investigation of axotomy-induced neuronal degeneration, applicable to a wide range of CNS disorders. Morphometric analysis permits quantification of neuronal cell health, as well as inferred information regarding synaptic connectivity and functional ability. I have demonstrated that morphometric data can highlight a therapeutic window in which to probe mechanisms implicated in neuronal pathology and neuroprotection. In this model it has been shown that the activation of TrkB provides potent neuroprotection to RGC dendritic arbors, and may promote dendritic remodelling. Although CSPG digestion is unlikely to be therapeutically useful in combination with BDNF treatment in this model, my data supports cell-based delivery of BDNF, which may be optimised using magnetic fields.

7.5 Conclusions

References

Abuhatzira, L. et al. 2007. MeCP2 deficiency in the brain decreases BDNF levels by REST/CoREST-mediated repression and increases TRKB production. *Epigenetics* 2(4), pp. 214-222.

Adlard, P. A. et al. 2004. The timecourse of induction of brain-derived neurotrophic factor mRNA and protein in the rat hippocampus following voluntary exercise. *Neurosci Lett* 363(1), pp. 43-48.

Aid, T. et al. 2007. Mouse and rat BDNF gene structure and expression revisited. *J Neurosci Res* 85(3), pp. 525-535.

Alderson, R. F. et al. 1990. Brain-derived neurotrophic factor increases survival and differentiated functions of rat septal cholinergic neurons in culture. *Neuron* 5(3), pp. 297-306.

Allen, S. J. et al. 1999. Profound and selective loss of catalytic TrkB immunoreactivity in Alzheimer's disease. *Biochem Biophys Res Commun* 264(3), pp. 648-651.

Amir, R. E. et al. 1999. Rett syndrome is caused by mutations in X-linked MECP2, encoding methyl-CpG-binding protein 2. *Nat Genet* 23(2), pp. 185-188.

Amthor, F. R. et al. 1984. Morphology of on-off direction-selective ganglion cells in the rabbit retina. *Brain Res* 298(1), pp. 187-190.

An, J. J. et al. 2008. Distinct role of long 3' UTR BDNF mRNA in spine morphology and synaptic plasticity in hippocampal neurons.*Cell*. Vol. 134. United States, pp. 175-187.

Anderson, C. M. and Swanson, R. A. 2000. Astrocyte glutamate transport: review of properties, regulation, and physiological functions. *Glia* 32(1), pp. 1-14.

Andres, D. A. et al. 2008. Rit signaling contributes to interferon-gamma-induced dendritic retraction via. *J Neurochem* 107(5), pp. 1436-1447.

Aoki, T. et al. 1969. Antigenic structure of cell surfaces. An immunoferritin study of the occurrence and topography of H-2' theta, and TL alloantigens on mouse cells. *J Exp Med* 130(5), pp. 979-1001.

Assawachananont, J. et al. 2014. Transplantation of Embryonic and Induced Pluripotent Stem Cell-Derived 3D Retinal Sheets into Retinal Degenerative Mice. *Stem Cell Reports* 2(5), pp. 662-674.

Astafurov, K. et al. 2014. Complement expression in the retina is not influenced by short-term pressure elevation. *Mol Vis* 20, pp. 140-152.

Babincova, M. et al. 2004. In vivo heating of magnetic nanoparticles in alternating magnetic field. *Med Phys* 31(8), pp. 2219-2221.

Babincova, M. et al. 2002. AC-magnetic field controlled drug release from magnetoliposomes: design of a method for site-specific chemotherapy. *Bioelectrochemistry* 55(1-2), pp. 17-19.

Babincová, M. et al. 2001. Superparamagnetic gel as a novel material for electromagnetically induced hyperthermia. *Journal of Magnetism and Magnetic Materials* 225(1–2), pp. 109-112.

Badea, T. C. et al. 2009. Distinct roles of transcription factors brn3a and brn3b in controlling the development, morphology, and function of retinal ganglion cells. *Neuron* 61(6), pp. 852-864.

Baden, T. et al. 2016. The functional diversity of retinal ganglion cells in the mouse. *Nature* 529(7586), pp. 345-350.

Bahi, A. and Dreyer, J. L. 2012. Hippocampus-specific deletion of tissue plasminogen activator "tPA" in adult mice impairs depression- and anxiety-like behaviors. *Eur Neuropsychopharmacol* 22(9), pp. 672-682.

Bai, Y. et al. 2010. An Agonistic TrkB mAb Causes Sustained TrkB Activation, Delays RGC Death, and Protects the Retinal Structure in Optic Nerve Axotomy and in Glaucoma. *Investigative Ophthalmology & Visual Science* 51(9), pp. 4722-4731.

Baker, P. S. and Brown, G. C. 2009. Stem-cell therapy in retinal disease. *Current Opinion in Ophthalmology* 20(3), pp. 175-181.

Bamji, S. X. et al. 1998. The p75 Neurotrophin Receptor Mediates Neuronal Apoptosis and Is Essential for Naturally Occurring Sympathetic Neuron Death. *J Cell Biol* 140(4), pp. 911-923.

Banfield, M. J. et al. 2001. Specificity in Trk receptor:neurotrophin interactions: the crystal structure of TrkB-d5 in complex with neurotrophin-4/5. *Structure* 9(12), pp. 1191-1199.

Bannerman, P. G. et al. 2005. Motor neuron pathology in experimental autoimmune encephalomyelitis: studies in THY1-YFP transgenic mice. *Brain* 128, pp. 1877-1886.

Baquet, Z. C. et al. 2004. Early striatal dendrite deficits followed by neuron loss with advanced age in the absence of anterograde cortical brain-derived neurotrophic factor. *Journal of Neuroscience* 24(17), pp. 4250-4258.

Barber, A. C. et al. 2012. Repair of the degenerate retina by photoreceptor transplantation. *Proc Natl Acad Sci U S A*.

Barde, Y. A. et al. 1982. Purification of a new neurotrophic factor from mammalian brain. *Embo j* 1(5), pp. 549-553.

Barlow, H. B. and Levick, W. R. 1965. The mechanism of directionally selective units in rabbit's retina. *J Physiol* 178(3), pp. 477-504.

Barnstable, C. J. and Drager, U. C. 1984. Thy-1 antigen: a ganglion cell specific marker in rodent retina. *Neuroscience* 11(4), pp. 847-855.

Barton, B. et al. 2014. Paradoxical visuomotor adaptation to reversed visual input is predicted by BDNF Val66Met polymorphism. *J Vis* 14(9).

Bartus, K. et al. 2012. Chondroitin sulphate proteoglycans: key modulators of spinal cord and brain plasticity. *Exp Neurol* 235(1), pp. 5-17.

Baumgartner, J. et al. 2013. Magnetotactic bacteria form magnetite from a phosphate-rich ferric hydroxide via nanometric ferric (oxyhydr)oxide intermediates.*Proc Natl Acad Sci U S A*. Vol. 110. pp. 14883-14888.

Baydyuk, M. and Xu, B. 2014. BDNF signaling and survival of striatal neurons. *Front Cell Neurosci* 8.

Beattie, M. S. et al. 2002. ProNGF induces p75-mediated death of oligodendrocytes following spinal cord injury. *Neuron* 36(3), pp. 375-386.

Beauquis, J. et al. 2013. Environmental enrichment prevents astroglial pathological changes in the hippocampus of APP transgenic mice, model of Alzheimer's disease. *Exp Neurol* 239, pp. 28-37.

Benchenane, K. et al. 2007. Anti-NR1 N-terminal-domain vaccination unmasks the crucial action of tPA on NMDA-receptor-mediated toxicity and spatial memory. *J Cell Sci* 120(Pt 4), pp. 578-585.

Benedetti, M. et al. 1993. Differential expression of nerve growth-factor receptors leads to altered binding-affinity and neurotrophin responsiveness. *Proceedings of the National Academy of Sciences of the United States of America* 90(16), pp. 7859-7863.

Bennett, J. L. et al. 1999. Patterned expression of BDNF and NT-3 in the retina and anterior segment of the developing mammalian eye. *Invest Ophthalmol Vis Sci* 40(12), pp. 2996-3005.

Berry, C. C. and Curtis, A. S. G. 2003. Functionalisation of magnetic nanoparticles for applications in biomedicine. *Journal of Physics D-Applied Physics* 36(13), pp. R198-R206.

Bibel, M. and Barde, Y. A. 2000. Neurotrophins: key regulators of cell fate and cell shape in the vertebrate nervous system. *Genes Dev* 14(23), pp. 2919-2937.

Bibel, M. et al. 1999. Biochemical and functional interactions between the neurotrophin receptors trk and p75NTR. *Embo j* 18(3), pp. 616-622.

Bibel, M. et al. 2004. Differentiation of mouse embryonic stem cells into a defined neuronal lineage. *Nat Neurosci* 7(9), pp. 1003-1009.

Billger, M. et al. 1988. Proteolysis of tubulin and microtubule-associated proteins 1 and 2 by calpain I and II. Difference in sensitivity of assembled and disassembled microtubules. *Cell Calcium* 9(1), pp. 33-44.

Binley, K. E. et al. 2014. Sholl analysis: a quantitative comparison of semi-automated methods. *J Neurosci Methods* 225, pp. 65-70.

Blackshaw, S. et al. 2004. Genomic analysis of mouse retinal development. *PLoS Biol* 2(9), p. E247.

Bloomfield, S. A. and Dacheux, R. F. 2001. Rod vision: pathways and processing in the mammalian retina. *Prog Retin Eye Res* 20(3), pp. 351-384.

Blurton-Jones, M. et al. 2009. Neural stem cells improve cognition via BDNF in a transgenic model of Alzheimer disease. *Proc Natl Acad Sci U S A* 106(32), pp. 13594-13599.

Bodnarenko, S. R. and Chalupa, L. M. 1993. Stratification of ON and OFF ganglion cell dendrites depends on glutamate-mediated afferent activity in the developing retina. *Nature* 364(6433), pp. 144-146.

Boles, L. C. and Lohmann, K. J. 2002. True navigation and magnetic maps in spiny lobsters. *Nature* 421, pp. 60-63.

Bonnemain, B. 1998. Superparamagnetic agents in magnetic resonance imaging: physicochemical characteristics and clinical applications. A review. *J Drug Target* 6(3), pp. 167-174.

Bonnet, D. et al. 2004. Brain-derived neurotrophic factor signalling in adult pig retinal ganglion cell neurite regeneration in vitro. *Brain Research* 1007(1-2), pp. 142-151.

Bosco, A. and Linden, R. 1999. BDNF and NT-4 differentially modulate neurite outgrowth in developing retinal ganglion cells.*J Neurosci Res*. Vol. 57. United States: 1999 Wiley-Liss, Inc., pp. 759-769.

Boulle, F. et al. 2012. Epigenetic regulation of the BDNF gene: implications for psychiatric disorders. *Mol Psychiatry* 17(6), pp. 584-596.

Bourne, J. N. and Harris, K. M. 2008. Balancing structure and function at hippocampal dendritic spines. *Annu Rev Neurosci* 31, pp. 47-67.

Bradbury, E. J. et al. 2002. Chondroitinase ABC promotes functional recovery after spinal cord injury. *Nature* 416(6881), pp. 636-640.

Brahimi, F. et al. 2014. Combinatorial assembly of small molecules into bivalent antagonists of TrkC or TrkA receptors. *PLoS One* 9(3), p. e89617.

Bramblett, D. E. et al. 2004. The transcription factor Bhlhb4 is required for rod bipolar cell maturation. *Neuron* 43(6), pp. 779-793.

Brown, J. M. and Wilson, G. 2003. Apoptosis genes and resistance to cancer therapy: what does the experimental and clinical data tell us? *Cancer Biol Ther* 2(5), pp. 477-490.

Brown, S. P. et al. 2000. Receptive field microstructure and dendritic geometry of retinal ganglion cells. *Neuron* 27(2), pp. 371-383.

Bruckner, G. et al. 1993. Perineuronal nets provide a polyanionic, glia-associated form of microenvironment around certain neurons in many parts of the rat brain. *Glia* 8(3), pp. 183-200.

Bukhari, N. et al. 2011. Axonal regrowth after spinal cord injury via chondroitinase and the tissue plasminogen activator (tPA)/plasmin system. *J Neurosci* 31(42), pp. 14931-14943.

Bull, N. D. et al. 2011. Use of an Adult Rat Retinal Explant Model for Screening of Potential Retinal Ganglion Cell Neuroprotective Therapies. *Investigative Ophthalmology & Visual Science* 52(6), pp. 3309-3320.

Bulte, J. W. 2009. In vivo MRI cell tracking: clinical studies. *AJR Am J Roentgenol* 193(2), pp. 314-325.

Bulte, J. W. and Kraitchman, D. L. 2004. Iron oxide MR contrast agents for molecular and cellular imaging. *NMR Biomed* 17(7), pp. 484-499.

Busskamp, V. and Roska, B. 2011. Optogenetic approaches to restoring visual function in retinitis pigmentosa. *Curr Opin Neurobiol* 21(6), pp. 942-946.

Calverley, R. K. S. and Jones, D. G. 1990. CONTRIBUTIONS OF DENDRITIC SPINES AND PERFORATED SYNAPSES TO SYNAPTIC PLASTICITY. *Brain Research Reviews* 15(3), pp. 215-249.

Cano, J. et al. 1986. Morphological changes in the retina of ageing rats.*Arch Gerontol Geriatr*. Vol. 5. Netherlands, pp. 41-50.

Caprioli, J. et al. 1996. Hyperthermia and hypoxia increase tolerance of retinal ganglion cells to anoxia and excitotoxicity. *Invest Ophthalmol Vis Sci* 37(12), pp. 2376-2381.

Carenza, E. et al. 2014. In vitro angiogenic performance and in vivo brain targeting of magnetized endothelial progenitor cells for neurorepair therapies. *Nanomedicine* 10(1), pp. 225-234.

Carter, B. D. et al. 1996. Selective activation of NF-kappa B by nerve growth factor through the neurotrophin receptor p75. *Science* 272(5261), pp. 542-545.

Carulli, D. et al. 2010. Animals lacking link protein have attenuated perineuronal nets and persistent plasticity. *Brain* 133(Pt 8), pp. 2331-2347.

Cassens, C. 2010. Binding of the Receptor Tyrosine Kinase TrkB to the Neural Cell Adhesion Molecule (NCAM) Regulates Phosphorylation of NCAM and NCAM-dependent Neurite Outgrowth. Vol. 285. pp. 28959-28967.

Cellerino, A. and Kohler, K. 1997. Brain-derived neurotrophic factor/neurotrophin-4 receptor TrkB is localized on ganglion cells and dopaminergic amacrine cells in the vertebrate retina. *J Comp Neurol* 386(1), pp. 149-160.

Chang, M. L. et al. 2007. Reactive changes of retinal astrocytes and Müller glial cells in kainate-induced neuroexcitotoxicity. *J Anat* 210(1), pp. 54-65.

Chao, M. V. 2003. Neurotrophins and their receptors: a convergence point for many signalling pathways. *Nat Rev Neurosci* 4(4), pp. 299-309.

Chen, H. and Weber, A. J. 2001. BDNF enhances retinal ganglion cell survival in cats with optic nerve damage. *Invest Ophthalmol Vis Sci* 42(5), pp. 966-974.

Chen, J. et al. 2013. Guidance of stem cells to a target destination in vivo by magnetic nanoparticles in a magnetic field. *ACS Appl Mater Interfaces* 5(13), pp. 5976-5985.

Chen, L. T. and Weiss, L. 1973. The role of the sinus wall in the passage of erythrocytes through the spleen. *Blood* 41(4), pp. 529-537.

Chen, R. Z. et al. 2001. Deficiency of methyl-CpG binding protein-2 in CNS neurons results in a Rett-like phenotype in mice. *Nat Genet* 27(3), pp. 327-331.

Chen, Z. Y. et al. 2005. Sortilin controls intracellular sorting of brain-derived neurotrophic factor to the regulated secretory pathway. *J Neurosci* 25(26), pp. 6156-6166.

Chen, Z. Y. et al. 2004. Variant brain-derived neurotrophic factor (BDNF) (Met66) alters the intracellular trafficking and activity-dependent secretion of wild-type BDNF in neurosecretory cells and cortical neurons. *J Neurosci* 24(18), pp. 4401-4411.

Cheng, B. and Mattson, M. P. 1994. NT-3 and BDNF protect CNS neurons against metabolic/excitotoxic insults. *Brain Res* 640(1-2), pp. 56-67.

Cheng, C. W. et al. 2005. The Iroquois homeobox gene, Irx5, is required for retinal cone bipolar cell development. *Dev Biol* 287(1), pp. 48-60.

Cheng, K. et al. 2012. Magnetic enhancement of cell retention, engraftment, and functional benefit after intracoronary delivery of cardiac-derived stem cells in a rat model of ischemia/reperfusion. *Cell Transplant* 21(6), pp. 1121-1135.

Chiu, K. et al. 2008. Retrograde labeling of retinal ganglion cells by application of fluoro-gold on the surface of superior colliculus. *J Vis Exp* (16).

Choi, H. S. et al. 2007. Renal clearance of quantum dots. *Nature Biotechnology* 25(10), pp. 1165-1170.

Christian, K. M. et al. 2011. Chronic stress-induced hippocampal dendritic retraction requires CA3 NMDA receptors. *Neuroscience* 174, pp. 26-36.

Christianson, M. G. and Lo, D. C. 2011. Development of a low-pressure microtargeting biolistic device for transfection of retinal explants.*Mol Vis*. Vol. 17. United States, pp. 2947-2955.

Chua, J. et al. 2013. Early remodeling of muller cells in the rd/rd mouse model of retinal dystrophy. *Journal of Comparative Neurology* 521(11), pp. 2439-2453.

Coleman, H. R. et al. 2008. Age-related macular degeneration. *Lancet* 372(9652), pp. 1835-1845.

Congdon, N. et al. 2004. Causes and prevalence of visual impairment among adults in the United States. *Arch Ophthalmol* 122(4), pp. 477-485.

Connor, B. et al. 1997. Brain-derived neurotrophic factor is reduced in Alzheimer's disease. *Brain Res Mol Brain Res* 49(1-2), pp. 71-81.

Coombs, J. et al. 2006. Morphological properties of mouse retinal ganglion cells. *Neuroscience* 140(1), pp. 123-136.

Cragg, B. G. 1975. The development of synapses in the visual system of the cat. *J Comp Neurol* 160(2), pp. 147-166.

Cui, Q. et al. 2002. Expression of trkA, trkB, and trkC in injured and regenerating retinal ganglion cells of adult rats. *Invest Ophthalmol Vis Sci* 43(6), pp. 1954-1964.

D'Amelio, M. et al. 2010. Neuronal caspase-3 signaling: not only cell death. *Cell Death Differ* 17(7), pp. 1104-1114.

Dabin, I. and Barnstable, C. J. 1995. Rat retinal Muller cells express Thy-1 following neuronal cell death. *Glia* 14(1), pp. 23-32.

Dani, V. S. and Nelson, S. B. 2009. Intact LTP but reduced connectivity between neocortical Layer 5 pyramidal neurons in a mouse model of Rett Syndrome. *J Neurosci* 29(36), pp. 11263-11270.

De Felice, C. et al. 2014. Oxidative brain damage in Mecp2-mutant murine models of Rett syndrome. *Neurobiol Dis* 68, pp. 66-77.

De Roo, M. et al. 2008. Spine dynamics and synapse remodeling during LTP and memory processes. *Prog Brain Res* 169, pp. 199-207.

Dechant, G. and Barde, Y. A. 1997. Signalling through the neurotrophin receptor p75NTR. *Curr Opin Neurobiol* 7(3), pp. 413-418.

Dechant, G. et al. 1997. The neurotrophin receptor p75 binds neurotrophin-3 on sympathetic neurons with high affinity and specificity. *J Neurosci* 17(14), pp. 5281-5287.

Decherchi, P. et al. 1997. Dual staining assessment of Schwann cell viability within whole peripheral nerves using calcein-AM and ethidium homodimer. *J Neurosci Methods* 71(2), pp. 205-213.

Deisseroth, K. 2011. Optogenetics.*Nat Methods*. Vol. 8. United States, pp. 26-29.

Deisseroth, K. et al. 2004. Excitation-neurogenesis coupling in adult neural stem/progenitor cells. *Neuron* 42(4), pp. 535-552.

Dekkers, M. P. et al. 2013. Cell biology in neuroscience: Death of developing neurons: new insights and implications for connectivity. *J Cell Biol* 203(3), pp. 385-393.

Denk, N. et al. 2015. Development of a murine ocular posterior segment explant culture for the study of intravitreous vector delivery. *Can J Vet Res* 79(1), pp. 31-38.

Dheen, S. T. et al. 2007. Microglial activation and its implications in the brain diseases. *Curr Med Chem* 14(11), pp. 1189-1197.

Dhingra, A. et al. 2008. Probing neurochemical structure and function of retinal ON bipolar cells with a transgenic mouse. *J Comp Neurol* 510(5), pp. 484-496.

Dimos, J. T. et al. 2008. Induced pluripotent stem cells generated from patients with ALS can be differentiated into motor neurons. *Science* 321(5893), pp. 1218-1221.

Dobelle, W. H. et al. 1974. Artifical vision for the blind: electrical stimulation of visual cortex offers hope for a functional prosthesis. *Science* 183(4123), pp. 440-444.

Doi, M. et al. 1995. Morphological classification of retinal ganglion cells in mice. *J Comp Neurol* 356(3), pp. 368-386.

Domenici, L. et al. 2014. Rescue of retinal function by BDNF in a mouse model of glaucoma. *PLoS One* 9(12), p. e115579.

Dong, E. et al. 2014. DNA-methyltransferase1 (DNMT1) binding to CpG rich GABAergic and BDNF promoters is increased in the brain of schizophrenia and bipolar disorder patients. *Schizophr Res*.

Dowling, P. et al. 1999. Up-regulated p75NTR neurotrophin receptor on glial cells in MS plaques. *Neurology* 53(8), pp. 1676-1682.

Dreyer, E. B. et al. 1995. An astrocytic binding site for neuronal Thy-1 and its effect on neurite outgrowth. *Proc Natl Acad Sci U S A* 92(24), pp. 11195-11199.

Dryja, T. P. et al. 1990. A point mutation of the rhodopsin gene in one form of retinitis-pigmentosa. *Nature* 343(6256), pp. 364-366.

Dunaevsky, A. et al. 1999. Developmental regulation of spine motility in the mammalian central nervous system. *Proceedings of the National Academy of Sciences of the United States of America* 96(23), pp. 13438-13443.

Dwivedi, Y. 2012. Frontiers in Neuroscience
Brain-Derived Neurotrophic Factor in Suicide Pathophysiology. In: Dwivedi, Y. ed. *The Neurobiological Basis of Suicide*. Boca Raton (FL): CRC Press
Llc.

East, E. et al. 2005. A Role for the Plasminogen Activator System in Inflammation and Neurodegeneration in the Central Nervous System during Experimental Allergic Encephalomyelitis. *Am J Pathol* 167(2), pp. 545-554.

Egan, M. F. et al. 2003. The BDNF val66met polymorphism affects activity-dependent secretion of BDNF and human memory and hippocampal function. *Cell* 112(2), pp. 257-269.

Ekstrom, P. et al. 1988. Accumulation of glial fibrillary acidic protein in Muller radial glia during retinal degeneration. *Invest Ophthalmol Vis Sci* 29(9), pp. 1363-1371.

El-Danaf, R. N. and Huberman, A. D. 2015. Characteristic patterns of dendritic remodeling in early-stage glaucoma: evidence from genetically identified retinal ganglion cell types.*J Neurosci*. Vol. 35. United States: 2015 the authors 0270-6474/15/352329-15$15.00/0., pp. 2329-2343.

Elmore, S. 2007. Apoptosis: A review of programmed cell death. *Toxicologic Pathology* 35(4), pp. 495-516.

Elston, G. N. et al. 2009. Spinogenesis and Pruning Scales across Functional Hierarchies. *Journal of Neuroscience* 29(10), pp. 3271-3275.

Erkman, L. et al. 1996. Role of transcription factors Brn-3.1 and Brn-3.2 in auditory and visual system development. *Nature* 381(6583), pp. 603-606.

Ernfors, P. et al. 1989. Expression of nerve growth factor receptor mRNA is developmentally regulated and increased after axotomy in rat spinal cord motoneurons. *Neuron* 2(6), pp. 1605-1613.

Erskine, L. and Herrera, E. 2007. The retinal ganglion cell axon's journey: insights into molecular mechanisms of axon guidance.*Dev Biol*. Vol. 308. United States, pp. 1-14.

Erturk, A. et al. 2014. Local pruning of dendrites and spines by caspase-3-dependent and proteasome-limited mechanisms. *J Neurosci* 34(5), pp. 1672-1688.

Fahnestock, M. et al. 2002. Neurotrophic factors and Alzheimer's disease: are we focusing on the wrong molecule? *J Neural Transm Suppl* (62), pp. 241-252.

Fahnestock, M. et al. 2001. The precursor pro-nerve growth factor is the predominant form of nerve growth factor in brain and is increased in Alzheimer's disease. *Mol Cell Neurosci* 18(2), pp. 210-220.

Famiglietti, E. V., Jr. and Kolb, H. 1976. Structural basis for ON-and OFF-center responses in retinal ganglion cells. *Science* 194(4261), pp. 193-195.

Fawcett, J. W. 2015. The extracellular matrix in plasticity and regeneration after CNS injury and neurodegenerative disease. *Prog Brain Res* 218, pp. 213-226.

Fawcett, J. W. and Asher, R. A. 1999. The glial scar and central nervous system repair. *Brain Res Bull* 49(6), pp. 377-391.

Feng, J. F. et al. 2012. Guided migration of neural stem cells derived from human embryonic stem cells by an electric field. *Stem Cells* 30(2), pp. 349-355.

Fenstermaker, V. et al. 2004. Regulation of dendritic length and branching by semaphorin 3A. *J Neurobiol* 58(3), pp. 403-412.

Ferguson, L. R. et al. 2013. Retinal Thickness Normative Data in Wild-Type Mice Using Customized Miniature SD-OCT. In: Villoslada, P. ed. *PLoS One*. Vol. 8. San Francisco, USA.

Ferrer-Martin, R. M. et al. 2014. Microglial cells in organotypic cultures of developing and adult mouse retina and their relationship with cell death. *Experimental Eye Research* 121, pp. 42-57.

Fischer, A. J. et al. 2013. The ciliary margin zone (CMZ) in development and regeneration of the vertebrate eye. *Exp Eye Res* 116, pp. 199-204.

Fischer, M. et al. 1998. Rapid actin-based plasticity in dendritic spines. *Neuron* 20(5), pp. 847-854.

Flaumenhaft, R. and Rifkin, D. B. 1991. Extracellular matrix regulation of growth factor and protease activity. *Curr Opin Cell Biol* 3(5), pp. 817-823.

Frade, J. M. and Barde, Y. A. 1999. Genetic evidence for cell death mediated by nerve growth factor and the neurotrophin receptor p75 in the developing mouse retina and spinal cord. *Development* 126(4), pp. 683-690.

Friedman, W. J. 2000. Neurotrophins induce death of hippocampal neurons via the p75 receptor. *J Neurosci* 20(17), pp. 6340-6346.

Frischknecht, R. et al. 2009. Brain extracellular matrixaffects AMPA receptor lateral mobility and short-term synaptic plasticity. *Nature Neuroscience* 12, pp. 897-904.

Gajewski, P. D. et al. 2011. The Met-allele of the BDNF Val66Met polymorphism enhances task switching in elderly. *Neurobiol Aging* 32(12), pp. 2327.e2327-2319.

Gan, L. et al. 1999. POU domain factor Brn-3b is essential for retinal ganglion cell differentiation and survival but not for initial cell fate specification. *Dev Biol* 210(2), pp. 469-480.

Gan, L. et al. 1996. POU domain factor Brn-3b is required for the development of a large set of retinal ganglion cells. *Proc Natl Acad Sci U S A* 93(9), pp. 3920-3925.

Gan, W. B. et al. 2000. Multicolor "DiOlistic" labeling of the nervous system using lipophilic dye combinations.*Neuron*. Vol. 27. United States, pp. 219-225.

Gao, H. et al. 1997. Elevated mRNA expression of brain-derived neurotrophic factor in retinal ganglion cell layer after optic nerve injury. *Invest Ophthalmol Vis Sci* 38(9), pp. 1840-1847.

Garcia-Alias, G. et al. 2009. Chondroitinase ABC treatment opens a window of opportunity for task-specific rehabilitation. *Nature Neuroscience* 12(9), pp. 1145-U1116.

Garcia-Segura, L. M. and Perez-Marquez, J. 2014. A new mathematical function to evaluate neuronal morphology using the Sholl analysis. *J Neurosci Methods* 226, pp. 103-109.

Gavrieli, Y. et al. 1992. Identification of programmed cell death in situ via specific labeling of nuclear DNA fragmentation. *J Cell Biol* 119(3), pp. 493-501.

George, E. B. et al. 1995. Axotomy-induced axonal degeneration is mediated by calcium influx through ion-specific channels. *J Neurosci* 15(10), pp. 6445-6452.

Gerdts, J. et al. 2013. Sarm1-Mediated Axon Degeneration Requires Both SAM and TIR Interactions.*J Neurosci*. Vol. 33. pp. 13569-13580.

Gerdts, J. et al. 2016. Axon self-destruction: New links among SARM1, MAPKs, and NAD+ metabolism. *Neuron* 89(3), pp. 449-460.

Gogolla, N. et al. 2009. Perineuronal nets protect fear memories from erasure. *Science* 325(5945), pp. 1258-1261.

Goldberg, J. L. et al. 2002. Retinal ganglion cells do not extend axons by default: promotion by neurotrophic signaling and electrical activity. *Neuron* 33(5), pp. 689-702.

Golgi, C. 1873. Sulla struttura della sostanza grigia del cervello (comunicazione preventiva). *Gazzetaa Medica Italiana - Lombardia* (33), pp. 244-246.

Gordon, J. A. and Stryker, M. P. 1996. Experience-dependent plasticity of binocular responses in the primary visual cortex of the mouse. *J Neurosci* 16(10), pp. 3274-3286.

Gray, K. and Ellis, V. 2008. Activation of pro-BDNF by the pericellular serine protease plasmin. *FEBS Lett* 582(6), pp. 907-910.

Green, W. R. et al. 1985. Pathologic features of senile macular degeneration. *Ophthalmology* 92(5), pp. 615-627.

Greenberg, M. E. 2010. *The Harvey Lectures*. John Wiley & Sons.

Grieshaber, P. et al. 2010. Staining of fluorogold-prelabeled retinal ganglion cells with calcein-AM: A new method for assessing cell vitality. *J Neurosci Methods* 192(2), pp. 233-239.

Grimaldi, P. et al. 2005. Neuronal replacement and integration in the rewiring of cerebellar circuits. *Brain Res Brain Res Rev* 49(2), pp. 330-342.

Guerin, M. B. et al. 2011. Age-dependent rat retinal ganglion cell susceptibility to apoptotic stimuli: implications for glaucoma. *Clin Experiment Ophthalmol* 39(3), pp. 243-251.

Guimaraes, A. et al. 1990. Molecular and morphological changes in the cat lateral geniculate nucleus and visual cortex induced by visual deprivation are revealed by monoclonal antibodies Cat-304 and Cat-301. *J Neurosci* 10(9), pp. 3014-3024.

Gupta, V. K. et al. 2012. Shp-2 regulates the TrkB receptor activity in the retinal ganglion cells under glaucomatous stress. *Biochimica et Biophysica Acta (BBA) - Molecular Basis of Disease* 1822(11), pp. 1643-1649.

Guy, J. et al. 2001. A mouse Mecp2-null mutation causes neurological symptoms that mimic Rett syndrome. *Nat Genet* 27(3), pp. 322-326.

Hall, J. R. 2012. Biomarkers of basic activities of daily living in Alzheimer's disease. 31(2), pp. 429-437.

Han, C. et al. 2012. Integrins regulate repulsion-mediated dendritic patterning of drosophila sensory neurons by restricting dendrites in a 2D space.*Neuron*. Vol. 73. United States: 2012 Elsevier Inc, pp. 64-78.

Harada, C. et al. 2011. Glia- and neuron-specific functions of TrkB signalling during retinal degeneration and regeneration. *Nat Commun* 2, p. 189.

Harman, D. 1981. The aging process. *Proceedings of the National Academy of Sciences of the United States of America-Biological Sciences* 78(11), pp. 7124-7128.

Harrington, A. W. et al. 2002. Activation of Rac GTPase by p75 is necessary for c-jun N-terminal kinase-mediated apoptosis. *J Neurosci* 22(1), pp. 156-166.

Harrington, A. W. et al. 2004. Secreted proNGF is a pathophysiological death-inducing ligand after adult CNS injury. *Proc Natl Acad Sci U S A* 101(16), pp. 6226-6230.

Hartong, D. T. et al. 2006. Retinitis pigmentosa. *Lancet* 368(9549), pp. 1795-1809.

Hausmann, O. 2003. Post-traumatic inflawing spinal cord injury. *Spinal Cord* 41(7), pp. 369-378.

He, Z. et al. 2002. Knowing how to navigate: mechanisms of semaphorin signaling in the nervous system. *Sci STKE* 2002(119), p. re1.

Heymach, J. V., Jr. and Shooter, E. M. 1995. The biosynthesis of neurotrophin heterodimers by transfected mammalian cells. *J Biol Chem* 270(20), pp. 12297-12304.

Hilger, I. et al. 2001. Electromagnetic heating of breast tumors in interventional radiology: in vitro and in vivo studies in human cadavers and mice. *Radiology* 218(2), pp. 570-575.

Hocking, J. C. et al. 2009. LIMK1 acts downstream of BMP signaling in developing retinal ganglion cell axons. *Dev Biol* 330(2), pp. 273-285.

Hong, Y. K. and Chen, C. 2011. Wiring and rewiring of the retinogeniculate synapse. *Curr Opin Neurobiol* 21(2), pp. 228-237.

Horton, A. et al. 1997. NGF binding to p75 enhances the sensitivity of sensory and sympathetic neurons to NGF at different stages of development. *Mol Cell Neurosci* 10(3-4), pp. 162-172.

Hou, S. J. et al. 2009. Is dysfunction of the tissue plasminogen activator (tPA)-plasmin pathway a link between major depression and cardiovascular disease? *Med Hypotheses* 72(2), pp. 166-168.

Howell, G. R. et al. 2007. Axons of retinal ganglion cells are insulted in the optic nerve early in DBA/2J glaucoma.*J Cell Biol*. Vol. 179. United States, pp. 1523-1537.

Hu, B. et al. 1999. Expression of p75 neurotrophin receptor in the injured and regenerating rat retina. *Neuroreport* 10(6), pp. 1293-1297.

Hu, Y. et al. 2010. Neurotrophic Effect of a Novel TrkB Agonist on Retinal Ganglion Cells.*Invest Ophthalmol Vis Sci*. Vol. 51. pp. 1747-1754.

Hu, Y. Q. and Koo, P. H. 1998. Inhibition of phosphorylation of TrkB and TrkC and their signal transduction by alpha2-macroglobulin. *J Neurochem* 71(1), pp. 213-220.

Huang, W. et al. 2006. Downregulation of Thy1 in retinal ganglion cells in experimental glaucoma. *Curr Eye Res* 31(3), pp. 265-271.

Huang, Z. J. et al. 1999. BDNF regulates the maturation of inhibition and the critical period of plasticity in mouse visual cortex. *Cell* 98(6), pp. 739-755.

Humayun, M. S. et al. 2012. Interim results from the international trial of Second Sight's visual prosthesis. *Ophthalmology* 119(4), pp. 779-788.

Huttenlocher, P. R. 1979. Synaptic density in human frontal cortex - developmental changes and effects of aging. *Brain Res* 163(2), pp. 195-205.

Hyman, B. T. and Yuan, J. 2012. Apoptotic and non-apoptotic roles of caspases in neuronal physiology and pathophysiology. *Nat Rev Neurosci* 13(6), pp. 395-406.

Hynynen, K. et al. 2001. Noninvasive MR imaging-guided focal opening of the blood-brain barrier in rabbits. *Radiology* 220(3), pp. 640-646.

Ibanez, C. F. and Simi, A. 2012. p75 neurotrophin receptor signaling in nervous system injury and degeneration: paradox and opportunity. *Trends Neurosci* 35(7), pp. 431-440.

Imlay, J. A. et al. 1988. Toxic DNA damage by hydrogen peroxide through the Fenton reaction in vivo and in vitro. *Science* 240(4852), pp. 640-642.

Ippolito, D. M. and Eroglu, C. 2010. Quantifying Synapses: an Immunocytochemistry-based Assay to Quantify Synapse Number.*J Vis Exp*.

Ishikura, N. et al. 2005. Notch-1 activation and dendritic atrophy in prion disease.*Proc Natl Acad Sci U S A*. Vol. 102. United States, pp. 886-891.

Jeffery, G. 1997. The albino retina: An abnormality that provides insight into normal retinal development. *Trends in Neurosciences* 20(4), pp. 165-169.

Jensen, R. J. and Rizzo, J. F., 3rd. 2009. Activation of ganglion cells in wild-type and rd1 mouse retinas with monophasic and biphasic current pulses. *J Neural Eng* 6(3), p. 035004.

Jeon, J. Y. et al. 2008. Migration of human neural stem cells toward an intracranial glioma. *Experimental and Molecular Medicine* 40(1), pp. 84-91.

Ji, Y. et al. 2005. Cyclic AMP controls BDNF-induced TrkB phosphorylation and dendritic spine formation in mature hippocampal neurons. *Nat Neurosci* 8(2), pp. 164-172.

Jiang, P. et al. 2014. The Impacts of Swimming Exercise on Hippocampal Expression of Neurotrophic Factors in Rats Exposed to Chronic Unpredictable Mild Stress. *Evid Based Complement Alternat Med* 2014, p. 729827.

Johnsen, E. O. et al. 2012. Activation of neural progenitor cells in human eyes with proliferative. *Exp Eye Res* 98, pp. 28-36.

Johnsen, S. and Lohmann, K. J. 2005. The physics and neurobiology of magnetoreception. *Nat Rev Neurosci* 6(9), pp. 703-712.

Johnson, J. et al. 2007. Vesicular Glutamate Transporter 1 Is Required for Photoreceptor Synaptic Signaling But Not For Intrinsic Visual Functions. *J Neurosci* 27(27), pp. 7245-7255.

Johnson, T. V. et al. 2011. Neurotrophic factor delivery as a protective treatment for glaucoma. *Experimental Eye Research* 93(2), pp. 196-203.

Johnson, T. V. and Martin, K. R. 2008. Development and characterization of an adult retinal explant organotypic tissue culture system as an in vitro intraocular stem cell transplantation model. *Investigative Ophthalmology & Visual Science* 49(8), pp. 3503-3512.

Johnson, T. V. et al. 2016. Time-Lapse Retinal Ganglion Cell Dendritic Field Degeneration Imaged in Organotypic Retinal Explant Culture. *Invest Ophthalmol Vis Sci* 57(1), pp. 253-264.

Jones, B. W. and Marc, R. E. 2005. Retinal remodeling during retinal degeneration.*Exp Eye Res*. Vol. 81. England, pp. 123-137.

Jones, E. V. and Bouvier, D. S. 2014. Astrocyte-secreted matricellular proteins in CNS remodelling during development and disease. *Neural plasticity* 2014, pp. 321209-321209.

Judas, M. et al. 2003. Complex patterns and simple architects: molecular guidance cues for developing axonal pathways in the telencephalon. *Prog Mol Subcell Biol* 32, pp. 1-32.

Kador, K. E. et al. 2013. Tissue Engineering the Retinal Ganglion Cell Nerve Fiber Layer. *Biomaterials* 34(17), pp. 4242-4250.

Kageyama, R. et al. 2005. Roles of bHLH genes in neural stem cell differentiation.*Exp Cell Res*. Vol. 306. United States, pp. 343-348.

Karetko, M. and Skangiel-Kramska, J. 2009. Diverse functions of perineuronal nets. *Acta Neurobiol Exp (Wars)* 69(4), pp. 564-577.

Karpova, N. N. 2014. Role of BDNF epigenetics in activity-dependent neuronal plasticity. *Neuropharmacology* 76 Pt C, pp. 709-718.

Kashimoto, R. et al. 2008. Cilostazol promotes survival of axotomized retinal ganglion cells in adult rats. *Neurosci Lett* 436(2), pp. 116-119.

Kay, J. et al. 2011. Retinal ganglion cells with distinct directional preferences differ in molecular identity, structure and central projections. *J Neurosci* 31(21), pp. 7753-7762.

Kelly, S. et al. 2004. Transplanted human fetal neural stem cells survive, migrate, and differentiate in ischemic rat cerebral cortex. *Proc Natl Acad Sci U S A* 101(32), pp. 11839-11844.

Kettenmann, H. et al. 2011. Physiology of microglia. *Physiol Rev* 91(2), pp. 461-553.

Kirschvink, J. L. et al. 2001. Magnetite-based magnetoreception. *Curr Opin Neurobiol* 11(4), pp. 462-467.

Kisiswa, L. et al. 2010a. Cellular inhibitor of apoptosis (cIAP1) is down-regulated during retinal ganglion. *Exp Eye Res* 91(5), pp. 739-747.

Kisiswa, L. et al. 2010b. Retinal ganglion cell death postponed: giving apoptosis a break? *Ophthalmic Res* 43(2), pp. 61-78.

Klassen, H. J. et al. 2004. Multipotent retinal progenitors express developmental markers, differentiate into retinal neurons, and preserve light-mediated behavior. *Investigative Ophthalmology & Visual Science* 45(11), pp. 4167-4173.

Knoepfel, T. and Akemann, W. 2010. NANOBIOTECHNOLOGY Remote control of cells. *Nature Nanotechnology* 5(8), pp. 560-561.

Kobelt, L. J. et al. 2014. Short duration electrical stimulation to enhance neurite outgrowth and maturation of adult neural stem progenitor cells. *Ann Biomed Eng* 42(10), pp. 2164-2176.

Kobuch, K. et al. 2008. Maintenance of adult porcine retina and retinal pigment epithelium in perfusion culture: characterisation of an organotypic in vitro model. *Exp Eye Res* 86(4), pp. 661-668.

Koizumi, A. et al. 2007. Organotypic culture of physiologically functional adult mammalian retinas. *PLoS One* 2(2), p. e221.

Kolb, H. 1970. Organization of the outer plexiform layer of the primate retina: electron microscopy of Golgi-impregnated cells. *Philos Trans R Soc Lond B Biol Sci* 258(823), pp. 261-283.

Kolbeck, R. et al. 1999. Brain-derived neurotrophic factor levels in the nervous system of wild-type and neurotrophin gene mutant mice. *J Neurochem* 72(5), pp. 1930-1938.

Koo, Y. E. et al. 2006. Brain cancer diagnosis and therapy with nanoplatforms. *Adv Drug Deliv Rev* 58(14), pp. 1556-1577.

Kordower, J. H. et al. 1997. Grafts of EGF-responsive neural stem cells derived from GFAP-hNGF transgenic mice: trophic and tropic effects in a rodent model of Huntington's disease. *J Comp Neurol* 387(1), pp. 96-113.

Korte, M. et al. 1995. Hippocampal long-term potentiation is impaired in mice lacking brain-derived neurotrophic factor. *Proc Natl Acad Sci U S A* 92(19), pp. 8856-8860.

Kubota, R. et al. 2002. A comparative study of neurogenesis in the retinal ciliary margin zone of homeothermic vertebrates. *Brain Res Dev Brain Res* 134(1-2), pp. 31-41.

Kumar, C. and Mohammad, F. 2011. Magnetic Nanomaterials for Hyperthermia-based Therapy and Controlled Drug Delivery. *Adv Drug Deliv Rev* 63(9), pp. 789-808.

Kunzevitzky, N. J. et al. 2010. Amacrine Cell Gene Expression and Survival Signaling: Differences from Neighboring Retinal Ganglion Cells.*Invest Ophthalmol Vis Sci*. Vol. 51. pp. 3800-3812.

Kuo, C. T. et al. 2006. Identification of E2/E3 ubiquitinating enzymes and caspase activity regulating Drosophila sensory neuron dendrite pruning. *Neuron* 51(3), pp. 283-290.

Kyrtatos, P. G. et al. 2009. Magnetic tagging increases delivery of circulating progenitors in vascular injury. *JACC Cardiovasc Interv* 2(8), pp. 794-802.

Landi, S et al. 2007. Environmental enrichment effects on development of retinal ganglion cell dendritic tratification require retinal BDNF. *PLoS One* 2(4), e346.

Leask, M. J. M. 1977. A physiochemical mechanism for magnetic field detection by migratory birds and homing pigeons. *Nature* 267, pp. 144-145.

Lee, H. et al. 2012. Perineuronal nets play a role in regulating striatal function in the mouse. *PLoS One* 7(3), p. e32747.

Lee, K. F. et al. 1994. p75-deficient embryonic dorsal root sensory and neonatal sympathetic neurons display a decreased sensitivity to NGF. *Development* 120(4), pp. 1027-1033.

Lee, K. F. et al. 1992. Targeted mutation of the gene encoding the low affinity NGF receptor p75 leads to deficits in the peripheral sensory nervous system. *Cell* 69(5), pp. 737-749.

Lee, R. et al. 2001. Regulation of cell survival by secreted proneurotrophins. *Science* 294(5548), pp. 1945-1948.

Lee, W. S. et al. 1998. Thy-1, a novel marker for angiogenesis upregulated by inflammatory cytokines. *Circ Res* 82(8), pp. 845-851.

Leibiger, I. B. and Berggren, P. O. 2015. Regulation of glucose homeostasis using radiogenetics and magnetogenetics in mice. *Nat Med* 21(1), pp. 14-16.

Levi-Montalcini, R. et al. 1996. Nerve growth factor: from neurotrophin to neurokine. *Trends Neurosci* 19(11), pp. 514-520.

Li, L. et al. 2008. Direct-current electrical field guides neuronal stem/progenitor cell migration. *Stem Cells* 26(8), pp. 2193-2200.

Li, L. and Jiang, J. 2011. Regulatory factors of mesenchymal stem cell migration into injured tissues and their signal transduction mechanisms. *Front Med* 5(1), pp. 33-39.

Li, T. et al. 2013. Multipotent stem cells isolated from the adult mouse retina are capable of producing functional photoreceptor cells. *Cell Research* 23, pp. 788-802.

Liang, D. et al. 2007. Cytotoxic edema: mechanisms of pathological cell swelling. *Neurosurgical focus* 22(5), pp. E2-E2.

Liang, F. Q. and Godley, B. F. 2003. Oxidative stress-induced mitochondrial DNA damage in human retinal pigment epithelial cells: a possible mechanism for RPE aging and age-related macular degeneration. *Exp Eye Res* 76(4), pp. 397-403.

Liesi, P. et al. 1990. Thy-1 is a neuronal and glial surface antigen which interacts with matrix proteins and plasminogen activator. *Exp Brain Res* 79(3), pp. 642-650.

Lin, B. et al. 2008. Restoration of visual function in retinal degeneration mice by ectopic expression of melanopsin. *Proceedings of the National Academy of Sciences of the United States of America* 105(41), pp. 16009-16014.

Lin, P. et al. 2014. The VGF-derived peptide TLQP62 produces antidepressant-like effects in mice via the BDNF/TrkB/CREB signaling pathway. *Pharmacol Biochem Behav* 120, pp. 140-148.

Liu, C. et al. 2016. 7,8-dihydroxyflavone, a small molecular TrkB agonist, is useful for treating various BDNF-implicated human disorders. *Transl Neurodegener* 5, p. 2.

Lo, D. C. et al. 1994. Neuronal transfection in brain slices using particle-mediated gene transfer. *Neuron* 13(6), pp. 1263-1268.

Loebinger, M. R. et al. 2009. Magnetic resonance imaging of mesenchymal stem cells homing to pulmonary metastases using biocompatible magnetic nanoparticles. *Cancer Res* 69(23), pp. 8862-8867.

Lohmann, K. J. 1999. Long-distance navigation in sea turtles. *Ethol Ecol Evol* 11(1), pp. 1-23.

Lohmann, K. J. 2016. PROTEIN COMPLEXES A candidate magnetoreceptor. *Nature Materials* 15(2), pp. 136-138.

Lom, B. and Cohen-Cory, S. 1999. Brain-derived neurotrophic factor differentially regulates retinal ganglion cell dendritic and axonal arborization in vivo. *J Neurosci* 19(22), pp. 9928-9938.

London, A. et al. 2013. The retina as a window to the brain-from eye research to CNS disorders. *Nat Rev Neurol* 9(1), pp. 44-53.

Long, X. et al. 2015. Magnetogenetics: remote non-invasive magnetic activation of neuronal activity with a magnetoreceptor. *Sci Bull (Beijing)* 60, pp. 2107-2119.

Longair, M. H. et al. 2011. Simple Neurite Tracer: open source software for reconstruction, visualization and analysis of neuronal processes. *Bioinformatics* 27(17), pp. 2453-2454.

Longo, F. M. and Massa, S. M. 2013. Small-molecule modulation of neurotrophin receptors: a strategy for the treatment of neurological disease. *Nat Rev Drug Discov* 12(7), pp. 507-525.

Lorenzl, S. et al. 2003. Tissue inhibitors of matrix metalloproteinases are elevated in cerebrospinal fluid of neurodegenerative diseases. *J Neurol Sci* 207(1-2), pp. 71-76.

Lu, B. 2003. BDNF and activity-dependent synaptic modulation. *Learn Mem* 10(2), pp. 86-98.

Luo, Y. L. et al. 1993. Collapsin - a protein in brain that induces the collapse and paralysis of neuronal growth cones. *Cell* 75(2), pp. 217-227.

Lye, M. H. et al. 2007. Organotypic culture of adult rabbit retina. *J Vis Exp* (3), p. 190.

Ma, J. et al. 2011. Combining chondroitinase ABC and growth factors promotes the integration of murine retinal progenitor cells transplanted into Rho(-/-) mice. *Molecular Vision* 17(193).

Ma, Y. T. et al. 1998. BDNF injected into the superior colliculus reduces developmental retinal ganglion cell death. *J Neurosci* 18(6), pp. 2097-2107.

Macias, M. 2008. Injury induced dendritic plasticity in the mature central nervous system. *Acta Neurobiologiae Experimentalis* 68(2), pp. 334-346.

MacLaren, R. E. et al. 2006. Retinal repair by transplantation of photoreceptor precursors. *Nature* 444(7116), pp. 203-207.

Magarinos, A. M. and McEwen, B. S. 1995. Stress-induced atrophy of apical dendrites of hippocampal CA3c neurons: comparison of stressors. *Neuroscience* 69(1), pp. 83-88.

Magavi, S. S. et al. 2000. Induction of neurogenesis in the neocortex of adult mice. *Nature* 405(6789), pp. 951-955.

Magdesian, M. H. et al. 2016. Rapid Mechanically Controlled Rewiring of Neuronal Circuits. *J Neurosci* 36(3), pp. 979-987.

Maller, J. B. et al. 2007. Variation in complement factor 3 is associated with risk of age-related macular degeneration. *Nature Genetics* 39(10), pp. 1200-1201.

Mansergh, F. C. et al. 2010. Loss of photoreceptor potential from retinal progenitor cell cultures, despite improvements in survival. *Experimental Eye Research* 91(4), pp. 500-512.

Marc, R. E. et al. 2003. Neural remodeling in retinal degeneration.*Prog Retin Eye Res*. Vol. 22. England, pp. 607-655.

Marchetto, M. C. et al. 2010. A model for neural development and treatment of Rett syndrome using human induced pluripotent stem cells. *Cell* 143(4), pp. 527-539.

Margolis, D. J. et al. 2008. Functional stability of retinal ganglion cells after degeneration-induced changes in synaptic input. *J Neurosci* 28(25), pp. 6526-6536.

Marrs, G. S. et al. 2006. Dendritic arbors of developing retinal ganglion cells are stabilized by beta 1-integrins. *Mol Cell Neurosci*. Vol. 32. United States, pp. 230-241.

Martin-Piedra, M. A. et al. 2014. Cell viability and proliferation capability of long-term human dental pulp stem cell cultures. *Cytotherapy* 16(2), pp. 266-277.

Martinowich, K. et al. 2003. DNA methylation-related chromatin remodeling in activity-dependent BDNF gene regulation. *Science* 302(5646), pp. 890-893.

Massa, S. M. et al. 2010. Small molecule BDNF mimetics activate TrkB signaling and prevent neuronal degeneration in rodents. *J Clin Invest* 120(5), pp. 1774-1785.

Massey, J. M. et al. 2006. Chondroitinase ABC digestion of the perineuronal net promotes functional collateral sprouting in the cuneate nucleus after cervical spinal cord injury. *J Neurosci* 26(16), pp. 4406-4414.

Mataga, N. et al. 2002. Permissive proteolytic activity for visual cortical plasticity. *Proc Natl Acad Sci U S A* 99(11), pp. 7717-7721.

Matsumoto, T. et al. 2008. Biosynthesis and processing of endogenous BDNF: CNS neurons store and secrete BDNF, not pro-BDNF. *Nat Neurosci* 11(2), pp. 131-133.

Matsuzaki, M. 2007. Factors critical for the plasticity of dendritic spines and memory storage. *Neurosci Res* 57(1), pp. 1-9.

Mayer, E. J. et al. 2005. Neural progenitor cells from postmortem adult human retina. *Br J Ophthalmol* 89(1), pp. 102-106.

Mazzoni, F. et al. 2008. Retinal Ganglion Cells Survive and Maintain Normal Dendritic Morphology in a Mouse Model of Inherited Photoreceptor Degeneration. *Journal of Neuroscience* 28(52), pp. 14282-14292.

McAllister, A. K. et al. 1996. Neurotrophin regulation of cortical dendritic growth requires activity. *Neuron*. Vol. 17. United States, pp. 1057-1064.

McAllister, A. K. et al. 1995. Neurotrophins regulate dendritic growth in developing visual cortex. *Neuron*. Vol. 15. United States, pp. 791-803.

McBain, S. C. et al. 2008. Magnetic nanoparticles for gene and drug delivery. *International Journal of Nanomedicine* 3(2), pp. 169-180.

McCaig, C. D. et al. 2005. Controlling cell behavior electrically: current views and future potential. *Physiol Rev* 85(3), pp. 943-978.

McKernan, D. P. et al. 2007. A key role for calpains in retinal ganglion cell death. *Invest Ophthalmol Vis Sci* 48(12), pp. 5420-5430.

McRae, P. A. and Porter, B. E. 2012. The perineuronal net component of the extracellular matrix in plasticity and epilepsy. *Neurochem Int* 61(7), pp. 963-972.

Mejias, R. et al. 2011. Dimercaptosuccinic acid-coated magnetite nanoparticles for magnetically guided in vivo delivery of interferon gamma for cancer immunotherapy. *Biomaterials* 32(11), pp. 2938-2952.

Melvin, N. R. and Sutherland, R. J. 2010. Quantitative Caveats of Standard Immunohistochemical Procedures: Implications for Optical Disector–based Designs.*J Histochem Cytochem*. Vol. 58. pp. 577-584.

Meng, X. et al. 2011. PI3K mediated electrotaxis of embryonic and adult neural progenitor cells in the presence of growth factors. *Exp Neurol* 227(1), pp. 210-217.

Meng, Y. et al. 2004. Regulation of ADF/cofilin phosphorylation and synaptic function by LIM-kinase.*Neuropharmacology*. Vol. 47. England, pp. 746-754.

Middlemas, D. S. et al. 1994. Identification of TrkB autophosphorylation sites and evidence that phospholipase C-gamma 1 is a substrate of the TrkB receptor. *J Biol Chem* 269(7), pp. 5458-5466.

Miller, J. M. et al. 2007. Delayed neurotrophin treatment following deafness rescues spiral ganglion cells from death and promotes regrowth of auditory nerve peripheral processes: effects of brain-derived neurotrophic factor and fibroblast growth factor. *J Neurosci Res* 85(9), pp. 1959-1969.

Minichiello, L. et al. 2002. Mechanism of TrkB-mediated hippocampal long-term potentiation. *Neuron* 36(1), pp. 121-137.

Mitrecic, D. et al. 2010. Distribution, differentiation, and survival of intravenously administered neural stem cells in a rat model of amyotrophic lateral sclerosis. *Cell Transplant* 19(5), pp. 537-548.

Mocchetti, I. and Bachis, A. 2004. Brain-derived neurotrophic factor activation of TrkB protects neurons from HIV-1/gp120-induced cell death. *Crit Rev Neurobiol* 16(1-2), pp. 51-57.

Molteno, T. C. A. and Kennedy, W. L. 2009. Navigation by induction-based magnetoreception in elasmobranch fishes. *J Biophys* 2009, pp. 1-7.

Mora, C. V. et al. 2004. Magnetoreception and its trigeminal mediation in the homing pigeon. *Nature* 432(7016), pp. 508-511.

Moraes, L. et al. 2012. Neuroprotective effects and magnetic resonance imaging of mesenchymal stem cells labeled with SPION in a rat model of Huntington's disease. *Stem Cell Res* 9(2), pp. 143-155.

Morawski, M. et al. 2004. Perineuronal nets potentially protect against oxidative stress. *Exp Neurol* 188(2), pp. 309-315.

Morgan, J. E. 2002. Retinal ganglion cell shrinkage in glaucoma. *J Glaucoma* 11(4), pp. 365-370.

Morgan, J. E. 2012. Retina ganglion cell degeneration in glaucoma: an opportunity missed? A review. *Clin Experiment Ophthalmol* 40(4), pp. 364-368.

Morgan, J. L. et al. 2008. Developmental patterning of glutamatergic synapses onto retinal ganglion cells.*Neural Develop*. Vol. 3. p. 8.

Morgenstern, D. A. et al. 2002. Chondroitin sulphate proteoglycans in the CNS injury response. *Prog Brain Res* 137, pp. 313-332.

Morimoto, T. 2012. Role of electrical activity of neurons for neuroprotection. *Int Rev Neurobiol* 105, pp. 19-38.

Moritoh, S. et al. 2010. Organotypic tissue culture of adult rodent retina followed by particle-mediated acute gene transfer in vitro. *PLoS One* 5(9), p. e12917.

Morquette, B. et al. 2015. REDD2-mediated inhibition of mTOR promotes dendrite retraction induced by axonal injury.*Cell Death Differ*. Vol. 22. England, pp. 612-625.

Morquette, J. B. and Di Polo, A. 2008. Dendritic and synaptic protection: is it enough to save the retinal ganglion cell. *J Neuroophthalmol* 28(2), pp. 144-154.

Mouritsen, H. et al. 2004. Cryptochromes and neuronal-activity markers colocalize in the retina of migratory birds during magnetic orientation. *Proc Natl Acad Sci USA* 101(39), pp. 14294-14299.

Mouw, J. K. et al. 2014. Extracellular matrix assembly: a multiscale deconstruction. *Nat Rev Mol Cell Biol* 15(12), pp. 771-785.

Moysidis, S. N. et al. 2015. Magnetic field-guided cell delivery with nanoparticle-loaded human corneal endothelial cells. *Nanomedicine* 11(3), pp. 499-509.

Mufson, E. J. and Kordower, J. H. 1992. Cortical neurons express nerve growth factor receptors in advanced age and Alzheimer disease. *Proc Natl Acad Sci U S A* 89(2), pp. 569-573.

Mukai, J. et al. 2000. NADE, a p75NTR-associated cell death executor, is involved in signal transduction mediated by the common neurotrophin receptor p75NTR. *J Biol Chem* 275(23), pp. 17566-17570.

Muroski, M. E. et al. 2016. Controlled Payload Release by Magnetic Field Triggered Neural Stem Cell Destruction for Malignant Glioma Treatment. *PLoS One* 11(1), p. e0145129.

Muthana, M. et al. 2015. Directing cell therapy to anatomic target sites in vivo with magnetic resonance targeting. *Nature Communications* 6.

Na, E. S. et al. 2013. The Impact of MeCP2 Loss- or Gain-of-Function on Synaptic Plasticity. *Neuropsychopharmacology* 38(1), pp. 212-219.

Nadal-Nicolas, F. M. et al. 2012. Whole number, distribution and co-expression of brn3 transcription factors in retinal ganglion cells of adult albino and pigmented rats. *PLoS One* 7(11), p. e49830.

Nagahara, A. H. et al. 2009. Neuroprotective effects of brain-derived neurotrophic factor in rodent and primate models of Alzheimer's disease. *Nat Med* 15(3), pp. 331-337.

Nagele, R. G. et al. 2004. Contribution of glial cells to the development of amyloid plaques in Alzheimer's disease.*Neurobiol Aging*. Vol. 25. United States, pp. 663-674.

Nakamura, F. et al. 2000. Molecular basis of semaphorin-mediated axon guidance.*J Neurobiol*. Vol. 44. United States: 2000 John Wiley & Sons, Inc., pp. 219-229.

Nash, M. S. and Osborne, N. N. 1999. Assessment of Thy-1 mRNA levels as an index of retinal ganglion cell damage. *Invest Ophthalmol Vis Sci* 40(6), pp. 1293-1298.

Nawy, S. 1999. The metabotropic receptor mGluR6 may signal through G(o), but not phosphodiesterase, in retinal bipolar cells. *J Neurosci* 19(8), pp. 2938-2944.

Nawy, S. and Jahr, C. E. 1990. Suppression by glutamate of cGMP-activated conductance in retinal bipolar cells. *Nature* 346(6281), pp. 269-271.

Naylor, R. L. et al. 2002. A discrete domain of the human TrkB receptor defines the binding sites for BDNF and NT-4. *Biochem Biophys Res Commun* 291(3), pp. 501-507.

Neeper, S. A. et al. 1995. Exercise and brain neurotrophins. *Nature* 373(6510), p. 109.

Nelson, R. et al. 1978. Intracellular staining reveals different levels of stratification for on- and off-center ganglion cells in cat retina. *J Neurophysiol* 41(2), pp. 472-483.

Nicole, O. et al. 2001. The proteolytic activity of tissue-plasminogen activator enhances NMDA receptor-mediated signaling. *Nature Medicine* 7(1), pp. 59-64.

Nikoletopoulou, V. et al. 2010. Neurotrophin receptors TrkA and TrkC cause neuronal death whereas TrkB does not. *Nature* 467(7311), pp. 59-63.

Niyadurupola, N. et al. 2011. The development of human organotypic retinal cultures (HORCs) to study retinal neurodegeneration. *Br J Ophthalmol* 95(5), pp. 720-726.

Nobukata, H. et al. 2000. Long-term administration of highly purified eicosapentaenoic acid ethyl ester prevents diabetes and abnormalities of blood coagulation in male WBN/Kob rats. *Metabolism* 49(7), pp. 912-919.

Nomura, A. et al. 1994. Developmentally regulated postsynaptic localization of a metabotropic glutamate receptor in rat rod bipolar cells. *Cell* 77(3), pp. 361-369.

Nowicka, D. et al. 2009. Parvalbumin-containing neurons, perineuronal nets and experience-dependent plasticity in murine barrel cortex. *Eur J Neurosci* 30(11), pp. 2053-2063.

Obaidat, I. M. et al. 2015. Magnetic Properties of Magnetic Nanoparticles for Efficient Hyperthermia. *Nanomaterials* 5(1), pp. 63-89.

Ogilvie, J. M. et al. 1999. A reliable method for organ culture of neonatal mouse retina with long-term survival. *J Neurosci Methods* 87(1), pp. 57-65.

Orlando, C. et al. 2012. Perisynaptic chondroitin sulfate proteoglycans restrict structural plasticity in an integrin-dependent manner. *J Neurosci* 32(50), pp. 18009-18017, 18017a.

Owen, J. J. and Raff, M. C. 1970. Studies on the differentiation of thymus-derived lymphocytes. *J Exp Med* 132(6), pp. 1216-1232.

Pang, P. T. et al. 2004. Cleavage of proBDNF by tPA/plasmin is essential for long-term hippocampal plasticity. *Science* 306(5695), pp. 487-491.

Pang, Z. P. et al. 2011. Induction of human neuronal cells by defined transcription factors. *Nature* 476(7359), pp. 220-223.

Pankhurst, Q. A. et al. 2003. Applications of magnetic nanoparticles in biomedicine. *Journal of Physics D-Applied Physics* 36(13), pp. R167-R181.

Pardridge, W. M. 2012. Drug transport across the blood-brain barrier. *J Cereb Blood Flow Metab* 32(11), pp. 1959-1972.

Pasantes-Morales, H. and Tuz, K. 2006. Volume changes in neurons: hyperexcitability and neuronal death. *Contrib Nephrol* 152, pp. 221-240.

Pasutto, F. et al. 2009. Heterozygous NTF4 mutations impairing neurotrophin-4 signaling in patients with primary open-angle glaucoma. *Am J Hum Genet* 85(4), pp. 447-456.

Patt, S. et al. 1991. Pathological changes in dendrites of substantia nigra neurons in Parkinson's disease: a Golgi study. *Histol Histopathol* 6(3), pp. 373-380.

Pattabiraman, P. P. et al. 2005. Neuronal activity regulates the developmental expression and subcellular localization of cortical BDNF mRNA isoforms in vivo. *Mol Cell Neurosci* 28(3), pp. 556-570.

Pearson, R. A. et al. 2012. Restoration of vision after transplantation of photoreceptors. *Nature* 485(7396), pp. 99-103.

Peeters, A. et al. 2010. Quantifying the effect of intraocular pressure reduction on the occurrence of glaucoma. *Acta Ophthalmol* 88(1), pp. 5-11.

Peng, Q. et al. 2007. Structure and function of embryonic rat retinal sheet transplants. *Curr Eye Res* 32(9), pp. 781-789.

Perry, V. H. et al. 1984. Is Thy-1 expressed only by ganglion cells and their axons in the retina and optic nerve? *J Neurocytol* 13(5), pp. 809-824.

Petanjek, Z. et al. 2011. Extraordinary neoteny of synaptic spines in the human prefrontal cortex. *Proc Natl Acad Sci U S A* 108(32), pp. 13281-13286.

Phillips, H. S. et al. 1991. BDNF mRNA is decreased in the hippocampus of individuals with Alzheimer's disease. *Neuron* 7(5), pp. 695-702.

Pickard, G. E. and Sollars, P. J. 2012. Intrinsically photosensitive retinal ganglion cells. *Rev Physiol Biochem Pharmacol* 162, pp. 59-90.

Pizzorusso, T. et al. 2002. Reactivation of ocular dominance plasticity in the adult visual cortex. *Science* 298(5596), pp. 1248-1251.

Poduslo, J. F. and Curran, G. L. 1996. Permeability at the blood-brain and blood-nerve barriers of the neurotrophic factors: NGF, CNTF, NT-3, BDNF. *Brain Res Mol Brain Res* 36(2), pp. 280-286.

Polleux, F. et al. 2000. Semaphorin 3A is a chemoattractant for cortical apical dendrites. *Nature* 404(6778), pp. 567-573.

Pouille, F. et al. 2013. The contribution of synaptic location to inhibitory gain control in pyramidal cells. *Physiol Rep* 1(5), p. e00067.

Qian, M. D. et al. 2006. Novel agonist monoclonal antibodies activate TrkB receptors and demonstrate potent neurotrophic activities. *J Neurosci* 26(37), pp. 9394-9403.

Qin, S. et al. 2016. A magnetic protein biocompass. *Nat Mater* 15(2), pp. 217-226.

Qu, Z. et al. 2015. Transplantation of rat embryonic stem cell-derived retinal progenitor cells preserves the retinal structure and function in rat retinal degeneration. *Stem Cell Res Ther* 6, p. 219.

Quigley, H. A. 1995. Ganglion cell death in glaucoma: pathology recapitulates ontogeny. *Aust N Z J Ophthalmol* 23(2), pp. 85-91.

Quigley, H. A. 1996. Number of people with glaucoma worldwide. *British Journal of Ophthalmology* 80(5), pp. 389-393.

Quigley, H. A. and Broman, A. T. 2006. The number of people with glaucoma worldwide in 2010 and 2020. *Br J Ophthalmol* 90(3), pp. 262-267.

Quigley, H. A. et al. 1988. Chronic human glaucoma causing selectively greater loss of large optic-nerve fibers. *Ophthalmology* 95(3), pp. 357-363.

Quigley, H. A. et al. 1995. Retinal ganglion-cell death in experimental glaucoma and after axotomy occurs by apoptosis. *Investigative Ophthalmology & Visual Science* 36(5), pp. 774-786.

Quigley, H. A. et al. 1987. Chronic glaucoma selectively damages large optic nerve fibers. *Invest Ophthalmol Vis Sci* 28(6), pp. 913-920.

Raffa, V. et al. 2009. Cell creeping and controlled migration by magnetic carbon nanotubes. *Nanoscale Res Lett* 5(1), pp. 257-262.

Rajendra, P. et al. 2004. Biological effects of power frequency magnetic fields: Neurochemical and toxicological changes in developing chick embryos.*Biomagn Res Technol*. Vol. 2. London, p. 1.

Ramaswamy, B. et al. 2015. Movement of magnetic nanoparticles in brain tissue: mechanisms and impact on normal neuronal function. *Nanomedicine* 11(7), pp. 1821-1829.

Rao, A. et al. 2000. Mismatched appositions of presynaptic and postsynaptic components in isolated hippocampal neurons. *J Neurosci* 20(22), pp. 8344-8353.

Raposo, C. and Schwartz, M. 2014. Glial scar and immune cell involvement in tissue remodeling and repair following acute CNS injuries. *Glia* 62(11), pp. 1895-1904.

Rapraeger, A. C. et al. 1991. Requirement of heparan sulfate for bFGF-mediated fibroblast growth and myoblast differentiation. *Science* 252(5013), pp. 1705-1708.

Ratnu, V. S. et al. 2014. Activation-induced cytidine deaminase regulates activity-dependent BDNF expression in post-mitotic cortical neurons. *Eur J Neurosci*.

Ray, M. T. et al. 2014. Decreased BDNF and TrkB mRNA expression in multiple cortical areas of patients with schizophrenia and mood disorders. *Transl Psychiatry* 4, p. e389.

Reese, B. E. and Colello, R. J. 1992. Neurogenesis in the retinal ganglion cell layer of the rat.*Neuroscience*. Vol. 46. England, pp. 419-429.

Reid, B. et al. 2005. Wound healing in rat cornea: the role of electric currents. *Faseb j* 19(3), pp. 379-386.

Reimers, S. et al. 2007. Formation of perineuronal nets in organotypic mouse brain slice cultures is independent of neuronal glutamatergic activity. *Eur J Neurosci* 25(9), pp. 2640-2648.

Reiser, M. F. et al. 2007. *Magnetic Resonance Tomography*. Springer Science and Business Media.

Richards, J. M. et al. 2012. In vivo mononuclear cell tracking using superparamagnetic particles of iron oxide: feasibility and safety in humans. *Circ Cardiovasc Imaging* 5(4), pp. 509-517.

Ridley, A. J. et al. 1999. Rho family proteins and cell migration. *Biochem Soc Symp* 65, pp. 111-123.

Riegler, J. et al. 2013. Superparamagnetic iron oxide nanoparticle targeting of MSCs in vascular injury. *Biomaterials* 34(8), pp. 1987-1994.

Riegler, J. et al. 2010. Targeted magnetic delivery and tracking of cells using a magnetic resonance imaging system. *Biomaterials* 31(20), pp. 5366-5371.

Rihn, L. L. and Claiborne, B. J. 1990. Dendritic growth and regression in rat dentate granule cells during late postnatal development. *Brain Res Dev Brain Res* 54(1), pp. 115-124.

Ritz, T. et al. 2000. A model for photoreceptor-based magnetoreception in birds. *Biophys J* 78(2), pp. 707-718.

Rodger, J. et al. 2012. Long-term gene therapy causes transgene-specific changes in the morphology of regenerating retinal ganglion cells. *PLoS One* 7(2), p. e31061.

Rodier, M. et al. 2014. Exogenous t-PA administration increases hippocampal mature BDNF levels. plasmin- or NMDA-dependent mechanism? *PLoS One* 9(3), p. e92416.

Rodriguez-Muela, N. et al. 2012. Autophagy promotes survival of retinal ganglion cells after optic nerve axotomy in mice. *Cell Death Differ* 19(1), pp. 162-169.

Rodriguez-Tebar, A. et al. 1990. Binding of brain-derived neurotrophic factor to the nerve growth factor receptor. *Neuron* 4(4), pp. 487-492.

Roux, P. P. and Barker, P. A. 2002. Neurotrophin signaling through the p75 neurotrophin receptor. *Prog Neurobiol* 67(3), pp. 203-233.

Rudzinski, M. et al. 2004. Changes in retinal expression of neurotrophins and neurotrophin receptors induced by ocular hypertension. *J Neurobiol* 58(3), pp. 341-354.

Rumpf, S. et al. 2011. Neuronal remodeling and apoptosis require VCP-dependent degradation of the. *Development* 138(6), pp. 1153-1160.

Rutar, M. et al. 2012. 670-nm light treatment reduces complement propagation following retinal degeneration.*J Neuroinflammation*. Vol. 9. England, p. 257.

Ryden, M. et al. 1997. Differential modulation of neuron survival during development by nerve growth factor binding to the p75 neurotrophin receptor. *Journal of Biological Chemistry* 272(26), pp. 16322-16328.

Sagdullaev, B. T. et al. 2003. Retinal transplantation-induced recovery of retinotectal visual function in a rodent model of retinitis pigmentosa. *Invest Ophthalmol Vis Sci* 44(4), pp. 1686-1695.

Sanes, J. R. and Masland, R.H. 2015. The types of retinal ganglion cells: current status and implications for neuronal classification. *Annu Rev Neurosci* 38, pp. 221-246.

Santos, A. R. et al. 2012. beta1 Integrin-Focal Adhesion Kinase (FAK) Signaling Modulates Retinal Ganglion. *PLoS One* 7(10), p. e48332.

Sartori, C. R. et al. 2011. The antidepressive effect of the physical exercise correlates with increased levels of mature BDNF, and proBDNF proteolytic cleavage-related genes, p11 and tPA. *Neuroscience* 180, pp. 9-18.

Sattler, K. D. 2010. *Handbook of Nanophysics. Principles and Methods*. CRC Press.

Scaini, G. et al. 2015. Acute Administration of Branched-Chain Amino Acids Increases the Pro-BDNF/Total-BDNF Ratio in the Rat Brain. *Neurochem Res*.

Schillinger, U. et al. 2005. Advances in magnetofection - magnetically guided nucleic acid delivery. *Journal of Magnetism and Magnetic Materials* 293(1), pp. 501-508.

Schindelin, J. et al. 2012. Fiji: an open-source platform for biological-image analysis. *Nat Methods* 9(7), pp. 676-682.

Schlamp, C. L. et al. 2001. Changes in Thy1 gene expression associated with damaged retinal ganglion cells. *Molecular Vision* 7(27), pp. 192-201.

Schlomann, U. et al. 2009. The stimulation of dendrite growth by Sema3A requires integrin engagement and focal adhesion kinase.*J Cell Sci*. Vol. 122. England, pp. 2034-2042.

Schmid, D. A. et al. 2012. A TrkB small molecule partial agonist rescues TrkB phosphorylation deficits and improves respiratory function in a mouse model of Rett syndrome. *J Neurosci* 32(5), pp. 1803-1810.

Schmidt, T. M. et al. 2011. Intrinsically photosensitive retinal ganglion cells: many subtypes, diverse functions. *Trends Neurosci* 34(11), pp. 572-580.

Schoenmann, Z. 2010. Axonal degeneration is regulated by the apoptotic machinery or a NAD+-sensitive pathway in insects and mammals. *J Neurosci* 30(18), pp. 6375-6386.

Schraermeyer, U. et al. 2001. Subretinally transplanted embryonic stem cells rescue photoreceptor cells from degeneration in the RCS rats. *Cell Transplant* 10(8), pp. 673-680.

Schratt, G. M. et al. 2004. BDNF regulates the translation of a select group of mRNAs by a mammalian target of rapamycin-phosphatidylinositol 3-kinase-dependent pathway during neuronal development. *J Neurosci* 24(33), pp. 7366-7377.

Schuh, R. A. et al. 2005. Calcium-dependent dephosphorylation of brain mitochondrial calcium/cAMP response element binding protein (CREB). *J Neurochem* 92(2), pp. 388-394.

Seiler, M. J. and Aramant, R. B. 2012. Cell replacement and visual restoration by retinal sheet transplants. *Prog Retin Eye Res* 31(6), pp. 661-687.

Seiler, M. J. et al. 2009. Functional and structural assessment of retinal sheet allograft transplantation in feline hereditary retinal degeneration. *Vet Ophthalmol* 12(3), pp. 158-169.

Seki, M. et al. 2003. BDNF is upregulated by postnatal development and visual experience: quantitative and immunohistochemical analyses of BDNF in the rat retina. *Invest Ophthalmol Vis Sci* 44(7), pp. 3211-3218.

Selkoe, D. J. 2002. Alzheimer's disease is a synaptic failure. *Science* 298(5594), pp. 789-791.

Senyei, A. et al. 1978. Magnetic guidance of drug-carrying microspheres. *Journal of Applied Physics* 49(6), pp. 3578-3583.

Shi, Y. and Ethell, I. M. 2006. Integrins control dendritic spine plasticity in hippocampal neurons through NMDA receptor and Ca2+/calmodulin-dependent protein kinase II-mediated actin reorganization.*J Neurosci*. Vol. 26. United States, pp. 1813-1822.

Shi, Y. et al. 2010. Plasma BDNF and tPA are associated with late-onset geriatric depression. *Psychiatry Clin Neurosci* 64(3), pp. 249-254.

Shiells, R. A. and Falk, G. 1990. Glutamate receptors of rod bipolar cells are linked to a cyclic GMP cascade via a G-protein. *Proc Biol Sci* 242(1304), pp. 91-94.

Shiells, R. A. and Falk, G. 1992. The glutamate-receptor linked cGMP cascade of retinal on-bipolar cells is pertussis and cholera toxin-sensitive. *Proc Biol Sci* 247(1318), pp. 17-20.

Shirai, H. et al. 2016. Transplantation of human embryonic stem cell-derived retinal tissue in two primate models of retinal degeneration. *Proc Natl Acad Sci U S A* 113(1), pp. E81-90.

Sholl, D. A. 1953. Dendritic organization in the neurons of the visual and motor cortices of the cat. *Journal of Anatomy* 87(4), pp. 387-&.

Shou, T. et al. 2003. Differential dendritic shrinkage of alpha and beta retinal ganglion cells in cats with chronic glaucoma. *Invest Ophthalmol Vis Sci* 44(7), pp. 3005-3010.

Silver, R. A. 2010. Neuronal arithmetic. *Nat Rev Neurosci* 11(7), pp. 474-489.

Singh, M. S. et al. 2013. Reversal of end-stage retinal degeneration and restoration of visual function by photoreceptor transplantation.*Proc Natl Acad Sci U S A*.

Singh, S. K. et al. 2016. Astrocytes Assemble Thalamocortical Synapses by Bridging NRX1alpha and NL1 via Hevin. *Cell* 164(1-2), pp. 183-196.

Singhal, S. et al. 2008. Chondroitin sulfate proteoglycans and microglia prevent migration and integration. *Stem Cells* 26(4), pp. 1074-1082.

Sniadecki, N. J. 2010. Minireview: A Tiny Touch: Activation of Cell Signaling Pathways with Magnetic Nanoparticles. *Endocrinology* 151(2), pp. 451-457.

Snigdha, S. et al. 2012. Caspase-3 activation as a bifurcation point between plasticity and cell death. *Neurosci Bull* 28(1), pp. 14-24.

Sofroniew, M. V. 2005. Reactive astrocytes in neural repair and protection. *Neuroscientist* 11(5), pp. 400-407.

Sommer, C. A. and Mostoslavsky, G. 2013. The evolving field of induced pluripotency: Recent progress and future challenges. *Journal of Cellular Physiology* 228(2), pp. 267-275.

Song, M. et al. 2010. Using a neodymium magnet to target delivery of ferumoxide-labeled human neural stem cells in a rat model of focal cerebral ischemia. *Hum Gene Ther* 21(5), pp. 603-610.

Song W , K. et al. 2015. Treatment of Macular Degeneration Using Embryonic Stem Cell-Derived Retinal Pigment Epithelium: Preliminary Results in Asian Patients.*Stem Cell Reports*. Vol. 4. pp. 860-872.

Spruston, N. 2008. Pyramidal neurons: dendritic structure and synaptic integration. *Nat Rev Neurosci* 9(3), pp. 206-221.

Stasheff, S. F. 2008. Emergence of sustained spontaneous hyperactivity and temporary preservation of OFF responses in ganglion cells of the retinal degeneration (rd1) mouse. *Journal of Neurophysiology* 99(3), pp. 1408-1421.

Stoll, G. et al. 2002. Degeneration and regeneration of the peripheral nervous system: from Augustus Waller's observations to neuroinflammation. *J Peripher Nerv Syst* 7(1), pp. 13-27.

Stone, J. L. et al. 1992. Morphometric analysis of macular photoreceptors and ganglion cells in retinas with retinitis pigmentosa. *Arch Ophthalmol* 110(11), pp. 1634-1639.

Strettoi, E. et al. 2002. Morphological and functional abnormalities in the inner retina of the rd/rd mouse. *J Neurosci* 22(13), pp. 5492-5504.

Stroh, A. et al. 2011. Tracking Stem Cell Differentiation in the Setting of Automated Optogenetic Stimulation. *Stem Cells* 29(1), pp. 78-88.

Stryer, L. 1986. Cyclic GMP cascade of vision. *Annu Rev Neurosci* 9, pp. 87-119.

Stuber, G. D. and Mason, A. O. 2013. Integrating optogenetic and pharmacological approaches to study neural circuit function: current applications and future directions. *Pharmacol Rev* 65(1), pp. 156-170.

Sun, C. et al. 2008. Magnetic nanoparticles in MR imaging and drug delivery. *Adv Drug Deliv Rev* 60(11), pp. 1252-1265.

Sun, W. Z. et al. 2002. Large-scale morphological survey of mouse retinal ganglion cells. *Journal of Comparative Neurology* 451(2), pp. 115-126.

Sur, M. et al. 1988. Expression of a surface-associated antigen on Y-cells in the cat lateral geniculate nucleus is regulated by visual experience. *J Neurosci* 8(3), pp. 874-882.

Suter, U. et al. 1992. NGF BDNF chimeric proteins - analysis of neurotrophin specificity by homolog-scanning mutagenesis. *Journal of Neuroscience* 12(1), pp. 306-318.

Suzuki, A. et al. 1998. Localization of mRNA for trkB isoforms and p75 in rat retinal ganglion cells. *J Neurosci Res* 54(1), pp. 27-37.

Tagawa, Y. et al. 1999. Immunohistological studies of metabotropic glutamate receptor subtype 6-deficient mice show no abnormality of retinal cell organization and ganglion cell maturation. *J Neurosci* 19(7), pp. 2568-2579.

Takahashi, K. and Yamanaka, S. 2006. Induction of pluripotent stem cells from mouse embryonic and adult fibroblast cultures by defined factors. *Cell* 126(4), pp. 663-676.

Takebe, A. et al. 2012. Zebrafish respond to the geomagnetic field by bimodal and group-dependent orientation. *Sci Rep* 2, pp. 727.

Talcott, K. E. et al. 2011. Longitudinal Study of Cone Photoreceptors during Retinal Degeneration and in Response to Ciliary Neurotrophic Factor Treatment.*Invest Ophthalmol Vis Sci*. Vol. 52. pp. 2219-2226.

Tang, M. et al. 2014. Antidepressant-like effect of n-3 PUFAs in CUMS rats: role of tPA/PAI-1 system. *Physiol Behav* 139c, pp. 210-215.

Tao, X. et al. 1998. Ca2+ influx regulates BDNF transcription by a CREB family transcription factor-dependent mechanism. *Neuron* 20(4), pp. 709-726.

Tezel, G. and Yang, X. 2004. Caspase-independent component of retinal ganglion cell death, in vitro. *Invest Ophthalmol Vis Sci* 45(11), pp. 4049-4059.

Tezel, G. et al. 2012. An astrocyte-specific proteomic approach to inflammatory responses in experimental rat glaucoma. *Invest Ophthalmol Vis Sci* 53(7), pp. 4220-4233.

Thanos, S. et al. 1989. Survival and axonal elongation of adult-rat retinal ganglion-cells - invitro effects of lesioned sciatic-nerve and brain derived neurotrophic factor. *European Journal of Neuroscience* 1(1), pp. 19-26.

Thanos, S. et al. 1993. Treatment of the adult retina with microglia-suppressing factors retards axotomy-induced neuronal degradation and enhances axonal regeneration in vivo and in vitro. *J Neurosci* 13(2), pp. 455-466.

Thrivikraman, G. et al. 2014. Intermittent electrical stimuli for guidance of human mesenchymal stem cell lineage commitment towards neural-like cells on electroconductive substrates. *Biomaterials* 35(24), pp. 6219-6235.

Tibbetts, M. D. et al. 2012. Stem cell therapy for retinal disease. *Current Opinion in Ophthalmology* 23(3), pp. 226-234.

Titus, A. D. et al. 2007. Hypobaric hypoxia-induced dendritic atrophy of hippocampal neurons is associated with cognitive impairment in adult rats.*Neuroscience*. Vol. 145. United States, pp. 265-278.

Tomita, H. et al. 2009. Channelrhodopsins provide a breakthrough insight into strategies for curing blindness. *Journal of Genetics* 88(4).

Torre, V. and Poggio, T. 1978. Synaptic mechanism possibly underlying directional selectivity to motion. *Proceedings of the Royal Society Series B-Biological Sciences* 202(1148), pp. 409-416.

Traynelis, S. F. and Lipton, S. A. 2001. Is tissue plasminogen activator a threat to neurons? *Nat Med* 7(1), pp. 17-18.

Tribble, J. R. et al. 2014. A novel system for the classification of diseased retinal ganglion cells. *Vis Neurosci* 31(6), pp. 373-380.

Triplett, J. W. et al. 2014. Dendritic and axonal targeting patterns of a genetically-specified class of retinal ganglion cells that participate in image-forming circuits. *Neural Dev* 9(2), pp. 1749-8104.

Tsai, S. J. 2007. Statins may enhance the proteolytic cleavage of proBDNF: implications for the treatment of depression. *Med Hypotheses* 68(6), pp. 1296-1299.

Tukmachev, D. et al. 2015. An effective strategy of magnetic stem cell delivery for spinal cord injury therapy. *Nanoscale* 7(9), pp. 3954-3958.

van Praag, H. et al. 1999. Running enhances neurogenesis, learning, and long-term potentiation in mice.*Proc Natl Acad Sci U S A*. Vol. 96. pp. 13427-13431.

Vecino, E. et al. 2002. Rat retinal ganglion cells co-express brain-derived neurotrophic factor (BDNF) and its receptor TrkB. *Vision Res* 42(2), pp. 151-157.

Vecino, E. et al. 2015. Glia-neuron interactions in the mammalian retina. *Prog Retin Eye Res*.

Veraart, C. et al. 1998. Visual sensations produced by optic nerve stimulation using an implanted self-sizing spiral cuff electrode. *Brain Res* 813(1), pp. 181-186.

Vilar, M. et al. 2009. Activation of the p75 neurotrophin receptor through conformational rearrangement of disulphide-linked receptor dimers. *Neuron* 62(1), pp. 72-83.

Virgintino, D. et al. 2009. Differential distribution of aggrecan isoforms in perineuronal nets of the human cerebral cortex. *J Cell Mol Med* 13(9b), pp. 3151-3173.

Vishwakarma, S. K. et al. 2015. Magnetic nanoparticle tagged stem cell transplantation in spinal cord injury: A promising approach for targeted homing of cells at the lesion site.*Neurol India*. Vol. 63. India, pp. 460-461.

Vorobyov, V. et al. 2013. Effects of digesting chondroitin sulfate proteoglycans on plasticity in cat primary visual cortex. *J Neurosci* 33(1), pp. 234-243.

Vutskits, L. et al. 2001. PSA-NCAM modulates BDNF-dependent survival and differentiation of cortical neurons. *Eur J Neurosci* 13(7), pp. 1391-1402.

Vyas, A. et al. 2002. Chronic stress induces contrasting patterns of dendritic remodeling in hippocampal and amygdaloid neurons. *J Neurosci* 22(15), pp. 6810-6818.

Waller, A. 1850. Experiments on the Section of the Glossopharyngeal and Hypoglossal Nerves of the Frog, and Observations of the Alterations Produced Thereby in the Structure of Their Primitive Fibres. *Philosophical Transactions of the Royal Society of London* 140, pp. 423-429.

Wang, D. and Fawcett, J. 2012. The perineuronal net and the control of CNS plasticity. *Cell Tissue Res* 349(1), pp. 147-160.

Wang, H. et al. 2006. Dysregulation of brain-derived neurotrophic factor expression and neurosecretory function in Mecp2 null mice. *J Neurosci* 26(42), pp. 10911-10915.

Wang, S. W. et al. 2000. Abnormal polarization and axon outgrowth in retinal ganglion cells lacking the POU-domain transcription factor Brn-3b. *Mol Cell Neurosci* 16(2), pp. 141-156.

Wang, S. W. et al. 2002. Retinal ganglion cell differentiation in cultured mouse retinal explants. *Methods* 28(4), pp. 448-456.

Wang, X. F. et al. 1991. Expression cloning and characterization of the TGF-beta type III receptor. *Cell* 67(4), pp. 797-805.

Watanabe, Y. et al. 1992. Stress induces atrophy of apical dendrites of hippocampal ca3 pyramidal neurons. *Brain Research* 588(2), pp. 341-345.

Weber, A. J. and Harman, C. D. 2008. BDNF preserves the dendritic morphology of alpha and beta ganglion cells in the cat retina after optic nerve injury.*Invest Ophthalmol Vis Sci*. Vol. 49. United States, pp. 2456-2463.

Weber, A. J. et al. 2008. Effects of optic nerve injury, glaucoma, and neuroprotection on the survival, structure, and function of ganglion cells in the mammalian retina.*J Physiol*. Vol. 586. England, pp. 4393-4400.

Weber, A. J. et al. 1998. Morphology of single ganglion cells in the glaucomatous primate retina. *Invest Ophthalmol Vis Sci* 39(12), pp. 2304-2320.

Weickert, C. S. et al. 2003. Reduced brain-derived neurotrophic factor in prefrontal cortex of patients with schizophrenia. *Mol Psychiatry* 8(6), pp. 592-610.

West, A. E. et al. 2001. Calcium regulation of neuronal gene expression. *Proc Natl Acad Sci U S A* 98(20), pp. 11024-11031.

White, K. E. et al. 2009. OPA1 Deficiency Associated with Increased Autophagy in Retinal Ganglion Cells in a Murine Model of Dominant Optic Atrophy. *Investigative Ophthalmology & Visual Science* 50(6), pp. 2567-2571.

Whitesides, G. M. et al. 1983. Magnetic separations in biotechnology. *Trends in Biotechnology* 1(5), pp. 144-148.

Widder, K. J. et al. 1980. In vitro release of biologically active adriamycin by magnetically responsive albumin microspheres. *Cancer Res* 40(10), pp. 3512-3517.

Wiese, S. et al. 2012. Astrocytes as a source for extracellular matrix molecules and cytokines. *Front Pharmacol* 3, p. 120.

Wiesel, T. N. and Hubel, D. H. 1963. Effects of visual deprivation on morphology and physiology of cells in cats lateral geniculate body. *Journal of Neurophysiology* 26(6), pp. 978-&.

Wilkins, A. et al. 2009. Human bone marrow-derived mesenchymal stem cells secrete brain-derived neurotrophic factor which promotes neuronal survival in vitro. *Stem Cell Res* 3(1), pp. 63-70.

Williams, D. W. et al. 2006. Local caspase activity directs engulfment of dendrites during pruning. *Nat Neurosci* 9(10), pp. 1234-1236.

Williams, P. A. et al. 2013a. Retinal ganglion cell dendritic atrophy in DBA/2J glaucoma.*PLoS One*. Vol. 8. United States, p. e72282.

Williams, P. A. et al. 2013b. Retinal ganglion cell dendritic degeneration in a mouse model of Alzheimer's disease. *Neurobiol Aging* 34(7), pp. 1799-1806.

Wilson, M. T. et al. 2000. Glutamate-induced changes in the pattern of hippocampal dendrite outgrowth: a role for calcium-dependent pathways and the microtubule cytoskeleton. *J Neurobiol* 43(2), pp. 159-172.

Woch, G. et al. 2001. Retinal transplants restore visually evoked responses in rats with photoreceptor degeneration. *Invest Ophthalmol Vis Sci* 42(7), pp. 1669-1676.

Wong, R. O. 1999. Retinal waves and visual system development. *Annu Rev Neurosci* 22, pp. 29-47.

Woo, N. H. et al. 2005. Activation of p75NTR by proBDNF facilitates hippocampal long-term depression. *Nat Neurosci* 8(8), pp. 1069-1077.

Wood, J. P. et al. 2011. Nanosecond pulse lasers for retinal applications. *Lasers Surg Med* 43(6), pp. 499-510.

Woronowicz, A. et al. 2010. Carboxypeptidase E knockout mice exhibit abnormal dendritic arborization and spine morphology in central nervous system neurons. *J Neurosci Res* 88(1), pp. 64-72.

Wu, A. et al. 2008a. Docosahexaenoic acid dietary supplementation enhances the effects of exercise on synaptic plasticity and cognition. *Neuroscience* 155(3), pp. 751-759.

Wu, S. et al. 2008b. Neural stem cells improve learning and memory in rats with Alzheimer's disease. *Pathobiology* 75(3), pp. 186-194.

Wurm, A. et al. 2009. Involvement of A(1) adenosine receptors in osmotic volume regulation of retinal glial cells in mice. *Mol Vis* 15, pp. 1858-1867.

Xia, Y. et al. 2006. State-dependent AMPA receptor trafficking in the mammalian retina. *Journal of Neuroscience* 26(19), pp. 5028-5036.

Xia, Y. et al. 2007. Activity-dependent synaptic plasticity in retinal ganglion cells. *Journal of Neuroscience* 27(45), pp. 12221-12229.

Xu, B. et al. 2000. Cortical degeneration in the absence of neurotrophin signaling: dendritic retraction and neuronal loss after removal of the receptor TrkB.*Neuron*. Vol. 26. United States, pp. 233-245.

Xu, H. P. and Tian, N. 2007. Retinal ganglion cell dendrites undergo a visual activity-dependent redistribution after eye opening. *J Comp Neurol* 503(2), pp. 244-259.

Xu, H. P. and Tian, N. 2008. Glycine receptor-mediated synaptic transmission regulates the maturation of ganglion cell synaptic connectivity. *J Comp Neurol* 509(1), pp. 53-71.

Xu, N. J. and Henkemeyer, M. 2012. Ephrin reverse signaling in axon guidance and synaptogenesis. *Semin Cell Dev Biol* 23(1), pp. 58-64.

Xu, Y. et al. 2007. Energy sources for glutamate neurotransmission in the retina: absence of the aspartate/glutamate carrier produces reliance on glycolysis in glia. *J Neurochem* 101(1), pp. 120-131.

Yacoubian, T. A. and Lo, D. C. 2000. Truncated and full-length TrkB receptors regulate distinct modes of dendritic growth. *Nat Neurosci* 3(4), pp. 342-349.

Yamashita, T. et al. 1999. Neurotrophin binding to the p75 receptor modulates Rho activity and axonal outgrowth. *Neuron* 24(3), pp. 585-593.

Yan, Q. and Johnson, E. M., Jr. 1988. An immunohistochemical study of the nerve growth factor receptor in developing rats. *J Neurosci* 8(9), pp. 3481-3498.

Yanai, A. et al. 2012. Focused magnetic stem cell targeting to the retina using superparamagnetic iron oxide nanoparticles. *Cell Transplant* 21(6), pp. 1137-1148.

Yang, F. et al. 2009. Pro-BDNF-induced synaptic depression and retraction at developing neuromuscular synapses. *J Cell Biol* 185(4), pp. 727-741.

Yang, G. and Masland, R. H. 1994. Receptive-fields and dendritic structure of directionally selective retinal ganglion-cells. *Journal of Neuroscience* 14(9), pp. 5267-5280.

Yang, H. W. et al. 2012. Potential of magnetic nanoparticles for targeted drug delivery.*Nanotechnol Sci Appl*. Vol. 5. pp. 73-86.

Yang, J. et al. 2015. Pathological Axonal Death through a MAPK Cascade that Triggers a Local Energy Deficit. *Cell* 160(1-2), pp. 161-176.

Yates, J. R. W. et al. 2007. Complement C3 variant and the risk of age-related macular degeneration. *New England Journal of Medicine* 357(6), pp. 553-561.

Yin, Y. et al. 2002. The brain-derived neurotrophic factor enhances synthesis of Arc in synaptoneurosomes. *Proc Natl Acad Sci U S A* 99(4), pp. 2368-2373.

Yoshii, A. and Constantine-Paton, M. 2007. BDNF induces transport of PSD-95 to dendrites through PI3K-AKT signaling after NMDA receptor activation. *Nat Neurosci* 10(6), pp. 702-711.

Yoshii, A. and Constantine-Paton, M. 2010. Postsynaptic BDNF-TrkB signaling in synapse maturation, plasticity, and disease. *Dev Neurobiol* 70(5), pp. 304-322.

Yuan, L. and Neufeld, A. H. 2001. Activated microglia in the human glaucomatous optic nerve head. *J Neurosci Res* 64(5), pp. 523-532.

Yuan, W. et al. 2002. Association between protease-specific proteolytic cleavage of brevican and synaptic loss in the dentate gyrus of kainate-treated rats. *Neuroscience* 114(4), pp. 1091-1101.

Zablotskii, V. et al. 2013. Life on magnets: stem cell networking on micro-magnet arrays. *PLoS One* 8(8), p. e70416.

Zagrebelsky, M. et al. 2005. The p75 neurotrophin receptor negatively modulates dendrite complexity and spine density in hippocampal neurons. *J Neurosci* 25(43), pp. 9989-9999.

Zhang, J. et al. 2012. Visual map development depends on the temporal pattern of binocular activity in mice. *Nat Neurosci* 15(2), pp. 298-307.

Zhang, J. et al. 2011. rAAV-mediated delivery of brain-derived neurotrophic factor promotes neurite outgrowth and protects neurodegeneration in focal ischemic model. *Int J Clin Exp Pathol* 4(5), pp. 496-504.

Zhang, N. et al. 2010. Characterization of Human Huntington's Disease Cell Model from Induced Pluripotent Stem Cells. *PLoS currents* 2, pp. RRN1193-RRN1193.

Zhang, S. et al. 2009. Size-Dependent Endocytosis of Nanoparticles. *Adv Mater* 21, pp. 419-424.

Zhang, X. M. and Yang, X. J. 2001. Regulation of retinal ganglion cell production by Sonic hedgehog. *Development* 128(6), pp. 943-957.

Zhang, Y. et al. 2007. CNS progenitor cells promote a permissive environment for neurite outgrowth via a. *J Neurosci* 27(17), pp. 4499-4506.

Zhang, Y. et al. 2002. Surface modification of superparamagnetic magnetite nanoparticles and their intracellular uptake. *Biomaterials* 23(7), pp. 1553-1561.

Zhao, H. et al. 2015. Specific Intensity Direct Current (DC) Electric Field Improves Neural Stem Cell Migration and Enhances Differentiation towards betaIII-Tubulin+ Neurons. *PLoS One* 10(6), p. e0129625.

Zhao, M. et al. 2006. Electrical signals control wound healing through phosphatidylinositol-3-OH kinase-gamma and PTEN. *Nature* 442(7101), pp. 457-460.

Zheng, F. et al. 2012. Regulation of brain-derived neurotrophic factor expression in neurons. *Int J Physiol Pathophysiol Pharmacol* 4(4), pp. 188-200.

Zhou, L. et al. 2013. Upregulation of blood proBDNF and its receptors in major depression. *J Affect Disord* 150(3), pp. 776-784.

Zhu, C. et al. 2005. The influence of age on apoptotic and other mechanisms of cell death after cerebral hypoxia-ischemia. *Cell Death Differ* 12(2), pp. 162-176.

Zivin, J. A. 2009. Acute stroke therapy with tissue plasminogen activator (tPA) since it was approved by the U.S. Food and Drug Administration (FDA). *Ann Neurol* 66(1), pp. 6-10.

Appendix

Chemotaxis measurements equations

All Chemotaxis equations from Chemotaxis and Migration Tool Version 1.01, Ibidi, accessed from http://ibidi.com/xtproducts/en/Software-and-Image-Analysis/Manual-Image-Analysis/Chemotaxis-and-Migration-Tool, last accessed 28.02.16.

$$xFMI(cell) = \frac{x_{NET}}{\text{accumulated distance}}$$

$$xFMI(mean) = \frac{1}{n}\sum_{i=1}^{n} xFMI(cell)_i$$

Equation S1. X forward migration index

$$yFMI(cell) = \frac{y_{NET}}{\text{accumulated distance}}$$

$$yFMI(mean) = \frac{1}{n}\sum_{i=1}^{n} yFMI(cell)_i$$

Equation S2. Y forward migration index

$$x \text{ centre of mass} = \frac{1}{n}\sum \text{endpoint } x$$

Equation S3. X centre of mass

$$\text{y centre of mass} = \frac{1}{n} \sum \text{endpoint y}$$

Equation S4. Y centre of mass

Papers arising from this thesis

Binley, K. E., Ng, W. S., Tribble, J. R., Song, B., Morgan, J. E., 2014. Sholl analysis: a quantitative comparison of semi-automated methods. *J Neurosci Methods* 225, pp. 65-70.

Binley, K. E., Ng, W.S., Barde, Y. A., Song, B., Morgan, J. E., 2016. Brain-derived neurotrophic factor prevents dendritic retraction of adult mouse retinal ganglion cells. *Eur J Neurosci* 44(3), pp. 2028-2039.